^{13}C metabolic flux analysis of recombinant Chinese hamster ovary (CHO) cell cultures

By

Neil Templeton

Dissertation

Submitted to the Faculty of the

Graduate School of Vanderbilt University

in partial fulfillment of the requirements

for the degree of

DOCTOR OF PHILOSOPHY

in

Chemical Engineering

December, 2014

Nashville, Tennessee

Approved:

Jamey D. Young, Ph.D.

M. Douglas LeVan, Ph.D.

Scott A. Guelcher, Ph.D.

David L. Tabb, Ph.D.

Science will only fulfill its promises when the benefits are equally shared by the really poor of the world.

César Milstein

1984 Nobel Prize in Physiology or Medicine

ACKNOWLEDGEMENTS

Is there such a thing as a typical PhD? I'm not entirely sure that there is. I am sure that my PhD experience was anything but typical. I've only begun to comprehend how fortunate I have been throughout the process.

In 2009, an assistant professor took a chance on an unknown kid from the other side of the Appalachian who didn't fit the bill and didn't have a chemical engineering degree-not fairy tale material. Perhaps he enjoys Robert Frost poetry (or perhaps not), but for whatever reason, the path less traveled was chosen when he selected me. I was signed on to his lab before I had even arrived on campus-an easy choice that I never once regretted. Whether it was chance, circumstance, or simply meant to be, the project I was assigned to was basically a dream match. I worked directly with a Janssen pharmaceuticals, at first remotely and then directly, performing research that was genuinely meaningful to me. Jamey taught me how to use MFA (keep reading if you wish to know what that means) and Janssen provided the materials, facilities, and funds that allowed me to perform the kind of research that most academic labs could only dream of doing. I owe a great deal to Kevin Smith for making this industrial collaboration work, Hamanti Dorai for getting us started, and Steve Lang for his continuous support.

Along the way, I met a wonderful man named Douglas LeVan, who gave his time and talents freely to help a struggling math student...even when it was greatly inconvenient to do so. While he may not have known it, this gave me a greatly need shot of confidence to continue forward. To this day I think the Dos Equis *most interesting man in the world* commercials are about him. About this same time, I met David Tabb, who first exposed me to the realm of bioinformatics. He introduced me Eric Bozko, who had past experience with bioreactors and

was a natural fit to my committee. While Erik moved on to other pursuits, I will never forget the comedy he provided to my first committee meeting-I genuinely wish I had recorded it. Erik provided me with directly applicable technical insight to my work, not to mention a few free lunches, and I am thankful for it. When Erik left the university, and I had to find a new committee member immediately, David Tabb stepped in to take his place-even when it was not convenient for him to do so. When I was struggling with my future plans post defense, fellow Hokie Scott Guelcher provided me with career insight that retrospectively, I'm not sure I could have gained from anyone else. His frank appraisal about experiences from working in industry and subsequent transition to academia are the sort of information you simply cannot gain by Googling. I am also appreciative of the part Scott played in opening the department up to students with non-traditional backgrounds. If not for his success upon arrival at Vanderbilt four years prior, I'm not sure I would have been accepted.

Jamey once shared with me the analogy that the student-advisor relationship has to that of a father-son. After being his PhD student the past five years, I can say that this relationship honestly holds.

When I arrived on-site for my 2 month tour as a visiting scientist at Janssen, several people told me that they couldn't believe I actually made it (if you want to collaborate with a company, get ready for legal hurdles). As an analogy, when I consider the intensity of the past five years, I can hardly believe I've made it myself. To my fellow travelers that I've met along this path, I hope I've contributed as much to your journey as you have to mine. Thank you for believing me in me (especially when I didn't). It was you that made all the difference.

TABLE OF CONTENTS

Page

LIST OF TABLES

Tables of Appendices

LIST OF FIGURES

Figures of Appendices

I: INTRODUCTION

Antibodies, and more generally protein therapeutics, are one of the most exciting breakthroughs of modern medicine [1]. They are treating an ever expanding list of diseases and disorders that span the gamut, including but not limited to: cancer, diabetes, cardiovascular disease, infertility, asthma, and rheumatoid arthritis. However, while these medicines have the capacity to change medicine today, they face one of the great problems of the 21st century. Like so many of the medical advances of the past 25 years, they offer little to no benefit outside the rich world. Protein therapeutics are cost prohibitive. Much of this can be owed to the research and development costs necessary to bring a drug to market. In the case of antibodies, much of this cost emerges from the front-loaded development costs associated with generating sufficient antibody to perform clinical trials [2–4]. The objective of this work is to conduct the fundamental research that we believe to be necessary to drive down the sales price to patients.

The timing of this work is critical. The era of biosimilars is arriving, with an estimated $33 billion USD worth of biopharmaceuticals (which are dominated by protein therapeutics) that will come off patent by 2016 [5]. Biosimilars are roughly the generic equivalent of chemical based drugs, having similar efficacy and pharmacokinetics as the brand name. Growth factors, perhaps the simplest variety of protein therapeutics, have already seen significant cost reduction associated with increased competition following patent expiration [6]. Can the same happen with antibodies? As was mentioned prior, much of the development costs are associated with generating sufficient product to perform clinical trials. Given the difficulty that a given company has in consistently producing its own patented antibody, it isn't clear how rapid biosimilars will expand into antibodies. The scientific community is literally at the frontline of this changing

environment, where the development of a fundamental understanding of what leads to high volumetric productivity is paramount. This is how our work aims to accomplish its objective, and the timing is anything but arbitrary.

Here we investigate the causes of poor volumetric productivity through a metabolic lens. A systems biology approach was applied to this industrial research problem, with the goal of:

1) Elucidating the metabolic phenotypes associated with high protein productivity

2) Exploration and evaluation of techniques to encourage productivity

This can be achieved by increases to specific growth rate, increases to peak viable cell densities attained, lengthening cell culture lifespan, and by increasing specific productivity.

3) Minimizing metabolic pathways known to associate negatively with antibody productivity

Major emphasis is placed on understanding the causation and minimization of lactate production.

Reducing lactate production has multiple benefits to industrial cell culture. First, it leads to a drop in culture pH. To compensate, pH can be adjusted by base additions. While effective, base additions increase osmolarity. When osmolarity reaches a certain threshold, it negatively affects final titer [7]. If lactate production can be avoided in the first place, these potential issues are avoided. Furthermore, large scale studies have found lactate production to negatively correlate with antibody production [8].

In the early 1940's, antibiotics were a cost-prohibitive novelty. Penicillin cost $11,000/kg in 1944. However, through much effort and innovation, this cost experienced exponential

decline. Penicillin was changed from a specialty chemical to commodity status, and sold for $18/kg in 1977 [9]. Why can't the same be achieved in protein therapeutics?

The dissertation is divided as follows:

Chapter II provides background and significance to the research offered in chapters III, IV, V, and VI. Prior work exploring the role of lactate production/consumption upon protein therapeutic production is explored. The mathematical basis for metabolic flux analysis (MFA), a powerful technique used to explore the metabolic phenotypes associated with antibody production, is provided. Finally, MFA studies relevant to industrial mammalian cell culture are summarized.

Chapter III examines the metabolic rewiring which occurs over time in an industrial fed-batch production process. A dihydroxyfolate reductase (DHFR) deficient Chinese Hamster Ovary (CHO) cell was used, the most widely used cell line for antibody production in industry. Increased oxidative pentose phosphate pathway (oxPPP) flux and TCA cycle both correlated positively with antibody production. Alongside the observed correlations, total lactate production decreased considerably over the culture lifespan, providing detail of how cell culture metabolism changes over time.

Chapter IV considers the role of engineered apoptotic resistance in CHO metabolism. Bcl-2Δ was expressed, and had considerable impact in reducing lactate production and later increasing consumption. Integrated viable cell density (IVCD) was increased by Bcl-2Δ. The impact upon mitochondrial metabolism was evaluated through both MFA and enzymatic activity analysis.

Chapter V explores the role of limiting glutamine availability in cell culture. As glutamine was exhausted from culture, net lactate production reversed. Furthermore, when the initial glutamine concentration was halved, lactate production reduced and growth rate increased.

Chapter VI embarks on the largest MFA study ever conducted upon antibody producing CHO cells. Here, glutamine synthetase (GS) based antibody expression (popular method, alternative to DHFR, used for industrial antibody expression) was examined in multiple clones in an early stationary-like phase. Oxidative metabolism again positively corresponded with specific productivity, true for several independently generated clones. Furthermore, the role that Bcl-2Δ played in increasing antibody production was considered.

Chapter VII provides conclusion by reexamining the significant findings of this work.

References

[1] Z. A. An, "Monoclonal antibodies — a proven and rapidly expanding therapeutic modality for human diseases," *J Protein Cell*, vol. 1, no. 4, pp. 319–330, 2010.

[2] A. K. Pavlou and M. J. Belsey, "The therapeutic antibodies market to 2008.," *Eur. J. Pharm. Biopharm.*, vol. 59, no. 3, pp. 389–96, Apr. 2005.

[3] S. S. Farid, "Process economics of industrial monoclonal antibody manufacture.," *J. Chromatogr. B. Analyt. Technol. Biomed. Life Sci.*, vol. 848, no. 1, pp. 8–18, Mar. 2007.

[4] J. Zhang, "Mammalian Cell Culture for Biopharmaceutical Production," in *Manual of Industrial Microbiology and Biotechnology*, 3rd ed., no. 104, R. H. Baltz, A. L. Demain, and J. E. Davies, Eds. Washington, DC: ASM Press, 2010, pp. 157–178.

[5] N. Carinhas, R. Oliveira, P. M. Alves, M. J. T. Carrondo, and A. P. Teixeira, "Systems biotechnology of animal cells: the road to prediction.," *Trends Biotechnol.*, vol. 30, no. 7, pp. 377–85, Jul. 2012.

[6] S. R. Aggarwal, "What's fueling the biotech engine-2011 to 2012.," *Nat. Biotechnol.*, vol. 30, no. 12, pp. 1191–7, Dec. 2012.

[7] J. S. Ryu, M. S. Lee, and G. M. Lee, "Effects of cloned gene dosage on the response of recombinant CHO cells to hyperosmotic pressure in regard to cell growth and antibody production.," *Biotechnol. Prog.*, vol. 17, no. 6, pp. 993–9, 2001.

[8] S. Charaniya, H. Le, H. Rangwala, K. Mills, K. Johnson, G. Karypis, and W.-S. Hu, "Mining manufacturing data for discovery of high productivity process characteristics.," *J. Biotechnol.*, vol. 147, no. 3–4, pp. 186–97, Jun. 2010.

[9] G. Seth, P. Hossler, J. Chong, and Y. W. Hu, "Engineering Cells for Cell Culture Bioprocessing – Physiological Fundamentals," *Adv Biochem Engin/Biotechnol*, vol. 101, no. June, pp. 119–164, 2006.

II: BACKGROUND AND SIGNIFICANCE

Importance to Healthcare

Protein therapeutics have the capacity to change medicine on a global scale. They comprise a broad class of drugs, and their market composition (based upon US sales) is categorized in descending order as follows: antibodies, hormones, growth factors, fusion proteins, cytokines, enzymes, blood factors, vaccines, and anti-coagulants [1]. Protein therapeutics are protein based drugs, and unlike small molecular weight drugs, they are too complex to synthesize chemically. Therefore, they, and more generally biologics, are produced in cell culture. While the majority of the biologics market is dominated by protein therapeutics, some hormones and vaccines are not protein therapeutics. All protein therapeutics are biologics, but not all biologics are protein therapeutics. This work focuses on protein therapeutics, which comprise greater than 90% of biologics [1].

To produce a protein therapeutic, the cell culture is genetically modified to express a biologically active protein that the human body will recognize. Following generation of a cell line, it is cultured in a specially designed media to maximize production, with multiple environmental controls (oxygen, pH, temperature, stir rate) optimized to do the same. Such work is often labeled upstream processing. After a process that typically ranges from several days to a few weeks, the protein therapeutic must be purified from the cell culture media, in such a fashion that maximal recovery and minimal degradation to the protein is achieved. Following purification, it is packaged in optimal fashion to maximize shelf life. Purification and packaging is often labeled downstream processing. Considering the multiple levels of optimization

required for protein therapeutic production, the engineering challenges are substantial. This work focuses on the engineering challenges of upstream processing.

Post upstream and downstream processing, the protein therapeutic is finally ready for the clinic. In the clinic the therapeutic is administered and has pharmacokinetic activity, just like a small molecular weight drug would (e.g. Aspirin, Claritin, and the majority of drugs that are household names). Unlike a small molecular weight drug, however, protein therapeutics are most often administered intravenously. This is to minimize the acid hydrolysis, naturally taking place in the stomach, denaturing the protein therapeutic and damaging efficacy. Table 2-1 provides a general overview of the diversity of diseases and disorders that can be treated by protein therapeutics, as well as their overall functional class and purpose.

Table 2-1. Overview of protein therapeutics on the market today, broken down into 5 functional classes. Table has been adapted from a 2008 review from Leader [2].

Protein therapeutic functional classes		
Functional Class	Purpose	Treatment/Target
Enzymatic or regulatory activity	Replace a deficient or abnormal protein	Hormone deficiencies Hemostasis and thrombosis Pulmonary disorders Gastrointestinal disorders Immunodeficiencies Metabolic enzyme disorders
	Increase activity of existing pathway	Hematopoiesis Fertility Immunoregulation Hemostasis and Thrombosis Endocrine disorders Growth regulation
	Provide non-native activity/function	Enzymatic degradation of macromolecules Enzymatic degradation of metabolites Hemostasis and thrombosis
Special targeting capacity	Interfere with molecule, deliver compound to specific site	Cancer Immunoregulation Transplantation Pulmonary disorders Hemostasis and thrombosis Hormone deficiencies
Vaccines[1]	Protection against virus	Hepatitis B Human papillomavirus Lyme disease
	Autoimmune protection	Hemolytic disease of newborn
Diagnostics[2]	Identification	Infections Endocrine disorders Cancer

[1] Attention should be paid to the specificity associated with vaccines relative to the other functional classes. It is possible to list the treatments because recombinant vaccines are quite limited in number.
[2] While not technically a therapeutic, diagnostics are also listed. This is due to the fact that like the recombinant therapeutics, the diagnostics are recombinant proteins produced in similar fashion [21]

Coinciding with the breadth of diseases treatable, as shown by Table 2-1, it is worth considering the sheer number of patients being treated. Currently 9.3% of the American population is diabetic [3], and much of the insulin administered to patients today is a synthetic product derived from *E. coli*. Anyone who has received a hepatitis B vaccination has received a protein therapeutic [2], and currently laws exist (in various forms) in all 50 states' public school systems to vaccinate [4]. Therefore, whether the American public is aware of it, a large percentage of the US population has already benefitted from this important class of molecules. These benefits are often realized because of the fundamental advantages protein therapeutics have over small-molecule drugs [2], mostly derived from their incredible specificity and low immunogenicity. Antigen-specific drug targeting within the body is not readily possible with small-molecule drugs, but proteins have evolved the native capacity for selective binding to specific molecular targets. Here, the antigen is most often a protein or protein complex.

Still, most of the protein therapeutics in the marketplace are costly to provide. In 2006, Farid reviewed a number of drugs on the market, and found strikingly high costs per treatment. Many of the treatments involving antibodies can cost well over $10,000 per treatment [5]. While certainly this cost is shared by the patient and their insurance, it raises concerns over the current burden of drug costs on the American economy. This is especially provoking in light of the incoming Patient Protection and Affordable Care Act and the gradual aging of the US population [6].

Economics

Economics is the fundamental driver behind research to increase productivity of recombinant protein therapeutics. While the potential for protein therapeutics is remarkably high—indeed, they represent the fastest growing class of therapeutic agents [7]—accessibility remains low. If the goal is to reduce the time to market, a better understanding of the overall production process is fundamentally necessary. Achieving this goal is desirable for two reasons. First, it is attractive to medicine today because it increases the rate of novel drugs reaching the market and decreases product variability. Second, from an economic perspective, achieving faster timelines for bringing a drug to market reduces the front-loaded investment costs for a pharmaceutical company, allowing for resource reallocation for the exploration of other novel drugs. Thus, research into recombinant (in this case, meaning DNA derived from humans) protein production promotes the drug-development cycle, which is advantageous to the patient and industry alike. So far, industry efforts towards platform-based approaches have been beneficial in shortening timelines [8]. Platform approaches are the general recycling of a given condition that seems to have been effective in prior processes. A condition could be in regards to environmental culture conditions, cell culture media, or even the way a cell line is generated. However, sacrifices to productivity have been made to maximize the speed to market.

Due to the fact that the majority of protein therapeutics that enter the development pipeline do not reach market [9], it is difficult to rationalize substantial time expenditure to obtain a high-producing clone in the initial stages of drug development. This is unfortunate, as antibody therapies (the largest class of protein therapeutics [1]) require large amounts of product to determine safety and efficacy in clinical trials. Nonetheless, the industry's reliance on limiting platform processes is clear here, as low productivity and high variability (leading to much of

your product being jettisoned) are simply "accepted" [10] as a means to generate enough product for phase I and II clinical trials. This is no doubt stymying drug development and approval rates, as a substantial portion of the total drug development cost is attributed to generating a sufficient amount of antibody for clinical trials [11,12]. When a drug has passed phase I and II, only then is the production process optimized. Yet even at this stage the ability to make improvements is limited by our knowledge of host cell physiology. In a 2011 FDA-lead drug shortage workshop, 54% of the actual or potential problems were due to product quality issues and/or manufacturing shortages in sterile injectable products (including protein therapeutics) [13]. Therefore, fundamental improvements in the production process are necessary to accelerate research and improve manufacturability of protein therapeutics, and examination of the molecular and cellular mechanisms underlying recombinant protein production is warranted.

Lastly, to identify the significance of efforts made to improve the scientific community's understanding of protein therapeutics production, consider the nation's present pharmaceutical expenditures. The United States spent $261 billion in 2012 on pharmaceuticals. This is equivalent to 1.7% of the US GDP, and expenditures are projected to grow at 6.5% annually over the next 10 years [14]. $64 billion went to biologics, or roughly 25% of total pharmaceutical costs [1]. However, in 2008, only 19% of pharmaceutical costs were related to biologics [15]. This trend is expected to continue, as in 2012 biologics grew at a rate seven times that of the overall pharmaceutical industry [1]. It is generally agreed upon that biologics will continue to grow at a rate faster than their small-molecule counterparts. However, their growth rate has varied wildly over the past 10 years (a mark of an immature industry) between 4% and 24% [1,15]. Regardless of the exact growth rate in biologics sales, this industry will play a critical role in the future US economy.

Techniques to increase antibody production

Achieving higher titers and volumetric productivities of recombinant proteins have been the main goals of the cell culture industry for the past several decades. There are two primary means to accomplish this end. The first is by achieving higher integrated viable cell densities (IVCD), with Equation 2-1 defining the benefit.

$$\frac{dp}{dt} = q_p X \qquad (2\text{-}1)$$

Where p is product concentration, t time, q_p specific productivity and X viable cell density. With a greater number of viable cells maintained over time, greater titers and volumetric productivities can be achieved. The second is to increase the cell-specific productivity. If either or both can be accomplished, without impairing the other, higher titers and volumetric productivities can be achieved. In this dissertation, attention has focused on elucidating metabolic adaptations of host cells that lead to enhanced protein productivity or increased IVCD, since both of these factors contribute to enhancing cell culture performance.

Over the past thirty years, final titers have increased over two orders of magnitude from about 0.05 g/L to over 10 g/L [16,17]. Most of this increase is attributable to increases in IVCD [18]. Peak cell concentrations in a fed-batch process rarely rose above 4 x 10^6 cells/mL in 1986; now they routinely exceed 15 x 10^6 cells/mL [19]. Additionally, while it was once difficult to culture beyond one week, now processes routinely run for three weeks or more. Increases in specific productivity have also been achieved, but has not increased by an order of magnitude (like IVCD) [20].

Regarding cell-specific productivities, in 1991, 50 pg/cell/day of product was achievable in a hybridoma cell line [16]. Compared to specific productivities reported today in literature,

this would be considered above average [21]. Considering an average CHO cell to be 350 pg, and a typical doubling time of 1 day in exponential phase, CHO cells are already capable of producing 260 pg of protein a day (host cell protein). This assumes that roughly 75% of the cell mass is attributable to protein [22]. If growth rate were reduced to 20%, and specific productivity of total protein (including host cell protein) was assumed to remain constant (independent of growth rate), an excess of 200 pg/cell/day of product would be made. Furthermore, the sheer diversity of techniques that exist to increase specific productivity suggest an empirical approach [23]. The effort to increase specific productivity certainly exists, but the direction (or biological understanding) is not clear.

Choice of expression systems

Cell line. CHO cell cultures are the predominant system used for production of monoclonal antibodies (mAbs) today, a type of protein therapeutic. CHO cells are used largely because of their high productivity, robustness, and safety track record [24]. They are presently used to produce 60-70% of recombinant protein therapeutics on the market [25]. Proteins are complex in structure and often require post-translational modifications (PTMs), such as glycosylation, to have proper activity. CHO cells are efficient at performing PTMs and can generate glycosylation patterns that are similar to humans [26]. Additionally, expression of antibody can be achieved with two different vectors. This is not possible for all mammalian cell lines (such as NS0) [27]. Initially, simpler organisms with less challenging growth requirements were used, such as *E. coli* and yeast. In time, *E. coli* proved to be quite effective for the production of simpler proteins without PTM requirements, such as insulin and the now controversial bovine growth hormone (rBGH) [28,29]. Promise has also been shown in using

microbes to produce antibody fragments [30]. To this date, considerably more is known about yeast and *E. coli* as they have proven to be more broadly useful to the biotech industry [31]. However, in the pursuit of more complex protein therapeutics, such as therapeutic antibodies, microbes have proven to be largely unsuccessful. This is due to their general lack of mammalian protein processing machinery and/or lack of specific enzymes required for human-like PTMs. In particular, failure to produce therapeutic antibodies with proper glycosylation frequently leads to inactivity in the body and rapid clearance rates [32].

There are multiple mammalian alternatives to CHO. Initially, most mAb production was conducted using hybridoma cell lines. Mouse hybridoma cell lines, generated from the fusion of an antibody-producing B-lymphocyte cell with a myeoloma cell (cancerous plasma B-cell), were the first reliable sources of monoclonal antibodies [33]. However, innovations in recombinant DNA technology allowed for movement away from hybridoma into what are today more widely used mammalian hosts. The most common host cell lines used today are CHO, murine myeloma (NS0), human embryonic kidney (HEK), and baby hamster kidney cells (BHK) [34].

Expression vectors. One simple reason for CHO's predominance could have more to do with timing and convenience than logic. Around the time when the protein therapeutic industry was beginning in the early 1980's, a dihydrofolate reductase deficient ($DHFR^-$) CHO line was generated by a biologist interested in performing metabolic studies [35]. In this cell line, both alleles encoding the dihydrofolate reductase (DHFR) enzyme were either mutated or eliminated. This became CHO-DUK-XB11, one of the most widely used CHO cell lines on the market today [36]. Just a few years later, an additional $DHFR^-$ line was generated (by the same biologist) where both DHFR alleles were deleted [37]. It was named CHO-DG44, another predominant CHO cell line on the market. Since DHFR is a critical enzyme required for the biosynthesis of

purine and pyrimidine nucleotides, cells lacking it cannot grow unless DHFR is expressed recombinantly. This was quite useful for protein therapeutics production, as it provided a mammalian selection system that did not involve antibiotics, a critical requirement. Antibiotics are generally avoided, as their addition (for host selection) will require subsequent removal in downstream purification, requiring increased purification costs.

DHFR selection involves first cloning the target genes required for protein production into a recombinant plasmid that contains the DHFR gene. The plasmid DNA is transfected into the host, and the resulting clones are cultured in the presence of methotrexate (MTX) to inhibit background DHFR activity [10]. Only the clones that successfully integrated the DHFR-containing plasmid into their chromosomes will be able to survive in the presence of MTX. The surviving clones not only tolerate the MTX inhibition, but also produce protein therapeutic since the target genes were included on the same DNA construct with the DHFR gene. Gradually, the MTX concentration is increased as the cultures grow more tolerant, theoretically leading to better producing clones. Gene copy number has been found to increase to several hundred in the best producing clones. However, there is a drawback to this approach: time. DHFR selection requires several rounds of gene amplification, often taking up to 6 months [27].

While perhaps obvious, MTX selection is most effective when a DHFR vector is transfected into a $DHFR^-$ host cell. When this is not the case, antibiotic resistance can be added to the plasmid to provide selection [10]. No doubt in part because of the limitations of the DHFR system, the glutamine synthetase (GS) system was developed (Figure 2-1).

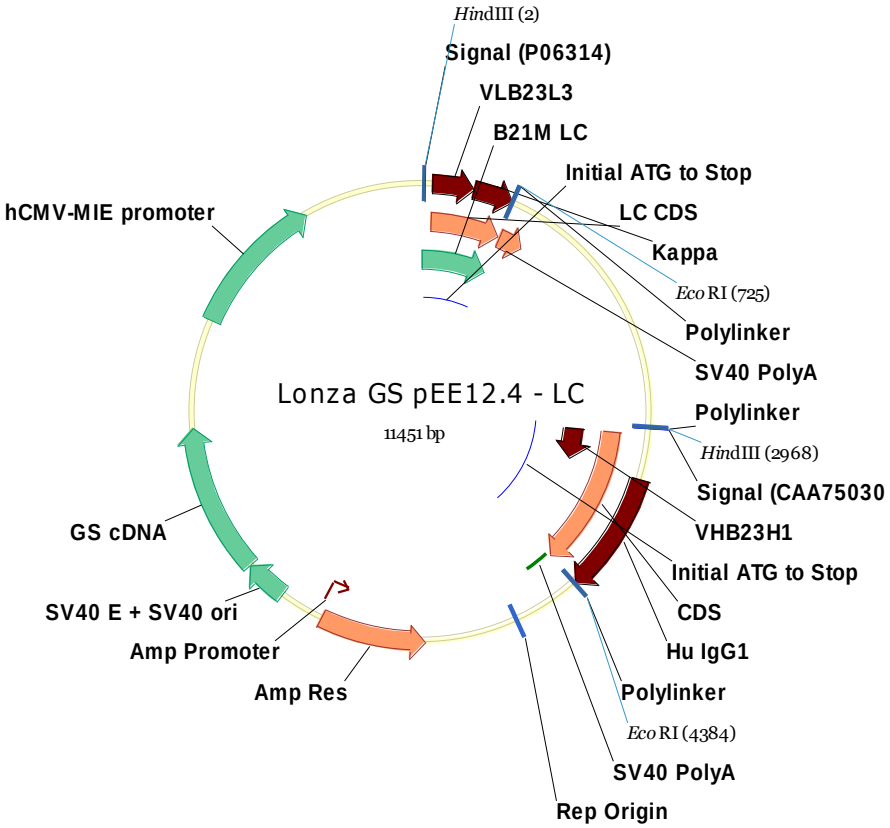

Figure 2-1. Glutamine Synthetase (GS) plasmid.

GS allows glutamine synthesis from glutamate and ammonia, outlined in Figure 2-2.

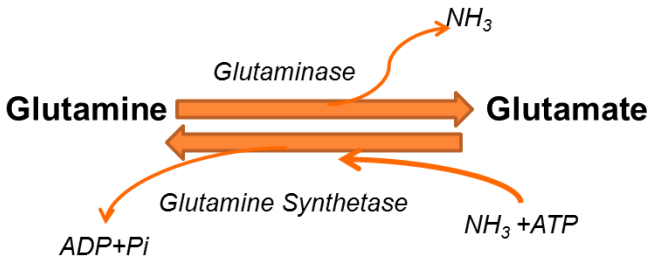

Figure 2-2. The role of glutamine synthetase (GS).

GS deficiency is a characteristic of most (if not all) CHO cell lines, making it an excellent selection system. GS expression is so low in NS0 lines that it is often designated GS^- [38]. The effectiveness of GS selection, like DHFR selection, is maximized by the addition of a chemical inhibitor. This chemical, methionine sulfoximine (MSX), is an inhibitor of GS. Following transfection, the necessary concentration of MSX is added to limit growth of cells that lack expression of the recombinant GS construct. Gene amplification (through gradual increases in MSX concentration) is typically not necessary with GS, even though only 4-10 copies are found in each individual clone [10,27]. This allows effective clones to be produced in roughly half the time of DHFR selection. As an additional benefit, GS expression significantly reduces the accumulation of ammonia [39], since glutamine does not need to be supplied in the growth medium to achieve maximal growth [40]. Ammonia is a major byproduct of glutamine metabolism but is inhibitory to cell cultures at sufficient concentrations [41,42]. Eliminating glutamine from the medium effectively removes the threat of ammonia accumulation to toxic concentrations. Considering the benefits of the GS system, it has taken a large market share away from DHFR, even though it was released on the market roughly ten years following DHFR [43]. However, while GS was patented by Lonza, DHFR is not owned by any company. It seems unlikely that patent protection (which recently expired) has limited the adoption of GS, as GS licensing from Lonza is trivial compared to the entire R&D cost required to put a drug on the market [44]. Regardless, DHFR still manages to be widely used despite its disadvantages [36,45].

The role of lactate production in mammalian cell culture

In spite of the fact that the industry has achieved two orders of magnitude of improvement in final titer, many of the same problems from thirty years ago remain today [19]. Lactate production, and the inefficient use of carbon resources associated with it, is still limiting the achievement of higher titers [46]. Lactate production reduces the pH of culture, forcing the addition of base. When base is added, the osmolarity begins to rise. This effect is most pronounced in fed-batch cultures. Osmotic pressure can be tolerated to reasonably high concentrations by CHO cells, but eventually it begins to negatively impact specific growth and productivity [47]. In addition to the potential problems posed by osmotic pressure, increased lactate production is statistically correlated with decreased productivity [48]. Efforts to reduce lactate production, or increase lactate consumption, correlate with increased antibody production. While industry has taken advantage of this observation, no one has proven why this correlation is observed.

Cell viability, obviously necessary for antibody production, can be significantly improved by reducing lactate production [19]. While the reasons for lactate production in a well-oxygenated environment are still elusive, its impact upon metabolism is beginning to be better understood. First, it is important to realize just how significant the lactate production flux actually is, and how it relates to glucose consumption (Figure 2-3).

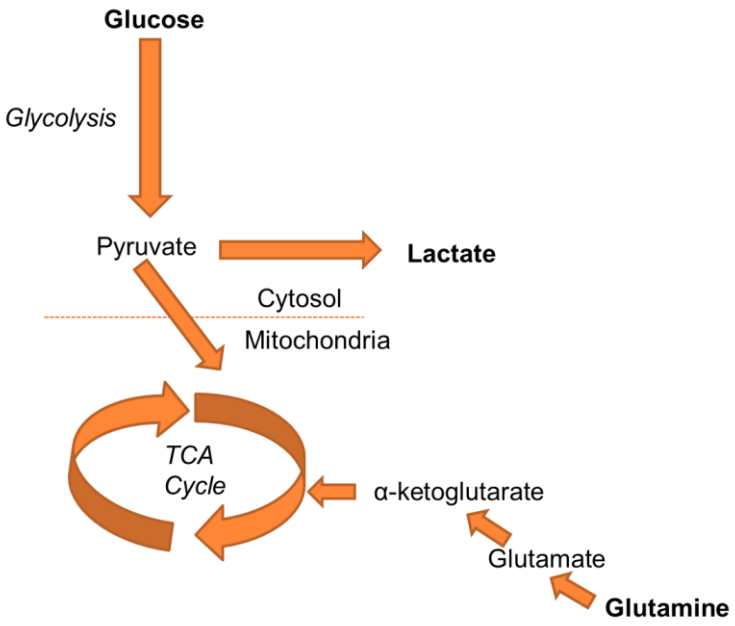

Figure 2-3. The metabolic connection between glucose, lactate, and glutamine.

Glucose is typically the largest incoming carbon flux in cell culture, and lactate production can account for over half of glucose carbon. During exponential growth, molar yields of lactate on glucose have been reported in the range from 49% to 80% in antibody producing cultures of hybridoma, CHO, and BHK cell lines [49], [50], [51]. In our own work examining a CHO cell line optimized for industrial production by Amgen, we've found that up to 38% of total carbon consumption can be tied to lactate production despite achieving antibody titers in excess of 3 g/L [52]. This fact underlies the minimal progress that has been made in decreasing lactate production. Yet, this lack of progress is not due to a lack of effort. Tables 2-2: 2-4 summarize a plethora of strategies that have been used to intentionally (and occasionally unintentionally) limit lactate accumulation in mammalian culture.

Environmental manipulations. Industrial strategies most often focus on media/environmental manipulations. One such strategy is a reduction in temperature, as seen in

Table 2-2, from a typical culture condition of 37°C to 30-35°C [11,53,54]. Temperature drops are most effective when employed in peak production stage when cell growth is already minimal. When correctly timed, reports of doubling in titers are possible [54].

Table 2-2. Environmental manipulations impacting lactate metabolism.

Manipulation	Metabolic Impact	Cell Line	Operation	Ref.
Reduce temperature from 37 to 33°C	Lactate and glucose flux reduced, but lactate/glucose ratio remains unaffected; Titer doubles largely due to doubling in specific productivity	CHO-K1, BHK	Batch	[54]
Increase osmolarity from 290-435mOsM	Specific productivity increased, titer unaffected; Lactate and glucose flux reduced but lactate/glucose ratio unaffected; Growth rate reduced by ~ 50%	Hybridoma	Batch	[55]
Increase osmolarity from 290-450mOsM	Slight increase in specific productivity and final titer; Growth rate reduced, but overall IVCD similar; Increase in lactate production/glucose consumption	NS0	Batch	[56]
Increase pCO_2	Effectively increased osmolarity; Decreased growth rate and increased specific productivity; No impact upon final titer; Increased lactate production/glucose consumption	CHO	Fed-batch	[57]

Previous work has found temperature reductions to force the cell into a G_0/G_1 state where growth was arrested and antibody specific productivity frequently increased. When the temperature was reduced, it led to an overall reduction in metabolic activity (i.e., less glucose consumed and less lactate produced). However, it had a minimal effect upon the lactate/glucose flux ratio, suggesting an insignificant change in the partitioning between glycolytic/mitochondrial carbon utilization.

Another strategy to increase specific productivity involves increasing the osmolarity. While there are several ways to accomplish an increase in osmolarity, the rationale for doing so is to increase specific productivity by promoting G_0/G_1 growth arrest. However, while a temperature drop typically reduces overall metabolic activity and reduces nutrient consumption,

forcing hypertonic conditions does not always have the same effect. In two similar studies on mammalian culture, specific glucose consumption increased when osmolarity was raised from 290 to 450 mOsM in NS0 [56], yet glucose consumption decreased when it was raised from 290 to 435 mOsM in hybridoma [55]. Osmolarity spikes likely have significant cell line dependencies [53,58]. While increasing osmolarity generally increases specific productivity, if increased too far, it negatively affects the final titer [58]. Additionally, osmotic pressures are somewhat difficult to control, as run-to-run there will always be variations in osmolarity (any and all metabolic byproducts and substrates impact culture osmolarity).

Media manipulations. Several media optimization strategies have been developed and implemented to enhance culture performance. One of the most common techniques is to limit the availability of a given nutrient, often glucose or glutamine. This strategy has been generally effective for limiting the production of lactate, and has been implemented for a number of years in fed-batch processes. However, as can be seen in Table 2-3, media manipulation results have been varied.

Table 2-3. Media manipulations impacting lactate metabolism.

Manipulation	Metabolic Impact	Cell Line	Operation	Ref.
Media				
Add copper to media at 20x standard concentration	Induces lactate re-uptake to consume nearly all the lactate previously produced; Increased titer by ~60%	CHO-DUK-XB11	Fed-batch	[59]
Co-limitation of glucose and Gln	Increased biomass yield on glucose; Production of NH_3, lactate, and Ala virtually eliminated; IVCD and final titer slightly increased	Hybridoma	Fed-batch	[60]
Limit glucose availability, feed based upon OUR	Fed glucose based upon oxygen uptake rate (OUR), lactate/glucose ratio was reduced over time, if only mildly; Final titer increased 22%	Myeloma	Fed-batch	[61]
Limit glucose availability, feed based upon OUR	As OUR was increased over culture life, lactate/glucose ratio decreased; Growth phase extended, peak VCD increased by factor of 6, when compared to batch; Data from batch culture not shown	Hybridoma	Fed-batch	[62]
Limit glucose availability	Reduced the fraction of glucose attributable to lactate from 81% to 9%; Increased fraction of glucose entering TCA cycle from 2% to 48%; Growth rate reduced; Final titer increased 100x	Hybridoma	Fed-batch	[49]
Limit glucose availability, feed glucose based upon pH rise	Reduced lactate production; doubled final titer as a result of higher IVCD and specific productivity	CHO-K1	Fed-batch	[63]
Feed lactate to culture as alternative to CO_2	Reduced ammonia production following exhaustion of lactate from culture; specific productivity, glycosylation, and growth rate unaffected	CHO-DUK-XB11	Fed-batch	[64]
Feed lactate to culture at various concentrations to determine inhibitory impact	Decreased yield of lactate on glucose; Specific productivity increased but IVCD decreased; No net change in final titer; Slight increase in ammonia production rate; Suggests effects of lactate addition were the result of osmolarity increases rather than lactate per se	Hybridoma	Batch	[41]
Determined inhibitory concentration of ammonia, lactate, osmolarity, CO_2	Using principal component analysis, applied optimal conditions to increase peak VCD by 17%, final titer by 40%; Did not report lactate data, just final result	CHO	Fed-batch	[65]
Co-culture galactose with glucose	Switched culture from lactate production to lactate consumption; Did not impact final titer; Slight increase in IVCD and slight decrease in specific productivity	CHO	Fed-batch	[66,67]
Limiting Gln availability	When glutamine had been nearly exhausted from culture, lactate switched from net production to consumption	CHO-S	Batch	[68]

Substitute Gln for pyruvate	Reduced glucose consumption and reduced lactate production, minimal change in lactate/glucose ratio; No impact upon growth rate	CHO, BHK, MDCK	Batch [3]	[69]

In two separate studies, when glucose was limited the production of lactate was practically eliminated, leading to a lactate/glucose ratio of nearly zero [49,60]. However, either the peak VCD achieved was diminished or growth rate was reduced, both fundamental problems for protein production. However, in another study, the IVCD achieved was actually increased, in addition to reduced specific lactate production, leading to a doubling in the final product titer [63]. While this achievement certainly benefited from the increased sensitivity derived from using pH measurements to control glucose addition (rather than glucose measurements), it is not clear if glucose limitations will be consistently effective. Another strategy is to substitute glucose for another sugar, such as galactose. Altamirano et al. showed how this could be effective in limiting lactate production in two separate studies [66,67]. Unfortunately, these efforts did not result in a higher final titer, and generally limited the growth rate, making the reduction in lactate production less meaningful.

One of the more interesting strategies explored was perhaps the most counterintuitive. Li et al. explored the effect of feeding lactate to cell culture, as a substitute for CO_2 [64]. Considering the universal usage of CO_2 as a media buffering agent (in tandem with HCO_3^-), and the universal interest to limit lactate accumulation in media, this study stood in stark contrast to other approaches. In terms of consumption fluxes, lactate was actually the preferred substrate to glucose (following addition). While final titer was not increased, ammonia production was

[3] This study induced the production of a vaccine with the inoculation of the flu virus, and media was changed upon inoculation, therefore technically making it a fed-batch process, but at least initially having features of a batch culture.

reduced considerably. It is possible the excess ammonia was stored as alanine, since significant alanine accumulation occurred. This is significant, as ammonia has been previously shown to negatively impact antibody glycosylation quality [25]. Osmolarity and IVCD were also not affected.

Genetic manipulations. At present, the industry is reluctant to consider genetic manipulations to their host cell lines. This is likely due to a combination of factors. The first issue deals with time. Media can be altered and its effects tested immediately in culture. Improvements to media formulation can also be more easily implemented with other processes (using different cell lines). Companies are unsure how the FDA will regulate genetic modifications to their cell lines, as outside of the DHFR and GS expression systems, there are not many precedents for using genetically engineered host cells. Perhaps only when genetic modification(s) enable considerable economic advantage will the industry reconsider this approach. Of all the genetic manipulations listed, the only one that has gained significant acceptance in the industry is GS [38,70]. Regardless, this has not stifled the academic interest or pursuit of uncovering meaningful and useful genetic alterations (Table 2-4).

Table 2-4. Genetic manipulations impacting lactate metabolism.

Manipulation	Metabolic Impact	Cell Line	Operation	Ref.
Genetic				
Downregulate LDH with RNAi	Reduced lactate production, glucose consumption; Negligible change in glucose/lactate ratio, IVCD; Increased titer more than 2x compared to control	CHO	Batch	[71]
Overexpress GAPDH and Anti-Sense LDH	Anti-LDH: Reduced lactate production; Increased IVCD, No impact upon final titer. Anti-LDH + GAPDH: Limited lactate production; Increased IVCD, titer doubled	CHO ($DHFR^-$)	Batch	[72]
Partial knockout of LDH	Increased IVCD, doubled final titer; Reduced lactate production by ~50%, glucose consumption by ~25%	Hybridoma	Batch	[73]
Knockdown of LDH and PDHK	Transfected cell to express siRNA for PDHK and LDH; Reduced lactate production by 90%; Increased specific productivity by 75%; IVCD not significantly effected	CHO-DUK-XB11	Fed-batch	[74]
Overexpress anti-apoptotic genes E1B19K, Aven, XIAP	Increased IVCD, prolonged culture life; Increased capacity to consume lactate, decreased ammonia accumulation; Nearly doubled final titer	CHO-K1-SV	Batch	[75]
Express cytosolic PC	Doubled final titer; Increased cellular ATP content; Lactate/glucose ratio reduced; Increased viability in later stages of culture	BHK	Batch, Continuous	[76, 77]
Express cytosolic PC	Reduced lactate and ammonia accumulation; Slight increase in peak VCD; Final titer not affected	HEK 293	Fed-batch	[78]
Express cytosolic PC	Reduced lactate and ammonia production; Increased IVCD by ~1/3; Increased titer by ~1/3	HEK 293	Batch	[79]
Express cytosolic PC	Increased IVCD; Doubled final titer; Reduced lactate production; Increased specific productivity as much as 80%	CHO-K1, BHK-21	Batch	[54]
Express Glut5 fructose transporter	Decreased lactate production and fructose consumption; Unfortunately decreased IVCD, too	CHO-DUK-XB11	Batch	[80]
Reduce Glut1 activity	Knocked down Glut1 activity through anti-sense expression, reduced glucose consumption; Widely varying growth rates among clones generated, expression of Glut1 anti-sense unstable over time	Hybridoma	Batch	[81]
Overexpress Asp/Glu Transporter and Timm8a1	Neither Timm8A1 or Aralar1 significantly affected glucose consumption; Reversed lactate production; Decreased lactate accumulation; Titer not reported	CHO	Batch	[82]
Overexpress Asp/Glu Transporter	Increased mitochondrial ATP production using 2 separate isoforms of Asp/Glu transporter; Did not measure glucose uptake or lactate production	CHO	Batch	[83]
Overexpress ALT	Increased volumetric productivity by ~60%; Reduced ammonia and lactate accumulation; Increased IVCD	CHO-DUK-XB11	Fed-batch	[84]

The strategy to overexpress pyruvate carboxylase (PC) deserves special attention, as five separate studies were conducted upon it. Specifically, the cytosolic variety of pyruvate carboxylase was expressed, which does not endogenously exist in the CHO genome [85] and was cloned from yeast. This enzyme is responsible for the carbon fixing reaction that uses pyruvate as a substrate and generates the four-carbon molecule oxaloacetate. Oxaloacetate is then converted into malate, via cytosolic malate dehydrogenase, and subsequently transported into the mitochondria (Figure 2-4).

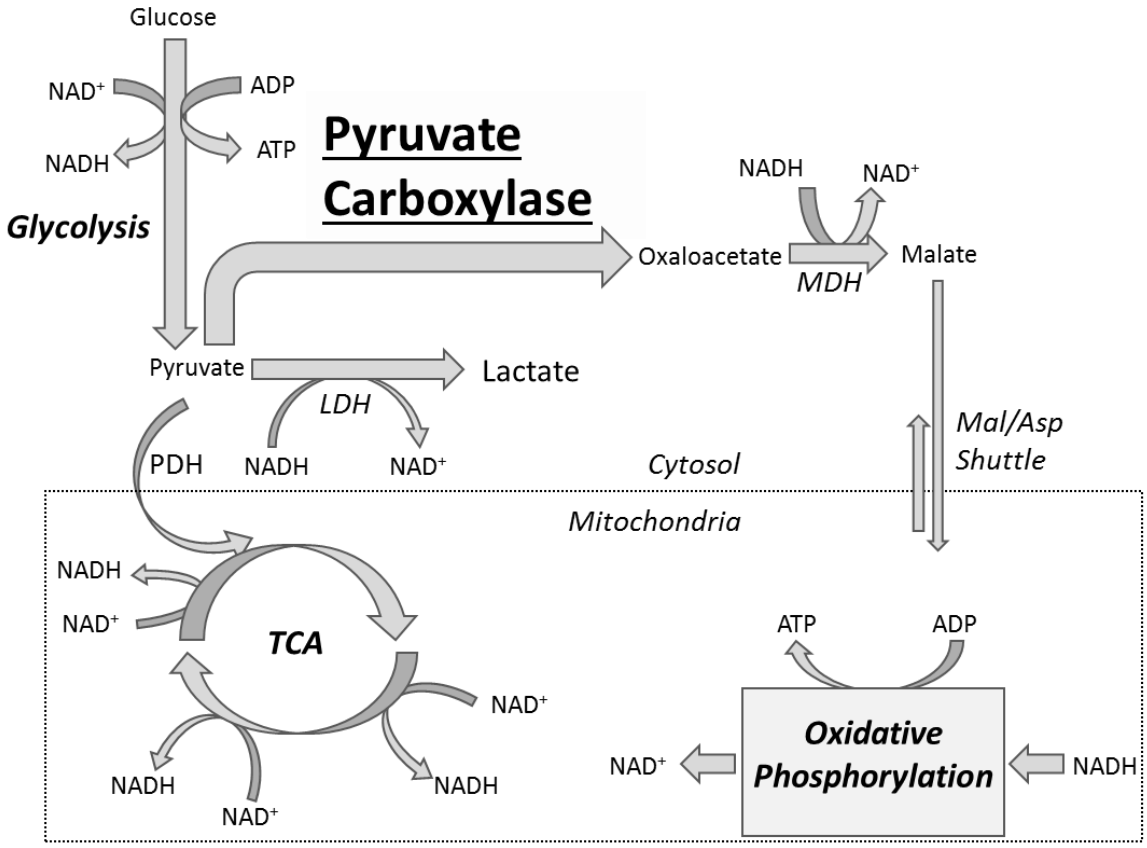

Figure 2-4. The impact of yeast-based cytosolic pyruvate carboxylase (PC) expression.

This provided an additional path, in addition to pyruvate dehydrogenase, for carbon to be transported to the mitochondria. Since this process oxidizes NADH into NAD^+, it has the added advantage of generating a redox cofactor likely in short supply in the cytosol. Not surprisingly, when cytosolic PC was expressed, lactate production was reduced. Moreover, all five studies reported practical benefits as a result of PC expression, where higher IVCD [54,79] was often achieved in addition to higher specific productivity [54] and final titer [54,77,79].

Another effective strategy to limit lactate accumulation was examined by Dorai where multiple anti-apoptotic genes were overexpressed [75]. Here, perhaps as a consequence of limiting the progression of apoptosis, IVCD was increased by 80%. This led to the final titer being increased by 78%, an achievement owed largely to an increase in IVCD. However, the expression of the anti-apoptotic genes had an additional effect, where accumulation of lactate was significantly reduced. This largely was an effect of augmented lactate consumption, which perhaps was facilitated by the measured enhancement in mitochondrial potential.

A general theme emerges upon examination of the environmental, media, and genetic developments that have been made. First is the realization that both the industry and academics have went to great lengths to reduce the production of a natural metabolic byproduct, lactate. Furthermore, of all the environmental, media, and genetic strategies, there are two common themes. One is the reduction in the total amount of nutrients, namely glucose, being consumed [55,63,69,71,80,81]. The other is the redistribution of the nutrients that have been consumed, commonly represented in the glucose/lactate flux ratio [62,64,72,74,78,79,84]. Often, both of these themes can be simultaneously achieved [49,54,60–62,68,73,76,77,82]. A redistribution of the nutrients consumed (change in glucose/lactate flux ratio) is often more desirable, as this doesn't deplete the availability of incoming substrates to allocate towards the production of

biomass or product protein. Among the six studies that resulted solely in a reduction of incoming nutrients, only 1 out of 6 clearly had a positive outcome [71]. In this case, a positive impact is defined as an increase in growth rate or IVCD (biomass) or an increase in specific productivity or final titer (product). Comparatively, 5 out of 7 studies associated with nutrient redistributions clearly had positive impacts, with the remaining 2 reducing ammonia accumulation. Lastly, among the ten studies where total nutrient uptake was decreased and redistributed, 8 out of 10 studies had positive impacts, with the remaining 2 lacking the reported data to judge. Considering all 23 studies considered here, the data clearly suggest that reducing lactate production, without having any nutrient consumption redistribution, is insufficient to have a positive outcome on production. Therefore, glucose/lactate ratio serves as a much more reliable indicator of cell culture performance.

It should be noted that while the glucose/lactate ratio is meaningful, it has limitations. Simply quantifying glucose and lactate flux does not provide any information as to what is the source of the lactate. It also doesn't consider the other metabolic byproducts that are typically produced during a production process. However, lactate is the largest carbon output besides biomass production during exponential growth [52], so this ratio provides insight into the cellular carbon budget. With less glucose converted to lactate, more can be shuttled into the mitochondria to engage in oxidative metabolism. This in turn can fuel improved protein productivity, as evidenced by a positive correlation between oxygen uptake rate (OUR) and volumetric productivity [17].

As can be clearly identified from Tables 2-4, strategies to limit/eliminate lactate production over the past twenty years have been varied in approach and success. Nonetheless,

previous work provides insight on how to improve the process as the industry moves more from an empirical to a systems-based approach [18].

Cellular physiology of lactate production. Figure 2-5 illustrates how lactate production and consumption affects cytosolic reduction/oxidation (redox).

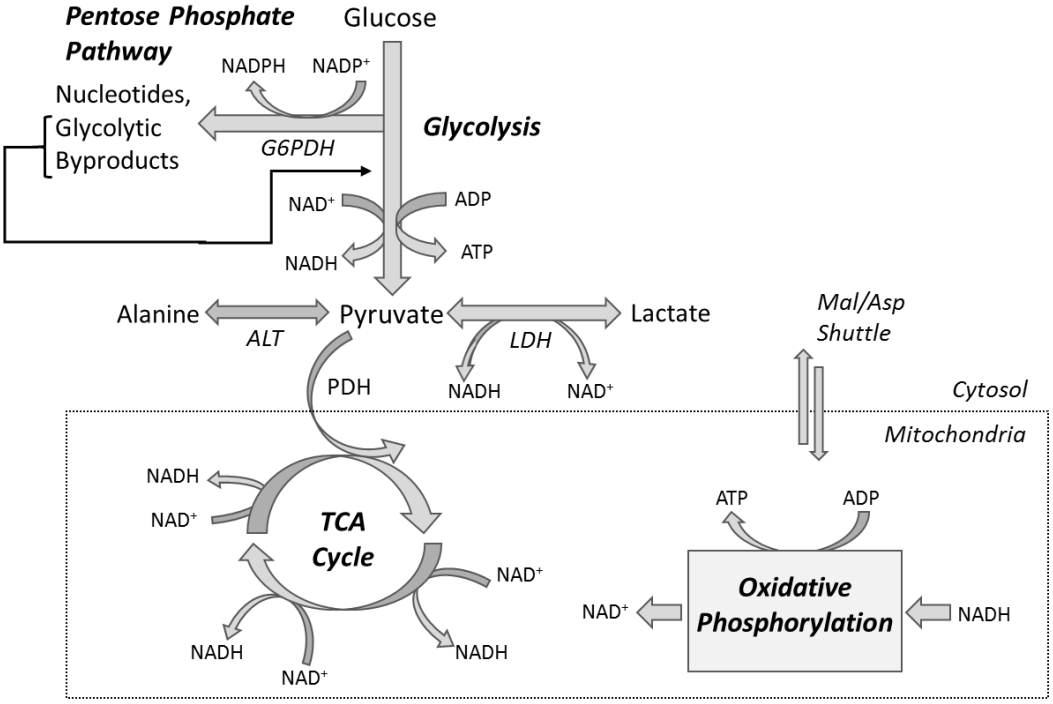

Figure 2-5. Cellular redox and energetics surrounding lactate production.

Figure 2-5 also highlights the significance of the lactate/glucose ratio. When glucose is catabolized to pyruvate, NAD^+ is reduced to NADH. For glycolysis to continue, NAD^+ must be regenerated. This is a major function of lactate production, to generate NAD^+ by oxidizing NADH. NADH reducing equivalents can also be transported into the cytosol using the malate-aspartate (Mal/Asp) shuttle. Nucleotides such as NADH cannot pass across the mitochondrial

membrane. Therefore, NADH is used to reduce oxaloacetate to malate, which can be transported into the mitochondrial matrix and oxidized as a way to transfer NADH reducing equivalents from the cytosol to the mitochondria, as shown in Figure 2-6.

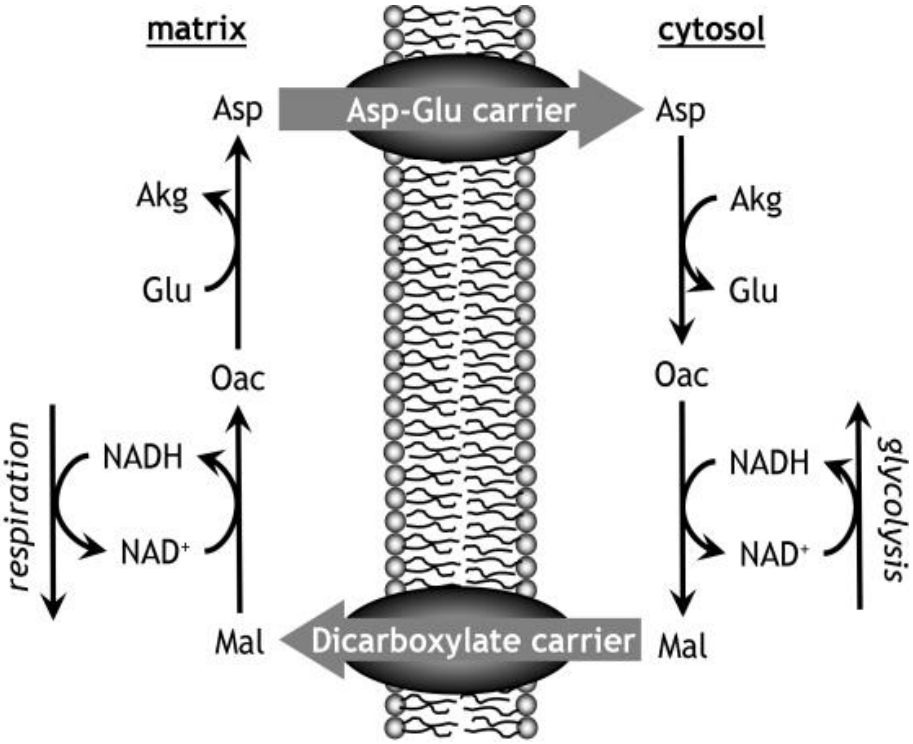

Figure 2-6. The malate/aspartate shuttle. The critical role of glycolysis and respiration in both mitochondrial and cytosolic redox states has been highlighted.

The Mal/Asp shuttle is typically not sufficient to satisfy the glycolytic demand for NAD^+ when the glucose consumption rate is high. In this instance, conversion of pyruvate to lactate can be used as a rapid source of cytosolic NAD^+. This underlies the significance of the lactate/glucose ratio. If the ratio falls, it is probable that the mitochondria are playing a greater role in redox provision. If it remains constant despite a fall in lactate production, it indicates a proportionate decrease in both glycolytic and mitochondrial metabolism. It is for this reason that

we and others have suggested the importance of the mitochondrial/glycolytic ratio [86]. The mitochondrial/glycolytic ratio considers the ratio of carbon directed to the mitochondria, compared to carbon directed to lactate, at the pyruvate node. This differs from the glucose to lactate ratio in that it takes into account the carbon flux lost to CO_2, when traveling through the pentose phosphate pathway.

The role of upstream mRNA and protein expression

While this work primarily focuses on metabolism studies, useful insight can be collected from upstream genomic/transcriptomic/proteomic studies. Since it is reasonable to question whether central metabolism, or energy related pathways, are the limiting factor for antibody production, we explore it here.

A transcriptomic study considered mRNA expression associated with an antibody producing line, and a wild-type non-expressing cell line [87]. Specifically, the mRNA related to protein synthesis and ribosomes was considered. Interestingly, the wild-type line had considerably more mRNA expression than the antibody secreting line. Therefore, it was argued that antibody expression plays a rather small role in the total protein being synthesized. This indicated the potential for considerable ground to be gained in specific productivity. Other work has considered the relative abundance of light and heavy chain mRNA. Under exponential growth, there is a correlation between specific productivity and expression level of antibody mRNA. However, as the culture moves into stationary phase, where the majority of antibody is generated, this correlation was lost [53]. Another study asked the question if sufficient machinery existed to generate/secrete protein, and used proteomics to quantify the relative

unfolded protein response (UPR) as indication of bottlenecks [88]. Again, the authors found no evidence to suggest UPR in antibody producing cell lines. Lastly, karytopic studies have been done on CHO cells in an effort to determine if genetic stability has a correlation with specific productivity [89]. One author's findings indicated that while significant aneuploidy existed in CHO cells (the Chinese Hamster is naturally diploid), and revealed that chromosomal aberations in general do occur in the presence of any transfection, there was no correlation between genetic stability and specific productivity. Taken collectively, these findings suggest that the rate limiting step to increasing specific productivity may not present itself in upstream limitations, it may be associated with central metabolism.

^{13}C metabolic flux analysis (MFA)

Fundamentally, metabolic flux analysis (MFA) aims to quantify the intracellular rates of metabolism. It is most useful when a given hypothesis cannot be tested without quantitative knowledge of intracellular rates of reactions. Many types of metabolic measurements (e.g., glucose/lactate ratio) can provide partial information about central metabolism without applying metabolic flux analysis. However, the interpretation of these measurements has limitations and is subject to various approximations. On the other hand, MFA allows researchers to quantitatively map the flow of carbon through intracellular metabolic pathways, providing rich information about the relative importance of carbon sources and sinks within the metabolic network and the partitioning of carbon among these various pathways (Figure 2-7).

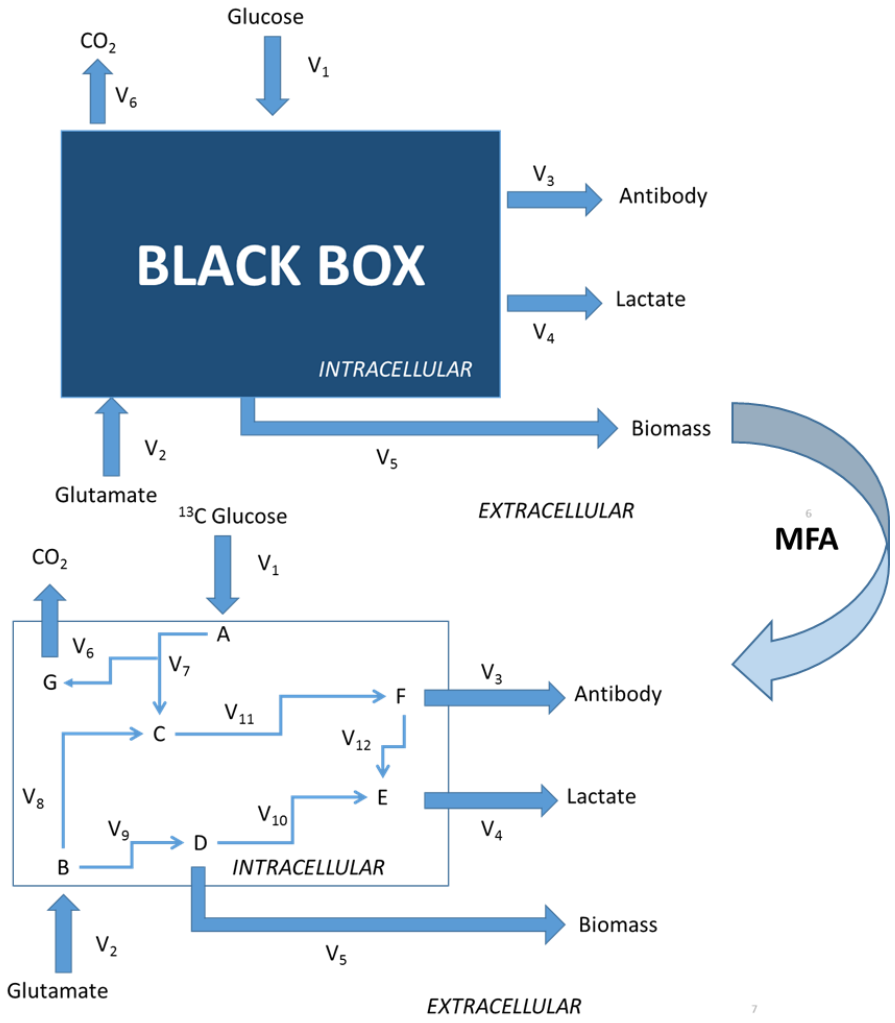

Figure 2-7. ^{13}C metabolic flux analysis can be used to supplement the information provided by metabolic studies. Without MFA, the cell is often viewed as a black box. All of the inputs and outputs can be quantified, but due to metabolic complexities, it is impossible to define the intracellular fluxes without additional information. Such additional information can be provided by the application of ^{13}C tracers. V_i represents an individual flux, and A-G are generic intracellular metabolites.

^{13}C metabolic flux analysis simply refers to the usage of ^{13}C tracers. This could be glucose, as shown in Figure 2-7, or most any other nutrient consumed by the cell (provided it is available for purchase).

^{13}C MFA provides additional constraints to a metabolic network, proportional to the number of metabolites measured. Metabolite labeling is measured through mass spectral analysis. When the selected source (^{13}C tracer) is consumed, the labeled carbon is turned over into other metabolites. The resultant mass spectral metabolite detail provides further constraints to a metabolic model, allowing cyclic pathways (such as the pentose phosphate pathway or tricarboxylic acid (TCA) cycle), which are typically undeterminable, to be quantified. This is achieved through a mathematical model that integrates mass spectral data and extracellular fluxes to calculate the intracellular fluxes of a metabolic model.

Model inputs

There are two types of measured inputs used to calculate fluxes with ^{13}C MFA. The first deals with extracellular fluxes, encompassing all the production and consumption fluxes of the cell. As can be seen in Figure 2-7, a product can be a simple metabolite, such as lactate, or a complex macromolecule, such as biomass or antibody. These inputs effectively contribute mass balance constraints to the model. The other input involves the information acquired from using a ^{13}C tracer. As a tracer incorporates itself into downstream metabolites, information is provided as to not only the source but the path that the tracer took to get there. This is because different pathways produce different carbon rearrangements, which results in unique labeling patterns in the downstream products. As an example, consider the pentose phosphate pathway (PPP) shown schematically in Figure 2-5. If [1,2-$^{13}C_2$]glucose is fed to the culture, either doubly or singly labeled pyruvate will emerge depending on the relative contributions of glycolysis versus PPP, respectively (Figure 2-8).

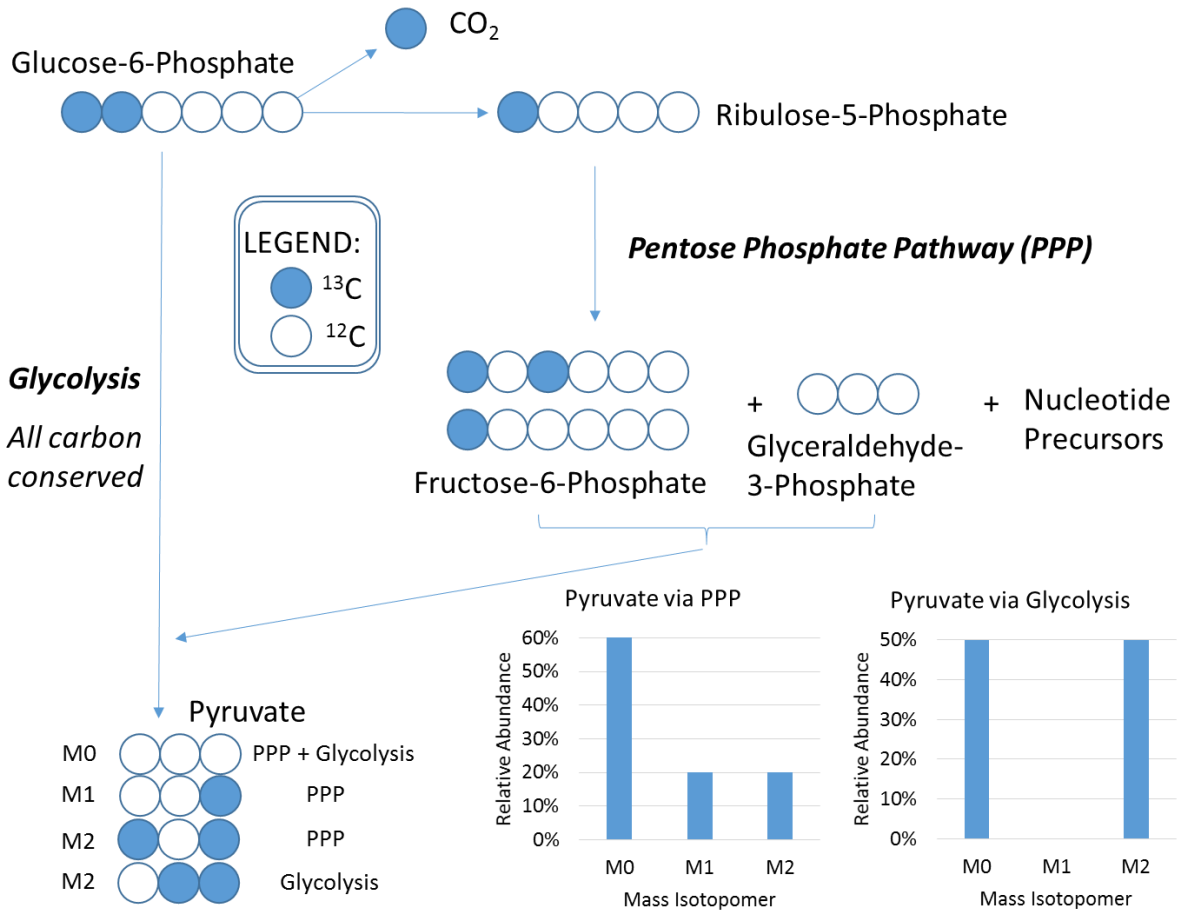

Figure 2-8. Discerning between the split of glycolysis and the pentose phosphate pathway. The mass isotopomer distribution of pyruvate, if generated purely through PPP or glycolysis, is shown. Any linear combination of the two can also exist, as the cell will often utilize both pathways simultaneously. Linear regression can be used to determine the actual glycolysis/PPP split ratio by fitting the experimental measurements to a mathematical model that accounts for the stoichiometry and atom rearrangements of the metabolic network.

Mass isotopomers are molecules that have the same chemical composition but different masses, due to differing incorporation of ^{13}C. Gas chromatography-mass spectroscopy (GC-MS) can accurately separate and determine the relative abundances of different mass isotopomers from the same metabolite. As stated previously, the relative abundances of these mass isotopomers are dictated by the selected tracer and the path that the tracer took as it moved

through the network. Therefore, while only mass balances can be formed from extracellular fluxes input to the model, addition of mass spectral (MS) data allows the model to be extended to include isotopomer balances. This typically results in an overdetermined system of equations that can be solved by least-squares regression to estimate the fluxes of interest. In the example provided in Figure 2-8, the ratio of the PPP flux compared to glycolysis is determined by the MS data acquired.

One key limitation of conducting ^{13}C MFA based on MS measurements has to do with the inability of MS to determine position-specific labeling. As can be seen in Figure 2-8, there is no way to distinguish between the M2 signal generated from the PPP and glycolysis. Nuclear magnetic resonance (NMR) can determine this positional information, and this provides an alternative technique to acquire labeling data for ^{13}C MFA studies. However, NMR requires considerably more sample volume and is much more costly to operate than MS [90,91]. Both are viable platforms and have experienced significant methodological development for MFA application in the past twenty years [92]. In this dissertation, mass spectral analysis is used exclusively.

All of the MFA studies presented in this dissertation depend upon two assumptions. The first is metabolic steady-state, which implies that the metabolic fluxes are constant over time. This is assessed by monitoring the changing concentration of nutrients/products/byproducts in the media to identify phases when the cell-specific rates of change are constant. Typically, measurements of viable cell density (VCD) and nutrient concentrations are made over a minimum of 2 days to determine these extracellular fluxes. Secondly, the models assume isotopic steady-state. This requires sufficient time for the tracer to equilibrate with the system,

with 2 days post-administration generally found to be sufficient for most intracellular metabolites in CHO cells [93].

Mathematics of MFA

MFA attempts to represent the entire experimental data set as accurately as possible by adjusting the flux parameters to minimize the differences between model-simulated and experimentally determined values. The MFA objective function is constructed to minimize the sum-of-squared residuals. Therefore, some experimental measurements may be fit by the model better than others. This could be a result of an inaccurate experimental measurement or by an error or omission in the model. Once the overall fit has been optimized, the goodness-of-fit is determined through a chi-squared test and by assessing the distribution of the residuals [94]. It is through this simulation and comparison process that the model is adjusted to best estimate each individual flux, indicated by V_i in Figure 2-9.

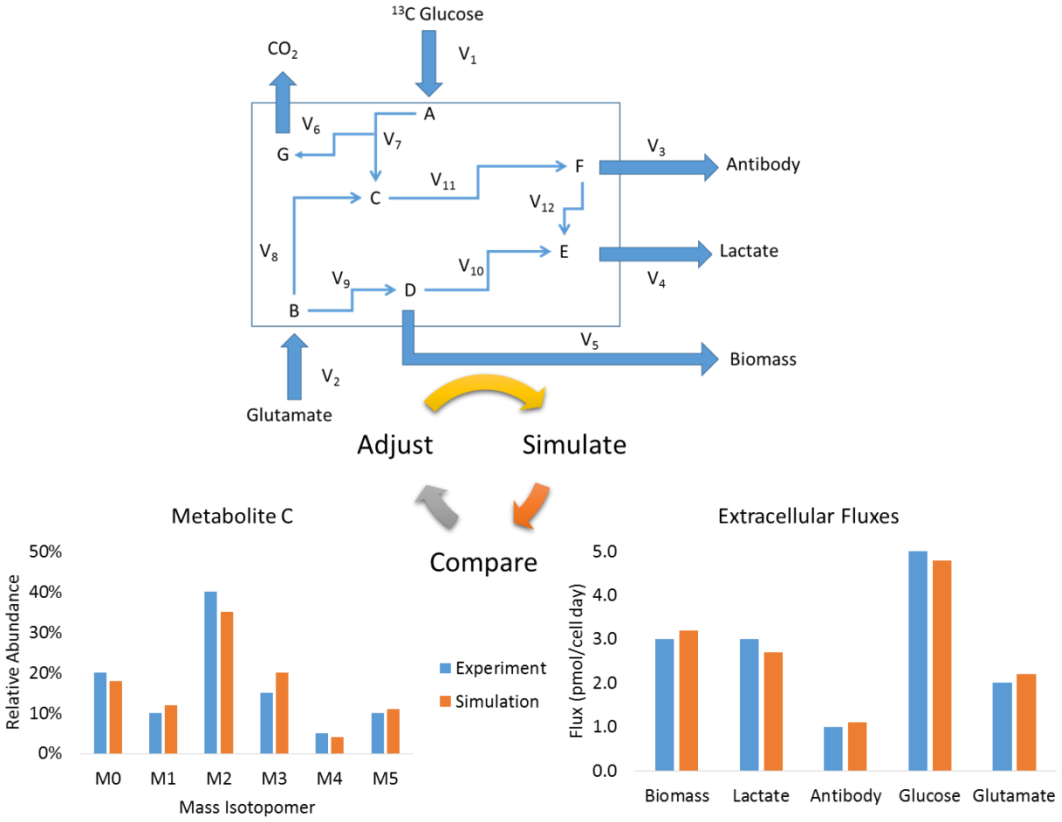

Figure 2-9. ^{13}C metabolic flux analysis. The network diagram has been borrowed from Figure 2-7. These two varieties of measurements, extracellular fluxes and mass isotopomer abundances, are used in tandem to estimate the intracellular fluxes. Fluxes V_i are adjusted to optimize the fit between simulated and experimental values.

After constructing the appropriate reaction network to represent the system of interest, this information can be used to construct a *stoichiometric matrix S* and unknown flux vector *v*. The steady-state metabolite mass balances can be written in matrix form using the following equation

$$S \cdot v = 0$$

The stoichiometric matrix *S* is *m x n*, where *m* is the number of balanced metabolites and *n* is the number of fluxes. However, only (*n*–*r*) fluxes can be freely adjusted, where *r* is the rank of *S*,

and the remaining *r* fluxes are dependent on these "free" fluxes as a result of mass conservation [94]. The full flux vector can be determined from the free fluxes through a linear transformation

$$v = K \cdot u$$

where *K* is the nullspace matrix of *S* and *u* is the vector of free fluxes. The nullspace matrix is not unique, but can be constructed from any collection of vectors that form a basis for the nullspace of *S*. The size of the nullspace matrix is $n \times (n-r)$.

Typically, there are not enough extracellular measurements available to determine all $(n-r)$ free fluxes, and the system is underdetermined. Flux balance analysis (FBA) is an approach closely related to MFA that aims to explore the set of possible solutions to this underdetermined set of equations [95]. However, FBA doesn't utilize the added information provided by ^{13}C tracers. Consequently, assumptions must be made to determine the system, and statistical analysis of any kind is limited [95]. On the other hand, inclusion of mass spectral measurements and isotopomer balances into the model results in an overdetermined system, which can be solved for a unique flux solution using least-squares regression. Furthermore, the flux solution can be subjected to statistical goodness-of-fit and uncertainty analyses that enable, for example, 95% confidence intervals to be determined for each flux.

The objective function of the ^{13}C MFA procedure can be expressed mathematically as

$$\min \Phi = (x(u) - x^{obs})^T \cdot \Sigma_x^{-1} \cdot (x(u) - x^{obs})$$

$$\text{subject to } K \cdot u \geq 0$$

where Φ is the sum-of-squares objective function, $x(u)$ is the simulated measurements vector, and x^{obs} is the experimental measurements vector. Σ_x is the covariance matrix of the

experimental measurements. It includes the individual measurement variance on the diagonal of the matrix. Σ_x serves to make the objective function covariance-weighted. Solution of the above optimization is accomplished by application of the Levenberg-Marquardt gradient-based algorithm [96], or any other suitable minimization technique.

In order to perform the optimization, the isotopomer balances must be solved at each iteration to simulate the MS measurements contained in the vector *x* for a given guess of the free flux vector *u*. The most efficient approach for solving these balance equations involves decomposing the metabolites into a collection of elementary metabolite units (EMUs), which are unique subsets of the atoms that comprise each metabolite [97]. For each molecule of atom size *N*, there are a maximum of 2^N-1 EMUs. However, not all EMUs are required to simulate the limited MS measurements that are available. Therefore, the EMU approach is computationally efficient because it only solves for the isotopomer distributions of EMUs that contribute to an actual experimental measurement [98]. Prior to the inception of the EMU approach, all isotopomers were balanced and solved simultaneously, leading to vastly larger systems of equations that required significantly more computational time. The first systematic approach to enumerate and solve all isotopomer balances was introduced by Schmidt et al. [99], which paved the way for modern approaches based on cumomer or EMU balances [91].

Using the EMU approach, EMUs can be grouped based upon their size (i.e., the number of atoms they contain). Like a mass balance constructed around a metabolite, balance equations can be formed around EMUs in order to simulate the experimental labeling. EMU balances can be arranged as a cascaded system of linear equations and expressed in matrix form as

$$A_1 \cdot X_1 = B_1 \cdot Y_1\left(y_1^{in}\right)$$

$$A_2 \cdot X_2 = B_2 \cdot Y_2\left(y_2^{in}, X_1\right)$$

…

$$A_n \cdot X_n = B_n \cdot Y_n\left(y_n^{in}, X_{n-1}, X_{n-2}, \ldots, X_1\right)$$

Where A_i and B_i are matrices that depend on the free flux values, X_i is an unknown matrix that contains the mass isotopomer distributions (MIDs) of all balanced EMUs of size i, and Y_i is a matrix of known source MIDs (y_i^{in}) or previously calculated MIDs (X_1, X_2, …). The source metabolites could be the isotopic tracer applied, or an unlabeled metabolite. At the i^{th} step, the system is solved for X_i. The EMU balances are solved in ascending size order, e.g., the EMUs of size i=1 must be solved before the EMUs of size i=2, as Y_2 depends upon X_1. It is through these EMU balances and the sum-of-squares minimization that the experimentally measured extracellular fluxes and mass spectral data (MIDs) are merged together to estimate the unknown free fluxes of the system.

Alternatives to ^{13}C MFA

In the absence of MFA, the cell can be modeled as a black box. This allows for all of the metabolic inputs and outputs to be accounted for using a stoichiometric analysis [49]. Stoichiometric analysis involves quantifying the rates of all major incoming and outgoing metabolic fluxes, so that carbon and redox balance can be assessed. Biomass and antibody generation are accounted for, and the metabolic demands for their synthesis are defined.

A natural next step to a stoichiometric analysis is the application of all the associated measurements to a metabolic model. This can involve the application of FBA to estimate

unknown intracellular fluxes based on mass balancing. However, central metabolism involves cycles, split pathways, and reversible reactions, all of which are not possible to fully resolve based solely on the extracellular measurements [100]. Therefore, additional assumptions and constraints are imposed upon the model. Constraints typically involve using cofactor balances, i.e. ATP, NADH, and NADPH. Unfortunately, applying cofactor balances is rather difficult and can lead to metabolic models that poorly represent metabolism. First, it is challenging to determine the efficiency in conversion of NADH to ATP [101]. Second, determining cell maintenance requirements for cofactors is equally difficult [90]. Simply put, it is impossible to accurately know all the energy producing/consuming reactions in the cell, and therefore difficult to appropriately apply cofactor balances [100]. Furthermore, imposing cofactor balances generally fall short of determining a metabolic network [102].

If a single solution is to be determined, additional assumptions can be made. This involves the application of linear programming to optimize a cellular objective [103], i.e., to maximize or minimize a given product. To provide an example, the objective could be to maximize/minimize ATP or NAD(P)H. A freely available software (named COBRA) can be used to calculate FBA solutions for any user-specified objective function [104]. However, these solutions are, by definition, found at the extreme edge of a bounded multidimensional solution space [90]. This may or may not be a biologically relevant representation of the metabolism exhibited. Only through comparison to a flux map derived from ^{13}C MFA can this solution be properly validated.

While these shortcomings clearly point towards the advantages of ^{13}C MFA, there are a few key advantages to FBA. Unlike ^{13}C MFA, it doesn't require the purchase of isotope tracers. Generally, this does limit ^{13}C MFA experiments to bench-top scale [92]. Additionally, FBA is

simpler and considerably less laborious than ^{13}C MFA [102]. The relative importance of accuracy vs monetary/time cost must be balanced, in order to assess the usefulness of FBA versus ^{13}C MFA.

MFA is a powerful tool to generate representative flux maps that characterize an experimental system. For predictive models, often kinetics-based approaches are more useful [105,106]. As an added benefit, they do not require metabolic steady-state assumptions (a requirement of both MFA and FBA). However, as is the case with all kinetic models, they require identification of suitable rate expressions and kinetic constants before reliable predictions can be obtained, which is often difficult to achieve in biologically relevant networks.

Past applications of MFA to investigate mammalian hosts capable of protein production

MFA has been applied to several past mammalian cell culture studies that explored the effects of media alterations, environmental changes, and the changes to cell metabolism occuring over a culture's operational lifetime. Industrially relevant fed-batch and perfusion processes have both been investigated. Some of the significant findings, to advance MFA technique and enhance industrial cell culture understanding, are discussed here.

Continuous culture. It is important to realize that metabolic steady-state can be more readily achieved in a continuous or perfusion setup, as compared to fed-batch. Continuous cultures hold a relatively constant media condition and cell density. Many of the earlier MFA studies took advantage of this detail. Sharfstein et al. took this a step further in 1994, when she conducted ^{13}C MFA using in-vivo NMR [107] with a hybridoma cell line. In this case, the entire

reactor was placed directly in the magnetic field (of NMR) over the course of the experiment. This design allows metabolites to be quantified in real-time, whereas the majority of ^{13}C MFA must conduct offline analysis. Due to a lack of signal sensitivity, however, high cell densities are required by this in-vivo approach. For this reason, Sharfstein et al. utilized a hollow fiber reactor, known for being capable of especially high cell densities [108]. This allowed for increased signal to be generated for a given metabolite. Labeling patterns of glycolytic intermediates, amino acids, and lipids were all determined. Independent experiments were conducted using either [1-$^{13}C_1$]glucose or [3-$^{13}C_1$]glutamine as the labeled source. The experiment tested the impact of decreasing glutamine concentration upon antibody production. Two conditions were considered, including glutamine at 1.7 and 4 mM concentration. Changing glutamine concentration did not substantially impact the PPP or glycolysis. When glutamine concentration was reduced however, amino acids (mostly glutamine) entering the TCA cycle via α-ketoglutarate were roughly halved. Additionally, when the concentration was reduced, relative specific antibody production significantly increased. Based upon these findings, Sharfstein et al. reported antibody production might not be limited by energy production. Final titer was roughly 25 mg/L, at least 2 orders of magnitude less than typical titers achieved at present. The miniscule antibody production of this study may explain the lack of correlation with energy production. Finally, this work determined that significant exchange fluxes were occurring between TCA intermediates and extracellular amino acids, a point still relevant to ^{13}C MFA studies today.

As a follow up study to this, using the same reactor setup, Mancuso et al. further examined the effect of limiting glutamine upon hybridoma [109]. In this study only [1-$^{13}C_1$]glucose was used, and metabolite labeling determined by NMR. Glycolytic intermediates,

lipids, and amino acids were measured. When glutamine was abruptly eliminated from culture, specific productivity was significantly increased (more than doubled). With it, glycolytic flux was not significantly affected, but overall ATP production reduced by 20% (based upon reduction in oxygen uptake rate). Lipid synthesis (growth) was unaffected. Mancuso et al. concluded that antibody production was not limited by energy, as was the case in Sharfstein's study. However, it is important to note that maximal specific productivity here was approximately 1 pg/cell/day. This is considerably less than the excess of 50 pg/cell/day achieved more recently [52].

Metabolic steady-state is essential to MFA, but it doesn't mean that multiple metabolic steady-states cannot exist. Two separate hybridoma FBA studies proved just this. In the first study, Follstad et al. used a chemostat and experimentally set out to experimentally determine the effect of various dilution rates upon metabolism [110]. Here, as the initial (control) residence time of approximately 5.2 days was stepped down to lesser dilution rates (eventually ¼ the control condition), an increased fraction of pyruvate was transported into the mitochondria to participate in the TCA cycle. Dilution rates were held constant for a minimum of 5 residence times (in most cases more), and after 68 days of culture, dilution rates were increased back to the control. Even though the dilution rate was the same, viable cell density at steady-state was approximately doubled and lactate production reduced by 18%.

In the second study exploring multiple metabolic steady-states, Europa et al. conducted another FBA study upon hybridoma. Initially cultured in fed batch, the experimental condition was fed at low glucose concentrations (approximately $1/20^{th}$ the control), and the control at relatively high glucose concentrations (approximately 19mM). After culturing for 12 hours, both cultures were moved into a chemostat. Upon moving into chemostat with a residence time of

approximately 6 days, two different metabolic steady-states were observed, even though glucose concentration was now equal and constant for both conditions. In the control, the lactate/glucose flux ratio was 1.4. In the experimental condition, glucose flux was reduced to ¼ the control, and lactate/glucose ratio <0.1. Impressively, antibody specific production was not affected in spite of this, and maintained at 0.45 pg/cell/day. While metabolic fluxes were generally reduced across the board, TCA cycle fluxes were reduced by 90% in the experimental condition. Alongside, glucose and glutamine fluxes were only reduced by 75% in the experimental condition. Again, it did not appear that energetics were limiting to antibody production at the given rate. Multiple metabolic steady-states in NS0 and HeLa have also been confirmed in more recent kinetic studies from Mulukutla et al. [111,112]. Mulukutla's work models a continuous solution space, based upon experimental results, of a given metabolic steady-state. As a consequence, his computational model provides insight to conditions not explicitly tested, a useful result for industry.

In a semi-continuous reactor design, Sheikholeslami et al. performed ^{13}C MFA upon an inducible antibody producing CHO cell [113] cultured in shake flasks. [1-$^{13}C_1$], [6-$^{13}C_1$], and [U-$^{13}C_6$]glucose served as tracers, along with [U-$^{13}C_5$]glutamine, in four separate parallel studies. LC-MS was used to determine the labeling of extracellular lactate, glutamate, aspartate, and alanine. Here, 30% of the culture volume was abruptly replaced on a daily interval, making this a semi-continous design, by centrifuging the culture and partially replacing the supernatant accordingly. Cultures appeared to exhibit exponential growth during the labeled experiment, and maintained a specific productivity of 13.7 pg/cell/day. When antibody production was induced, the oxPPP flux was nearly halved. TCA cycle fluxes reportedly increased by an average of 17%. Application of the results from this study should be carefully considered alongside the fact that

the culture conditions were not really continuous or fed-batch. However, the fact that oxPPP flux reduced when antibody production was induced is a surprising result. To date, it is the only MFA study which offers comparison of the oxPPP flux of an antibody producing and control line during exponential growth.

Fed batch culture. MFA has also been applied to fed-batch bioreactors. Sengupta et al. used ^{13}C MFA to evaluate the impact of differing environmental conditions (partial pressure CO_2, dissolved oxygen (DO), temperature) and feed volumes upon stationary phase metabolism [114]. Specifically, the labeled experiment was conducted between day 17 and 20 of culture. GS-CHO was cultured in the presence of both [U-$^{13}C_6$] and [1-$^{13}C_1$]glucose. LC-MS was used to determine metabolite labeling of various glycolytic intermediates. While MS data was collected for TCA intermediates and amino acids, it was not used as a constraint in the model. The authors omitted the data because isotopic steady-state had not been reached in 4 hours' time for amino acids or TCA intermediates in the preliminary labeling experiment. Seemingly contrasting with the findings of Sheikholeslami et al., Sengupta et al. reported that nearly all glycolytic flux was directed to the oxPPP, regardless of the environmental conditions tested. In some cases, there was even evidence of a glycolytic recycle, allowing the oxPPP flux to be in excess of the glucose flux. However, it is important to remember that here the stationary phase is being considered, not the exponential phase. Furthermore, there is no comparison to a control cell line not secreting antibody. The conditions most associated with high (more specifically, recycle) oxPPP flux were associated with low dissolved CO_2 (low partial pressure). Notably, pH was held constant for all conditions. The condition with the highest pyruvate flux directed to the mitochondria was associated with the highest antibody productivity. The two conditions with the

reduced oxPPP activity were associated with increased antibody productivity, drawing comparison to the findings of Sheikholeslami et al.

Ahn et al. used a similar approach to Sengupta et al. in that they too performed ^{13}C stationary MFA only upon glycolytic intermediates measurements [115]. Here, Ahn et al. used [1,2-$^{13}C_2$]glucose as the labeled source, and cultured adherent CHO-K1 in T-25 flasks. Metabolite labeling results were assessed using a GC-MS. After performing stationary MFA to determine glycolytic and PPP fluxes, isotopic non-stationary (INST) MFA was applied to the MS results of TCA intermediates, amino acids, and fatty acids. This calculated all remaining fluxes, including those associated with the TCA cycle. INST-MFA was used because isotopic steady-state was not achieved in the TCA intermediates. This work analyzed the changes to metabolism which occur during the exponential growth phase and stationary phase. The growth phase correlated with high glycolytic flux, high lactate production, and high cycling anaplerotic fluxes (PC and malic enzyme (ME)). As the culture shifted to stationary phase, a similar profile to Sengupta's work was observed, with increased oxPPP and TCA cycling. Lactate production actually reversed during the stationary phase, in agreement with other work exploring the exponential and stationary phase in CHO [116].

As a follow up study to this, Ahn et al. explored a means to shorten the required length of time to perform steady-state ^{13}C MFA [117]. In two parallel studies, [U-$^{13}C_5$]glutamine and [1,2-$^{13}C_2$]glucose were used. Still using CHO-K1 in T-25 flasks, he largely replicated the results of his prior study. However, he found through GC-MS that isotopic steady-state could be achieved in TCA intermediates in just 3 hours, and glycolytic intermediates in only 1.5 hours. This experimental design development would potentially be useful where metabolic steady-state of the period of interest was known/hypothesized to be limited in time. The INST-MFA

technique previously mentioned addtionally serves as a situational option. INST-MFA does not require assumptions about isotopic steady-state, but does require additional measurements, and involves additional computational complexity [118].

Metabolism is dynamic. To this end, much effort has been placed in developing dynamic MFA approaches [119,120]. Whilst ^{13}C dynamic MFA has yet to be accomplished, it is being developed. Fortunately, even fed-batch processes exhibit quasi- steady-state metabolism for a sufficient period of time to perform MFA in the midst of changing nutrient availability. Regardless, the steady-state assumption can be a challenge to consistently satisfy without a priori knowledge of a given system.

In summary, all the MFA approaches listed here are useful when used in the appropriate situation. Time, cost, scale, and predictive/representative capacity of metabolic steady-state are the major factors to consider when determining which type of metabolic model to use.

References

[1] S. R. Aggarwal, “What ’ s fueling the biotech engine — 2012 to 2013,” vol. 32, no. 1, 2014.

[2] B. Leader, Q. J. Baca, and D. E. Golan, “Protein therapeutics: a summary and pharmacological classification.,” *Nat. Rev. Drug Discov.*, vol. 7, no. 1, pp. 21–39, Jan. 2008.

[3] American Diabetes Association, “Statistics About Diabetes.” [Online]. Available: http://www.diabetes.org/diabetes-basics/statistics/. [Accessed: 06-Dec-2014].

[4] Center for Disease Control, “State Vaccination Requirements.” [Online]. Available: http://www.cdc.gov/vaccines/imz-managers/laws/state-reqs.html. [Accessed: 06-Dec-2014].

[5] S. S. Farid, “Established Bioprocesses for Producing Antibodies as a Basis for Future Planning,” *Adv. Biochem. Eng. Biotechnol.*, vol. 101, pp. 1–42, 2006.

[6] US Department of Health and Human Services, “Projected future growth of the older population,” 2014.

[7] A. Beck, T. Wurch, C. Bailly, and N. Corvaia, “Strategies and challenges for the next generation of therapeutic antibodies.,” *Nat. Rev. Immunol.*, vol. 10, no. 5, pp. 345–52, May 2010.

[8] B. Boghigian, G. Seth, R. Kiss, and B. Pfeifer, “Metabolic flux analysis and pharmaceutical production.,” *Metab. Eng.*, vol. 12, no. 2, pp. 81–95, Mar. 2010.

[9] M. Hay, D. W. Thomas, J. L. Craighead, C. Economides, and J. Rosenthal, “Clinical development success rates for investigational drugs.,” *Nat. Biotechnol.*, vol. 32, no. 1, pp. 40–51, Jan. 2014.

[10] J. Zhang, “Manufacture of Mammalian Cell Biopharmaceuticals,” in *Manual of Industrial Microbiology and Biotechnology*, 3rd ed., R. Baltz, Ed. ASM Press, 2010, pp. 179–195.

[11] J. Zhang, “Mammalian Cell Culture for Biopharmaceutical Production,” in *Manual of Industrial Microbiology and Biotechnology*, no. 104, R. Baltz, Ed. ASM Press, 2010, pp. 157–178.

[12] S. S. Farid, “Process economics of industrial monoclonal antibody manufacture.,” *J. Chromatogr. B. Analyt. Technol. Biomed. Life Sci.*, vol. 848, no. 1, pp. 8–18, Mar. 2007.

[13] A. Davidson and S. S. Farid, “Innovation in Biopharmaceutical Manufacture,” in *Bioprocess International*, 2014, pp. 12–19.

[14] Center for Medicare and Medicaid Services, “National Health Expenditure Projections 2012 - 2022,” 2013.

[15] S. Aggarwal, “What’s fueling the biotech engine--2008.,” *Nat. Biotechnol.*, vol. 27, no. 11, pp. 987–93, Nov. 2009.

[16] F. M. Wurm, “Production of recombinant protein therapeutics in cultivated mammalian cells.,” *Nat. Biotechnol.*, vol. 22, no. 11, pp. 1393–8, Nov. 2004.

[17] Y.-M. Huang, W. Hu, E. Rustandi, K. Chang, H. Yusuf-makagiansar, and T. Ryll, “Maximizing productivity of CHO cell-based fed-batch culture using chemically defined media conditions and typical manufacturing equipment.,” *Biotechnol. Prog.*, vol. 26, no. 5, pp. 1400–10, 2010.

[18] N. Carinhas, R. Oliveira, P. M. Alves, M. J. T. Carrondo, and A. P. Teixeira, “Systems biotechnology of animal cells: the road to prediction.,” *Trends Biotechnol.*, vol. 30, no. 7, pp. 377–85, Jul. 2012.

[19] K. P. Jayapal, K. F. Wlaschin, M. G. S. Yap, and W.-S. Hu, “Recombinant Protein Therapeutics from CHO Cells — 20 Years and Counting,” *SBE Spec. Sect. CHO Consort.*, pp. 40–47, 2006.

[20] Y. Lim, N. S. C. Wong, Y. Y. Lee, S. C. Y. Ku, D. C. F. Wong, and M. G. S. Yap, “Engineering mammalian cells in bioprocessing - current achievements and future perspectives.,” *Biotechnol. Appl. Biochem.*, vol. 55, no. 4, pp. 175–89, Apr. 2010.

[21] E. Jain and A. Kumar, “Upstream processes in antibody production: evaluation of critical parameters.,” *Biotechnol. Adv.*, vol. 26, no. 1, pp. 46–72, 2008.

[22] K. Sheikh, J. Fo, and L. K. Nielsen, “Modeling Hybridoma Cell Metabolism Using a Generic Genome-Scale Metabolic Model of Mus musculus,” *Biotechnol. Prog.*, vol. 21, no. 1, pp. 112–121, 2005.

[23] N. Carinhas, T. M. Duarte, L. C. Barreiro, M. J. T. Carrondo, P. M. Alves, and A. P. Teixeira, “Metabolic signatures of GS-CHO cell clones associated with butyrate treatment and culture phase transition.,” *Biotechnol. Bioeng.*, vol. 110, no. 12, pp. 3244–3257, Jun. 2013.

[24] P. Meleady, P. Doolan, M. Henry, N. Barron, J. Keenan, F. O’Sullivan, C. Clarke, P. Gammell, M. W. Melville, M. Leonard, and M. Clynes, “Sustained productivity in recombinant Chinese hamster ovary (CHO) cell lines: proteome analysis of the molecular basis for a process-related phenotype.,” *BMC Biotechnol.*, vol. 11, no. 1, p. 78, Jan. 2011.

[25] A. G. McAtee, N. Templeton, and J. D. Young, “Role of Chinese hamster ovary central carbon metabolism in controlling the quality of secreted biotherapeutic proteins,” *Pharm. Bioprocess.*, vol. 2, pp. 63–74, 2014.

[26] J. R. Birch and A. J. Racher, “Antibody production.,” *Adv. Drug Deliv. Rev.*, vol. 58, no. 5–6, pp. 671–85, Aug. 2006.

[27] M. Butler, “Animal cell cultures: recent achievements and perspectives in the production of biopharmaceuticals.,” *Appl. Microbiol. Biotechnol.*, vol. 68, no. 3, pp. 283–91, Aug. 2005.

[28] J. R. Swartz, “Advances in Escherichia coli production of therapeutic proteins.,” *Curr. Opin. Biotechnol.*, vol. 12, no. 2, pp. 195–201, Apr. 2001.

[29] J. L. Martínez, L. Liu, D. Petranovic, and J. Nielsen, “Pharmaceutical protein production by yeast: towards production of human blood proteins by microbial fermentation.,” *Curr. Opin. Biotechnol.*, vol. 23, no. 6, pp. 965–71, Dec. 2012.

[30] M. Arbabi-Ghahroudi, J. Tanha, and R. MacKenzie, “Prokaryotic expression of antibodies.,” *Cancer Metastasis Rev.*, vol. 24, no. 4, pp. 501–19, Dec. 2005.

[31] H. F. Kildegaard, D. Baycin-Hizal, N. E. Lewis, and M. J. Betenbaugh, “The emerging CHO systems biology era: harnessing the ’omics revolution for biotechnology.,” *Curr. Opin. Biotechnol.*, pp. 1–6, Mar. 2013.

[32] M. J. Coloma, a Clift, L. Wims, and S. L. Morrison, “The role of carbohydrate in the assembly and function of polymeric IgG.,” *Mol. Immunol.*, vol. 37, no. 18, pp. 1081–90, Dec. 2000.

[33] P. J. Hudson and C. Souriau, “Engineered antibodies.,” *Nat. Med.*, vol. 9, no. 1, pp. 129–34, Jan. 2003.

[34] J. Zhu, “Mammalian cell protein expression for biopharmaceutical production.,” *Biotechnol. Adv.*, vol. 30, no. 5, pp. 1158–70, 2012.

[35] G. Urlaub and L. a Chasin, “Isolation of Chinese hamster cell mutants deficient in dihydrofolate reductase activity.,” *Proc. Natl. Acad. Sci. U. S. A.*, vol. 77, no. 7, pp. 4216–20, Jul. 1980.

[36] F. M. Wurm and D. Hacker, “First CHO genome.,” *Nat. Biotechnol.*, vol. 29, no. 8, pp. 718–20, Aug. 2011.

[37] G. Urlaub, E. Käs, A. Carothers, and L. Chasin, “Deletion of the diploid dihydrofolate reductase locus from cultured mammalian cells,” *Cell*, vol. 33, no. June, pp. 405–412, 1983.

[38] L. M. Barnes, C. M. Bentley, and A. J. Dickson, “Advances in animal cell recombinant protein production: GS-NS0 expression system.,” *Cytotechnology*, vol. 32, no. 2, pp. 109–23, Feb. 2000.

[39] M. C. de la Cruz Edmonds, M. Tellers, C. Chan, P. Salmon, D. K. Robinson, and J. Markusen, “Development of transfection and high-producer screening protocols for the CHOK1SV cell system.,” *Mol. Biotechnol.*, vol. 34, no. 2, pp. 179–90, Oct. 2006.

[40] M. Taschwer, M. Hackl, J. A. Hernández Bort, C. Leitner, N. Kumar, U. Puc, J. Grass, M. Papst, R. Kunert, F. Altmann, and N. Borth, “Growth, productivity and protein glycosylation in a CHO EpoFc producer cell line adapted to glutamine-free growth.,” *J. Biotechnol.*, vol. 157, no. 2, pp. 295–303, Jan. 2012.

[41] S. S. Ozturk, M. R. Riley, and B. O. Palsson, “Effects of ammonia and lactate on hybridoma growth, metabolism, and antibody production.,” *Biotechnol. Bioeng.*, vol. 39, no. 4, pp. 418–31, Feb. 1992.

[42] T. Hassell, S. Gleave, and M. Butler, “Growth inhibition in animal cell culture,” *Appl. Biochem. Biotechnol.*, vol. 30, no. 1, pp. 29–41, 1991.

[43] C. Bebbington, G. Renner, S. Thomson, D. King, D. Abrams, and Y. Yarranton, “High-level expression of a recombinant antibody from myeloma cells using a glutamine synthetase gene as an amplifiable selectable marker,” *Nat. Biotechnol.*, vol. 10, pp. 169–175, 1992.

[44] K. Smith, “Cost of Lonza Glutamine Synthetase (GS) system.” 2013.

[45] S. D. Jones, F. J. Castillo, and H. L. Levine, “Advances inthe Development of Therapeutic Monoclonal Antibodies,” no. October, 2007.

[46] V. S. Martínez, S. Dietmair, L.-E. Quek, M. P. Hodson, P. Gray, and L. K. Nielsen, “Flux balance analysis of CHO cells before and after a metabolic switch from lactate production to consumption.,” *Biotechnol. Bioeng.*, vol. 110, no. 2, pp. 660–6, Mar. 2013.

[47] M. Takagi, H. Hayashi, and T. Yoshida, “The effect of osmolarity on metabolism and morphology in adhesion and suspension chinese hamster ovary cells producing tissue plasminogen activator.,” *Cytotechnology*, vol. 32, no. 3, pp. 171–9, Mar. 2000.

[48] S. Charaniya, H. Le, H. Rangwala, K. Mills, K. Johnson, G. Karypis, and W.-S. Hu, “Mining manufacturing data for discovery of high productivity process characteristics.,” *J. Biotechnol.*, vol. 147, no. 3–4, pp. 186–97, Jun. 2010.

[49] L. Xie and D. I. Wang, “Material balance studies on animal cell metabolism using a stoichiometrically based reaction network.,” *Biotechnol. Bioeng.*, vol. 52, no. 5, pp. 579–90, Dec. 1996.

[50] A. P. Zeng, W. S. Hu, and W. D. Deckwer, “Variation of stoichiometric ratios and their correlation for monitoring and control of animal cell cultures.,” *Biotechnol. Prog.*, vol. 14, no. 3, pp. 434–41, 1998.

[51] K. F. Wlaschin and W. Hu, “Fedbatch Culture and Dynamic Nutrient Feeding,” *Adv. Biochem. Eng.*, no. 101, pp. 43–74, 2006.

[52] N. Templeton, J. Dean, P. Reddy, and J. D. Young, “Peak antibody production is associated with increased oxidative metabolism in an industrially relevant fed-batch CHO cell culture.,” *Biotechnol. Bioeng.*, vol. 110, no. 7, pp. 2013–2024, Feb. 2013.

[53] P. M. O’Callaghan and D. C. James, “Systems biotechnology of mammalian cell factories.,” *Brief. Funct. Genomic. Proteomic.*, vol. 7, no. 2, pp. 95–110, Mar. 2008.

[54] M. B. Fogolín, R. Wagner, M. Etcheverrigaray, and R. Kratje, “Impact of temperature reduction and expression of yeast pyruvate carboxylase on hGM-CSF-producing CHO cells.,” *J. Biotechnol.*, vol. 109, no. 1–2, pp. 179–91, Apr. 2004.

[55] S. Ozturk and B. Palsson, “Effect of medium osmolarity on hybridoma growth, metabolism, and antibody production,” *Biotechnol. Bioeng.*, vol. 37, no. April, pp. 989–993, 1991.

[56] M.-H. Wu, G. Dimopoulos, A. Mantalaris, and J. Varley, “The effect of hyperosmotic pressure on antibody production and gene expression in the GS-NS0 cell line.,” *Biotechnol. Appl. Biochem.*, vol. 40, no. Pt 1, pp. 41–6, Aug. 2004.

[57] M. M. Zhu, A. Goyal, D. L. Rank, S. K. Gupta, T. Vanden Boom, and S. S. Lee, “Effects of elevated pCO2 and osmolality on growth of CHO cells and production of antibody-fusion protein B1: a case study.,” *Biotechnol. Prog.*, vol. 21, no. 1, pp. 70–7, 2005.

[58] J. S. Ryu, M. S. Lee, and G. M. Lee, “Effects of cloned gene dosage on the response of recombinant CHO cells to hyperosmotic pressure in regard to cell growth and antibody production.,” *Biotechnol. Prog.*, vol. 17, no. 6, pp. 993–9, 2001.

[59] W. Luo, H. Hu, R. Chang, J. Zhong, M. Knabel, R. O. Meally, and R. N. Cole, “Pyruvate Kinase M2 Is a PHD3-Stimulated Coactivator for Hypoxia-Inducible Factor 1,” *Cell*, vol. 145, no. 5, pp. 732–744, 2011.

[60] J. Ljunggren and L. Haggstrom, “Catabolic Control of Hybridoma Cells by Glucose and Glutamine Limited Fed Batch Cultures,” *Biotechnol. Bioeng.*, vol. 44, pp. 808–818, 1994.

[61] A. Gambhir, A. F. Europa, and W. S. Hu, “Alteration of cellular metabolism by consecutive fed-batch cultures of mammalian cells.,” *J. Biosci. Bioeng.*, vol. 87, no. 6, pp. 805–10, Jan. 1999.

[62] W. Zhou, J. Rehm, and W. S. Hu, “High viable cell concentration fed-batch cultures of hybridoma cells through on-line nutrient feeding.,” *Biotechnol. Bioeng.*, vol. 46, no. 6, pp. 579–87, Jun. 1995.

[63] M. Gagnon, G. Hiller, Y.-T. Luan, A. Kittredge, J. DeFelice, and D. Drapeau, “High-end pH-controlled delivery of glucose effectively suppresses lactate accumulation in CHO fed-batch cultures.,” *Biotechnol. Bioeng.*, vol. 108, no. 6, pp. 1328–37, Jun. 2011.

[64] J. Li, C. L. Wong, N. Vijayasankaran, T. Hudson, and A. Amanullah, “Feeding lactate for CHO cell culture processes: Impact on culture metabolism and performance.,” *Biotechnol. Bioeng.*, vol. 109, no. 5, pp. 1173–86, May 2012.

[65] Z. Xing, Z. Li, V. Chow, and S. S. Lee, “Identifying inhibitory threshold values of repressing metabolites in CHO cell culture using multivariate analysis methods.,” *Biotechnol. Prog.*, vol. 24, no. 3, pp. 675–83, 2008.

[66] C. Altamirano, A. Illanes, S. Becerra, J. J. Cairó, and F. Gòdia, “Considerations on the lactate consumption by CHO cells in the presence of galactose.,” *J. Biotechnol.*, vol. 125, no. 4, pp. 547–56, Oct. 2006.

[67] C. Altamirano, C. Paredes, a Illanes, J. J. Cairó, and F. Gòdia, “Strategies for fed-batch cultivation of t-PA producing CHO cells: substitution of glucose and glutamine and rational design of culture medium.,” *J. Biotechnol.*, vol. 110, no. 2, pp. 171–9, May 2004.

[68] F. Zagari, M. Jordan, M. Stettler, H. Broly, and F. M. Wurm, “Lactate metabolism shift in CHO cell culture: the role of mitochondrial oxidative activity.,” *N. Biotechnol.*, vol. 30, no. 2, pp. 238–245, Jun. 2013.

[69] Y. Genzel, J. B. Ritter, S. König, R. Alt, and U. Reichl, “Substitution of glutamine by pyruvate to reduce ammonia formation and growth inhibition of mammalian cells.,” *Biotechnol. Prog.*, vol. 21, no. 1, pp. 58–69, 2005.

[70] J. D. Young, “Metabolic flux rewiring in mammalian cell cultures,” *Curr. Opin. Biotechnol.*, pp. 1–8, May 2013.

[71] S. H. Kim and G. M. Lee, “Down-regulation of lactate dehydrogenase-A by siRNAs for reduced lactic acid formation of Chinese hamster ovary cells producing thrombopoietin.,” *Appl. Microbiol. Biotechnol.*, vol. 74, no. 1, pp. 152–9, Feb. 2007.

[72] D. Jeong, I. T. Cho, T. S. Kim, G. W. Bae, I.-H. Kim, and I. Y. Kim, “Effects of lactate dehydrogenase suppression and glycerol-3-phosphate dehydrogenase overexpression on cellular metabolism.,” *Mol. Cell. Biochem.*, vol. 284, no. 1–2, pp. 1–8, Mar. 2006.

[73] K. Chen, Q. Liu, L. Xie, P. a Sharp, and D. I. Wang, “Engineering of a mammalian cell line for reduction of lactate formation and high monoclonal antibody production.,” *Biotechnol. Bioeng.*, vol. 72, no. 1, pp. 55–61, Jan. 2001.

[74] M. Zhou, Y. Crawford, D. Ng, J. Tung, A. F. J. Pynn, A. Meier, I. H. Yuk, N. Vijayasankaran, K. Leach, J. Joly, B. Snedecor, and A. Shen, "Decreasing lactate level and increasing antibody production in Chinese Hamster Ovary cells (CHO) by reducing the expression of lactate dehydrogenase and pyruvate dehydrogenase kinases.," *J. Biotechnol.*, vol. 153, no. 1–2, pp. 27–34, Apr. 2011.

[75] H. Dorai, Y. S. Kyung, D. Ellis, C. Kinney, C. Lin, D. Jan, G. Moore, and M. J. Betenbaugh, "Expression of anti-apoptosis genes alters lactate metabolism of Chinese Hamster Ovary cells in culture.," *Biotechnol. Bioeng.*, vol. 103, no. 3, pp. 592–608, Jun. 2009.

[76] N. Irani, M. Wirth, J. van Den Heuvel, and R. Wagner, "Improvement of the primary metabolism of cell cultures by introducing a new cytoplasmic pyruvate carboxylase reaction.," *Biotechnol. Bioeng.*, vol. 66, no. 4, pp. 238–46, Jan. 1999.

[77] N. Irani, A. J. Beccaria, and R. Wagner, "Expression of recombinant cytoplasmic yeast pyruvate carboxylase for the improvement of the production of human erythropoietin by recombinant BHK-21 cells.," *J. Biotechnol.*, vol. 93, no. 3, pp. 269–82, Feb. 2002.

[78] C. B. Elias, E. Carpentier, Y. Durocher, L. Bisson, R. Wagner, and A. Kamen, "Improving glucose and glutamine metabolism of human HEK 293 and Trichoplusia ni insect cells engineered to express a cytosolic pyruvate carboxylase enzyme.," *Biotechnol. Prog.*, vol. 19, no. 1, pp. 90–7, 2003.

[79] O. Henry and Y. Durocher, "Enhanced glycoprotein production in HEK-293 cells expressing pyruvate carboxylase.," *Metab. Eng.*, vol. 13, no. 5, pp. 499–507, Sep. 2011.

[80] K. F. Wlaschin and W.-S. Hu, "Engineering cell metabolism for high-density cell culture via manipulation of sugar transport.," *J. Biotechnol.*, vol. 131, no. 2, pp. 168–76, Aug. 2007.

[81] C. Paredes, E. Prats, J. J. Cairó, F. Azorín, L. Cornudella, and F. Gòdia, "Modification of glucose and glutamine metabolism in hybridoma cells through metabolic engineering.," *Cytotechnology*, vol. 30, no. 1–3, pp. 85–93, Jul. 1999.

[82] F. Zagari, M. Stettler, H. Broly, M. Wurm, and M. Jordan, "High expression of the aspartate–glutamate carrier Aralar1 favors lactate consumption in CHO cell culture," *Pharm. Bioprocess.*, vol. 1, no. 1, pp. 19–27, 2013.

[83] F. M. Lasorsa, P. Pinton, L. Palmieri, G. Fiermonte, R. Rizzuto, and F. Palmieri, "Recombinant expression of the Ca(2+)-sensitive aspartate/glutamate carrier increases mitochondrial ATP production in agonist-stimulated Chinese hamster ovary cells.," *J. Biol. Chem.*, vol. 278, no. 40, pp. 38686–92, Oct. 2003.

[84] H. Tabuchi and T. Sugiyama, “Cooverexpression of alanine aminotransferase 1 in Chinese hamster ovary cells overexpressing taurine transporter further stimulates metabolism and enhances product yield.,” *Biotechnol. Bioeng.*, vol. 110, no. 8, pp. 2208–2215, Feb. 2013.

[85] S. Hammond, M. Kaplarevic, N. Borth, M. J. Betenbaugh, and K. H. Lee, “Chinese hamster genome database: An online resource for the CHO community at www.CHOgenome.org.,” *Biotechnol. Bioeng.*, vol. 109, no. 6, pp. 1353–1356, Nov. 2012.

[86] J. Wahrheit, A. Nicolae, and E. Heinzle, “Dynamics of growth and metabolism controlled by glutamine availability in Chinese hamster ovary cells.,” *Appl. Microbiol. Biotechnol.*, vol. 98, no. 4, pp. 1771–83, Feb. 2014.

[87] S. H. G. Khoo, F. Falciani, and M. Al-Rubeai, “A genome-wide transcriptional analysis of producer and non-producer NS0 myeloma cell lines.,” *Biotechnol. Appl. Biochem.*, vol. 47, no. Pt 2, pp. 85–95, Jun. 2007.

[88] D. M. Dinnis, S. H. Stansfield, S. Schlatter, C. M. Smales, D. Alete, J. R. Birch, A. J. Racher, C. T. Marshall, L. K. Nielsen, D. C. James, and L. Court, “Functional Proteomic Analysis of GS-NS0 Murine Myeloma Cell Lines With Varying Recombinant Monoclonal Antibody Production Rate,” 2006.

[89] M. Derouazi, D. Martinet, N. Besuchet Schmutz, R. Flaction, M. Wicht, M. Bertschinger, D. L. Hacker, J. S. Beckmann, and F. M. Wurm, “Genetic characterization of CHO production host DG44 and derivative recombinant cell lines.,” *Biochem. Biophys. Res. Commun.*, vol. 340, no. 4, pp. 1069–77, Feb. 2006.

[90] H. Bonarius, G. Schmid, and J. Tramper, “Flux analysis of underdetermined metabolic networks: the quest for the missing constraints,” *Trends Biotechnol.*, vol. 15, no. 8, pp. 308–314, Aug. 1997.

[91] W. Wiechert, M. Möllney, N. Isermann, M. Wurzel, and a a de Graaf, “Bidirectional reaction steps in metabolic networks: III. Explicit solution and analysis of isotopomer labeling systems.,” *Biotechnol. Bioeng.*, vol. 66, no. 2, pp. 69–85, Jan. 1999.

[92] C. Goudar, R. Biener, C. Boisart, R. Heidemann, J. Piret, A. de Graaf, and K. Konstantinov, “Metabolic flux analysis of CHO cells in perfusion culture by metabolite balancing and 2D [13C, 1H] COSY NMR spectroscopy.,” *Metab. Eng.*, vol. 12, no. 2, pp. 138–49, Mar. 2010.

[93] R. Deshpande, T. H. Yang, and E. Heinzle, “Towards a metabolic and isotopic steady state in CHO batch cultures for reliable isotope-based metabolic profiling.,” *Biotechnol. J.*, vol. 4, no. 2, pp. 247–63, Feb. 2009.

[94] M. R. Antoniewicz, J. K. Kelleher, and G. Stephanopoulos, “Determination of confidence intervals of metabolic fluxes estimated from stable isotope measurements.,” *Metab. Eng.*, vol. 8, no. 4, pp. 324–37, Jul. 2006.

[95] M. R. Antoniewicz, “Dynamic metabolic flux analysis--tools for probing transient states of metabolic networks.,” *Curr. Opin. Biotechnol.*, vol. 24, no. 6, pp. 973–8, Dec. 2013.

[96] J. D. Young, “INCA: a computational platform for isotopically non-stationary metabolic flux analysis.,” *Bioinformatics*, vol. 30, no. 9, pp. 1333–5, May 2014.

[97] M. R. Antoniewicz, J. K. Kelleher, and G. Stephanopoulos, “Elementary metabolite units (EMU): a novel framework for modeling isotopic distributions.,” *Metab. Eng.*, vol. 9, no. 1, pp. 68–86, Jan. 2007.

[98] L. J. Jazmin and J. D. Young, “Isotopically Nonstationary 13C Metabolic Flux Analysis,” in *Systems Metabolic Engineering: Methods and Protocols*, vol. 985, no. 3, H. S. Alper, Ed. Totowa, NJ: Humana Press, 2013, pp. 367–390.

[99] K. Schmidt, M. Carlsen, J. Nielsen, and J. Villadsen, “Modeling isotopomer distributions in biochemical networks using isotopomer mapping matrices.,” *Biotechnol. Bioeng.*, vol. 55, no. 6, pp. 831–40, Sep. 1997.

[100] W. Wiechert, “13C Metabolic Flux Analysis,” *Metab. Eng.*, vol. 3, pp. 195–206, Apr. 2001.

[101] U. Sauer and J. E. Bailey, “Estimation of P-to-O ratio in Bacillus subtilis and its influence on maximum riboflavin yield.,” *Biotechnol. Bioeng.*, vol. 64, no. 6, pp. 750–4, Sep. 1999.

[102] H. P. Bonarius, B. Timmerarends, C. D. de Gooijer, and J. Tramper, “Metabolite-balancing techniques vs. 13C tracer experiments to determine metabolic fluxes in hybridoma cells.,” *Biotechnol. Bioeng.*, vol. 58, no. 2–3, pp. 258–62, 1998.

[103] J. D. Orth, I. Thiele, and B. Ø. Palsson, “What is flux balance analysis?,” *Nat. Biotechnol.*, vol. 28, no. 3, pp. 245–248, Mar. 2010.

[104] S. a Becker, A. M. Feist, M. L. Mo, G. Hannum, B. Ø. Palsson, and M. J. Herrgard, “Quantitative prediction of cellular metabolism with constraint-based models: the COBRA Toolbox.,” *Nat. Protoc.*, vol. 2, no. 3, pp. 727–38, Jan. 2007.

[105] R. P. Nolan and K. Lee, “Dynamic model of CHO cellmetabolism.,” *Metab. Eng.*, pp. 1–17, Oct. 2010.

[106] R. P. Nolan and K. Lee, “Dynamic model of CHO cell metabolism.,” *Metab. Eng.*, vol. 13, no. 1, pp. 108–24, Jan. 2011.

[107] S. T. Sharfstein, S. N. Tucker, a Mancuso, H. W. Blanch, and D. S. Clark, “Quantitative in vivo nuclear magnetic resonance studies of hybridoma metabolism.,” *Biotechnol. Bioeng.*, vol. 43, no. 11, pp. 1059–74, May 1994.

[108] L. Chu and D. K. Robinson, “Industrial choices for protein production by large-scale cell culture.,” *Curr. Opin. Biotechnol.*, vol. 12, no. 2, pp. 180–7, Apr. 2001.

[109] A. Mancuso, S. T. Sharfstein, E. J. Fernandez, D. S. Clark, and H. W. Blanch, “Effect of extracellular glutamine concentration on primary and secondary metabolism of a murine hybridoma: an in vivo 13C nuclear magnetic resonance study.,” *Biotechnol. Bioeng.*, vol. 57, no. 2, pp. 172–86, Jan. 1998.

[110] B. D. Follstad, R. R. Balcarcel, G. Stephanopoulos, and D. I. Wang, “Metabolic flux analysis of hybridoma continuous culture steady state multiplicity.,” *Biotechnol. Bioeng.*, vol. 63, no. 6, pp. 675–83, Jun. 1999.

[111] B. C. Mulukutla, M. Gramer, and W.-S. Hu, “On metabolic shift to lactate consumption in fed-batch culture of mammalian cells.,” *Metab. Eng.*, vol. 14, no. 2, pp. 138–149, Jan. 2012.

[112] B. C. Mulukutla, A. Yongky, P. Daoutidis, and W. Hu, “Bistability in glycolysis pathway as a physiological switch in energy metabolism.,” *PLoS One*, vol. 9, no. 6, p. e98756, Jan. 2014.

[113] Z. Sheikholeslami, M. Jolicoeur, O. Henry, and Z. Sheikoleslami, “Probing the metabolism of an inducible mammalian expression system using extracellular isotopomer analysis.,” *J. Biotechnol.*, vol. 164, no. 4, pp. 469–78, May 2013.

[114] N. Sengupta, S. T. Rose, and J. A. Morgan, “Metabolic flux analysis of CHO cell metabolism in the late non-growth phase.,” *Biotechnol. Bioeng.*, vol. 108, no. 1, pp. 82–92, Jan. 2011.

[115] W. S. Ahn and M. R. Antoniewicz, “Metabolic flux analysis of CHO cells at growth and non-growth phases using isotopic tracers and mass spectrometry.,” *Metab. Eng.*, vol. 13, no. 5, pp. 598–609, Sep. 2011.

[116] N. Templeton, J. Dean, P. Reddy, and J. D. Young, “Peak antibody production is associated with increased oxidative metabolism in an industrially relevant fed-batch CHO cell culture.,” *Biotechnol. Bioeng.*, vol. 110, no. 7, pp. 2013–2024, Feb. 2013.

[117] W. S. Ahn and M. R. Antoniewicz, “Parallel labeling experiments with [1,2-(13)C]glucose and [U-(13)C]glutamine provide new insights into CHO cell metabolism.,” *Metab. Eng.*, vol. 15, pp. 34–47, Jan. 2013.

[118] J. D. Young, J. L. Walther, M. R. Antoniewicz, and H. Yoo, “An Elementary Metabolite Unit (EMU) Based Method of Isotopically Nonstationary Flux Analysis,” *Biotechnology*, vol. 99, no. 3, pp. 686–699, 2008.

[119] M. R. Antoniewicz, “Dynamic metabolic flux analysis--tools for probing transient states of metabolic networks.,” *Curr. Opin. Biotechnol.*, vol. 24, no. 6, pp. 973–8, Dec. 2013.

[120] R. W. Leighty and M. R. Antoniewicz, “Dynamic metabolic flux analysis (DMFA): A framework for determining fluxes at metabolic non-steady state.,” *Metab. Eng.*, vol. 13, no. 6, pp. 745–755, Oct. 2011.

III: PEAK ANTIBODY PRODUCTION IS ASSOCIATED WITH INCREASED OXIDATIVE METABOLISM IN AN INDUSTRIAL FED-BATCH CHO CELL CULTURE

Biotechnology and Bioengineering. 2013. 110 (7): 2013-2024

Abstract

Cell metabolism can vary considerably over the course of a typical fed-batch antibody production process. However, the intracellular pathway alterations associated with various phases of growth and antibody production have yet to be fully elucidated using industrially relevant production hosts. Therefore, we performed ^{13}C labeling experiments and metabolic flux analysis (MFA) to characterize CHO cell metabolism during four separate phases of an industrial fed-batch culture. First, we found that peak specific growth rate was associated with high lactate production and minimal TCA cycling. Conversely, we found that lactate metabolism switched from net production to net consumption as the culture transitioned from peak growth to peak antibody production. During the peak antibody production phase, energy was primarily generated through oxidative phosphorylation, which was also associated with elevated oxidative pentose phosphate pathway (oxPPP) activity. Interestingly, as TCA cycling and antibody production reached their peaks, specific growth rate continued to diminish as the culture entered stationary phase. However, TCA cycling and oxPPP activity remained high even as viable cell density began to decline. Overall, we found that a highly oxidative state of metabolism corresponded with peak antibody production, whereas peak cell growth was characterized by a highly glycolytic metabolic state.

Introduction

Chinese hamster ovary (CHO) cells are currently the preferred host for recombinant antibody production, supplying 60-70% of the nearly $100 billion global biotherapeutics market [2]. Production of recombinant antibodies is energetically costly to the host cell, requiring roughly three molecules of ATP to synthesize just one peptide bond [3]. A highly producing cell line can potentially generate 40 pg of antibody each day [3], representing up to 20% of the cell's total intracellular protein [4]. Despite these energy and material demands, mammalian cell lines often exhibit an inefficient glycolytic state of metabolism involving rapid conversion of glucose to lactate even in the presence of abundant oxygen [2]. Furthermore, increased consumption of glutamine is also exhibited by many continuous cell lines, but much of the nitrogen provided by this substrate is subsequently lost to the production of ammonia and alanine [5]. While minimizing wasteful byproduct accumulation has been a goal of the mammalian biotech industry for over twenty-five years, it still remains an unresolved issue. Furthermore, many production cultures will shift from net production to net consumption of these byproducts during the bioprocess run [6], however, the regulatory mechanisms that control this switch are still poorly understood.

Fed-batch bioreactors are the most common system of monoclonal antibody production used today [7]. Fed-batch reactors have a key advantage over other systems, such as perfusion culture, because a higher final product titer can be achieved. This limits the cost associated with downstream processing and purification [8]. One challenge of fed-batch designs is that culture metabolism changes substantially over the course of the production run. This can be attributed to changing nutrient availability and cell density that give rise to transitions between distinct growth phases (i.e., exponential, stationary, and decline). Furthermore, concentrations of lactate,

ammonia, and other waste products can accumulate during early growth phases to concentrations that inhibit cell growth and antibody productivity and impact protein glycosylation during later phases [9]. Byproduct accumulation can also lead to excessive increases to osmolarity, especially when online base addition is used to control pH [10]. To mitigate these effects, much prior work has examined the impacts of process parameters such as pH, temperature, CO_2, and osmolarity on process performance [7]. Information from these studies has been used to design optimal media formulations and feeding strategies that reduce byproduct accumulation by limiting the supply of glucose, glutamine, or other nutrients to the culture [8], [11]. Further work has examined metabolic engineering of CHO cells to enhance pyruvate entry into mitochondria by overexpressing the pyruvate carboxylase (PC) enzyme [12] or to resist cell toxicity by overexpressing various anti-apoptotic proteins [13].

While previous studies have led to substantial improvements in bioprocess rates and titers, the ability to precisely quantify cell metabolism throughout multiple growth phases is essential to further understand and optimize the industrial fed-batch production process. Metabolic flux analysis (MFA) provides a powerful approach to map intracellular carbon flows of cultured cells and thereby elucidate the functional behavior of entire biochemical networks, as opposed to studying individual reactions or nodes in isolation. MFA has been applied to a variety of bioprocess applications, including optimization of medium composition and feeding strategies [14], data reconciliation and error analysis of measured rates [15], and to draw comparisons between the metabolism of CHO cells and other continuous cell lines [16]. Most prior MFA studies on CHO cells have relied on classical metabolite balancing to estimate fluxes without the use of ^{13}C tracers [2]. This necessitates the use of simplified network models and *ad hoc* assumptions to determine fluxes based on measured nutrient uptake and product secretion rates.

Alternative approaches have also been developed to calculate upper and lower flux bounds using large-scale stoichiometric models without attempting to solve explicitly for the unidentifiable fluxes [16]. To our knowledge, only three prior MFA studies have applied ^{13}C tracing of CHO cell cultures to fully resolve fluxes through parallel and cyclic reaction pathways (e.g., oxPPP, PC, etc.) [17]–[19]. However, only Sengupta et al. [19] applied ^{13}C-MFA to examine fed-batch culture of an antibody-secreting CHO cell line, and their work was limited to the late stationary growth phase. On the other hand, Ahn and Antoniewicz [17] applied ^{13}C-MFA to compare flux maps between exponential and stationary growth phases of a fed-batch CHO culture, but their work examined an adherent CHO-K1 line that did not express recombinant antibody. Therefore, comprehensive understanding of CHO cell physiology based on ^{13}C-MFA is still lacking, especially in regards to how CHO metabolism adapts to changing growth and antibody secretion rates over the course of an industrially relevant fed-batch bioprocess.

In this study, we have performed ^{13}C labeling experiments and MFA to characterize cell metabolism throughout four separate phases of an industrial fed-batch process. A small-scale culture system with a highly productive (HP) recombinant antibody-producing CHO cell line was used to represent a typical manufacturing-scale serum-free process. Using MFA, we initially observed that the demands of peak growth were met by a highly glycolytic state of metabolism, but as time progressed the culture shifted to an increasingly oxidative state that coincided with peak antibody production. All major pathways of central metabolism were considered in our analysis, including glycolysis, pentose phosphate pathway, TCA cycle, and various cataplerotic and anaplerotic pathways. In a complementary study, both the expression and activity of several relevant enzy1mes within these pathways were verified [20]. To our

knowledge, this is the first time that MFA has been applied to characterize multiple phases of an industrial antibody-producing fed-batch CHO cell bioprocess.

Materials and Methods

Cell culture

A highly-productive (HP) CHO cell line was generated by transfecting plasmid DNA containing mAb light chain and heavy chain into a dihydrofolate reductase-deficient CHO cell line adapted to suspension and serum-free growth media. Prior to the experiment, these cell lines were passaged every three or four days at a density of $3x10^5$cells/mL in peptone- and methotrexate-containing growth media in a humidified incubator maintained at 36°C and 5% CO_2 with shaking at 150 RPM. For further information about culture conditions, refer to Dean and Reddy [20].

To initiate the fed-batch experiment, the culture was inoculated into a chemically defined production media at a viable cell density of approximately $5x10^5$ cells/mL. Fed-batch cultures were grown using 25 mL of culture volume in 125mL shake flasks or 3.6 mL in 24 deep-well plates in humidified incubators maintained at 36°C and 5% CO_2 with shaking at either 150 RPM (125mL shake flask) or 220 RPM (24 deep-well plate). The production was carried out for ten days by feeding 5%, 5%, and 9% of the initial culture volume of a chemically defined concentrated amino acid feed on days three, six, and eight. On days three, six, and eight, glucose concentrations were adjusted to 55.6 mM (10 g/L).

Determination of nutrient uptake and product excretion rates

Extracellular media samples were taken at multiple times throughout the experiment. Glucose and lactate concentrations were determined by enzymatic assay using an automated Poly-chem instrument (Polymedco, Cortlandt Manor, NY). Viable cell density (VCD) was determined by using a ViCell (Beckman Coulter, Fullerton, CA). Antibody titer was determined by high performance liquid chromatography (HPLC) using a Protein-A column. Amino acid concentration was determined by HPLC using a 6-aminoquinolyl-N-hydroxysuccinimidyl carbamate derivatization method. Extracellular pyruvate concentrations were determined using an organic acid Aminex HPX-87H column (Biorad, Hercules, CA) as previously described [21].

The specific growth rate and cell specific rates of nutrient uptake and product excretion were determined using the following equations:

$$\frac{dX}{dt} = \mu X \qquad (3\text{-}1)$$

$$\frac{dC_i}{dt} = -k_i C_i + q_i X \qquad (3\text{-}2)$$

where X represents viable cell density, μ represents specific growth rate, and t represents time. In the second equation, C_i represents concentration, q_i represents cell specific production rate (or consumption rate if negative), and k_i represents the first-order degradation rate of the i^{th} biochemical component in the extracellular medium. Degradation rate for most metabolites was negligible, with the lone exception of glutamine. The spontaneous rate of glutamine degradation, calculated in the absence of cells at incubation conditions, was found to be 0.087 day^{-1}. This rate of degradation was significant (relative to cell specific uptake), as has been reported previously in literature [22]. All specific rates were calculated using the method of Glacken et al. [23], where regression analysis was applied to the extracellular time course measurements.

Steady state labeling experiment

Steady-state labeling was achieved in free intracellular metabolites by feeding labeled substrate for a minimum of 48 hours prior to sampling, which has been previously shown to be sufficient to achieve isotopic equilibrium in CHO cell cultures [24]. Because the metabolism of the culture was changing gradually over time, the measured labeling represents a quasi-steady state condition based on the assumption that the dynamics of isotope labeling occur more rapidly than the metabolic transients. Some bias may be introduced into the MFA results to the extent that this assumption is not strictly satisfied; however, we expect that our key conclusions are robust to minor violations of this assumption.

Multiple parallel ^{13}C labeling experiments were performed to enable flux analysis of each growth phase (Table 3-1).

Table 3-1. Fed batch schedule for isotope labeling experiments. Parallel 13C-labeling experiments were carried out to enable flux analysis of each growth phase. The lightly shaded section indicates when the culture was exposed to 13C labeled substrates. The culture was regularly fed an optimized nutrient-rich complex on the days indicated by ‘‘Feed.’’ Fields labeled as ‘‘Quench’’ indicate the times when the culture was harvested for intracellular metabolite analysis. The darkly shaded section of the chart represents the post- experiment period. The culture had already been quenched and terminated prior to that time.

Day	0	1	2	3	4	5	6	7	8	9	10
Day 0-3	Seed			Quench							
Day 3-5	Seed			Feed		Quench					
Day 6-8	Seed			Feed			Feed		Quench		
Day 8-10	Seed			Feed			Feed		Feed		Quench

In the case of the Day 0-3 experiment, 72 hours were allowed to achieve isotopic steady state. Two separate tracer experiments were conducted in parallel for the Day 0-3 time interval. In the first experiment, a cocktail of glucose tracers was administered, composed of 50% [1, 2-$^{13}C_2$] glucose, 30% [U-$^{13}C_6$] glucose, and 20% [1-^{13}C] glucose. [U-$^{13}C_6$] glucose has been previously shown to be an effective tracer for estimating TCA cycle fluxes, while [1, 2-$^{13}C_2$] glucose and [1-^{13}C] glucose provide information on the branch ratio between glycolysis and oxPPP [25]. The tracer mixture was optimized using the approach of Möllney et al. [26]. In the second experiment, [U-$^{15}N_2$, U-$^{13}C_5$] glutamine was used to achieve increased labeling of TCA cycle intermediates, since a large fraction of the glucose substrate was diverted to lactate during the initial Day 0-3 time interval. The labeling data from both experiments were simultaneously fitted to the same isotopomer model in order to estimate metabolic fluxes. The three other fed-batch phases of interest for this study (Day 3-5, Day 6-8, and Day 8-10) used 100% [U-^{13}C] glucose as the labeled substrate. This tracer was chosen in order to maximize identifiability of TCA cycle and amphibolic mitochondrial pathway fluxes. In these latter experiments, labeling was allowed 48 hours to equilibrate.

Metabolite quenching and extraction

Due to the fact that some intracellular metabolites are turned over on a seconds time scale, rapid quenching is necessary to capture an accurate snapshot of intracellular metabolism [27]. With this in mind, an ammonium bicarbonate (AMBIC) quench was performed [28]. Here, AMBIC makes up 0.85% w/v of the aqueous portion of the quench solution, which is a 60/40 mixture of methanol/AMBIC pre-cooled to -40°C. At each sample time point, an aliquot of culture medium containing approximately 10 million viable cells was drawn into a syringe and

rapidly ejected into the quench solution. Following the quench, metabolite extraction was performed using the Folch method [29].

Derivatization and gas chromatography mass spectrometry (GC-MS) analysis

Derivatization for GC-MS was initiated by dissolving evaporated metabolite extracts in 50 µL of methoxyamine reagent (MOX; Pierce, Rockford, IL). Following 30 minutes of sonication at room temperature, the sample was incubated for 90 minutes at 40°C. Then, 70µL of MTBSTFA + 1% TBDMCS (Pierce, Rockford, IL) in pyridine was added, and the solution was incubated for 30 minutes at 70°C. Lastly, the samples were centrifuged at 14,000 RPM to remove any solid precipitates.

Derivatized extracts were analyzed with a HP5-MS capillary column (30 m × 0.25 mm i.d. × 0.25 µm; Agilent J&W Scientific) installed in an Agilent 7890A gas chromatograph (GC). The injection volume was 1 µL and all samples were run in split mode (50:1) with an inlet temperature of 270°C. Helium flowrate was set to 1 mL/min. The GC oven temperature was held at 80°C for 5 minutes, ramped at 20°C/min to 140°C and held for 0 minutes, and ramped once more at 4°C/min to 280°C and held for 5 minutes. Mass spectra were obtained using scan mode over the range of 100 to 500 m/z. Raw ion chromatograms were integrated using a custom MATLAB program that applied consistent integration bounds and baseline correction to each fragment ion [30].

Isotopomer network model

A reaction network was generated to accurately represent the central metabolism of CHO cells. This network consisted of glycolysis, TCA cycle, pentose phosphate pathway, multiple

cataplerotic and anaplerotic reactions, and both catabolism and anabolism of amino acids. ATP and NAD(P)H were not included in the stoichiometric balances, as they have been shown to produce inconsistent results in mammalian cell cultures [31]. In total, there were 71 reactions that made up this network with 23 extracellular metabolites and two macromolecular products, antibody and biomass. Further details of the reaction network are provided in the Supplementary Materials.

Biomass and antibody demands

In order to develop an accurate biomass equation, the dry weight of the HP cell line was determined to be approximately 329 pg on average. This was calculated after drying and weighing a known amount of cells in a plastic petri dish in a non-humidified 37^{o}C incubator. The composition of the cell mass was based upon previous work available in literature for hybridoma cells [32]. The included contents of the dry cell mass for the biomass equation were protein, glycogen, lipids, and nucleotides. Each macromolecule was stoichiometrically decomposed into its independent precursor building blocks. Protein composition was based upon the relative amount of each amino acid. Each glycogen monomer was assumed to be composed of one G6P. Lipids were broken down into cholesterol, phosphatidylcholine, phosphatidylethanolamine, phosphatidylinositol, phosphatidylserine, phosphatidylglycerol, diphosphatidylglycerol, and sphingomyelin. Biosynthesis of nucleotides was also considered, based on the demands of both DNA and RNA. The biosynthetic demands for recombinant antibody production were based solely upon its amino acid composition. For further information about both the antibody and biomass equations, refer to the Supplementary Materials.

Flux determination and statistical analysis

Isotopic steady-state MFA was applied based on both the measured cell specific uptake and excretion rates and the measured intracellular isotopomer abundances [30]. This approach involved solving an inverse problem where metabolic fluxes were determined by least-squares regression of experimental measurements using the isotopomer network model. Flux estimations were repeated a minimum of 100 times from a randomized initial guess to ensure the global solution was obtained. A chi-square statistical test was used to assess goodness-of-fit and a sensitivity analysis was performed to determine 95% confidence intervals associated with the reported flux values [33].

Results and Discussion

Stoichiometric analysis

A stoichiometric analysis was performed upon four separate growth phases of a 10-day fed-batch culture (Table 3-2), accounting for all major incoming and outgoing carbon fluxes except carbon dioxide.

Table 3-2. Key characteristics of each fed-batch phase. Standard error of the mean is reported for gross specific growth rates (μ_{gross}) and specific death rates (k_d). The difference between these two rates gives the net specific growth rate.

Time (Day)	Growth Rate (Day $^{-1}$)	Phase	Key Characteristic(s)
0-3	0.66±0.01	Early Exponential	Peak growth rate and glycolytic flux
3-5	0.52±0.04	Late Exponential	Peak oxPPP flux
6-8	0.17±0.02	Stationary	Peak antibody production and TCA cycling
8-10	-0.02±0.05	Decline	Viability drops/oxPPP and TCA maintained

Glucose and amino acids supplied essentially all of the incoming carbon flux to the culture, with pyruvate serving as an additional source during the initial growth phase. While glutamine was the most important amino acid during Early Exponential phase, other amino acids became important in later growth phases once glutamine had been depleted from the medium. During Early and Late Exponential phases, most of the carbon consumed was used for biomass production (Figure 3-1), with the balance largely converted to lactate (Figure 3-2).

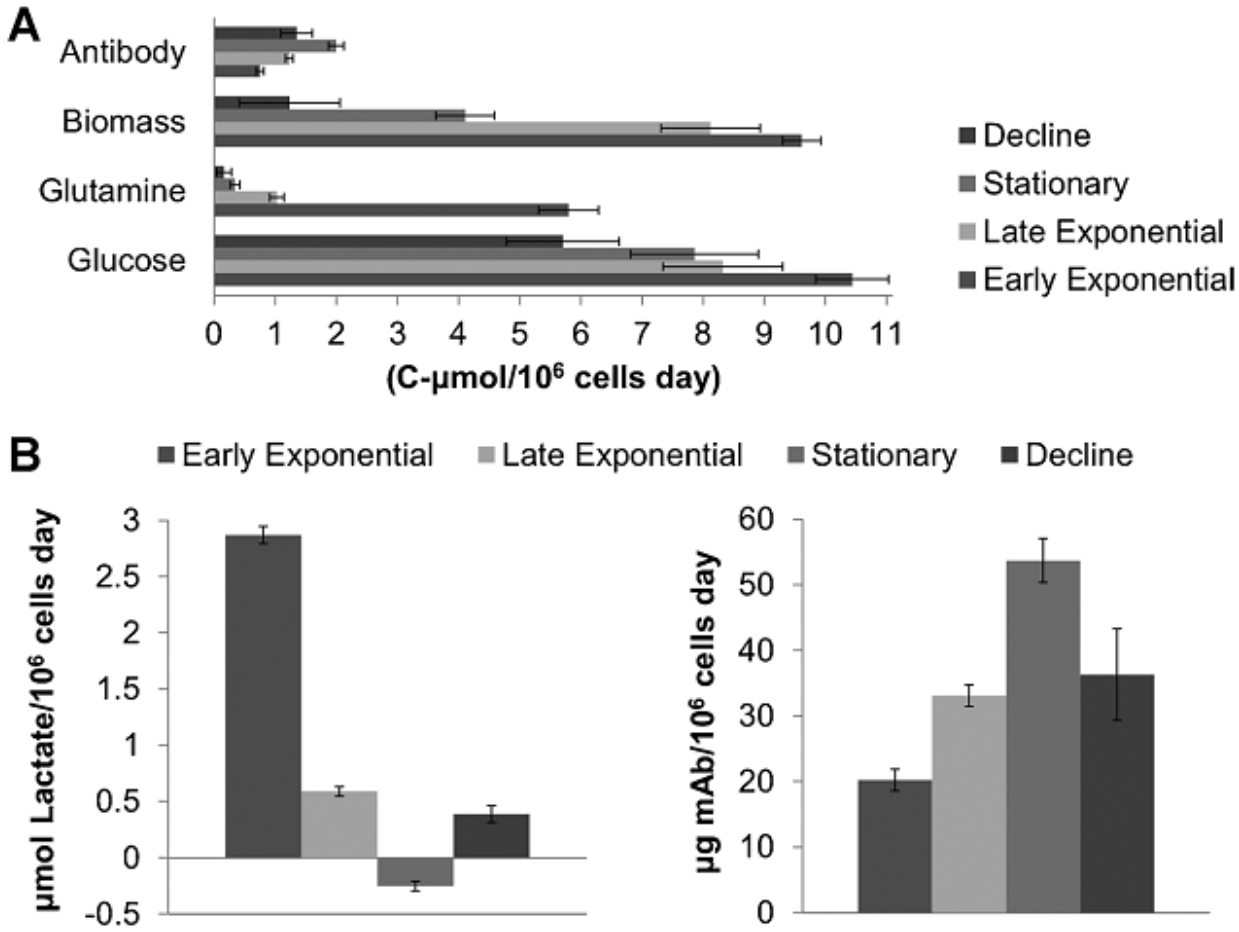

Figure 3-1. Major nutrient uptake and product formation rates. **A**: Key biosynthetic and nutrient uptake rates expressed on a carbon basis. Error bars indicate the standard error of the regressed rate parameters. **B**: Specific lactate and antibody fluxes during each phase.

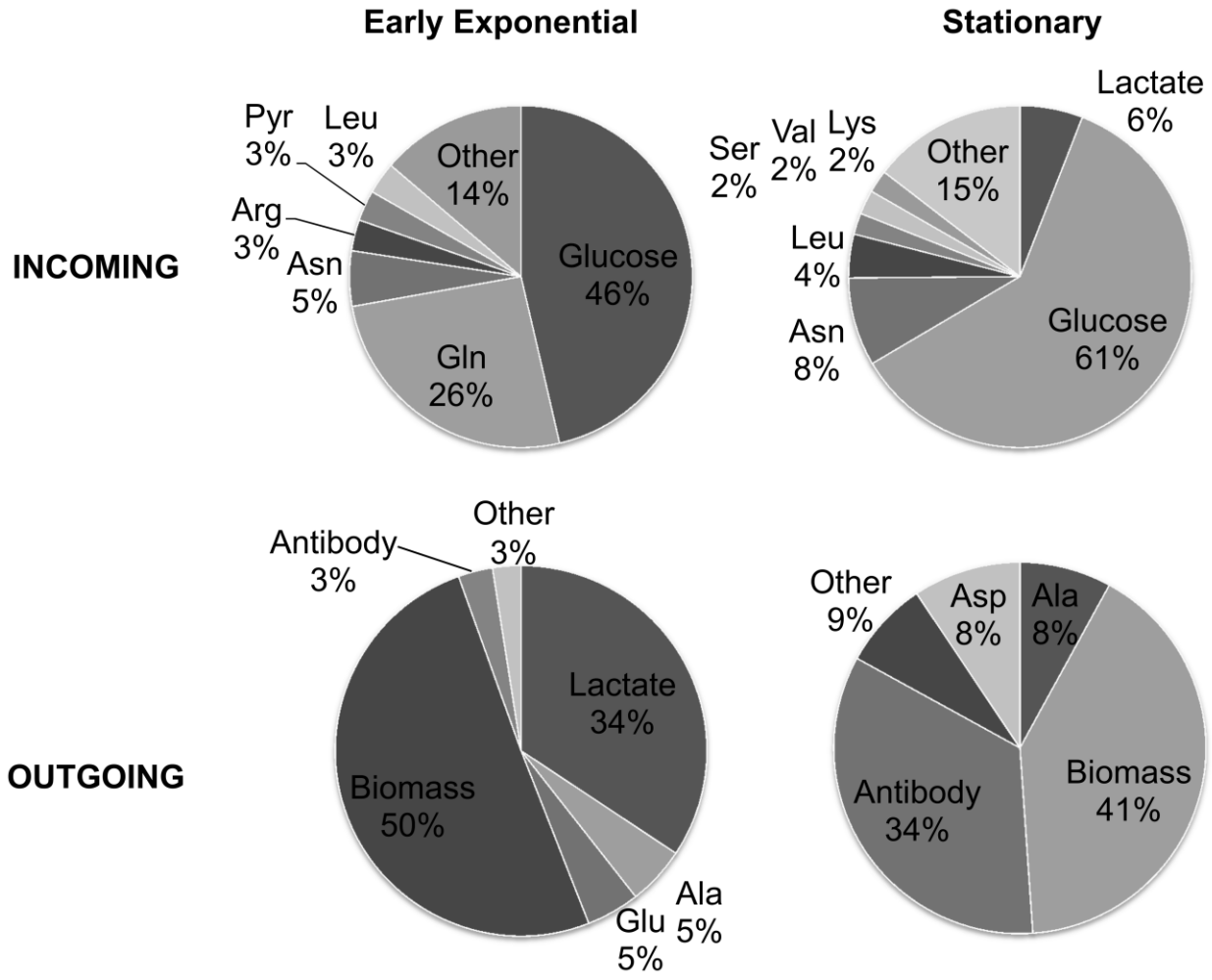

Figure 3-2. Stoichiometric analyses of measured nutrient uptake and product formation rates. Fractional contributions are expressed on a carbon basis and were calculated from direct measurements of extracellular medium composition over time, with the exception of carbon dioxide. The CO_2 contribution was estimated from the difference between measured incoming and outgoing carbon fluxes, as needed to complete the mass balance. The estimated CO_2 production rates were within the expected range based on experimentally determined rates of oxygen consumption and respiratory quotient obtained from independent bioreactor studies [33]. ‘‘Other’’ indicates the sum of several amino acids that make minor contributions to overall carbon flux.

At later phases, biomass synthesis was diminished and antibody production became a major component of the biosynthetic demand. Furthermore, lactate metabolism switched from net production to net consumption as the culture entered Stationary phase. The overall rate of

carbon consumption fell gradually at each fed batch stage (Figure 3-3), which can be largely attributed to the falling specific growth rate (Figure 3-1).

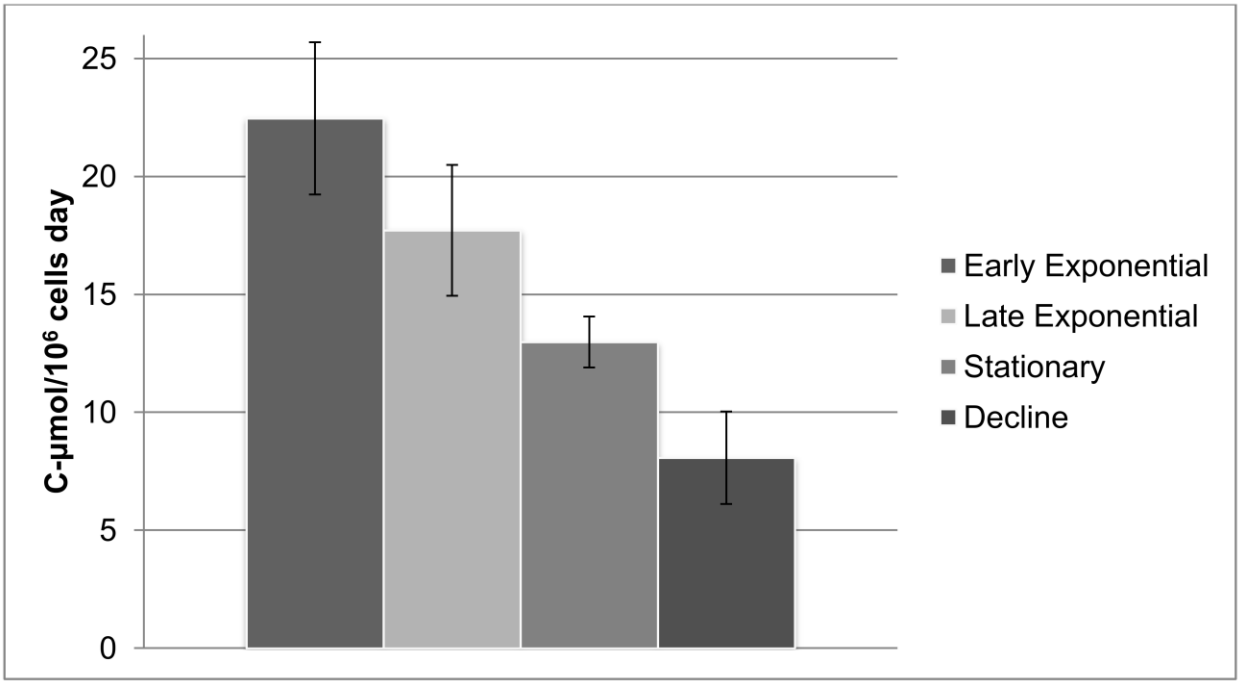

Figure 3-3. Total incoming carbon flux during each fed-batch phase. The contributions of all measured incoming carbon sources have been summed. Error bars indicate the propagated standard error.

Nutrient consumption. When glutamine and glucose carbon fluxes are summed, they compose approximately 65% of the total incoming extracellular flux during Early Exponential phase. Glutaminolysis was substantially reduced following this phase, but glucose consumption remained relatively high throughout all growth phases and never dropped below 50% of its initial rate. The rate of glutamine uptake during Early Exponential phase greatly exceeded the biosynthetic demand for biomass or antibody production. The excess glutamine consumed was catabolized to provide energy, as has been observed before [34]. Experiments using [U-$^{13}C_6$] and [U-$^{15}N_2$] glutamine showed that glutamine was largely converted to alanine and lactate [20].

The total amino acid contribution to incoming carbon flux was considerable over the entire fed-batch process (between 30% to 50% of total carbon), with the uptake of other amino acids increasing after glutamine was depleted. In particular, asparagine represented 5% of the incoming carbon flux during Early Exponential and 8% during Stationary phase.

Product formation. Antibody production was at its minimum during Early Exponential phase (only 3% of output carbon flux), but production rate more than doubled during Stationary phase (34% of output carbon flux) (Figure 3-2). Conversely, biomass production went from being the largest single flux (incoming or outgoing) at Early Exponential phase to being non-existent during Decline. In spite of this, we observed that antibody demand for incoming carbon flux was less than biomass demand in most phases, with the only exception being Decline phase when no biomass was generated. Following a similar pattern as biomass production, lactate production represented over 30% of the total outgoing carbon flux during Early Exponential phase. It was substantially reduced during Late Exponential, and it reversed direction during Stationary phase. The production of several amino acids such as glutamate, alanine, and aspartate was also observed, where glutamate excretion was associated with increased glutamine uptake and aspartate excretion was associated with increased asparagine uptake.

Metabolic flux analysis

To further investigate the intracellular pathway alterations associated with the various growth phases of this fed-batch process, ^{13}C labeling experiments were performed to enable comprehensive metabolic flux analysis. The MFA results for each growth phase are summarized in the flux maps shown in Figure 3-4.

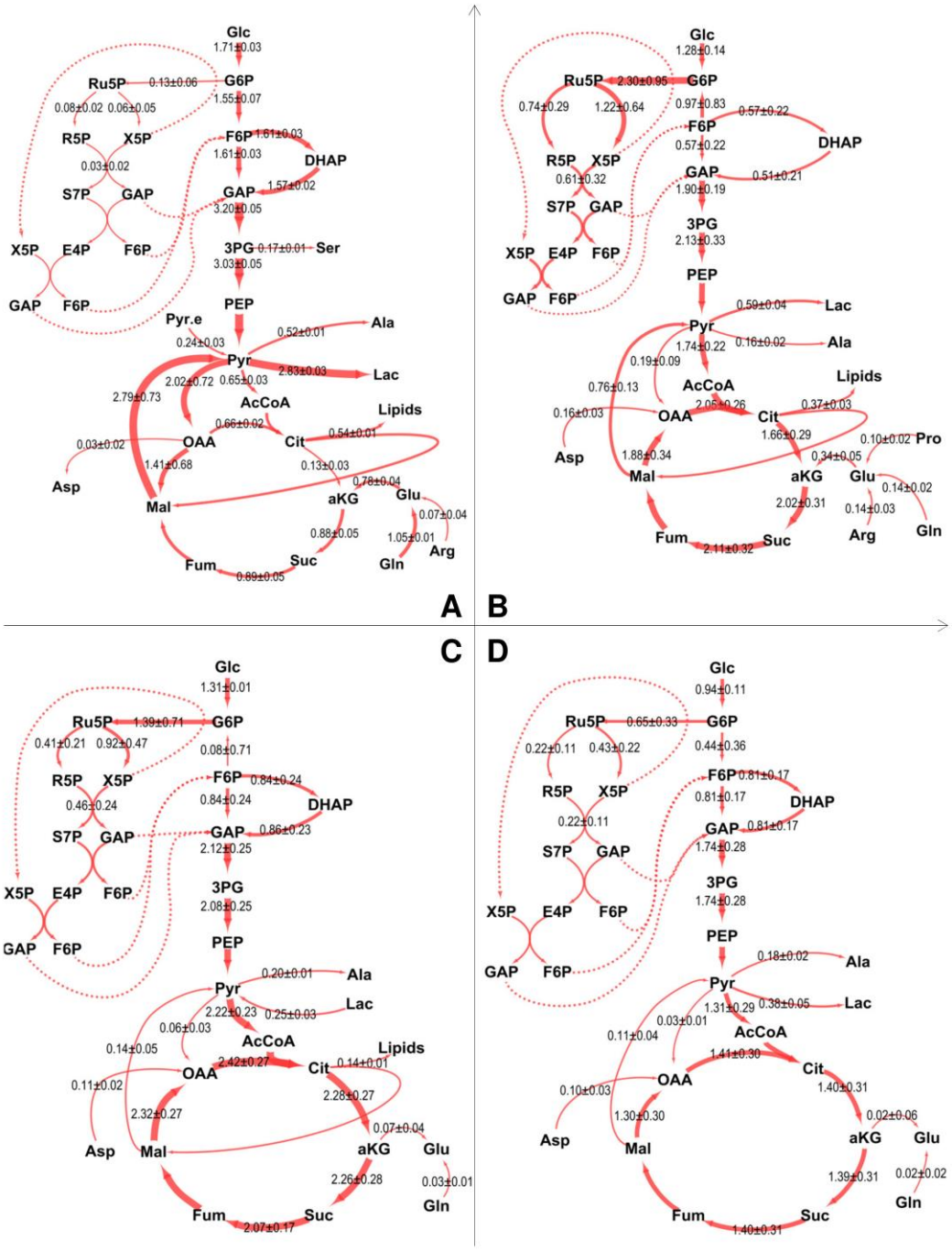

Figure 3-4. Metabolic flux maps for all growth phases. Reported fluxes (mmol/10^6 cells day) are the median of the 95% confidence interval, with associated standard errors shown. Arrow thickness is scaled proportional to the flux value. Dotted lines indicate transfer of identical metabolites involved in separate pathways, and are not actual fluxes included in the model. The flux maps were generated using Cytoscape, a freely available software [35]. **A**: Early Exponential; **B**: Late Exponential; **C**: Stationary; and **D**: Decline.

In the following, we discuss the key features of each major pathway and how the functional state of the network varies over time. Here, it is important to consider the total incoming carbon flux (Figure 3-3) in addition to the reported intracellular fluxes.

Glycolysis. Growth was at its maximum during Early Exponential phase, yet most of the incoming carbon from glucose was converted to lactate and alanine. Minimal flux was diverted into the oxidative pentose phosphate pathway (oxPPP), as over 90% of the incoming glucose was metabolized directly into glycolysis. High glycolytic activity, and specifically lactate production, has been previously associated with increased growth of mammalian cells. As stated in previous work [36], one hypothesis is that lactate production is an adaptation to increase the availability of biosynthetic precursors needed to generate biomass [37]–[39]. In contrast to Early Exponential phase, lactate production was substantially reduced following Early Exponential phase and even reversed itself during Stationary phase. Whereas lactate represented 30% of the total *outgoing* carbon flux during Early Exponential phase, it accounted for 6% of the *incoming* carbon flux during Stationary phase. However, glucose consumption and overall glycolytic flux decreased by roughly one-third following Early Exponential phase and remained relatively constant throughout Late Exponential, Stationary, and Decline phases.

Pentose Phosphate Pathway. Although essentially non-existent during Early Exponential phase, oxPPP flux was substantial during all later growth phases. Even during Decline phase, when total incoming carbon flux was reduced by 65%, glucose-6-phosphate dehydrogenase (G6PDH) flux was still larger than during Early Exponential phase. Further verification of changing oxPPP activity was provided in a parallel [1, 2-$^{13}C_2$]glucose study where only M+2

lactate mass isotopomers were observed during Early Exponential phase but substantial M+1 labeling was observed during Stationary phase [20].

Minimal oxPPP activity during exponential growth has been reported in other CHO cell MFA studies [17]. This does however raise the important question of where the necessary NAPDH for growth and maintenance of cellular redox was derived during Early Exponential phase. It has been estimated that 1-2 moles of NADPH are required per mole of acetyl-CoA incorporated into lipid [40]. ATP-citrate lyase (ACL) is the key enzyme responsible for decomposing citrate into acetyl-CoA for lipid generation. We estimated an ACL flux of 0.537 $\mu mol/10^6$ cells/day during Early Exponential phase. Since the G6PDH flux is only 25% of ACL flux during this period, another pathway must be primarily responsible for generating NAPDH for growth. This could be attributed to NADP-dependent isoforms of malic enzyme or isocitrate dehydrogenase (refer to Cataplerosis and Anaplerosis section).

Flux into oxPPP, via G6PDH, reached its peak during Late Exponential and Stationary phases. A portion of the NAPDH generated was likely used for maintenance of lipid membranes, and a parallel study found evidence of elevated palmitate turnover during Stationary phase [20]. Other studies have also observed significant G6PDH flux during the stationary phase of a fed-batch CHO cell culture [19], where nearly all of the incoming glucose was diverted to the oxPPP. In our work, all of the incoming glucose was diverted to the oxPPP during both Late Exponential and Stationary phases, which also corresponded with peak antibody production. In fact, G6PDH flux was greater than hexokinase (HK) during these periods, which implies that the oxPPP was operating in a cyclic mode with net conversion of F6P to G6P.

TCA Cycle. With a significant pyruvate flux routed into lactate during Early Exponential phase, little remained to be transported into mitochondria for oxidation. A parallel study found that multiple TCA metabolites derived substantial carbon from glutamine and asparagine during this period, leading to nearly half of the lipogenic palmitate being derived from these two amino acids [20]. Asparagine's contribution to the TCA cycle, via conversion to aspartate, remained high throughout all growth phases (unlike glutamine). Of the three NADH-producing dehydrogenase reactions in the TCA cycle, one of the three (malate dehydrogenase) was running in reverse, meaning that NADH was being consumed rather than generated. Therefore, in spite of substantial glutaminolysis, there was minimal NADH production associated with TCA cycle activity during Early Exponential phase. This result along with the high rate of lactate production indicates that minimal oxidative phosphorylation was taking place. Conversely, incoming flux to the TCA cycle from glycolysis peaked during Late Exponential and Stationary phases. Even in the Decline phase, absolute fluxes associated with TCA cycling were maintained at higher levels than during Early Exponential phase. This was even more impressive considering that the total incoming carbon flux was reduced by almost two-thirds (Figure 3-3).

One common trend across all phases was the correlation between oxPPP and TCA cycle fluxes. When oxPPP flux was minimal, TCA flux was also minimal and vice versa. One potential explanation for this trend could involve the role of NADPH in neutralizing mitochondrial-derived reactive oxygen species (ROS) through maintenance of reduced glutathione levels [19], [39]. ROS accumulation can lead to cell toxicity due to oxidation of cellular lipids, protein, and DNA [41], [42]. Therefore, increasing oxPPP flux could be an adaptive response to enhance antioxidant capacity in the presence of high mitochondrial activity.

Antibody Production. One significant result of our study was that increased antibody production (Figure 3-5) was closely associated with oxidative TCA cycle metabolism and oxPPP flux.

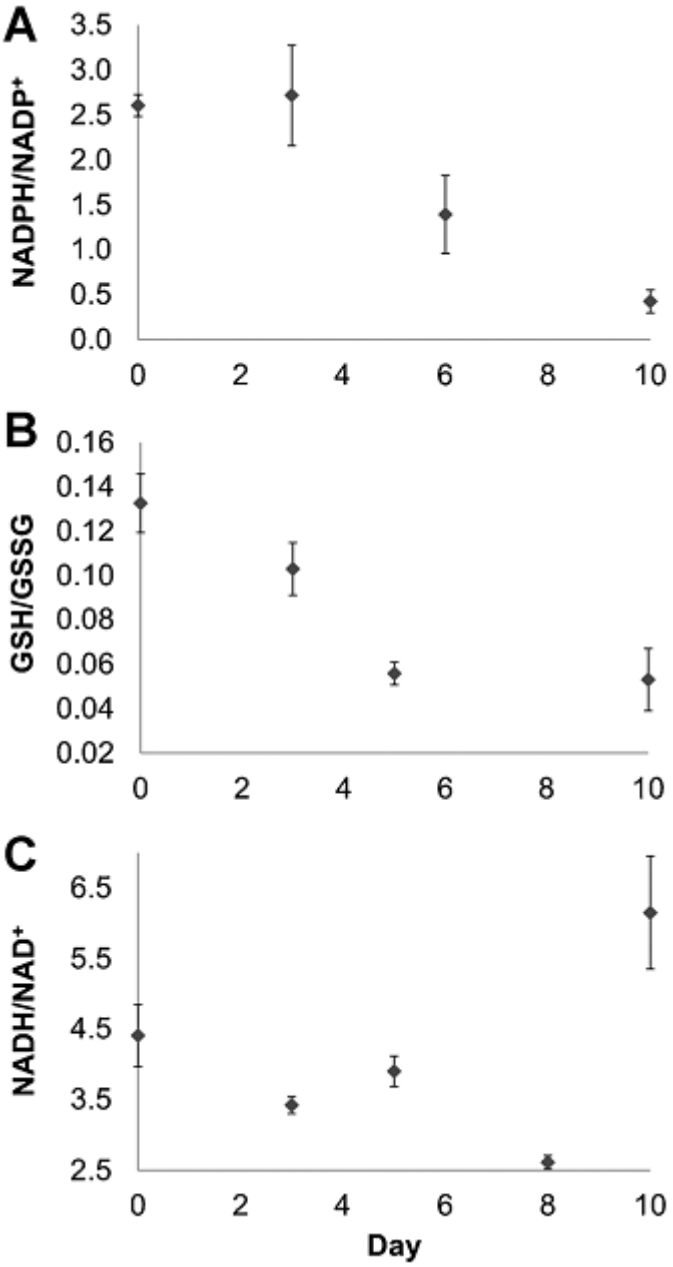

Figure 3-5. Intracellular redox ratios. **A**. Ratio of NADPH to $NADP^+$ as a function of time. **B**. Ratio of reduced (GSH) to oxidized (GSSG) glutathione. C. Ratio of NADH to NAD^+.

To our knowledge, this is the first MFA study to examine this relationship between oxidative metabolism and antibody production. Through comparison of four separate phases of the fed-batch process, we observed a positive correlation between antibody production and

isocitrate dehydrogenase (IDH) flux, which is representative of oxidative TCA cycle activity (Figure 3-6).

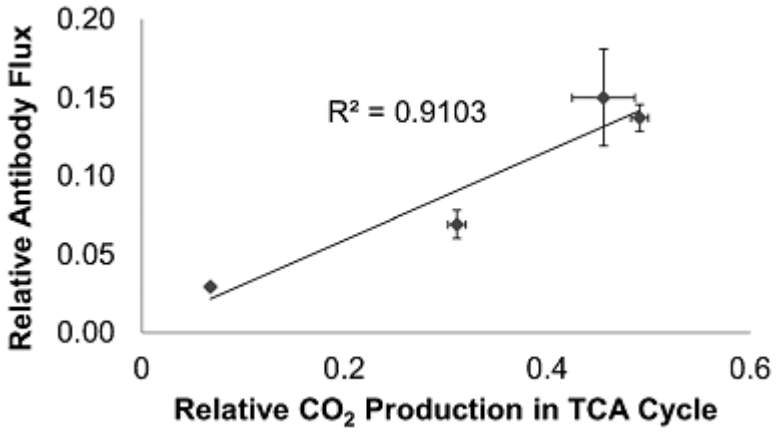

Figure 3-6. Correlation between oxidative TCA cycle flux and antibody production. Each point represents a separate phase of the fed-batch process, with TCA cycle and antibody fluxes normalized to the corresponding total incoming carbon flux reported in Figure 3-3. Oxidative TCA cycle flux was calculated by summing the rates of all three CO_2-producing TCA cycle reactions: PDH, IDH, and ADH. Error bars indicate standard errors.

IDH is an indicator of TCA activity because it represents the glycolytic carbon (via pyruvate) to progress through the TCA cycle, and not the carbon lost for cytosolic lipid synthesis via ATP-citrate lyase, as was very much the case during Early Exponential phase. On the other hand, peak growth corresponded with peak glycolytic flux but minimal oxidative metabolism. Based upon our results, metabolic engineering to increase flux to TCA cycle during production phase has potential to enhance rates of specific antibody formation. Additional steps may be required to simultaneously divert more flux into oxPPP in order to maintain redox homeostasis and avoid ROS accumulation.

Cataplerosis and Anaplerosis. During Early Exponential phase, substantial flux was diverted into mitochondrial cataplerotic and anaplerotic pathways. Conversely, there was a large reduction in these fluxes during subsequent growth phases. During Early Exponential phase, ATP-citrate lyase (ACL) accounted for more than 75% of the flux leaving citrate. In another prior MFA study, ACL was determined to be a negligible flux during exponential phase [17] However, our work used a serum-free medium without substantial fatty acid content, so cell growth required *de novo* lipid synthesis that in turn relied on ACL to supply AcCoA building blocks.

Substantial malic enzyme (ME) flux was also observed during Early Exponential phase, and although there was a large uncertainty associated with this value, closer examination of the 95% confidence interval reveals that even the lower bound of 1.3 μmol/ 10^6 cells/day is high in comparison to most other fluxes estimated during this growth phase. Like ME, phosphoenolpyruvate carboxykinase (PEPCK) could also be contributing cataplerotic flux from the TCA cycle to glycolysis; however, we cannot distinguish between these two pathways based upon our isotopomer measurements and have therefore lumped them together. ME in combination with anaplerotic pyruvate carboxylase (PC) flux effectively create a separate cycle overlapping with the TCA cycle. PC was found to have substantial flux during Early Exponential phase, returning much of the pyruvate generated by ME to the TCA cycle. PC can often be ignored in quiescent cells, but can carry a substantial flux in growing cultures [43]. Our analysis determined that the PC flux was at least as significant as pyruvate dehydrogenase (PDH) for channeling pyruvate into the TCA cycle during the initial growth period. The activity of PC was independently confirmed in a separate experiment using [1-^{13}C]pyruvate, the results of which can be found in the Supplementary Materials.

The high cycling through ME and PC could potentially explain the minimal oxPPP activity during Early Exponential phase, as NADP-dependent ME isoforms could have supplied the majority of cellular NADPH demands and thereby made additional oxPPP flux unnecessary. However, all three ME isoforms are known to exist in CHO cells [44] and our MFA results cannot distinguish between them. Activity of the NADP-dependent ME1 isoform was confirmed for this study (results not shown), but results were inconclusive regarding the activity of ME2 and ME3. Therefore, it is difficult to state which isoform, if any, was dominant in catalyzing conversion of malate to pyruvate. Lastly, in addition to ME, isocitrate dehydrogenase (IDH) is also capable of producing NADPH. In general, the presence of multiple isoforms of both IDH and ME make it difficult to determine their contribution to the overall NAD(P)H production rates based on our MFA results.

Conclusions

As CHO cells transition from peak growth to peak antibody production, cell metabolism can change considerably over the course of a typical industrial fed-batch bioprocess. We aimed to quantify these global metabolic alterations using ^{13}C labeling experiments and metabolic flux analysis. We found that high glycolytic flux positively correlated with peak growth, and specific lactate production was highest when specific growth rate was also highest. On the contrary, a highly oxidative state of metabolism was associated with increased antibody production, a result that, to our knowledge, has not been previously reported in MFA studies. During peak specific antibody production (i.e., during Stationary phase), TCA cycling was at its maximum and lactate production was at its minimum. In fact, lactate was not produced at all, but instead was consumed. Furthermore, high oxidative pentose phosphate pathway flux was found to positively

correlate with high TCA cycling and antibody production. This suggests that promoting oxidative TCA cycle metabolism and pentose phosphate pathway flux may provide a possible strategy to increase specific antibody production and reduce lactate accumulation during the production phase of industrial fed-batch CHO cell cultures.

Acknowledgments

The authors of this work have no pertinent conflicts of interest to report. Funding for this project was provided by Amgen Contract # 2010529686. The authors would like to thank all the Amgen analysts involved in this work; special thanks to Sheila Kingrey-Grebe for AA analysis, Jennifer Kerr for GC-MS set up, Louiza Dudin, Rajnita Charan, and Sumana Dey for cell culture media, and Angie Ziebart for mAb titer measurements. Thanks to Amgen for supporting Jason Dean's postdoctoral training.

Nomenclature

3PG: 3-Phosphoglycerate

AcCoA: Acetyl-CoA

ACL: ATP Citrate Lyase

aKG: α-Ketoglutarate

Ala: Alanine

AMBIC: Ammonium Bicarbonate

Arg: Arginine

Asp: Aspartate

ATP: Adenosine-5'-Triphosphate

CHO: Chinese Hamster Ovary

Cit: Citrate

DHAP: Dihydroxyacetone Phosphate

E4P: Erythrose-4-Phosphate

F6P: Fructose 6-Phosphate

Fum: Fumarate

G6P: Glucose-6-Phosphate

G6PDH: Glucose-6-Phosphate Dehydrogenase

GAP: Glyceraldehyde-3-Phosphate

GC-MS: Gas Chromatography-Mass Spectrometry

Glc: Glucose

Gln: Glutamine

Glu: Glutamate

HK: Hexokinase

HPLC: High Performance Liquid Chromatography

Lac: Lactate

mAb: Monoclonal Antibody

Mal: Malate

ME: Malic Enzyme

MFA: Metabolic Flux Analysis

MOX: Methoxyamine

MTBSTFA: N-Methyl-N-(t-butyldimethylsilyl) trifluoroacetamide

NADH: Nicotinamide Adenine Dinucleotide

NADPH: Nicotinamide Adenine Dinucleotide phosphate

OAA: Oxaloacetate

PC: Pyruvate Carboxylase

PEP: Phosphoenolpyruvate

oxPPP: Oxidative Pentose Phosphate Pathway

Pro: Proline

Pyr.e: Extracellular Pyruvate

Pyr: Pyruvate

R5P: Ribose-5-Phosphate

ROS: Reactive Oxygen species

RPM: Revolutions Per Minute

Ru5P: Ribulose-5-Phosphate

S7P: Sedoheptulose-7-Phosphate

Suc: Succinate

TBDMCS: Tert-Butyldimethylchlorosilane

TCA Cycle: Tri-Carboxylic Acid Cycle

VCD: Viable Cell Density

X5P: Xylulose-5-Phosphate

Appendix

Metabolic flux analysis assumptions

The reaction network for all four models generated, including the reported fluxes and their associated 95% confidence intervals, can be found in a separate Excel spreadsheet. The following assumptions were made in regards to generating the models:

1. Metabolism is at a steady state during each of the four phases of the fed-batch. The reported fluxes therefore represent averages over the corresponding time interval.
2. Intracellular isotopic labeling has reached quasi-steady state at the time of sample quenching and removal.
3. Succinate and fumarate are symmetric molecules that don't retain any particular orientation when metabolized by TCA cycle enzymes.
4. The labeling patterns of mitochondrial and cytosolic metabolites are assumed to be in isotopic equilibrium.
5. Change in individual cell size (mass) over the fed-batch lifetime is assumed to be negligible.
6. All major carbon sources of the complex industrial media have been included.
7. The amount of carbon required for antibody glycosylation is assumed to be negligible.
8. Exchange fluxes are employed to account for dilution by unlabeled carbon sources in the medium (e.g., lactate, alanine, aspartate).

Confirmation of pyruvate carboxylase (PC) activity

Pyruvate carboxylase (PC) was found to have substantial flux during Early Exponential phase, returning much of the pyruvate generated by malic enzyme to the TCA cycle. The activity of PC was also independently confirmed in a separate experiment using [1-^{13}C] pyruvate. Here, the first carbon of pyruvate was labeled and spiked into the media either at Day 0 or Day 6, and intracellular metabolites were analyzed on either Day 2 or Day 7. Metabolite labeling was assessed by GC-MS to determine the path of entry of pyruvate into the TCA cycle. If PC was active, a portion of the labeled carbon from [1-^{13}C] pyruvate would have appeared in oxaloacetate (OAA) and malate (Figure 3-A-1). Alternatively, if pyruvate predominantly entered the TCA cycle through pyruvate dehydrogenase (PDH), there would be no ^{13}C labeling in malate. This is because the first carbon of pyruvate is lost to CO_2 in the PDH reaction (Figure 3-A-1). As shown in Table 3-A-1, the results indicate that PC was active during Early Exponential phase but was inactive during Stationary phase.

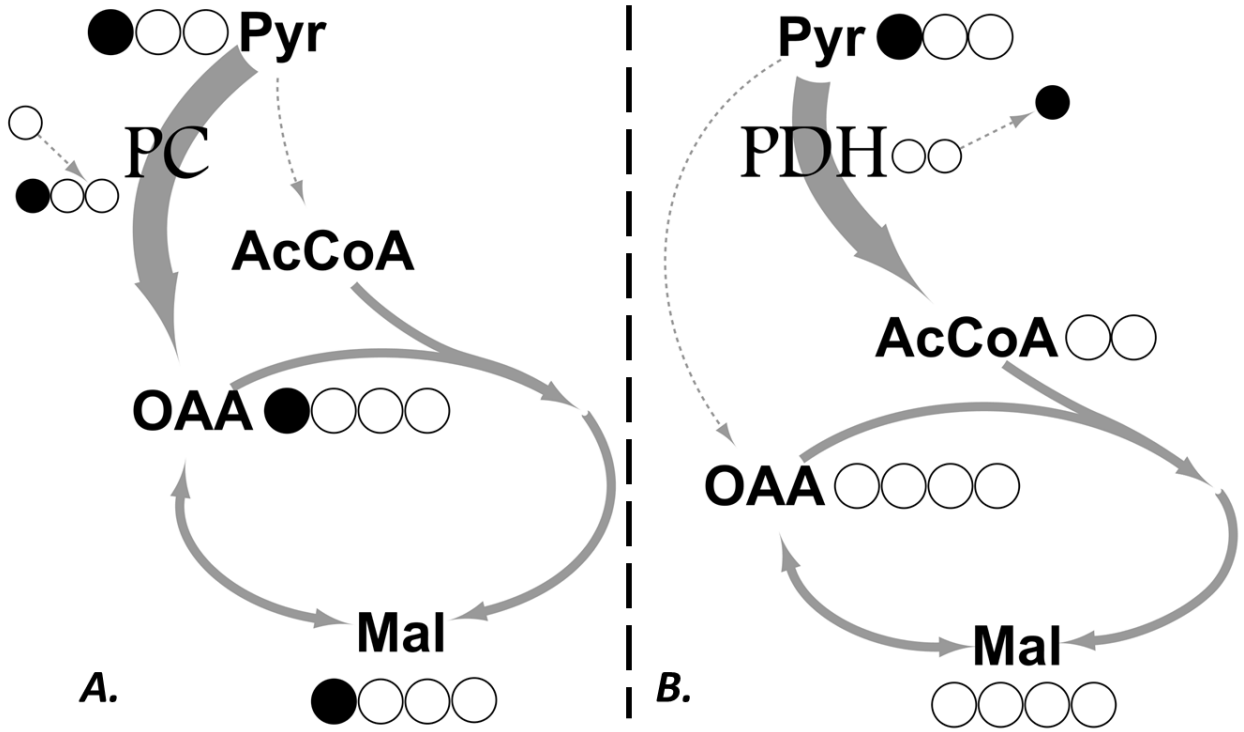

Figure 3-A-1. **[1-^{13}C] pyruvate experiment to determine path of entry to TCA cycle**. **A**. Expected labeling if pyruvate carboxylase (PC) is the dominant route of entry to TCA cycle. **B**. Expected labeling if PDH is the dominant route of entry to the TCA cycle.

Table 3-A-1. **Measured malate labeling in [1-^{13}C] pyruvate experiments** performed during Day 0-2 and Day 6-7 of the fed-batch culture.

	Day 2	Day 7
Malate M1 Labeling	0.12 ±0.01	Not Detectable

Additional stoichiometric analysis

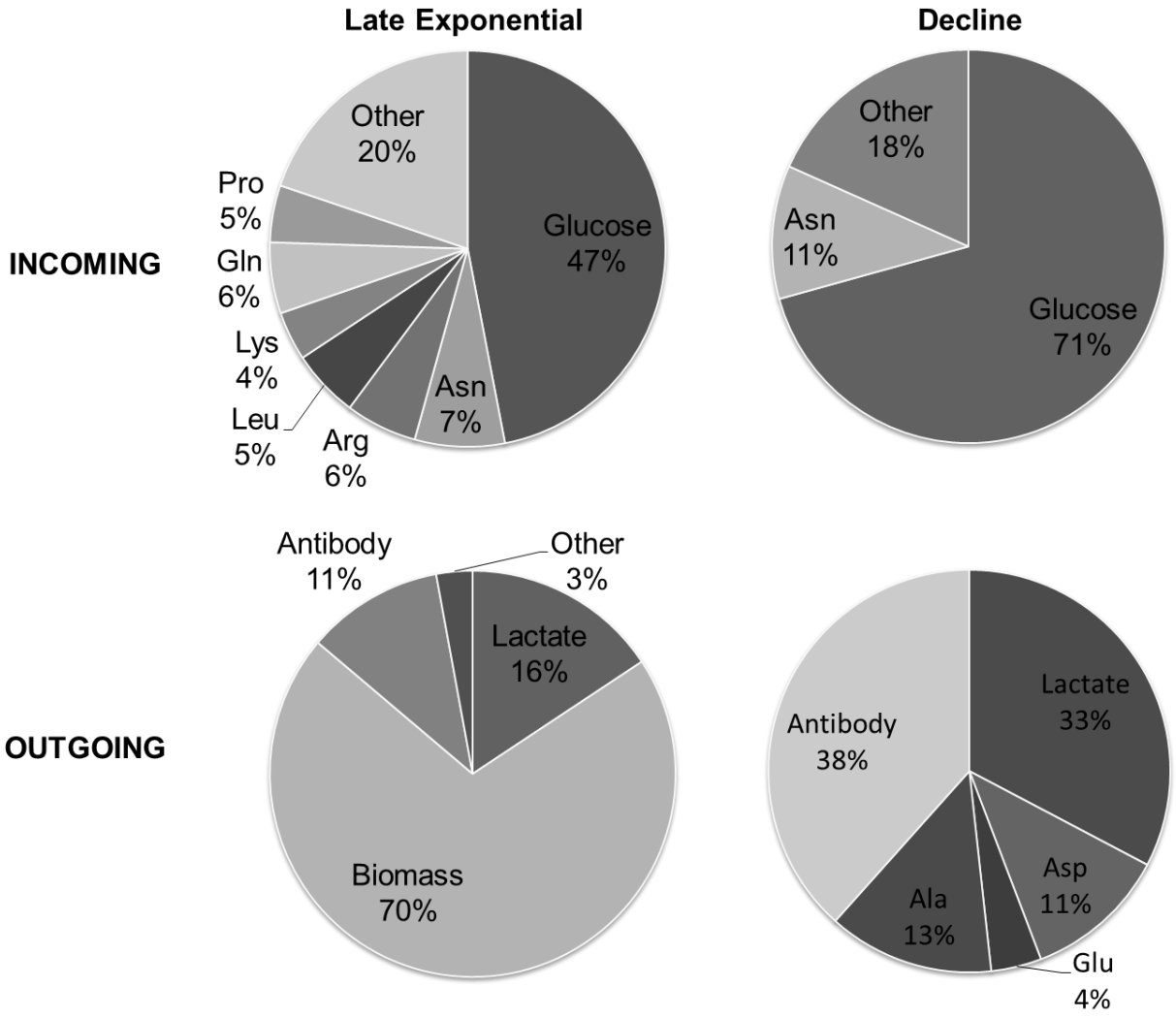

Figure 3-A-2. **Stoichiometric analysis of measured nutrient uptake and product formation rates**. Carbon dioxide generation not measured. "Other" indicates the sum of several amino acids that make minor contributions to carbon flux.

Intracellular metabolites examined for labeling

Table 3-A-2. Ion fragments quantified via GCMS for the purpose of MFA. The number listed in the ion fragment column corresponds to the mass of fragment.

Ion Fragment	Node ID	Labeled Atom	Unlabeled Atom
Lac 233	Lac	2 3	C8 H25 O2 Si2
Lac 261	Lac	1 2 3	C8 H25 O2 Si2
Ala 232	Ala	2 3	C8 H26 O N Si2
Ala 260	Ala	1 2 3	C8 H26 O2 N Si2
Ser 288	Ser	2 3	C12 H34 N O Si2
Ser 302	Ser	1 2	C12 H32 N O2 Si2
Ser 362	Ser	2 3	C14 H40 N O2 Si3
Ser 390	Ser	1 2 3	C14 H40 N O3 Si3
akG 346	aKG	1 2 3 4 5	C9 H28 O5 N Si2
Mal 419	Mal	1 2 3 4	C14 H39 O5 Si3
Asp 302	Asp	1 2	C12 H32 N O2 Si2
Asp 376	Asp	1 2	C14 H38 N O3 Si3
Asp 390	Asp	2 3 4	C14 H40 N O3 Si3
Asp 418	Asp	1 2 3 4	C14 H40 O4 N Si3
Glu 330	Glu	2 3 4 5	C14 H36 N O2 Si2
Glu 358	Glu	1 2 3 4 5	C12 H36 N O3 Si2
Glu 432	Glu	1 2 3 4 5	C14 H42 O4 N Si3
Asn 417	Asn	1 2 3 4	C14 H41 N2 O3 Si3
Gln 431	Gln	1 2 3 4 5	C14 H43 N2 O3 Si3
Suc 289	Suc	1 2 3 4	C8 H25 O4 Si2
Cit 459	Cit	1 2 3 4 5 6	C14 H39 O6 Si3

Carbon atom mapping of reaction network

Table 3-A-3. Reaction network carbon transitions.

Glycolysis	
PGI	G6P (abcdef) <-> F6P (abcdef)
PFK	F6P (abcdef) -> DHAP (cba) + GAP (def)
TPI	DHAP (abc) <-> GAP (abc)
GADPH	GAP (abc) <-> 3PG (abc)
Eno	3PG (abc) <-> PEP (abc)
PK	PEP (abc) -> Pyr (abc)
HK	Glc (abcdef) -> G6P (abcdef)
LDH Reversible	Lac (abc) <-> Pyr (abc)
Pentose Phosphate Pathway	
6PGDH	G6P (abcdef) -> Ru5P (bcdef) + CO2 (a)
R5PE	Ru5P (abcde) <-> X5P (abcde)
R5PI	Ru5P (abcde) <-> R5P (abcde)
TK1	X5P (abcde) + R5P (fghij) <-> GAP (hij) + S7P (fgabcde)
TK2	S7P (abcdefg) + GAP (hij) <-> E4P (defg) + F6P (abchij)
TK3	X5P (abcde) + E4P (fghi) <-> GAP (cde) + F6P (abfghi)
TCA Cycle	
PDH	Pyr (abc) -> AcCoA (bc) + CO2 (a)
CS	OAA (abcd) + AcCoA (ef) -> Cit (dcbfea)
IDH	Cit (abcdef) -> aKG (abcde) + CO2 (f)
ADH	aKG (abcde) -> Suc (bcde) + CO2 (a)
SDH	Suc (abcd) <-> Fum (abcd)
Fum	Fum (abcd) <-> Mal (abcd)
MDH	Mal (abcd) <-> OAA (abcd)
Transport	
Glc IN	Glc.e (abcdef) -> Glc (abcdef)
Glc Labeled	Glc.l (abcdef) -> Glc.e (abcdef)
Glc Unlabeled	Glc.u (abcdef) -> Glc.e (abcdef)
Lys IN	Lys.e (abcdef) -> Lys (abcdef)
Thr IN	Thr.e (abcd) -> Thr (abcd)
Phe IN	Phe.e (abcdefghi) -> Phe (abcdefghi)
Tyr IN	Tyr.e (abcdefghi) -> Tyr (abcdefghi)
Val IN	Val.e (abcde) -> Val (abcde)
Leu IN	Leu.e (abcdef) -> Leu (abcdef)
Ile IN	Ile.e (abcdef) -> Ile (abcdef)
Trp IN	Trp.e (abcdefghijk) -> Trp (abcdefghijk)
His IN	His.e (abcdef) -> His (abcdef)
Met IN	Met.e (abcde) -> Met (abcde)
aKG Produced via Glu	DummyaKG <-> aKGSink

Anaplerotic reactions	
ME	Mal (abcd) -> Pyr (abc) + CO2 (d)
PYC	Pyr (abc) + CO2 (d) -> OAA (abcd)
ACL	Cit (abcdef) -> AcCoA.c (ed) + Mal (fcba)
Amino Acid Metabolism	
ASNS	Asp (abcd) <-> Asn (abcd)
CBXase + Mutase	ProCoA (abc) + CO2 (d) -> Suc (abcd)
GLS	Gln (abcde) <-> Glu (abcde)
GluPro Mtbl	Glu (abcde) <-> Pro (abcde)
GS + SHT	CO2 (a) + MEETHF (b) -> Gly (ab)
Met Mtbl	Met (abcde) + Ser (fgh) -> Methyl (e) + Cys (fgh) + Suc (abcd)
PheTyr Mtbl	Phe (abcdefghi) -> Tyr (abcdefghi)
SHT	Ser (abc) <-> Gly (ab) + MEETHF (c)
Thr Mtbl	Thr (abcd) -> Pyr (abc) + CO2 (d)
Trp Mtbl	Trp (abcdefghijk) -> CO2 (d) + CO2 (e) + Ala (abc) + aKetoadi (fghijk)
Trp2 Mtbl	aKetoadi (abcdef) -> CO2 (a) + CO2 (f) + AcCoA (bc) + AcCoA (de)
*GDH	aKG (abcde) + DummyaKG <-> Glu (abcde)
*ALT	Ala (abc) + aKG (defgh) + DummyaKG <-> Pyr (abc) + Glu (defgh)
*Ile Mtbl	Ile (abcdef) + aKG (ghijk) + DummyaKG -> AcCoA (de) + CO2 (a) + ProCoA (bcf) + Glu (ghijk)
*Leu Mtbl	Leu (abcdef) + aKG (ghijk) + CO2 (l) + DummyaKG -> CO2 (a) + AcCoA (bc) + AcCoA (ld) + AcCoA (ef) + Glu (ghijk)
*Tyr Mtbl	Tyr (abcdefghi) + aKG (jklmn) + DummyaKG -> CO2 (a) + Mal (defg) + AcCoA (bc) + AcCoA (hi) + Glu (jklmn)
*AST	OAA (abcd) + Glu (efghi) <-> Asp (abcd) + aKG (efghi) + DummyaKG
*Arg Mtbl	Arg (abcdef) + aKG (ghijk) + DummyaKG -> Glu (abcde) + Urea (f) + Glu (ghijk)
*PST	3PG (abc) + Glu (defgh) -> Ser (abc) + aKG (defgh) + DummyaKG
*Cys Mtbl	Cys (abc) + aKG (defgh) + DummyaKG -> Pyr (abc) + Glu (defgh)
Lumped Antibody Equation	
Antibody	610.6*Ala + 213.6*Arg + 249.8*Asn + 323.1*Asp + 212.9*Cys + 333.2*Gln + 331*Glu + 859.2*Gly + 110.9*His + 141.8*Ile + 568*Leu + 411.8*Lys + 95.84*Met + 234.3*Phe + 597.6*Pro + 1118*Ser + 709.4*Thr + 105.3*Trp + 221.3*Tyr + 758*Val -> Antibody
Lumped Biomass Equation	
Biomass 329pg	0.1552*Asp + 0.127*Glu + 0.0948*Asn + 0.1451*Ser + 0.047*His + 0.2165*Gly + 0.124*Arg + 0.1974*Ala + 0.0599*Tyr + 0.0477*Cys + 0.1369*Val + 0.0454*Met + 0.0721*Phe + 0.1066*Ile + 0.1856*Leu + 0.1875*Lys + 0.1059*Gln + 0.0145*Trp + 0.103*Pro + 0.127*Thr + 0.0839*MEETHF + 0.0766*CO2 + 0.8143*AcCoA.c + 0.04*DHAP + 0.0766*R5P + 0.0949*G6P -> Biomass
Transport Exchange	
DummySer	Ser.e (abc) <-> Ser (abc) + dummySer

Ser IN	dummySer -> Sink
DummyAla	Ala (abc) <-> Ala.e (abc) + dummyAla
Ala OUT	dummyAla -> Sink
DummyArg	Arg.e (abcdef) <-> Arg (abcdef) + dummyArg
Arg IN	dummyArg -> Sink
DummyAsp	Asp (abcd) <-> Asp.e (abcd) + dummyAsp
Asp OUT	dummyAsp -> Sink
DummyCys	Cys.e (abc) <-> Cys (abc) + dummyCys
Cys IN	dummyCys -> Sink
DummyGlu	Glu (abcde) <-> Glu.e (abcde) + dummyGlu
Glu OUT	dummyGlu -> Sink
DummyGln	Gln.e (abcde) <-> Gln (abcde) + dummyGln
Gln IN	dummyGln -> Sink
DummyGly	Gly.e (ab) <-> Gly (ab) + dummyGly
Gly IN	dummyGly -> Sink
DummyPro	Pro.e (abcde) <-> Pro (abcde) + dummyPro
Pro IN	dummyPro -> Sink
DummyAsn	Asn.e (abcd) <-> Asn (abcd) + dummyAsn
Asn IN	dummyAsn -> Sink
DummyLac	Lac.e (abc) <-> Lac (abc) + dummyLac
Lac IN	dummyLac -> Sink

95% confidence intervals associated with individual fluxes

Table 3-A-4. **Net fluxes associated with Figure 3-4a**. Early exponential phase of culture.

Pathway	Enzyme	Rxn	LB 95% CI	UB 95% CI	Value
Glycolysis	PGI	G6P <-> F6P	1.412	1.687	1.549
	PFK	F6P -> DHAP + GAP	1.542	1.675	1.609
	TPI	DHAP <-> GAP	1.516	1.624	1.570
	GAPDH	GAP <-> 3PG	3.096	3.307	3.202
	ENO	3PG <-> PEP	2.929	3.131	3.030
	PK	PEP -> Pyr	2.929	3.131	3.030
	HK	Glc -> G6P	1.641	1.772	1.707
	LDH	Lac <-> Pyr	-2.925	-2.767	-2.846
PPP	6PGDH	G6P -> Ru5P + CO2	0.000	0.254	0.127
	R5PE	Ru5P <-> X5P	-0.035	0.146	0.056
	R5PI	Ru5P <-> R5P	0.033	0.118	0.076
	TK1	X5P + R5P <-> GAP + S7P	-0.018	0.073	0.028
	TK2	S7P + GAP <-> E4P + F6P	-0.018	0.073	0.028
	TK3	X5P + E4P <-> GAP + F6P	-0.018	0.073	0.028
TCA	PDH	Pyr -> AcCoA + CO2	0.584	0.713	0.649
	SDH	Suc <-> Fum	0.779	0.992	0.886
	FUM	Fum <-> Mal	0.779	0.992	0.886
	MDH	Mal <-> OAA	-2.774	-0.037	-1.405
	CS	OAA + AcCoA -> Cit	0.608	0.713	0.660
	ADH	aKG -> Suc + CO2	0.778	0.990	0.884
	IDH	Cit -> aKG + CO2	0.075	0.183	0.129
Transport	Ser IN	Ser.e -> Ser	0.121	0.157	0.139
	Ala OUT	Ala -> Ala.e	0.360	0.409	0.385
	Arg IN	Arg.e -> Arg	0.084	0.235	0.159
	Asp OUT	Asp -> Asp.e	0.119	0.154	0.137
	Glu OUT	Glu -> Glu.e	0.234	0.273	0.254
	Gln IN	Gln.e -> Gln	1.110	1.140	1.125
	Pro IN	Pro.e -> Pro	0.077	0.082	0.080
	Asn IN	Asn.e -> Asn	0.246	0.322	0.284
	Gly OUT	Gly -> Gly.e	2.767	2.925	2.846
	Cys OUT	Cys -> Cys.e	0.001	0.037	0.019
	Pyr IN	Pyr.e -> Pyr	0.019	0.055	0.037
	Lys IN	Lys.e -> Lys	0.127	0.136	0.131
	Thr IN	Thr.e -> Thr	0.093	0.100	0.096
	Phe IN	Phe.e -> Phe	0.050	0.065	0.057
	Tyr IN	Tyr.e -> Tyr	0.032	0.079	0.055

	Val IN	Val.e -> Val	0.101	0.108	0.104
	Leu IN	Leu.e -> Leu	0.128	0.137	0.133
	Ile IN	Ile.e -> Ile	0.070	0.076	0.073
	Trp IN	Trp.e -> Trp	0.012	0.025	0.018
	His IN	His.e -> His	0.032	0.038	0.035
	Met IN	Met.e -> Met	0.031	0.054	0.043
Anaplerosis	ME	Mal -> Pyr + CO2	1.321	4.252	2.787
	PYC	Pyr + CO2 -> OAA	0.578	3.466	2.022
	ACL	Cit -> AcCoA.c + Mal	0.520	0.557	0.538
Amino	GLS	Gln <-> Glu	1.033	1.064	1.049
Acid	ASNS	Asp <-> Asn	-0.254	-0.178	-0.216
Metabolism	SHT	Ser <-> Gly + MEETHF	0.107	0.126	0.117
	CYST	Ser <-> Cys	0.044	0.090	0.067
	GS + SHT	CO2 + MEETHF -> Gly	0.052	0.071	0.061
	Met Mtbl	Met + Ser -> Methyl + Cys + Suc	0.000	0.023	0.012
	PheTyr Mtbl	Phe -> Tyr	0.000	0.012	0.006
	Thr Mtbl	Thr -> Pyr + CO2	0.000	0.004	0.002
	Histidase	His -> FormTHF + Glu	0.000	0.014	0.007
	CBXase + Mutase	ProCoA + CO2 -> Suc	0.000	0.010	0.005
	Trp Mtbl	Trp -> CO2 + CO2 + Ala + aKetoadi	0.000	0.013	0.006
	Trp2 Mtbl	aKetoadi -> CO2 + CO2 + AcCoA + AcCoA	0.000	0.012	0.006
	GDH	aKG <-> Glu	-0.230	0.051	-0.089
	ALT	Ala + aKG <-> Pyr + Glu	-0.549	-0.496	-0.523
	Ile Mtbl	Ile + aKG -> AcCoA + CO2 + ProCoA + Glu	0.000	0.011	0.006
	Leu Mtbl	Leu + aKG + CO2 -> CO2 + AcCoA + AcCoA + AcCoA + Glu	0.000	0.006	0.003
	Tyr Mtbl	Tyr + aKG -> CO2 + Mal + AcCoA + AcCoA + Glu	0.000	0.038	0.019
	Val Mtbl	Val + aKG -> Glu + CO2 + CO2 + ProCoA	0.000	0.007	0.003
	Lys Mtbl	Lys + aKG + aKG -> Glu + Glu + aKetoadi	0.000	0.008	0.004
	AST	OAA + Glu <-> Asp + aKG	-0.013	0.072	0.029
	Arg Mtbl	Arg + aKG -> Glu + Urea + Glu	0.000	0.145	0.072
	PST	3PG + Glu -> Ser + aKG	0.140	0.196	0.168

Biomass Production	Biomass 329pg	0.1552*Asp + 0.127*Glu + 0.0948*Asn + 0.1451*Ser + 0.047*His + 0.2165*Gly + 0.124*Arg + 0.1974*Ala + 0.0599*Tyr + 0.0477*Cys + 0.1369*Val + 0.0454*Met + 0.0721*Phe + 0.1066*Ile + 0.1856*Leu + 0.1875*Lys + 0.1059*Gln + 0.0145*Trp + 0.103*Pro + 0.127*Thr + 0.0839*MEETHF + 0.0766*CO2 + 0.8143*AcCoA.c + 0.04*DHAP + 0.0766*R5P + 0.0949*G6P -> Biomass	0.638	0.684	0.661
Antibody Production	Antibody	610.6*Ala + 213.6*Arg + 249.8*Asn + 323.1*Asp + 212.9*Cys + 333.2*Gln + 331*Glu + 859.2*Gly + 110.9*His + 141.8*Ile + 568*Leu + 411.8*Lys + 95.84*Met + 234.3*Phe + 597.6*Pro + 1118*Ser + 709.4*Thr + 105.3*Trp + 221.3*Tyr + 758*Val -> Antibody	1.72E-05	2.14E-05	1.93E-05

Table 3-A-5. Exchange fluxes associated with Figure 3-4a. Early exponential phase of culture. Only fluxes which could be determined are shown.

Pathway	Enzyme	Rxn	LB 95% CI	UB 95% CI	Value
Glycolysis	LDH	Lac <-> Pyr	0.0E+00	4.4E+00	2.2E+00
Amino Acid Metabolism	GLS	Gln <-> Glu	1.0E-07	9.1E-01	4.5E-01
	SHT	Ser <-> Gly + MEETHF	5.7E-01	3.1E+00	1.8E+00
	ALT	Ala + aKG + DummyaKG <-> Pyr + Glu	0.0E+00	3.0E+00	1.5E+00
	AST	OAA + Glu <-> Asp + aKG + DummyaKG	1.7E+01	5.8E+01	3.8E+01

Table 3-A-6. **Net fluxes associated with Figure 3-4b**. Late exponential phase of culture.

Pathway	Enzyme	Rxn	LB 95% CI	UB 95% CI	Value
Glycolysis	PGI	G6P <-> F6P	-2.586	0.652	-0.967
	PFK	F6P -> DHAP + GAP	0.137	1.003	0.570
	TPI	DHAP <-> GAP	0.116	0.900	0.508
	GAPDH	GAP <-> 3PG	1.526	2.273	1.899
	ENO	3PG <-> PEP	1.482	2.768	2.125
	PK	PEP -> Pyr	1.482	2.768	2.125
	LDH	Pyr <-> Lac	0.511	0.675	0.593
	HK	Glc -> G6P	1.006	1.537	1.272
PPP	6PGDH	G6P -> Ru5P + CO2	0.443	4.151	2.297
	R5PE	Ru5P <-> X5P	-0.027	2.475	1.224
	R5PI	Ru5P <-> R5P	0.163	1.316	0.739
	TK1	X5P + R5P <-> GAP + S7P	-0.014	1.237	0.612
	TK2	S7P + GAP <-> E4P + F6P	-0.014	1.237	0.612
	TK3	X5P + E4P <-> GAP + F6P	-0.014	1.237	0.612
TCA	PDH	Pyr -> AcCoA + CO2	1.308	2.181	1.744
	CS	OAA + AcCoA -> Cit	1.544	2.546	2.045
	IDH	Cit -> aKG + CO2	1.090	2.234	1.662
	ADH	aKG -> Suc + CO2	1.414	2.624	2.019
	SDH	Suc <-> Fum	1.490	2.728	2.109
	FUM	Fum <-> Mal	1.490	2.728	2.109
	MDH	Mal <-> OAA	1.212	2.557	1.884
Transport	Trp IN	Trp.e -> Trp	0.012	0.040	0.026
	Lys IN	Lys.e -> Lys	0.103	0.145	0.124
	His IN	His.e -> His	0.026	0.055	0.041
	Met IN	Met.e -> Met	0.032	0.060	0.046
	Thr IN	Thr.e -> Thr	0.076	0.107	0.092
	Phe IN	Phe.e -> Phe	0.041	0.065	0.053
	Tyr IN	Tyr.e -> Tyr	0.011	0.036	0.023
	Val IN	Val.e -> Val	0.098	0.138	0.118
	Leu IN	Leu.e -> Leu	0.161	0.167	0.164
	Ile IN	Ile.e -> Ile	0.064	0.095	0.079
	Ser IN	Ser.e -> Ser	0.123	0.159	0.141
	Ala OUT	Ala -> Ala.e	0.048	0.090	0.069
	Arg IN	Arg.e -> Arg	0.155	0.254	0.205
	Glu IN	Glu .e -> Glu	0.000	0.017	0.008
	Gln IN	Gln.e-> Gln	0.157	0.249	0.203
	Gly IN	Gly.e-> Gly	0.029	0.062	0.046
	Pro IN	Pro.e-> Pro	0.125	0.202	0.164
	Asn IN	Asn.e-> Asn	0.271	0.376	0.324

	Asp OUT	Asp -> Asp.e	0.016	0.044	0.030
	Cys IN	Cys.e -> Cys	0.051	0.080	0.065
Anaplerosis	ACL	Cit -> AcCoA.c + Mal	0.300	0.445	0.372
	ME	Mal -> Pyr + CO2	0.510	1.014	0.762
	PC	Pyr + CO2 -> OAA	0.003	0.368	0.185
Amino	ASNS	Asp <-> Asn	-0.326	-0.219	-0.272
Acid	CBXase + Mutase	ProCoA + CO2 -> Suc	0.023	0.094	0.057
Metabolism	GLS	Gln <-> Glu	0.096	0.191	0.144
	GluPro Mtbl	Glu <-> Pro	-0.137	-0.057	-0.097
	GS + SHT	CO2 + MEETHF -> Gly	0.010	0.032	0.022
	Histidase	His -> FormTHF + Glu	0.001	0.031	0.016
	Met Mtbl	Met + Ser -> Methyl + Cys + Suc	0.008	0.038	0.023
	PheTyr Mtbl	Phe -> Tyr	0.002	0.029	0.013
	SHT	Ser <-> Gly + MEETHF	0.041	0.076	0.060
	Thr Mtbl	Thr -> Pyr + CO2	0.000	0.032	0.010
	Trp Mtbl	Trp -> CO2 + CO2 + Ala + aKetoadi	0.001	0.030	0.016
	Trp2 Mtbl	aKetoadi -> CO2 + CO2 + AcCoA + AcCoA	0.010	0.072	0.041
	ALT	Ala + aKG <-> Pyr + Glu	-0.195	-0.129	-0.163
	Arg Mtbl	Arg + aKG -> Glu + Urea + Glu	0.090	0.192	0.141
	AST	OAA + Glu <-> Asp + aKG	-0.222	-0.103	-0.161
	Cys Mtbl	Cys + aKG -> Pyr + Glu	0.037	0.082	0.059
	GDH	aKG <-> Glu	-0.949	-0.406	-0.654
	Ile Mtbl	Ile + aKG -> AcCoA + CO2 + ProCoA + Glu	0.008	0.045	0.026
	Leu Mtbl	Leu + aKG + CO2 -> CO2 + AcCoA + AcCoA + AcCoA + Glu	0.044	0.082	0.061
	Lys Mtbl	Lys + aKG + aKG -> Glu + Glu + aKetoadi	0.000	0.054	0.025
	PST	3PG + Glu -> Ser + aKG	0.018	0.078	0.044
	Tyr Mtbl	Tyr + aKG -> CO2 + Mal + AcCoA + AcCoA + Glu	0.000	0.025	0.000
	Val Mtbl	Val + aKG -> Glu + CO2 + CO2 + ProCoA	0.007	0.056	0.031

Biomass Production	Biomass 329pg	0.1552*Asp + 0.127*Glu + 0.0948*Asn + 0.1451*Ser + 0.047*His + 0.2165*Gly + 0.124*Arg + 0.1974*Ala + 0.0599*Tyr + 0.0477*Cys + 0.1369*Val + 0.0454*Met + 0.0721*Phe + 0.1066*Ile + 0.1856*Leu + 0.1875*Lys + 0.1059*Gln + 0.0145*Trp + 0.103*Pro + 0.127*Thr + 0.0839*MEETHF + 0.0766*CO2 + 0.8143*AcCoA.c + 0.04*DHAP + 0.0766*R5P + 0.0949*G6P -> Biomass	0.368	0.547	0.457
Antibody Production	Antibody	610.6*Ala + 213.6*Arg + 249.8*Asn + 323.1*Asp + 212.9*Cys + 333.2*Gln + 331*Glu + 859.2*Gly + 110.9*His + 141.8*Ile + 568*Leu + 411.8*Lys + 95.84*Met + 234.3*Phe + 597.6*Pro + 1118*Ser + 709.4*Thr + 105.3*Trp + 221.3*Tyr + 758*Val -> Antibody	2.97E-05	3.62E-05	3.29E-05

Table 3-A-7. Exchange fluxes associated with Figure 3-4b. Late exponential phase of culture. Only fluxes which could be determined are shown.

Pathway	Enzyme	Rxn	LB 95% CI	UB 95% CI	Value
TCA	SDH	Suc <-> Fum	7.4E-01	9.9E+00	5.3E+00
	FUM	Fum <-> Mal	8.4E-01	1.0E+07	5.0E+06
	MDH	Mal <-> OAA	6.2E+01	1.0E+07	5.0E+06
Amino	SHT	Ser <-> Gly + MEETHF	0.088	0.4804	2.8E-01
Acid	ALT	Ala + aKG <-> Pyr + Glu	0	4.3856	2.2E+00
Metabolism	AST	OAA + Glu <-> Asp + aKG	1.9013	4.6045	3.3E+00

Table 3-A-8. **Net fluxes associated with Figure 3-4c**. Stationary phase of culture.

Pathways	Enzyme	Rxn	LB 95% CI	UB 95% CI	Value
Glycolysis	PGI	G6P <-> F6P	-1.482	1.316	-0.083
	PFK	F6P -> DHAP + GAP	0.364	1.311	0.838
	TPI	DHAP <-> GAP	0.420	1.305	0.863
	GAPDH	GAP <-> 3PG	1.629	2.610	2.119
	ENO	3PG <-> PEP	1.590	2.573	2.081
	PK	PEP -> Pyr	1.590	2.573	2.081
	HK	Glc -> G6P	1.276	1.344	1.310
	LDH	Lac <-> Pyr	0.194	0.313	0.253
PPP	6PGDH	G6P -> Ru5P + CO2	0.000	2.785	1.392
	R5PE	Ru5P <-> X5P	-0.009	1.861	0.926
	R5PI	Ru5P <-> R5P	0.008	0.821	0.415
	TK1	X5P + R5P <-> GAP + S7P	-0.005	0.931	0.463
	TK2	S7P + GAP <-> E4P + F6P	-0.005	0.931	0.463
	TK3	X5P + E4P <-> GAP + F6P	-0.005	0.931	0.463
TCA	PDH	Pyr -> AcCoA + CO2	1.763	2.670	2.216
	CS	OAA + AcCoA -> Cit	1.887	2.961	2.424
	IDH	Cit -> aKG + CO2	1.754	2.806	2.280
	ADH	aKG -> Suc + CO2	1.704	2.817	2.260
	SDH	Suc <-> Fum	1.725	2.411	2.068
	Fum	Fum <-> Mal	1.725	2.411	2.068
	MDH	Mal <-> OAA	1.794	2.847	2.321
Transport	Lys IN	Lys.e -> Lys	0.047	0.058	0.053
	Thr IN	Thr.e -> Thr	0.054	0.062	0.058
	Phe IN	Phe.e -> Phe	0.024	0.034	0.029
	Tyr IN	Tyr.e -> Tyr	0.021	0.031	0.026
	Val IN	Val.e -> Val	0.058	0.066	0.062
	Leu IN	Leu.e -> Leu	0.076	0.114	0.095
	Ile IN	Ile.e -> Ile	0.034	0.050	0.042
	Trp IN	Trp.e -> Trp	0.008	0.017	0.012
	His IN	His.e -> His	0.012	0.015	0.014
	Met IN	Met.e -> Met	0.012	0.020	0.016
	Ser IN	Ser.e -> Ser	0.074	0.090	0.082
	Ala OUT	Ala -> Ala.e	0.118	0.152	0.135
	Arg IN	Arg.e -> Arg	0.028	0.044	0.036
	Asp OUT	Asp -> Asp.e	0.074	0.097	0.085
	Cys IN	Cys.e -> Cys	0.040	0.051	0.045
	Glu OUT	Glu -> Glu.e	0.013	0.032	0.022
	Gln IN	Gln.e-> .Gln	0.041	0.084	0.062
	Gly IN	Gly.e-> Gly	0.009	0.029	0.019

	Pro IN	Pro.e-> Pro	0.029	0.060	0.044
	Asn IN	Asn.e-> Asn	0.238	0.293	0.266
Anaplerosis	ME	Mal -> Pyr + CO2	0.051	0.231	0.141
	PYC	Pyr + CO2 -> OAA	0.000	0.116	0.058
	ACL	Cit -> AcCoA.c + Mal	0.110	0.163	0.136
Amino	ASNS	Asp <-> Asn	-0.265	-0.209	-0.237
Acid	CBXase + Mutase	ProCoA + CO2 -> Suc	0.009	0.025	0.017
Metabolism	GLS	Gln <-> Glu	0.006	0.050	0.028
	GluPro Mtbl	Glu <-> Pro	-0.012	0.020	0.004
	GS + SHT	CO2 + MEETHF -> Gly	0.018	0.029	0.024
	Met Mtbl	Met + Ser -> Methyl + Cys + Suc	0.000	0.008	0.004
	PheTyr Mtbl	Phe -> Tyr	0.000	0.010	0.005
	SHT	Ser <-> Gly + MEETHF	0.031	0.044	0.038
	Thr Mtbl	Thr -> Pyr + CO2	0.000	0.003	0.001
	Trp Mtbl	Trp -> CO2 + CO2 + Ala + aKetoadi	0.000	0.009	0.005
	Trp2 Mtbl	aKetoadi -> CO2 + CO2 + AcCoA + AcCoA	0.000	0.009	0.005
	GDH	aKG <-> Glu	0.002	0.140	0.071
	ALT	Ala + aKG <-> Pyr + Glu	-0.214	-0.176	-0.195
	Ile Mtbl	Ile + aKG -> AcCoA + CO2 + ProCoA + Glu	0.009	0.025	0.017
	Leu Mtbl	Leu + aKG + CO2 -> CO2 + AcCoA + AcCoA + AcCoA + Glu	0.016	0.054	0.035
	Tyr Mtbl	Tyr + aKG -> CO2 + Mal + AcCoA + AcCoA + Glu	0.002	0.018	0.010
	AST	OAA + Glu <-> Asp + aKG	-0.140	-0.079	-0.109
	Arg Mtbl	Arg + aKG -> Glu + Urea + Glu	0.000	0.013	0.006
	PST	3PG + Glu -> Ser + aKG	0.027	0.053	0.040
	Cys Mtbl	Cys + aKG -> Pyr + Glu	0.022	0.037	0.029
Biomass Production	Biomass 329pg	0.1552*Asp + 0.127*Glu + 0.0948*Asn + 0.1451*Ser + 0.047*His + 0.2165*Gly + 0.124*Arg + 0.1974*Ala + 0.0599*Tyr + 0.0477*Cys + 0.1369*Val + 0.0454*Met + 0.0721*Phe + 0.1066*Ile + 0.1856*Leu + 0.1875*Lys + 0.1059*Gln + 0.0145*Trp + 0.103*Pro + 0.127*Thr + 0.0839*MEETHF + 0.0766*CO2 + 0.8143*AcCoA.c + 0.04*DHAP + 0.0766*R5P + 0.0949*G6P -> Biomass	0.135	0.200	0.167

Antibody Production	Antibody	610.6*Ala + 213.6*Arg + 249.8*Asn + 323.1*Asp + 212.9*Cys + 333.2*Gln + 331*Glu + 859.2*Gly + 110.9*His + 141.8*Ile + 568*Leu + 411.8*Lys + 95.84*Met + 234.3*Phe + 597.6*Pro + 1118*Ser + 709.4*Thr + 105.3*Trp + 221.3*Tyr + 758*Val -> Antibody	4.700E-05	5.580E-05	5.140E-05

Table 3-A-9. Exchange fluxes associated with Figure 3-4c. Stationary phase of culture. Only fluxes which could be determined are shown.

Pathway	Enzyme	Rxn	LB 95% CI	UB 95% CI	Value
Amino Acid Metabolism	ASNS	Asp <-> Asn	0.0E+00	7.2E+00	3.6E+00
	GLS	Gln <-> Glu	1.0E-07	3.7E+05	1.9E+05
	GluPro Mtbl	Glu <-> Pro	1.0E-07	1.4E-01	7.2E-02
	SHT	Ser <-> Gly + MEETHF	2.7E-02	1.4E-01	8.5E-02
	ALT	Ala + aKG <-> Pyr + Glu	1.0E-07	8.2E+06	4.1E+06
	AST	OAA + Glu <-> Asp + aKG	3.2E+00	7.3E+00	5.2E+00

Table 3-A-10. **Net fluxes associated with Figure 3-4d**. Decline phase of culture.

Pathways	Enzyme	Rxn	LB 95% CI	UB 95% CI	Value
Glycolysis	PGI	G6P <-> F6P	-0.263	1.144	0.441
	PFK	F6P -> DHAP + GAP	0.479	1.144	0.811
	TPI	DHAP <-> GAP	0.479	1.144	0.811
	GAPDH	GAP <-> 3PG	1.215	2.288	1.752
	Eno	3PG <-> PEP	1.201	2.276	1.738
	PK	PEP -> Pyr	1.201	2.276	1.738
	LDH	Pyr <-> Lac	0.282	0.487	0.384
	HK	Glc -> G6P	0.730	1.146	0.938
PPP	6PGDH	G6P -> Ru5P + CO2	0.000	1.302	0.651
	R5PE	Ru5P <-> X5P	0.000	0.868	0.434
	R5PI	Ru5P <-> R5P	0.000	0.434	0.217
	TK1	X5P + R5P <-> GAP + S7P	0.000	0.434	0.217
	TK2	S7P + GAP <-> E4P + F6P	0.000	0.434	0.217
	TK3	X5P + E4P <-> GAP + F6P	0.000	0.434	0.217
TCA	PDH	Pyr -> AcCoA + CO2	0.748	1.879	1.314
	CS	OAA + AcCoA -> Cit	0.809	1.998	1.404
	IDH	Cit -> aKG + CO2	0.809	1.998	1.403
	ADH	aKG -> Suc + CO2	0.787	1.993	1.390
	SDH	Suc <-> Fum	0.796	2.006	1.401
	Fum	Fum <-> Mal	0.796	2.006	1.401
	MDH	Mal <-> OAA	0.713	1.892	1.302
Transport	Trp IN	Trp.e -> Trp	0.003	0.005	0.004
	Lys IN	Lys.e -> Lys	0.012	0.038	0.025
	His IN	His.e -> His	0.003	0.012	0.008
	Met IN	Met.e -> Met	0.003	0.011	0.007
	Thr IN	Thr.e -> Thr	0.021	0.042	0.031
	Phe IN	Phe.e -> Phe	0.007	0.022	0.015
	Tyr IN	Tyr.e -> Tyr	0.011	0.023	0.017
	Val IN	Val.e -> Val	0.020	0.048	0.034
	Leu IN	Leu.e -> Leu	0.016	0.065	0.041
	Ile IN	Ile.e -> Ile	0.004	0.028	0.016
	Ser IN	Ser.e -> Ser	0.019	0.049	0.034
	Ala OUT	Ala -> Ala.e	0.116	0.199	0.157
	Arg IN	Arg.e -> Arg	0.006	0.023	0.015
	Glu OUT	Glu -> Glu.e	0.015	0.042	0.028
	Gln IN	Gln.e -> Gln	0.001	0.067	0.034
	Gly IN	Gly.e -> Gly	0.000	0.035	0.017
	Pro IN	Pro.e -> Pro	0.000	0.049	0.025
	Asn IN	Asn.e -> Asn	0.169	0.277	0.223

	Asp OUT	Asp -> Asp.e	0.069	0.131	0.100
	Cys IN	Cys.e -> Cys	0.026	0.040	0.033
Anaplerosis	ACL	Cit -> AcCoA.c + Mal	0.000	0.001	0.001
	ME	Mal -> Pyr + CO2	0.027	0.201	0.114
	PC	Pyr + CO2 -> OAA	0.000	0.053	0.027
Amino	ASNS	Asp <-> Asn	-0.268	-0.160	-0.214
Acid	CBXase + Mutase	ProCoA + CO2 -> Suc	0.000	0.035	0.017
Metabolism	GLS	Gln <-> Glu	-0.011	0.055	0.022
	GluPro Mtbl	Glu <-> Pro	-0.028	0.024	-0.002
	GS + SHT	CO2 + MEETHF -> Gly	0.000	0.018	0.009
	Histidase	His -> FormTHF + Glu	0.000	0.008	0.004
	Met Mtbl	Met + Ser -> Methyl + Cys + Suc	0.000	0.008	0.004
	PheTyr Mtbl	Phe -> Tyr	0.000	0.014	0.007
	SHT	Ser <-> Gly + MEETHF	0.000	0.018	0.009
	Thr Mtbl	Thr -> Pyr + CO2	0.000	0.018	0.009
	GDH	aKG <-> Glu	-0.093	0.140	0.023
	ALT	Ala + aKG <-> Pyr + Glu	-0.221	-0.137	-0.179
	Ile Mtbl	Ile + aKG -> AcCoA + CO2 + ProCoA + Glu	0.000	0.023	0.012
	Leu Mtbl	Leu + aKG + CO2 -> CO2 + AcCoA + AcCoA + AcCoA + Glu	0.000	0.045	0.023
	Tyr Mtbl	Tyr + aKG -> CO2 + Mal + AcCoA + AcCoA + Glu	0.004	0.025	0.015
	Val Mtbl	Val + aKG -> Glu + CO2 + CO2 + ProCoA	0.000	0.022	0.011
	Lys Mtbl	Lys + aKG + aKG -> Glu + Glu + aKetoadi	0.000	0.024	0.012
	AST net	OAA + Glu <-> Asp + aKG	-0.163	-0.038	-0.101
	Arg Mtbl	Arg + aKG -> Glu + Urea + Glu	0.000	0.016	0.008
	PST	3PG + Glu -> Ser + aKG	0.002	0.037	0.020
	Cys Mtbl	Cys + aKG -> Pyr + Glu	0.018	0.037	0.027
	Lys Mtbl2	aKetoadi -> CO2 + CO2 + AcCoA + AcCoA	0.000	0.024	0.012

Biomass Production	Biomass 329pg	0.1552*Asp + 0.127*Glu + 0.0948*Asn + 0.1451*Ser + 0.047*His + 0.2165*Gly + 0.124*Arg + 0.1974*Ala + 0.0599*Tyr + 0.0477*Cys + 0.1369*Val + 0.0454*Met + 0.0721*Phe + 0.1066*Ile + 0.1856*Leu + 0.1875*Lys + 0.1059*Gln + 0.0145*Trp + 0.103*Pro + 0.127*Thr + 0.0839*MEETHF + 0.0766*CO2 + 0.8143*AcCoA.c + 0.04*DHAP + 0.0766*R5P + 0.0949*G6P -> Biomass	0.000	0.001	0.001
Antibody Production	Antibody	610.6*Ala + 213.6*Arg + 249.8*Asn + 323.1*Asp + 212.9*Cys + 333.2*Gln + 331*Glu + 859.2*Gly + 110.9*His + 141.8*Ile + 568*Leu + 411.8*Lys + 95.84*Met + 234.3*Phe + 597.6*Pro + 1118*Ser + 709.4*Thr + 105.3*Trp + 221.3*Tyr + 758*Val -> Antibody	2.7E-05	4.4E-05	3.6E-05

Table 3-A-11. Exchange fluxes associated with Figure 3-4d. Decline phase of culture. Only fluxes which could be determined are shown.

Pathway	Enzyme	Rxn	LB 95% CI	UB 95% CI	Value
Amino	ASNS	Asp <-> Asn	0.0E+00	1.6E+00	8.2E-01
Acid	SHT	Ser <-> Gly + MEETHF	2.9E-03	1.9E-01	9.6E-02
Metabolism	GDH	aKG <-> Glu	1.0E-07	3.7E+00	1.9E+00
	ALT	Ala + aKG <-> Pyr + Glu	0.0E+00	3.7E+00	1.9E+00
	AST	OAA + Glu <-> Asp + aKG	4.0E-02	4.7E-01	2.5E-01

References

[1] W. S. Ahn and M. R. Antoniewicz, "Towards dynamic metabolic flux analysis in CHO cell cultures.," *Biotechnol. J.*, vol. 7, no. 1, pp. 61–74, Jan. 2012.

[2] G. Seth, P. Hossler, J. Chong, and Y. W. Hu, "Engineering Cells for Cell Culture Bioprocessing – Physiological Fundamentals," *Adv Biochem Engin/Biotechnol*, vol. 101, no. June, pp. 119–164, 2006.

[3] G. B. Nyberg, R. R. Balcarcel, B. D. Follstad, G. Stephanopoulos, and D. I. Wang, "Metabolism of peptide amino acids by Chinese hamster ovary cells grown in a complex medium.," *Biotechnol. Bioeng.*, vol. 62, no. 3, pp. 324–35, Feb. 1999.

[4] H. A. Hansen and C. Emborg, "Influence of ammonium on growth, metabolism, and productivity of a continuous suspension Chinese hamster ovary cell culture.," *Biotechnol. Prog.*, vol. 10, no. 1, pp. 121–124, 1994.

[5] R. P. Nolan and K. Lee, "Dynamic model of CHO cell metabolism.," *Metab. Eng.*, vol. 13, no. 1, pp. 108–24, Jan. 2011.

[6] J. R. Birch and A. J. Racher, "Antibody production," *Adv. Drug Deliv. Rev.*, vol. 58, no. 5–6, pp. 671–685, Aug. 2006.

[7] C. Altamirano, C. Paredes, a Illanes, J. J. Cairó, and F. Gòdia, "Strategies for fed-batch cultivation of t-PA producing CHO cells: substitution of glucose and glutamine and rational design of culture medium.," *J. Biotechnol.*, vol. 110, no. 2, pp. 171–9, May 2004.

[8] K. F. Wlaschin and W. Hu, "Fedbatch Culture and Dynamic Nutrient Feeding," *Adv. Biochem. Eng.*, no. 101, pp. 43–74, 2006.

[9] T. Omasa, K. Higashiyama, S. Shioya, and K. Suga, "Effects of lactate concentration on hybridoma culture in lactate-controlled fed-batch operation.," *Biotechnol. Bioeng.*, vol. 39, no. 5, pp. 556–64, Mar. 1992.

[10] C. Altamirano, A. Illanes, S. Becerra, J. J. Cairó, and F. Gòdia, "Considerations on the lactate consumption by CHO cells in the presence of galactose.," *J. Biotechnol.*, vol. 125, no. 4, pp. 547–56, Oct. 2006.

[11] M. B. Fogolín, R. Wagner, M. Etcheverrigaray, and R. Kratje, "Impact of temperature reduction and expression of yeast pyruvate carboxylase on hGM-CSF-producing CHO cells.," *J. Biotechnol.*, vol. 109, no. 1–2, pp. 179–91, Apr. 2004.

[12] H. Dorai, Y. S. Kyung, D. Ellis, C. Kinney, C. Lin, D. Jan, G. Moore, and M. J. Betenbaugh, "Expression of anti-apoptosis genes alters lactate metabolism of Chinese

Hamster Ovary cells in culture.," *Biotechnol. Bioeng.*, vol. 103, no. 3, pp. 592–608, Jun. 2009.

[13] Z. Xing, B. Kenty, I. Koyrakh, M. Borys, S.-H. Pan, and Z. J. Li, "Optimizing amino acid composition of CHO cell culture media for a fusion protein production," *Process Biochem.*, vol. 46, no. 7, pp. 1423–1429, Jul. 2011.

[14] C. T. Goudar, R. Biener, K. B. Konstantinov, and J. M. Piret, "Error Propagation from Prime Variables into Specific Rates and Metabolic Fluxes for Mammalian Cells in Perfusion Culture," *Biotechnol. Prog.*, vol. 25, no. 4, pp. 986–998, 2009.

[15] L.-E. Quek, S. Dietmair, J. O. Krömer, and L. K. Nielsen, "Metabolic flux analysis in mammalian cell culture.," *Metab. Eng.*, vol. 12, no. 2, pp. 161–71, Mar. 2010.

[16] W. S. Ahn and M. R. Antoniewicz, "Metabolic flux analysis of CHO cells at growth and non-growth phases using isotopic tracers and mass spectrometry.," *Metab. Eng.*, vol. 13, no. 5, pp. 598–609, Sep. 2011.

[17] C. Goudar, R. Biener, C. Boisart, R. Heidemann, J. Piret, A. de Graaf, and K. Konstantinov, "Metabolic flux analysis of CHO cells in perfusion culture by metabolite balancing and 2D [13C, 1H] COSY NMR spectroscopy.," *Metab. Eng.*, vol. 12, no. 2, pp. 138–49, Mar. 2010.

[18] N. Sengupta, S. T. Rose, and J. a Morgan, "Metabolic flux analysis of CHO cell metabolism in the late non-growth phase.," *Biotechnol. Bioeng.*, vol. 108, no. 1, pp. 82–92, Jan. 2011.

[19] J. Dean and P. Reddy, "Metabolic analysis of antibody producing CHO cells in fed-batch production.," *Biotechnol. Bioeng.*, vol. 110, no. 6, pp. 1735–1747, Jan. 2013.

[20] J. T. Dean, L. Tran, S. Beaven, P. Tontonoz, K. Reue, K. M. Dipple, and J. C. Liao, "Resistance to diet-induced obesity in mice with synthetic glyoxylate shunt.," *Cell Metab.*, vol. 9, no. 6, pp. 525–36, Jun. 2009.

[21] S. S. Ozturk and B. O. Palsson, "Chemical decomposition of glutamine in cell culture media: effect of media type, pH, and serum concentration.," *Biotechnol. Prog.*, vol. 6, no. 2, pp. 121–8, 1990.

[22] M. W. Glacken, E. Adema, and a J. Sinskey, "Mathematical descriptions of hybridoma culture kinetics: I. Initial metabolic rates.," *Biotechnol. Bioeng.*, vol. 32, no. 4, pp. 491–506, Aug. 1988.

[23] R. Deshpande, T. H. Yang, and E. Heinzle, "Towards a metabolic and isotopic steady state in CHO batch cultures for reliable isotope-based metabolic profiling.," *Biotechnol. J.*, vol. 4, no. 2, pp. 247–63, Feb. 2009.

[24] C. M. Metallo, J. L. Walther, and G. Stephanopoulos, “Evaluation of 13C isotopic tracers for metabolic flux analysis in mammalian cells.,” *J. Biotechnol.*, vol. 144, no. 3, pp. 167–74, Nov. 2009.

[25] M. Möllney, W. Wiechert, D. Kownatzki, and a a de Graaf, “Bidirectional reaction steps in metabolic networks: IV. Optimal design of isotopomer labeling experiments.,” *Biotechnol. Bioeng.*, vol. 66, no. 2, pp. 86–103, Jan. 1999.

[26] S. Dietmair, N. E. Timmins, P. P. Gray, L. K. Nielsen, and J. O. Krömer, “Towards quantitative metabolomics of mammalian cells: development of a metabolite extraction protocol.,” *Anal. Biochem.*, vol. 404, no. 2, pp. 155–64, Sep. 2010.

[27] C. a Sellick, R. Hansen, A. R. Maqsood, W. B. Dunn, G. M. Stephens, R. Goodacre, and A. J. Dickson, “Effective quenching processes for physiologically valid metabolite profiling of suspension cultured Mammalian cells.,” *Anal. Chem.*, vol. 81, no. 1, pp. 174–83, Jan. 2009.

[28] J. Folch, M. Lees, and G. H. S. Stanley, “A simple method for the isolation and purification of total lipides from animal tissues,” *J. Biol. Chem.*, vol. 226, no. 1, pp. 497–509, Aug. 1957.

[29] M. R. Antoniewicz, J. K. Kelleher, and G. Stephanopoulos, “Elementary metabolite units (EMU): a novel framework for modeling isotopic distributions.,” *Metab. Eng.*, vol. 9, no. 1, pp. 68–86, Jan. 2007.

[30] H. P. Bonarius, B. Timmerarends, C. D. de Gooijer, and J. Tramper, “Metabolite-balancing techniques vs. 13C tracer experiments to determine metabolic fluxes in hybridoma cells.,” *Biotechnol. Bioeng.*, vol. 58, no. 2–3, pp. 258–62, 1998.

[31] K. Sheikh, J. Fo, and L. K. Nielsen, “Modeling Hybridoma Cell Metabolism Using a Generic Genome-Scale Metabolic Model of Mus musculus,” *Biotechnol. Prog.*, vol. 21, no. 1, pp. 112–121, 2005.

[32] M. R. Antoniewicz, J. K. Kelleher, and G. Stephanopoulos, “Determination of confidence intervals of metabolic fluxes estimated from stable isotope measurements.,” *Metab. Eng.*, vol. 8, no. 4, pp. 324–37, Jul. 2006.

[33] B. D. Follstad, “Personal Communication.” 2012.

[34] R. J. DeBerardinis, A. Mancuso, E. Daikhin, I. Nissim, M. Yudkoff, S. Wehrli, and C. B. Thompson, “Beyond aerobic glycolysis: transformed cells can engage in glutamine metabolism that exceeds the requirement for protein and nucleotide synthesis.,” *Proc. Natl. Acad. Sci. U. S. A.*, vol. 104, no. 49, pp. 19345–50, Dec. 2007.

[35] M. E. Smoot, K. Ono, J. Ruscheinski, P.-L. Wang, and T. Ideker, “Cytoscape 2.8: new features for data integration and network visualization.,” *Bioinformatics*, vol. 27, no. 3, pp. 431–2, Feb. 2011.

[36] J. Li, C. L. Wong, N. Vijayasankaran, T. Hudson, and A. Amanullah, “Feeding lactate for CHO cell culture processes: Impact on culture metabolism and performance.,” *Biotechnol. Bioeng.*, vol. 109, no. 5, pp. 1173–86, May 2012.

[37] R. J. DeBerardinis, J. J. Lum, G. Hatzivassiliou, and C. B. Thompson, “The biology of cancer: metabolic reprogramming fuels cell growth and proliferation.,” *Cell Metab.*, vol. 7, no. 1, pp. 11–20, Jan. 2008.

[38] R. J. Shaw, “Glucose metabolism and cancer.,” *Curr. Opin. Cell Biol.*, vol. 18, no. 6, pp. 598–608, Dec. 2006.

[39] M. G. Vander Heiden, L. C. Cantley, and C. B. Thompson, “Understanding the Warburg effect: the metabolic requirements of cell proliferation.,” *Science*, vol. 324, no. 5930, pp. 1029–33, May 2009.

[40] L. Xie and D. I. Wang, “Material balance studies on animal cell metabolism using a stoichiometrically based reaction network.,” *Biotechnol. Bioeng.*, vol. 52, no. 5, pp. 579–90, Dec. 1996.

[41] B. Halliwell, “Oxidative stress in cell culture: an under-appreciated problem?,” *FEBS Lett.*, vol. 540, no. 1–3, pp. 3–6, Apr. 2003.

[42] R. Scherz-Shouval and Z. Elazar, “ROS, mitochondria and the regulation of autophagy.,” *Trends Cell Biol.*, vol. 17, no. 9, pp. 422–7, Sep. 2007.

[43] F. Hyder, J. R. Chase, K. L. Behar, G. F. Mason, M. Siddeek, D. L. Rothman, and R. G. Shulman, “Increased tricarboxylic acid cycle flux in rat brain during forepaw stimulation detected with 1H[13C]NMR.,” *Proc. Natl. Acad. Sci. U. S. A.*, vol. 93, no. 15, pp. 7612–7, Jul. 1996.

[44] S. Hammond, M. Kaplarevic, N. Borth, M. J. Betenbaugh, and K. H. Lee, “Chinese hamster genome database: an online resource for the CHO community at www.CHOgenome.org.,” *Biotechnol. Bioeng.*, vol. 109, no. 6, pp. 1353–6, Jun. 2012.

IV: THE IMPACT OF ANTI-APOPTOTIC GENE BCL-2Δ EXPRESSION ON CHO CENTRAL METABOLISM

Metabolic Engineering. 25 (2014) 92-102.

Abstract

Anti-apoptosis engineering is an established technique to prolong the viability of mammalian cell cultures used for industrial production of recombinant proteins. However, the effect of overexpressing anti-apoptotic proteins on central carbon metabolism has not been systematically studied. We transfected CHO-S cells to express Bcl-2Δ, an engineered anti-apoptotic gene, and selected clones that differed in their Bcl-2Δ expression and caspase activity. ^{13}C metabolic flux analysis (MFA) was then applied to elucidate the metabolic alterations induced by Bcl-2Δ. Expression of Bcl-2Δ reduced lactate accumulation by redirecting the fate of intracellular pyruvate toward mitochondrial oxidation during the lactate-producing phase, and it significantly increased lactate re-uptake during the lactate-consuming phase. This flux redistribution was associated with significant increases in biomass yield, peak viable cell density (VCD), and integrated VCD. Additionally, Bcl-2Δ expression was associated with significant increases in isocitrate dehydrogenase and NADH oxidase activities, both rate-controlling mitochondrial enzymes. This is the first comprehensive ^{13}C MFA study to demonstrate that expression of anti-apoptotic genes has a significant impact on intracellular metabolic fluxes, especially in controlling the fate of pyruvate carbon, which has important biotechnology applications for reducing lactate accumulation and enhancing productivity in mammalian cell cultures.

Introduction

Chinese hamster ovary (CHO) cells have emerged as the most widely used mammalian cell line for recombinant protein production, accounting for nearly 70% of all biotherapeutics produced in what is approaching a $100 billion global marketplace [1,2]. This biologics market is growing at a rate 60% faster than the overall pharmaceutical market [2]. Some of the major advantages of CHO cells are their ability to secrete correctly folded and post-translationally modified recombinant proteins and their proven history of regulatory approval [3]. Increasing demand for biopharmaceutical products requires CHO hosts and culture systems to become more productive, as the costs associated with producing sufficient antibody to conduct clinical trials can account for a substantial portion of the total drug development cost [4,5]. Failure of the scientific community to develop rational approaches for increasing product titer and yield will result in high development costs that stymie both drug discovery and drug affordability.

Manipulating apoptotic pathways is one route that has been used to improve recombinant protein titers. After all, volumetric protein productivity is directly proportional to the integrated viable cell density (IVCD) of the culture [6], and apoptosis accounts for up to 80% of cell death in a typical bioreactor run [7]. Overexpressing anti-apoptotic genes, such as Bcl-2 or Bcl-xL, to limit the progression of apoptosis was shown to be effective at maintaining cell viability in response to a variety of adverse bioreactor conditions [8–12]. More recently, CHO cells overexpressing anti-apoptotic genes E1B-19K, Aven, and an XIAP mutant (XIAPΔ) provided a 60% increase in IVCD and 80% increase in final product titer [13]. Interestingly, the apoptosis-resistant clones were also found to accumulate less lactate during early-exponential phase and to be capable of faster lactate consumption during late-exponential and stationary phases [13]. This is a highly desirable trait for industrial bioprocesses, as a shift to lactate consumption during

production phase was found to be a prominent feature of high-titer runs identified through data-mining of 243 production trains at Genentech's Vacaville manufacturing facility [14]. Although it is known that proteins involved in apoptosis regulation may impinge on processes that control mitochondrial energy metabolism [15], the effects of these proteins on intracellular metabolic pathways have not been directly studied.

Several alternative approaches have been applied to directly engineer pathways involved in lactate production and energy metabolism, which have been summarized in a recent review [16]. These studies rely on quantitative analysis of cellular metabolic phenotypes to determine the impact of these genetic manipulations on carbon fluxes. For example, stoichiometric analysis involves the application of mass balances to determine the specific rates and relative ratios of extracellular metabolite transport [17]. This can be useful for assessing nutrient uptake and product excretion by cell cultures. ^{13}C metabolic flux analysis (MFA), on the other hand, leverages this stoichiometric information and combines it with ^{13}C labeling measurements to calculate intracellular metabolic fluxes. ^{13}C MFA has been previously used to map fluxes in both exponential [18,19] and stationary phase [18–20] CHO cultures. However, its application to quantify metabolic alterations in apoptosis-resistant cell lines has not been explored.

In this study, we performed ^{13}C labeling experiments and MFA on a commercially available CHO-S cell line and two apoptosis-resistant clones that were obtained by transfecting the parent CHO-S line with the engineered anti-apoptotic protein Bcl-2Δ. The two clones significantly differed in their level of Bcl-2Δ expression and caspase 3/7 activation. We observed significant rewiring of pyruvate metabolism in both Bcl-2Δ clones, with more pyruvate carbon directed toward mitochondrial oxidation rather than lactate production during the initial phase of growth. This shift in pyruvate metabolism correlated directly with the level of Bcl-2Δ

expression observed in each clone. It was also associated with an increase in carbon allocation to biomass relative to lactate in the Bcl-2Δ clones. Eventually, all three cultures shifted from lactate production to consumption, but the apoptosis-resistant clone with the highest Bcl-2Δ expression consumed lactate at an elevated rate compared to the untransfected control. Both Bcl-2Δ clones also exhibited increased activity of mitochondrial enzymes involved in the TCA cycle and oxidative phosphorylation, which may be partially responsible for the observed changes in flux. To our knowledge, this is the first ^{13}C MFA study to quantify the metabolic impacts of anti-apoptosis engineering, enabling a closer examination of the regulatory connections between metabolic and apoptotic pathways.

Materials and Methods

Clone generation

A parent CHO-S cell line (Life Technologies, Carlsbad, CA) was transfected with plasmid DNA containing a G418 antibiotic resistance marker to constitutively express Bcl-2Δ. A human CMV promoter was used to achieve high expression of Bcl-2Δ. Plasmid construction was previously described [21]. Following G418 selection, approximately 200 clonal populations were generated, and two clones were chosen for further study based upon caspase-3/7 activity. The highest Bcl-2Δ expressing clone (with the lowest caspase-3/7 activity) was designated as the "High-Expressing" (HE) clone, while another clone with moderate caspase activity and less Bcl-2Δ expression was designated as the "Low-Expressing" (LE) clone. The untransfected CHO-S parent was designated as the "Control" line.

Cell culture

Batch cultures were grown in 125 mL shake flasks at a working volume of 50 mL, using an orbital shaker (145 RPM, 0.45 RCF) inside a humidified incubator maintained at 37°C and 10% CO_2. Cultures were inoculated at 3 x 10^5 cells/mL and supplied glucose-free CD-CHO media (Life Technologies, Carlsbad, CA) supplemented with 50 mM glucose and 4 mM glutamine. All growth experiments were carried out for 10 days following inoculation with five separate replicates (N=5).

Caspase 3/7 activity assay

The Apo-ONE homogeneous caspase-3/7 assay (Promega, Madison, WI) was used to assess caspase-3/7 activity. Caspase activity was measured at days 5 and 8 of culture. Cell samples were exposed to rhodamine and lysis buffer for 2 hours inside a 37°C humidified incubator, shaken at 0.08 RCF (155 RPM) on a microplate orbital shaker. Measurements were promptly recorded using a fluorescence plate reader.

Determination of extracellular exchange rates

Culture samples were collected 2-3 times daily for measurement of specific growth rate and extracellular exchange rates. Viable cell density (VCD) was immediately determined using a trypan blue exclusion method with a Cedex XS automated counter (Roche, Basel, Switzerland). The remainder of the sample was promptly frozen. Glucose and lactate concentrations were determined in culture supernatants using a YSI 2300 biochemical analyzer (YSI, Yellow Springs,

OH). Amino acid concentrations were determined using an Agilent 1200 series high performance liquid chromatograph (HPLC). To accurately quantify amino acid concentrations using ultraviolet (UV) absorbance detection, pre-injection derivatization with orthophthaldildehyde (OPA) was used, as described previously [22].

The net specific growth rate (μ_{net}), specific death rate (k_d), and gross growth rate (μ_g) were determined by regressing the viable cell density (X) and dead cell density (X_d) measurements using the following equations:

$$\frac{dX}{dt} = \mu_{net} X \quad (4\text{-}1)$$

$$\frac{dX_d}{dt} = k_d X \quad (4\text{-}2)$$

$$\mu_{net} = \mu_g - k_d \quad (4\text{-}3)$$

The specific production rate of extracellular metabolites was determined by regressing the concentration measurements using the following equation:

$$\frac{dC_i}{dt} = q_i X - k_i C_i \quad (4\text{-}4)$$

Here, C_i represents the concentration of the ith measured metabolite, q_i represents its specific production rate (negative if consumed), and k_i is its first-order degradation constant. The only component with a non-negligible chemical degradation rate was glutamine, and its half-life was found to be ~8 days. Regression analysis was performed using the ETA software package [23].

Determination of integrated viable cell density

IVCD was determined by trapezoidal integration of the entire measured growth curve, using the following formula:

$$IVCD = \sum_{i=0}^{n} \left[(t_{i+1} - t_i) \left(\frac{X_{i+1} + X_i}{2} \right) \right] \qquad (4\text{-}5)$$

where *X* is viable cell density, *t* is time, and *n* is the total number of VCD measurements.

Isotope labeling experiments

To initiate isotope labeling experiments, cells were centrifuged, washed, and resuspended in CD-CHO media supplemented with a mixture of 50% [1,2-$^{13}C_2$]glucose and 50% [U-$^{13}C_6$]glucose at a total glucose concentration of 50 mM. A minimum of 2.7 days were allowed prior to sampling, as we have previously found that isotopic steady state is achieved in CHO cells after ~2 days of glucose labeling under similar culture conditions (data not shown). Cell culture samples containing approximately 10 million cells were removed and rapidly cold-quenched using a solution of 60% methanol and 40% aqueous ammonium bicarbonate (AMBIC, 0.85% w/v) pre-cooled to -40°C [24]. Cell pellets were extracted using a biphasic chloroform:methanol:water (8:4:3) solution immediately following removal of the quenching solution [25]. Polar metabolites were recovered in the methanol/water phase.

Gas chromatography mass spectrometry (GCMS) analysis

Evaporated polar samples were derivatized as described previously [19] and injected into an Agilent 7890 gas chromatograph equipped with a HP5-MS column (30m x 0.25mm i.d. x

0.25µm; Agilent J&W Scientific). Injection volume was varied between 0.2-2µL, and purge times between 30-60 seconds were used to obtain acceptable signal-to-noise ratios for each fragment ion. The GC outlet was fixed at 270°C, and helium flow rate was 1 mL/min. The GC oven was initially set at 80°C and held for 5 minutes, ramped at 20°C/min to 140°C, ramped at 4°C/min to 280°C, and held for 5 minutes. Scan mode allowed all mass spectra between 100-500 m/z to be recorded, and raw ion chromatograms were integrated using a custom MATLAB program which applied consistent integration bounds and baseline corrections to each fragment ion [26].

Reaction network

A reaction network was generated that included all major pathways of central carbon metabolism: glycolysis, pentose phosphate pathway (PPP), TCA cycle, anaplerotic/cataplerotic reactions, amino acid catabolic/anabolic reactions, and a lumped growth reaction. We used the cell composition values from Sheikh et al. [27] and determined cell dry weight to be 398, 361, and 343 pg/cell for the control, LE, and HE clone, respectively. This allowed the metabolite yield coefficients included in the lumped growth reaction to be identified [19]. Carbon atom transitions and subcellular compartmentation were specified for all reactions. ATP and NAD(P)H balances were not included in the reaction network [28]. In total, there were 116 reactions (including reversible reactions) in the network, 21 extracellular metabolites, and one macromolecular product (biomass). Refer to the supplementary material for a detailed description of the reaction network and modeling assumptions.

13C metabolic flux analysis (MFA)

The INCA analysis platform was used to generate mass balances and isotopomer balances required to simulate ^{13}C labeling within CHO central carbon metabolism [29] (accessible at http://mfa.vueinnovations.com/mfa). INCA applies an elementary metabolite unit (EMU) decomposition of the reaction network to efficiently simulate the effects of varying fluxes on the labeling of measurable metabolites [26,30]. We assumed that both metabolic and isotopic quasi-steady-state was obtained during the isotope labeling experiments. Metabolic fluxes were estimated by regression of experimentally determined mass isotopomer distributions (MIDs) and extracellular exchange rates using a Levenberg-Marquardt optimization algorithm. Flux estimation was repeated a minimum of 100 times from random initial values to ensure a global minimum was obtained. All results were subjected to a chi-square statistical test to assess goodness-of-fit, and accurate 95% confidence intervals were computed for all flux parameters by evaluating the sensitivity of the sum-of-squared residuals to parameter variations [31]. To effectively visualize the reaction network, flux maps were generated using Cytoscape [32] (accessible at http://www.cytoscape.org).

Enzyme activity assays

An isocitrate dehydrogenase (IDH) assay kit (Abcam, Cambridge, MA) was used to measure NAD^+ dependent IDH activity of whole CHO cells according to the manufacturer's instructions. Standards and samples were colorimetrically assayed on clear 96-well plates using a Genios plate reader (TECAN, Durham, NC) at 450 nm. A chemiluminescence assay was used to measure Complex I (NADH oxidase) activity in whole CHO cells harvested in PBS. Suspended cells ($5\text{-}6\times10^5$ cells per well) were placed on white 96-well plates in a solution

containing PBS and 20 μM lucigenin. Luminescence was monitored for 5 min using a VICTOR3 plate reader (Perkin-Elmer, Waltham, MA) to establish a baseline reading. Following stimulation with 45 μM NADH, luminescence was monitored for an additional 60 min.

Western blot

Whole cell protein lysates were collected in RIPA buffer. Following quantification of total protein concentration, 26 μg of total protein was loaded into a 4-20% Tris-HCl gel (Bio-Rad, Hercules, CA). Following electrophoresis and transfer, the membrane was blocked for 100 min with 5% non-fat milk. Next, the membrane was incubated with a Bcl-2 primary antibody that bound to both endogenous Bcl-2 and Bcl-2Δ (Santa Cruz Biotechnology, Santa Cruz, CA). Tubulin was used as a loading control. Incubation with primary antibody was performed at 1:900 (rabbit Bcl-2) and 1:6000 (mouse Tubulin) concentration in 5% non-fat milk for 60 min at room temperature. Incubation with a HRP-labeled secondary antibody (Perkin-Elmer, Waltham, MA) followed, and was performed at 1:1800 (anti-rabbit) and 1:3000 (anti-mouse) concentration in 5% non-fat milk for 60 min at room temperature. To visualize the bands through chemiluminescence, Western Lightning Plus ECL (Perkin Elmer, Waltham, MA) was used. Image quantification of the blots was performed using ImageJ [33].

Subcellular localization of Bcl-2 and Bcl-2Δ

Mitochondria-associated endoplasmic reticulum membrane (MAM) samples were prepared as described previously [34]. Following homogenization of the cultures grown on 15-cm dishes, the nuclear/whole cell (P1), crude mitochondrial, and microsomal fractions (P3) were

prepared by differential centrifugation. Supernatants were collected as the cytosolic fraction. The crude mitochondrial fraction in isolation buffer (250 mM mannitol, 5 mM HEPES, 0.5 mM EGTA, pH 7.4) was subjected to Percoll gradient centrifugation for separation of the MAM from mitochondria. Once all fractions were collected, samples were boiled in 2X sample buffer and analyzed by SDS-PAGE and western blotting.

Statistical analysis

One-way ANOVA was used to compare the Control, LE, and HE cell lines. If significance was found (α=0.05), we applied a Tukey-Kramer test to identify significant differences in mean values. If significance was not found at α=0.05, we proceeded to test at α=0.1, as noted in the figures.

Results

Clone selection

Two Bcl-2Δ expressing clones were selected that exhibited varying levels of apoptotic resistance based on a screen for caspase-3/7 activity (Figure 4-1a).

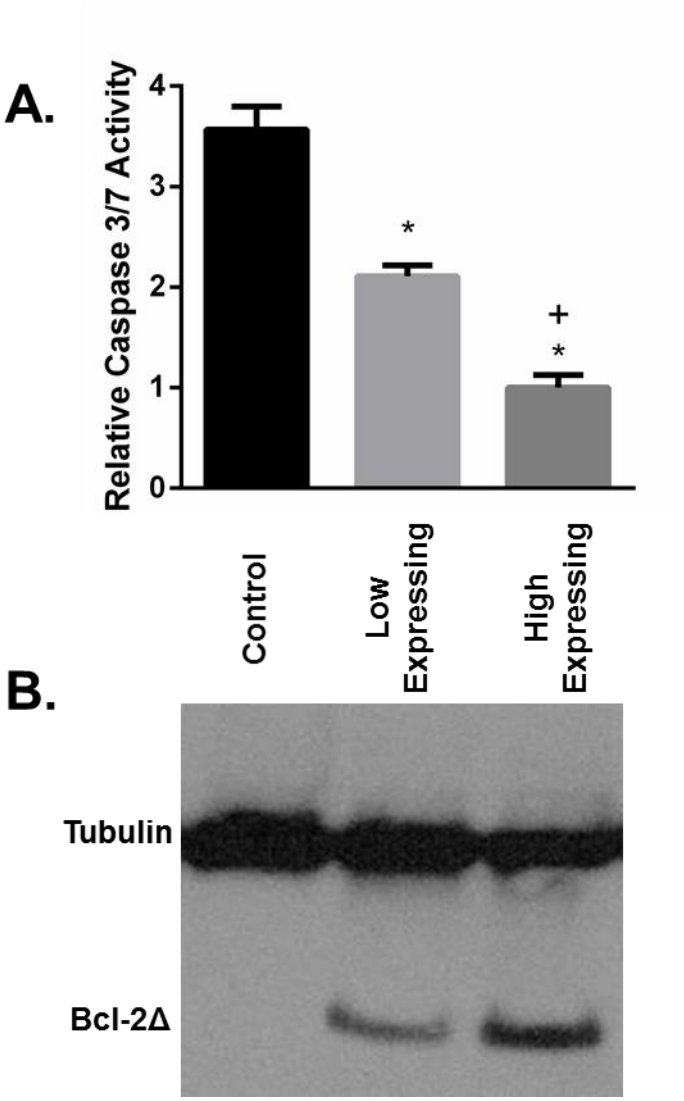

Figure 4-1. The relationship of caspase 3/7 activity and Bcl-2Δ expression. A. Caspase activity at day 5 of culture. Standard deviation is reported. * Indicates statistically significant difference compared to the control (p=0.05). + Indicates statistically significant difference between Low Expressing and High Expressing clones (p=0.05). **B.** Western blot for Bcl-2Δ at day 5 of culture. The primary antibody bound to both endogenous Bcl-2 and engineered Bcl-2Δ. Bcl-2Δ expression was substantially greater than Bcl-2, explaining why only one band was visible. For further confirmation of Bcl-2/Bcl-2Δ expression level, refer to Supplemental Figure 4-A-1.

Both clones exhibited significantly reduced caspase-3/7 activity compared to the untransfected control line at day 5 of culture. Western blot analysis revealed that Bcl-2Δ expression was

significantly increased in the high-expressing (HE) clone, roughly double that of the low-expressing (LE) clone (Figure 4-1b). This result corroborated the result of Figure 4-1a, as the HE clone had roughly half the caspase-3/7 activity of the LE clone at the same time point. Increased expression of the endogenous Bcl-2 protein was observed in the LE clone, but the expression level was substantially less than that of Bcl-2Δ (Figure 4-A-1). The localization of Bcl-2 was consistent with previously published data [35], and no differences in the subcellular distribution of Bcl-2 and Bcl-2Δ were observed (Figure 4-A-2). To ensure that the relative caspase activity of the clones did not change in a time-dependent manner, we repeated the measurement after approximately 8 days of culture. At this time, we found even more substantially reduced caspase-3/7 activity in both Bcl-2Δ expressing clones in comparison to the control (Figure 4-A-3).

Stoichiometric analysis

To investigate the metabolic consequences of Bcl-2Δ expression, we assessed cell growth rate (Figure 4-A-4) and extracellular exchange rates during two separate culture phases by expressing all rates on a C-mol basis (Figure 4-2).

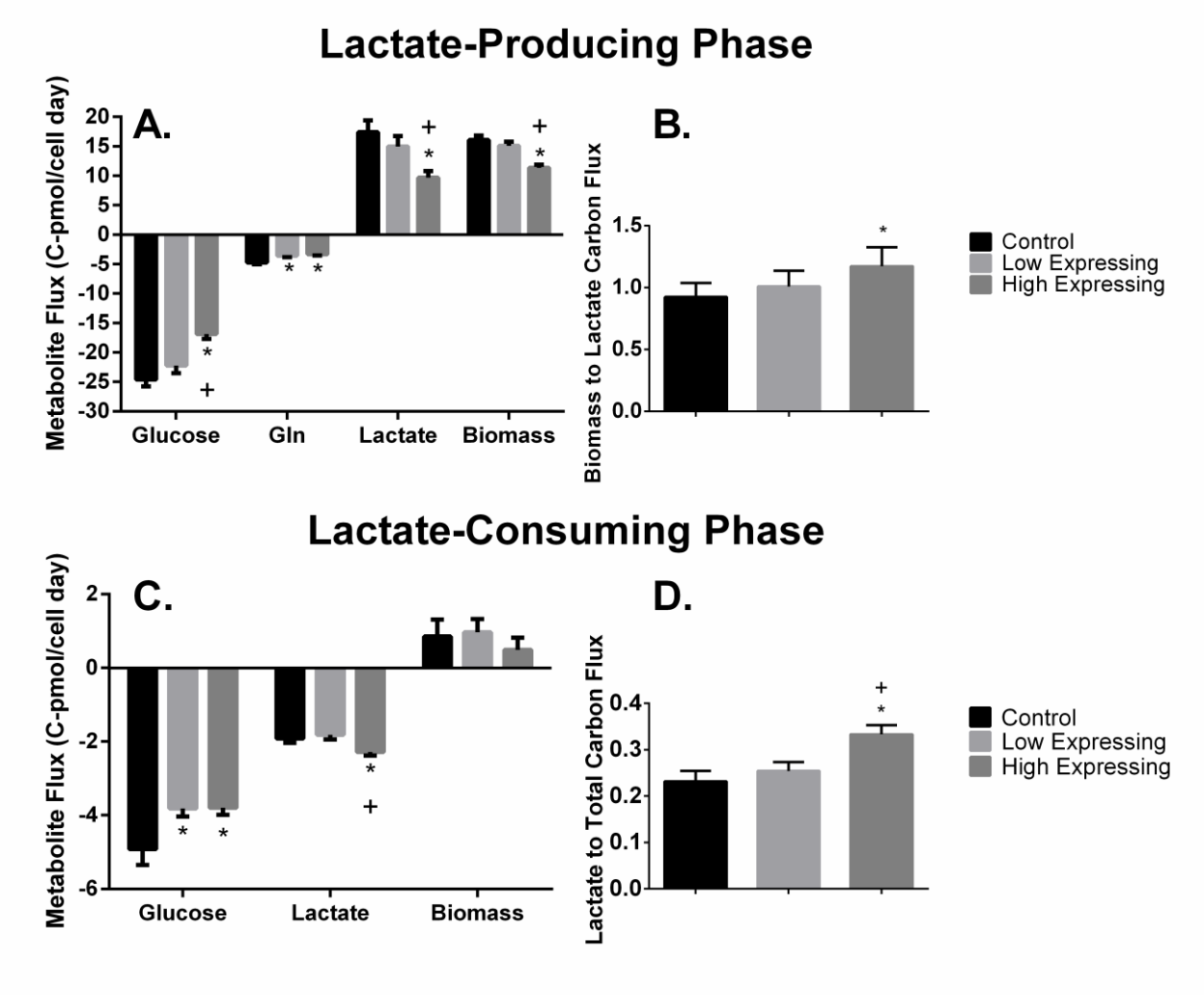

Figure 4-2. Major extracellular carbon fluxes. Carbon flux is determined by multiplying the flux (specific uptake rate, production rate) by the number of carbons in the molecule. Standard deviation is reported. * Indicates statistically significant difference compared to the control (p=0.05). + Indicates statistically significant difference between Low Expressing and High Expressing clones (p=0.05). **A.** Fluxes during the lactate-producing phase. The biomass carbon output corresponded with the following gross growth rates: Control 1.00±0.04 day^{-1}, Low Expressing 0.99±0.04 day^{-1}, and High Expressing 0.84±0.03 day^{-1}. **B.** Ratio of biomass to lactate carbon fluxes during the lactate-producing phase. **C.** Fluxes during the lactate-consuming phase. The biomass carbon output corresponded with the following gross growth rates: Control 0.05±0.02 day^{-1}, Low Expressing 0.06±0.01 day^{-1}, and High Expressing 0.03±0.01 day^{-1}. **D.** Ratio of incoming lactate carbon flux to total incoming carbon flux during the lactate-consuming phase.

Due to the fact that lactate flux switched from production to consumption during the course of the culture, an effect often observed in industrial CHO cell cultures [36], we examined the lactate-producing and lactate-consuming phases separately. These corresponded roughly with the exponential and stationary phases, as previously reported in literature [37].

Lactate-Producing Phase. In the lactate-producing phase (Figure 4-2a), the HE clone produced lactate at a rate that was approximately half that of the control. Alanine production also fell significantly in both the HE and LE clones. Biomass production was the only other substantial carbon output during this phase, with a magnitude comparable to lactate on a C-mol basis. However, while the control clone produced only 0.92±0.11 C-mol of biomass for every 1 C-mol of lactate, the HE clone was 27% more efficient in its carbon utilization, producing 1.17±0.15 C-mol of biomass for every 1 C-mol of lactate (Figure 4-2b). In terms of carbon inputs, the HE clone consumed glucose at a significantly lower rate than the LE clone and nearly a third less compared to the control. Glutamine consumption was significantly reduced in both Bcl-2Δ expressing clones. In general, amino acid consumption was reduced in both Bcl-2Δ expressing clones, but with the exception of glutamine, none of the other amino acid fluxes contributed substantially to the overall carbon balance.

Examination of the culture growth rates reveals further insight into the metabolic impact of Bcl-2Δ expression. The HE clone had a growth rate that was significantly reduced by 16% compared to the control (Figure 4-A-4). Previous work has found Bcl-2 overexpression to have a similar negative impact on growth [38]. However, the LE clone did not differ significantly from the control in growth rate despite diminished lactate production and reduced glucose

consumption (Figure 4-2a). This indicates that the reduction in nutrient uptake and lactate production in the LE clone reflects a direct effect of Bcl-2Δ expression on metabolic pathways rather than a growth-rate-dependent effect. Furthermore, the total incoming carbon flux was reduced by approximately 10% in the LE clone and by 30% in the HE clone during the lactate-producing phase (Figure 4-3).

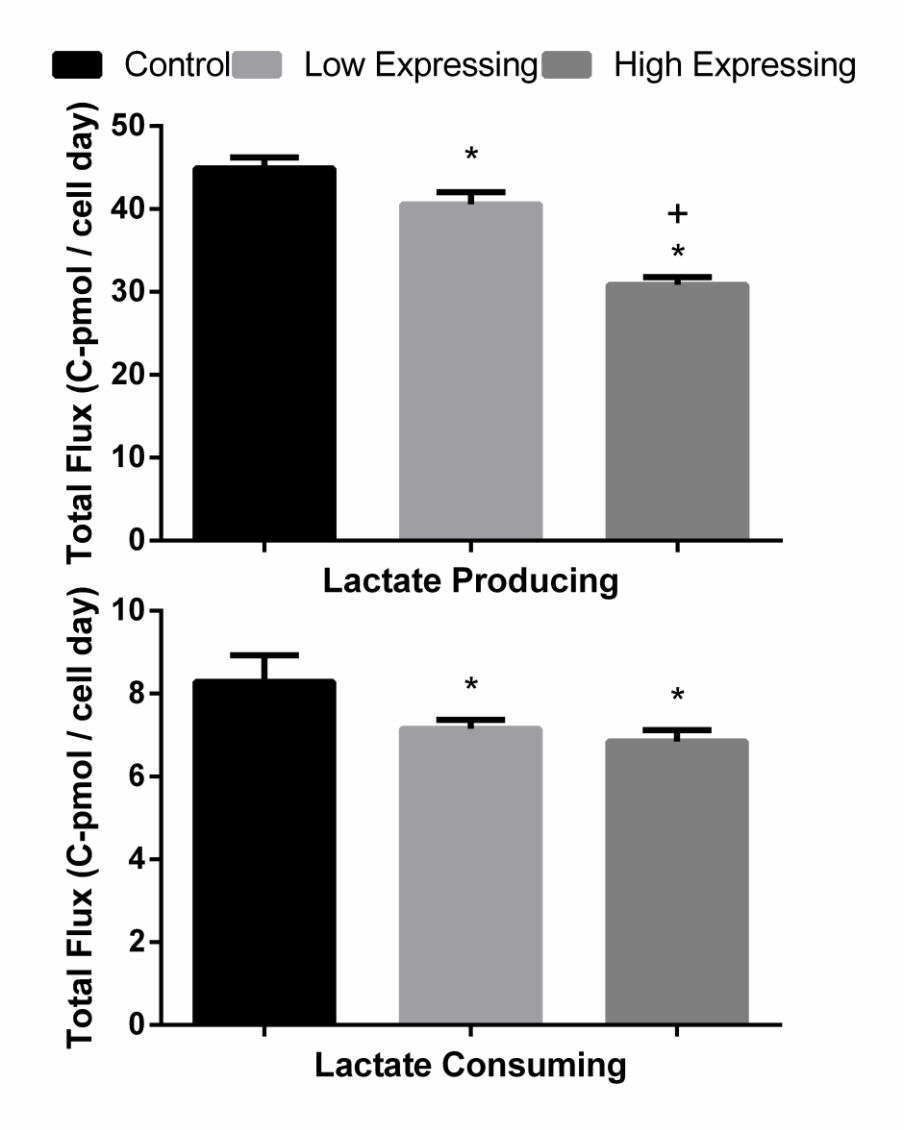

Figure 4-3. Total incoming carbon flux during each phase. Standard deviation is reported. * Indicates statistically significant differences compared to the control (p=0.05). + Indicates statistically significant differences between the Low Expressing and High Expressing clones (p=0.05).

Lactate-consuming phase. The lactate-consuming phase was notably different from the lactate-producing phase. The sum of the specific lactate and glucose consumption rates accounted for 79–89% of the total carbon consumed in the three clones. Outgoing carbon flux to biomass was limited during this phase, but was not negligible. Nearly all of the extracellular

carbon substrates were consumed during this phase, including several metabolites previously excreted during the lactate-producing phase. Incoming lactate flux was significantly higher in the HE line, while the LE clone consumed lactate at nearly the same rate as the control (Figure 4-2c). However, the glucose uptake rate was significantly reduced in both Bcl-2Δ expressing clones. The lactate-to-glucose ratio was 54% greater in the HE clone when compared to the control (Figure 4-A-5). Thus incoming lactate flux made up a significantly greater fraction of the total incoming carbon flux in the HE clone, a 44% increase compared to the control (Figure 4-2d). As expected, the culture was considerably less metabolically active relative to the lactate-producing phase, as indicated by drastic reductions in total carbon consumption (Figure 4-3).

^{13}C metabolic flux analysis (^{13}C MFA)

With significant rerouting of extracellular fluxes observed during both the lactate-producing and lactate-consuming phases, we sought to identify the fate of the incoming glucose carbon and to quantify the intracellular flux distributions of all three clones. We performed a ^{13}C labeling study followed by metabolic flux analysis (MFA) to calculate intracellular metabolic fluxes in both the lactate-producing and lactate-consuming phases.

Lactate-producing phase. The flux maps obtained by ^{13}C MFA during the lactate-producing phase are shown in Figure 4-4.

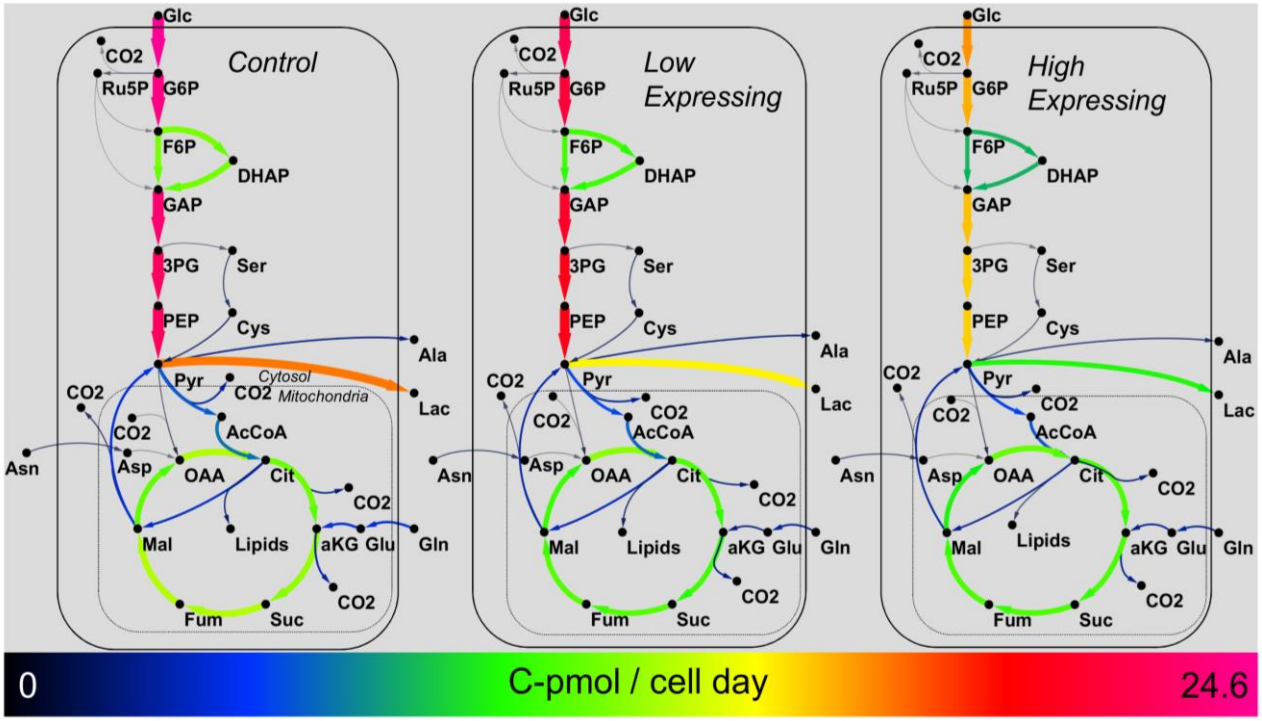

Figure 4-4. Metabolic flux maps during the lactate-producing phase. The magnitude of each net carbon flux corresponds with the color and width of the reaction arrow.

A few notable features are shared by all three clones. Minimal oxidative pentose phosphate pathway (oxPPP) activity was observed, and nearly all of the glucose consumed was directed through glycolysis to pyruvate. This result has been observed in previous ^{13}C MFA studies of exponential-phase CHO cultures [18]. Flux through malic enzyme (ME) was the most substantial cataplerotic flux leaving the TCA cycle during this phase. Still, nearly all of the pyruvate generated was attributable to the pyruvate kinase (PK) flux. A substantial portion of the pyruvate generated was converted into lactate; however, the HE clone diverted less pyruvate toward lactate production than the other cell lines.

Despite decreased total carbon consumption by both Bcl-2Δ expressing clones (Figure 4-3), TCA cycle fluxes were not significantly different among the three cell lines. Therefore, we

examined how the incoming carbon was partitioned at the pyruvate node to maintain consistent TCA cycle activity, since pyruvate is a central metabolic hub where fermentative and oxidative pathways bifurcate. To this end, we compared all incoming and outgoing pyruvate fluxes at the pyruvate node (Figure 4-5).

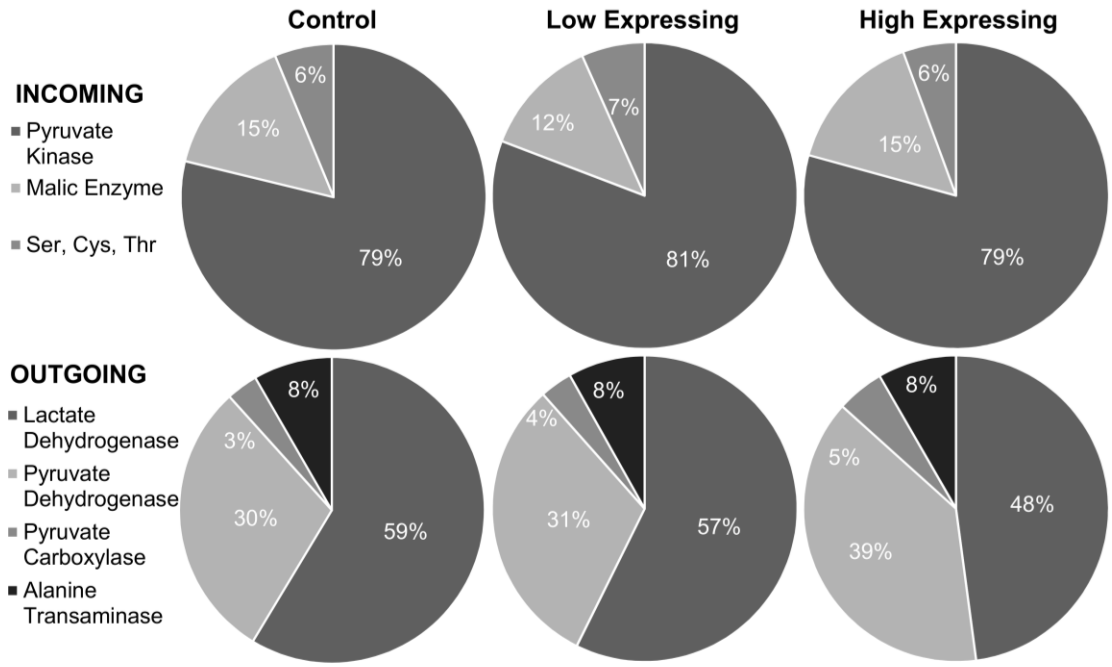

Figure 4-5. Distribution of flux at the pyruvate node during the lactate-producing phase. Cys, Ser, Thr represents the summed contributions of these three amino acids to pyruvate production.

In the control line, 33±7% of carbon leaving the pyruvate node was transferred to the mitochondria through pyruvate carboxylase (PC) and pyruvate dehydrogenase (PDH). However, as Bcl-2Δ expression level increased, a greater fraction of the incoming pyruvate was directed to the mitochondria, reaching as high as 44±7% in the HE clone.

With a higher fraction of pyruvate oxidized in mitochondria, we hypothesized that more mitochondrial NADH would be generated per glucose consumed and more oxidative metabolism would be detected in the Bcl-2Δ expressing clones. To test this hypothesis, and to identify a potential mechanism by which the Bcl-2Δ cells increased their mitochondrial activity, we measured the enzymatic activities of the mitochondrial enzymes isocitrate dehydrogenase (IDH) and NADH-coenzyme Q oxidoreductase (Complex I). IDH is a rate-controlling step in the TCA cycle that catalyzes the oxidative conversion of citrate to alpha-ketoglutarate, with concomitant evolution of CO_2 and generation of NADH. As indicated in Figure 4-6a, the IDH activity was at least 60% higher in both engineered cell lines relative to the control, which indicates a shift toward increased oxidative capacity in response to Bcl-2Δ expression.

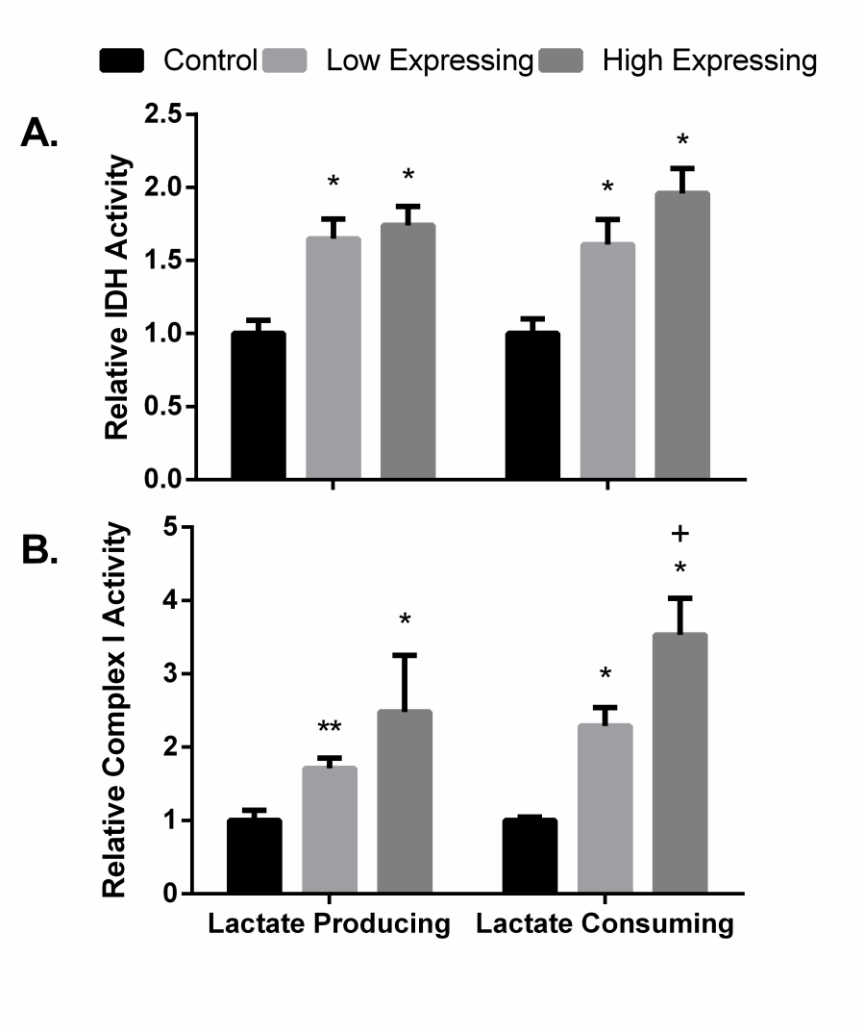

Figure 4-6. **Enzyme activity assays**. **A.** Relative enzymatic activity of isocitrate dehydrogenase (IDH). **B.** Relative enzymatic activity of Complex I (NADH oxidase). Standard deviation is reported. * Indicates statistically significant difference compared to the control (p=0.05). + Indicates statistically significant difference between the Low Expressing and High Expressing clones (p=0.05). Comparisons of both assays are relative to the control enzymatic activity, and are only appropriate when compared within a specific phase (i.e., within the lactate-producing phase or lactate-consuming phase). ** Indicates statistically significant difference compared to the control (p=0.1).

Similarly, both Bcl-2Δ expressing clones were determined to have significantly increased Complex I activity (Figure 4-6b). This enzyme functions to oxidize NADH produced in the TCA cycle and is a vital component of the mitochondrial electron transport chain.

Lactate-consuming phase. During the lactate-consuming phase, growth slowed dramatically and the total incoming carbon flux decreased by nearly an order of magnitude. This was due largely to decreased glucose consumption rates as all 3 clones transitioned into stationary phase (Figure 4-2c). Past work has found similar reductions in glucose flux following a switch to lactate consumption [39]. The majority of incoming glucose was diverting to the oxPPP, with fluxes ranging from 76% of total carbon uptake in the control line to 61% in the HE clone (Figure 4-7).

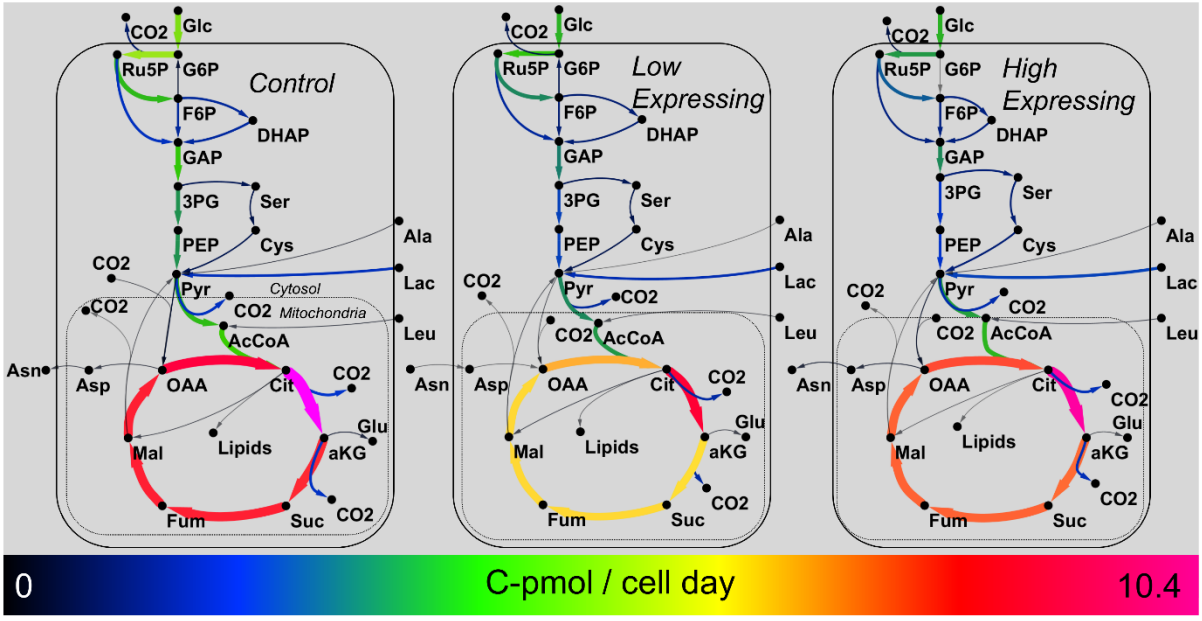

Figure 4-7. Metabolic flux map of lactate-consuming phase. The magnitude of each net carbon flux corresponds with the color and width of each reaction arrow.

Even so, the TCA cycle was the main focal point of central metabolism during the lactate-consuming phase, with the majority of incoming carbon ultimately directed there for oxidation to CO_2.

Figure 4-8 shows the distribution of carbon fluxes entering the pyruvate node during this phase.

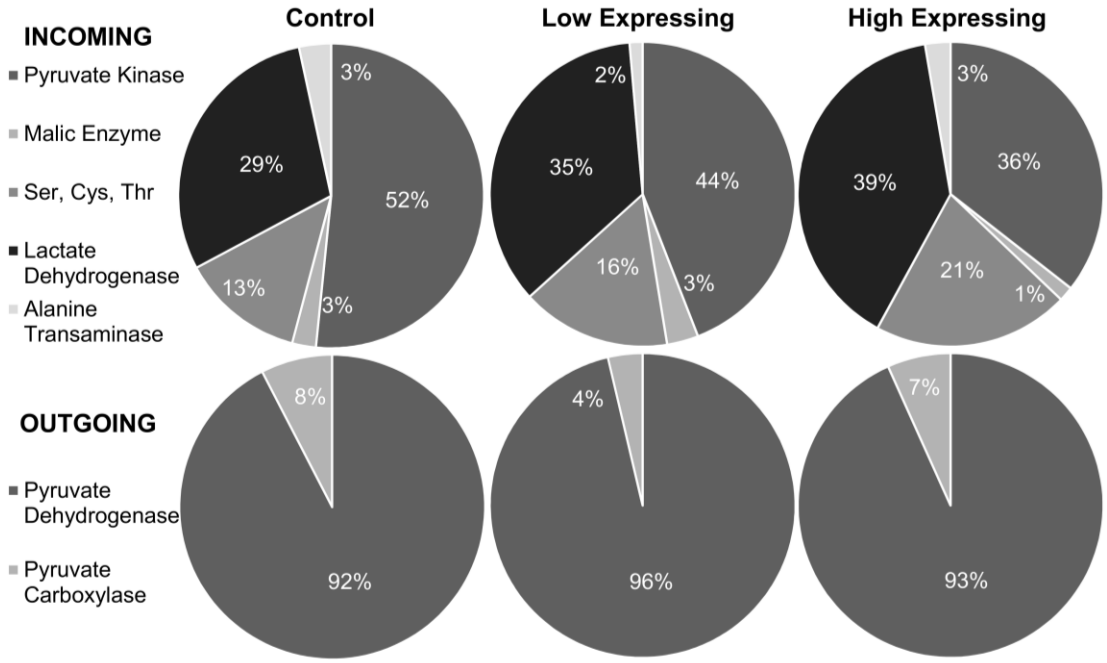

Figure 4-8. Distribution of carbon flux at the pyruvate node during the lactate-consuming phase.

Most of the incoming pyruvate carbon can be broken down into two components: the contribution from lactate and the contribution from glycolysis. Lactate accounted for 39±1% of

the input carbon in the HE clone compared to only 29±4% in the control line. The LE clone fell in the middle at 35±5%. Whether viewed on an absolute (Figure 4-2c) or relative basis (Figure 4-8), the utilization of lactate by the HE clone is significantly greater than the control. Since all of the outgoing flux from pyruvate was directed to the mitochondria during this phase, we again became interested in whether changes in carbon partitioning at the pyruvate node were associated with changes in mitochondrial oxidative capacity. Therefore, we measured IDH activity (Figure 4-6a) and Complex I activity (Figure 4-6b) in cells harvested during the lactate-consuming phase. As in the lactate-producing phase, the activities of both mitochondrial enzymes were significantly higher in the Bcl-2Δ expressing clones as compared to the control.

Discussion

Bcl-2 was originally known for its role as an oncogene, having been frequently found overexpressed in several different cancer cell types [40]—most notably B-cell lymphoma for which it is named. More recently, the biotechnology industry became interested in Bcl-2 and other anti-apoptotic genes due to their ability to increase survival of industrial cell lines with a potential impact on enhancing product yields [10,41,42]. In 2000, multiple laboratories including our group [9,43] found that Bcl-2 expression indeed retards apoptotic progression in CHO cells, including those producing recombinant proteins. Dorai et al. [13] later observed that antibody-producing CHO cells engineered to overexpress a variety of different anti-apoptotic genes exhibited less lactate accumulation during early exponential phase and more rapid lactate consumption during late exponential and stationary phases.

The current study builds upon this previous work to examine the metabolic response of CHO cells to recombinant expression of Bcl-2Δ, an engineered variant of Bcl-2 where both the BH2 and BH3 motifs have been removed. This serves to enhance protein stability, since several ubiquitination sites and regulatory motifs have been removed from the truncated sequence [41]. Expression of Bcl-2Δ in CHO cells has been previously shown to surpass wild-type Bcl-2 in its ability to extend culture survival in response to diverse insults [41]. In this study, the expression of Bcl-2Δ was greatly enhanced in our clones relative to the endogenous Bcl-2 level of control cells (Figure 4-A-1), presumably due to both the use of a strong constitutive CMV promoter and the increased stability of Bcl-2Δ. This resulted in rewiring of metabolic fluxes at the pyruvate node, both during the lactate-producing and lactate-consuming phases of culture. We sought to better understand the regulatory connections between these metabolic alterations and the known anti-apoptotic properties of Bcl-2.

Bcl-2 is known to regulate cell death by modulating mitochondrial membrane permeability [44] and is believed to function by preventing the release of cytochrome c from the intramembrane space, which is a committed step in several different apoptotic mechanisms [45]. There are multiple hypotheses surrounding how mitochondrial permeability is regulated by Bcl-2, as discussed in a recent review [46]. Some evidence supports a role for Bcl-2 in blocking permeability transition pore (PTP) activation, thus preventing dissipation of inner mitochondrial transmembrane potential ($\Delta\psi_m$) [47,48]. Bcl-2 has also been found to limit activity of the voltage-dependent anion channel (VDAC), a protein essential to the regulation of mitochondrial Ca^{2+} uptake [49]. These effects would be expected to simultaneously modulate metabolic pathway activities, since several mitochondrial enzymes are regulated by changes in Ca^{2+} and $\Delta\psi_m$ [15]. These include IDH and Complex I enzymes that catalyze important redox reactions in

the TCA cycle and oxidative phosphorylation (OXPHOS), respectively. Furthermore, the effect of Bcl-2 to prevent loss of cytochrome c from the intramembrane space may also function to regulate OXPHOS, as cytochrome c is a required part of the mitochondrial electron transport chain.

Our measurements indicate that Bcl-2Δ expression increased enzymatic activities of both IDH and Complex I (Figure 4-6), potentially enhancing mitochondrial oxidative capacity. The effect was accompanied by a greater fraction of pyruvate produced during the lactate-producing phase being directed to the mitochondria for oxidation (Figure 4-5). In addition, there was a significant increase in the lactate consumption rate (Figure 4-2c) and a significant increase in the fraction of pyruvate carbon derived from lactate (Figure 4-8) during the lactate-consuming phase. We hypothesize that these systems-level metabolic alterations stem, at least in part, from the changes in mitochondrial enzymatic activities we observed.

Bcl-2 has also been shown to enhance the activity of several Ca^{2+}-dependent mitochondrial transporters, including adenine nucleotide translocator (ANT) [50]. ANT exists in the inner mitochondrial membrane and enables exchange of ADP/ATP with the cytosol. Lack of mitochondrial ADP availability could lead to a potential bottleneck within the OXPHOS pathway of control cells. Removal of this bottleneck could be another potential explanation for the increased pyruvate shuttled to the mitochondria and enhanced Complex I activity observed in the HE clone. Others have found that there is a limitation in the Ca^{2+}-dependent Asp/Glu transporter of CHO cells, which is responsible for transport of NAD^+ equivalents into the cytosol as part of the malate-aspartate shuttle [51,52]. This could explain the reduced lactate production observed in the Bcl-2Δ clones, since the conversion of pyruvate to lactate by lactate dehydrogenase (LDH) provides an alternative pathway to oxidize NADH that is expected to

become less important as mitochondrial OXPHOS and malate-aspartate shuttle capacities increase. Based upon the lactate/glucose ratio, both Bcl-2Δ expressing clones exhibited reduced reliance on lactate production for maintaining cytosolic redox during the lactate-producing phase (Figure 4-A-5). Likewise, the enhanced lactate consumption exhibited by the HE clone after the lactate shift may be partially explained by increased mitochondrial transport and disposal of NADH equivalents generated by LDH acting in the reverse direction. Taken together, the known role of anti-apoptotic proteins such as Bcl-2 to alter mitochondrial Ca^{2+} flux and $\Delta\psi_m$ are important for regulating several aspects of mitochondrial metabolism that could explain our observations.

Even though recombinant expression of Bcl-2Δ did not positively impact the growth rate, it did clearly hinder the progression of cell death. Bcl-2Δ expression led to increases in IVCD of 40% in the HE culture and 20% in the LE culture (Figure 4-9).

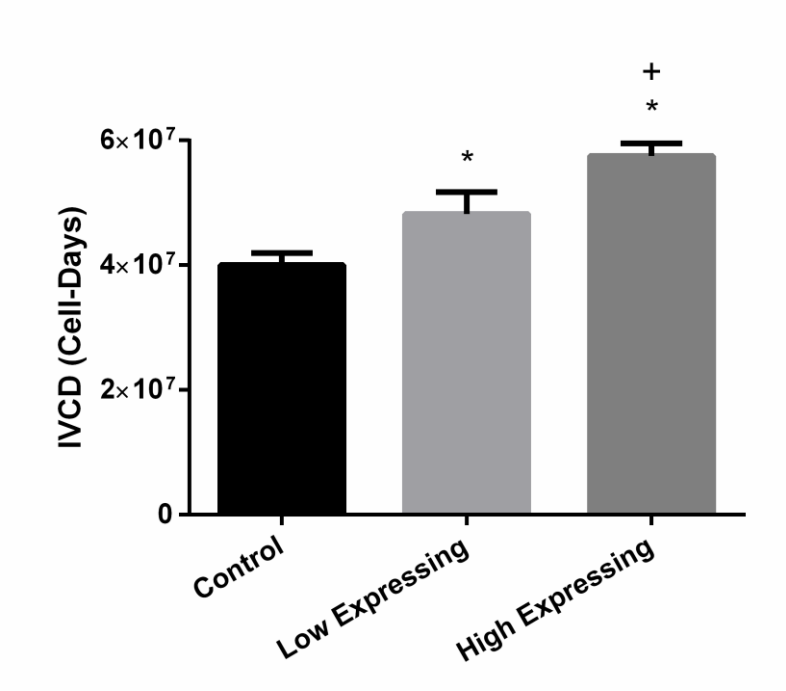

Figure 4-9. Integrated viable cell density (IVCD) over the culture life. Standard deviation is reported. * Indicates statistically significant difference compared to the control (p=0.05). + Indicates statistically significant difference between the Low Expressing and High Expressing clones (p=0.05).

This is in agreement with prior studies where Bcl-2 was found to inhibit cell death without increasing cell proliferation [53,54]. Peak VCD was also increased by nearly 50% in the HE clone and nearly 40% in the LE clone (Figure 4-A-6). This reflects an increase in biomass yield, as the Bcl-2Δ expressing cells directed more carbon flux to biomass production rather than lactate (Figure 4-2b). Additionally, glutamine consumption decreased significantly in the Bcl-2Δ clones, perhaps attributable to the redistribution of pyruvate carbon to the TCA cycle. This increased carbon efficiency is likely a result of enhanced TCA cycle activity relative to glycolysis, since OXPHOS provides more ATP per glucose consumed than lactate production. Further evidence for this increased carbon efficiency is reflected in the fact that the reductions in

growth rate observed in both Bcl-2Δ clones (HE down 16%; LE unaffected) was substantially less than the reductions in their total carbon consumption rate (HE down 30%; LE down 10%).

In addition to the enhancements in biomass yield, the accompanying reduction in lactate production would be expected to have further benefits in an industrial bioprocess, since elevated lactate concentrations have been found to hamper both growth and antibody production of CHO cell cultures [55]. The HE line allowed lactate to accumulate to marginally less (<10%) concentrations than the control, despite achieving ~50% higher peak VCD (Supplemental Figures 4-A-6 and 4-A-7). Furthermore, a culture capable of consuming the lactate that it previously produced is at an obvious advantage in a controlled bioreactor. A lactate-consuming culture requires less base addition to maintain pH and results in less rise in osmolarity [56], which has also been found to negatively affect growth. All cell lines examined in this study consumed previously produced lactate; however, the HE clone consumed lactate at a specific rate significantly greater than the others, confirming the result that Dorai et al. [13] obtained in their apoptosis-resistant lines.

Although prior work by Meents et al. (2002) found that Bcl-2 overexpression did not increase specific protein productivity, Bcl-2Δ clones have the potential to outperform Bcl-2 overexpressing clones in terms of protein production [41,42]. While the current study did not address the effects of Bcl-2Δ expression on protein production, recent work from our group has found a strong correlation between enhanced TCA cycling and peak antibody production [19]. Therefore, we expect that anti-apoptosis engineering may offer a path toward improving specific protein productivity while reducing lactate accumulation and improving biomass yields, in addition to its well-known effects to extend culture longevity.

The ^{13}C flux analysis performed in this study was dependent on assumptions of both isotopic and metabolic steady state. Although we did not obtain biomass samples during the initial two days of growth due to the low cell densities achieved during this period, multiple parallel experiments where tracers were administered to higher density cultures indicate that the ^{13}C enrichment of intracellular metabolites plateaus after ~2 days of labeling. Therefore, all samples used for ^{13}C isotopomer analysis were collected following more than two days of labeling, which we expect to be sufficient to achieve isotopic steady state. It is also possible that the metabolic steady-state assumption was violated due to dynamic changes that occur during the transition from lactate-producing to lactate-consuming phases of culture. While this is indeed a concern, there are currently no established methods for performing fully dynamic ^{13}C MFA under metabolic nonstationary conditions [1,57]. Therefore, in order to address industrially relevant culture conditions where metabolism is changing over time, it is necessary to invoke a quasi-steady-state assumption. This involves the premise that, after the initial tracer equilibration period, further changes in isotope labeling will track closely with changes in metabolism and can be analyzed by steady-state ^{13}C MFA to obtain a series of snapshots that describes the variation in metabolic fluxes over time. This is similar to the approach used by Antoniewicz et al. [58] to profile dynamic changes in *E. coli* metabolism during a fed-batch culture that exhibited both glycerol-producing and glycerol-consuming phases. Despite these limitations and assumptions, we expect that the ^{13}C MFA results are reliable because (i) the main findings related to pyruvate partitioning are consistent with extracellular flux measurements and with direct measurements of mitochondrial enzyme activities, (ii) the enrichments of pyruvate and lactate were maintained near their maximal levels throughout both phases of culture, (iii) we did not utilize samples collected immediately following the lactate shift, and (iv) the average ^{13}C

enrichments of metabolites from the control and HE lines were consistent within each phase, despite being collected at different times due to the delayed onset of lactate consumption in the HE culture (Figure 4-A-8).

Conclusions

Host cell engineering through recombinant Bcl-2Δ expression has considerable potential for industrial applications. It notably improves the total IVCD by delaying the onset of apoptosis. In addition, this study has shown that Bcl-2Δ expression promotes a shift toward increased mitochondrial oxidation of incoming carbon substrates. Bcl-2Δ's ability to limit lactate production and enhance lactate consumption is an especially attractive property, and will only become more so, as industry continues to push toward higher peak VCDs and longer culture lifespans. To our knowledge, this is the first ^{13}C MFA study to quantify the metabolic impact of Bcl-2Δ expression, enabling a closer examination of the interplay between apoptotic and metabolic regulatory functions of Bcl-2Δ through comprehensive analysis of central carbon metabolism.

Acknowledgements

This work was supported by NSF GOALI award CBET-1067766. The authors would like to acknowledge the contributions from Dawn Ellis in clone generation. The authors would also like to thank Daniel Wolozny for his general assistance in this study.

Nomenclature

3PG: 3-Phosphoglycerate

AcCoA: Acetyl-CoA

ACL: ATP Citrate Lyase

aKG: α-Ketoglutarate

Ala.e: Alanine.extracellular

AMBIC: Ammonium Bicarbonate

ANT: Adenine Nucleotide Translocator

Asn.e: Asparagine.extracellular

ATP: Adenosine-5'-Triphosphate

Bcl-2: B-cell lymphoma 2

CHO: Chinese Hamster Ovary

Cit: Citrate

DHAP: Dihydroxyacetone Phosphate

E4P: Erythrose-4-Phosphate

EMU: Elementary Metabolite Unit

F6P: Fructose 6-Phosphate

Fum: Fumarate

G6P: Glucose-6-Phosphate

G6PDH: Glucose-6-Phosphate Dehydrogenase

GAP: Glyceraldehyde-3-Phosphate

GCMS: Gas Chromatography-Mass Spectrometry

Glc: Glucose

Gln.e: Glutamine.extracellular

HE: High Expressing (of Bcl-2Δ)

HPLC: High Performance Liquid Chromatography

HRP: Horseradish Peroxidase

IDH: Isocitrate Dehydrogenase

IVCD: Integrated Viable Cell Density

Lac.e: Lactate.extracellular

Lac: Lactate

LDH: Lactate Dehydrogenase

LE: Low Expressing (of Bcl-2Δ)

Leu.e: Leucine.extracellular

Lys.e: Lysine.extracellular

Mal: Malate

ME: Malic Enzyme

MFA: Metabolic Flux Analysis

MID: Mass Isotopomer Distribution

MOX: Methoxyamine

MTBSTFA: N-Methyl-N-(t-butyldimethylsilyl) trifluoroacetamide

NADH: Nicotinamide Adenine Dinucleotide

NADPH: Nicotinamide Adenine Dinucleotide phosphate

OAA: Oxaloacetate

OPA: Orthophthaldildehyde

OXPHOS: Oxidative Phosphorylation

oxPPP: oxidative Pentose Phosphate Pathway

PC: Pyruvate Carboxylase

PDH: Pyruvate Dehydrogenase

PEP: Phosphoenolpyruvate

PPP: Pentose Phosphate Pathway

Pro: Proline

PTP: Permeability Transition Pore

Pyr: Pyruvate

R5P: Ribose-5-Phosphate

RCF: Relative Centrifugation Force

ROS: Reactive Oxygen species

Ru5P: Ribulose-5-Phosphate

S7P: Sedoheptulose-7-Phosphate

Ser.e: Serine.extracellular

Suc: Succinate

TBDMCS: Tert-Butyldimethylchlorosilane

TCA Cycle: Tri-Carboxylic Acid Cycle

Val.e: Valine.extracellular

VCD: Viable Cell Density

VDAC: Voltage Dependent Anion Channel

X5P: Xylulose-5-Phosphate

XIAP: X-linked Inhibitor of Apoptosis Protein

Appendix

Metabolic flux analysis assumptions

The reaction network for all three models generated, including the reported fluxes and their associated 95% confidence intervals, can be found in a separate Excel spreadsheet. The following assumptions were made in regards to generating the models:

1. Metabolism is at a steady state during each of the two phases of the batch culture. The reported fluxes therefore represent averages over the corresponding time interval.
2. Intracellular isotopic labeling has reached quasi-steady state at the time of sample quenching and removal.
3. Succinate and fumarate are symmetric molecules that don't retain any particular orientation when metabolized by TCA cycle enzymes.
4. Change in individual cell size (mass) over the fed-batch lifetime is assumed to be negligible.
5. All major carbon sources of the complex industrial media have been included.
6. Exchange fluxes are employed to account for dilution by unlabeled carbon sources in the medium (e.g., lactate, alanine, aspartate).
7. As a consequence of conducting the isotope labeling experiments for 5 days of time to reach the lactate-consuming phase, secondary tracers emerged as byproducts of the primary glucose tracer. This required mass spectral measurements of extracellular lactate, and the specification of secondary tracers entering the reaction network during the lactate-consuming phase. The secondary tracer sources for lactate were specified based upon the measured lactate labeling during the preceding lactate-producing phase.

Supplemental figures

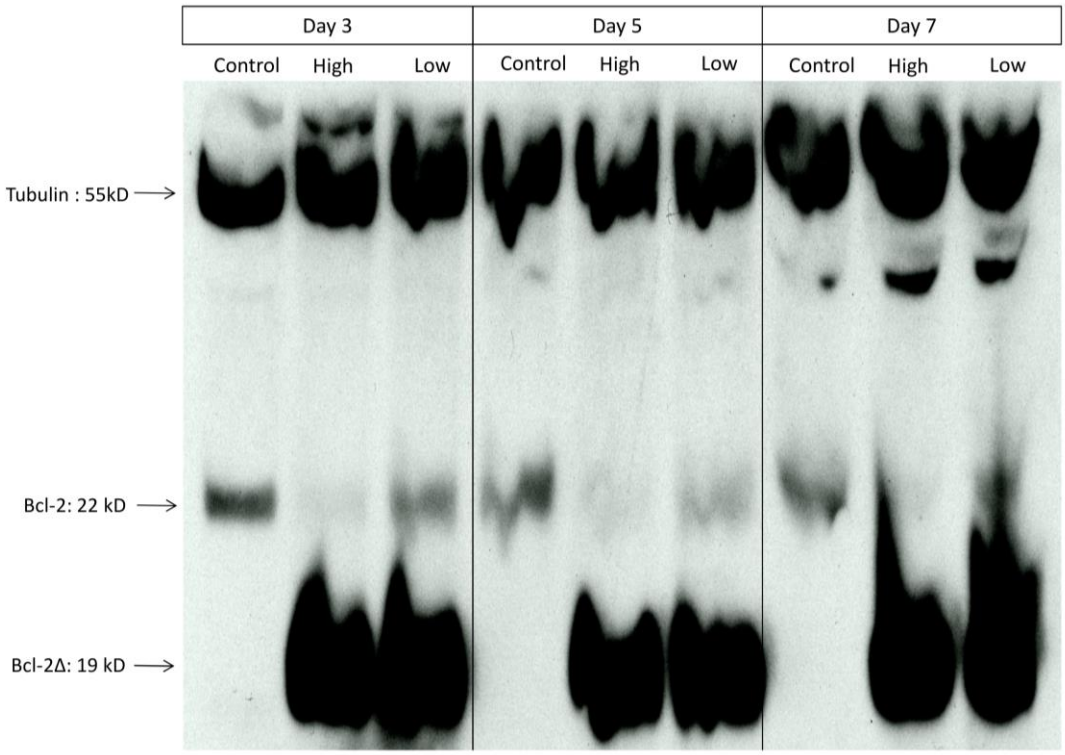

Figure 4-A-1. Western Blot of Bcl-2 and Bcl-2Δ (Isoform 2: 1G5O/1GJH). Low and High correspond with the expression level of Bcl-2Δ in the two transfected clones. Bcl-2 was expressed at considerably lower levels than Bcl-2Δ at all three sample times. To visualize Bcl-2, Bcl-2Δ had to be oversaturated.

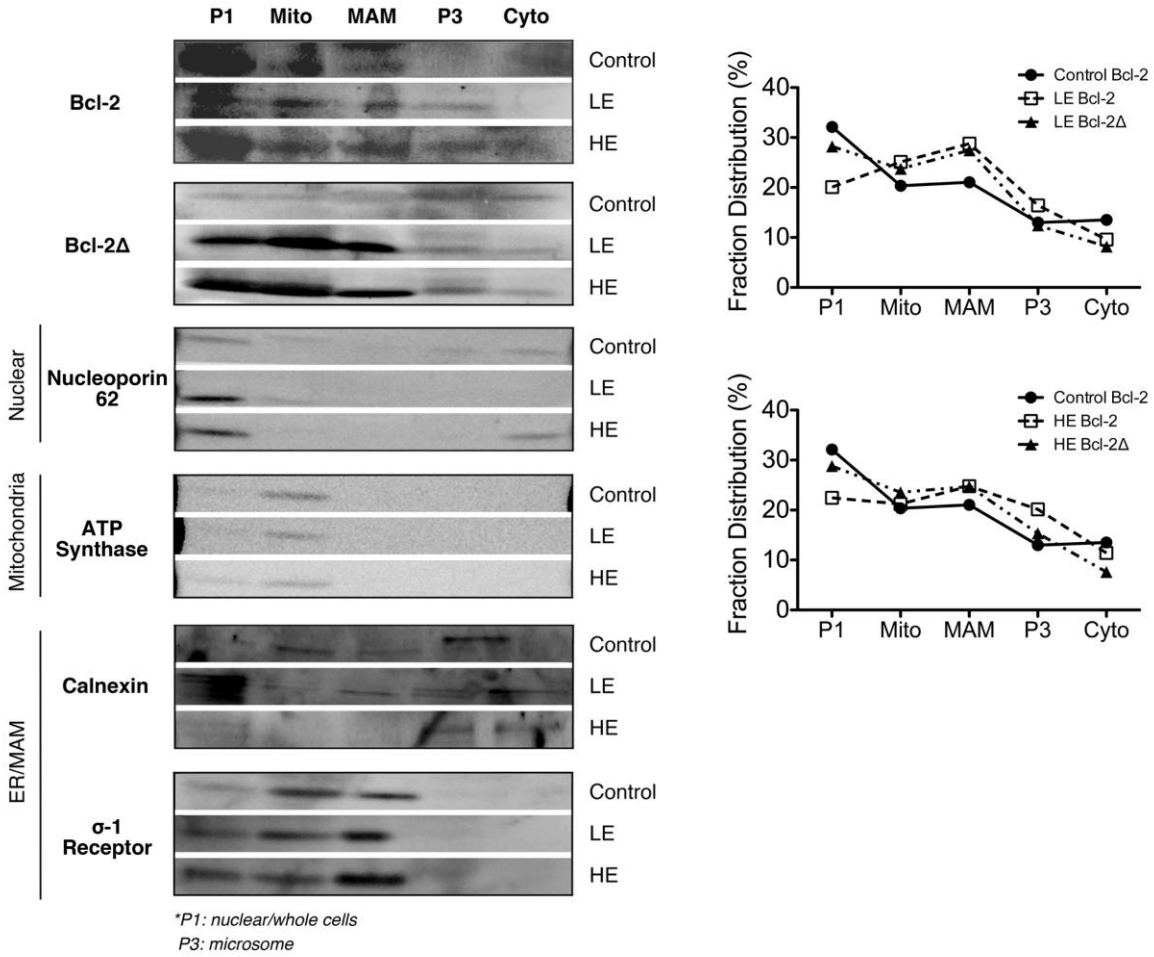

Figure 4-A-2. **Subcellular localization of Bcl-2 and Bcl-2Δ**. Cell fractionation study of control and Bcl-2Δ expressing clones showing P1 (whole cell and nuclear), mitochondrial (MITO), MAM, P3 (microsomal), and cytosolic (CYTO) fractions. Markers for known nuclear, mitochondrial, ER, and MAM proteins are used to validate the purity of fractions. The percent distribution of Bcl-2 and Bcl-2Δ in the LE and HE clones are graphed for each subcellular fraction in comparison to Bcl-2 expression in control cells. Data is representative of the varying levels of protein samples between all fractions collected and cannot be used as a comparison of total protein levels between cell lines.

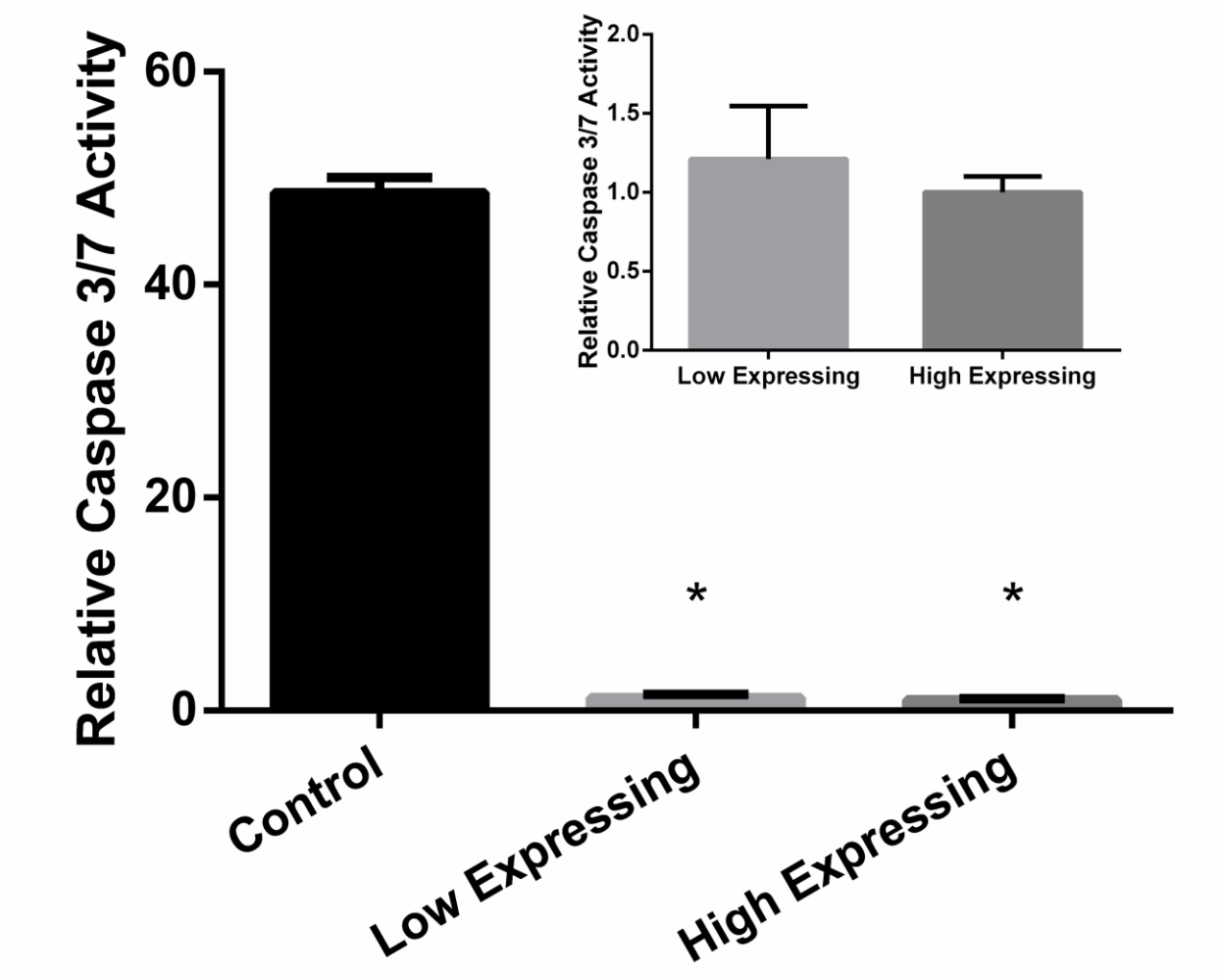

Figure 4-A-3. Caspase3/7 activity at day 8 of culture. Inset compares LE to HE clone. Standard deviation shown. * Indicates statistically significant difference compared to the control (p=0.05).

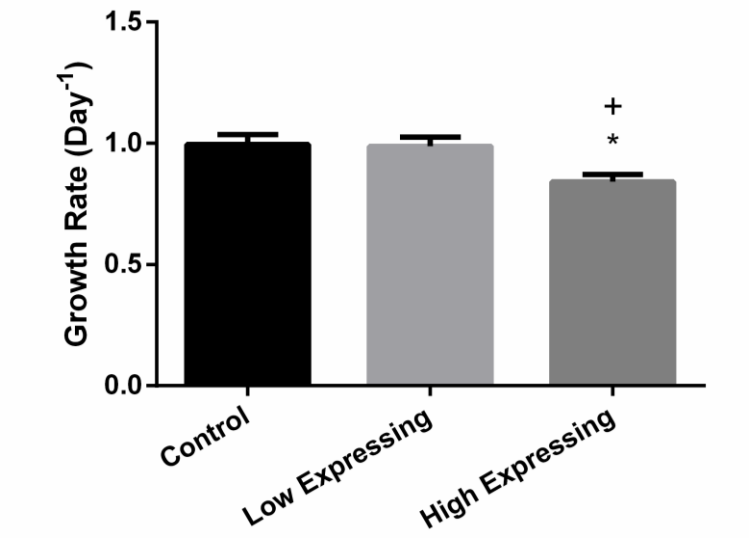

Figure 4-A-4. Net specific growth rate during the lactate-producing phase. Standard deviation shown. * Indicates statistically significant difference compared to the control (p=0.05). + Indicates statistically significant differences between the Low Expressing and High Expressing clones (p=0.05).

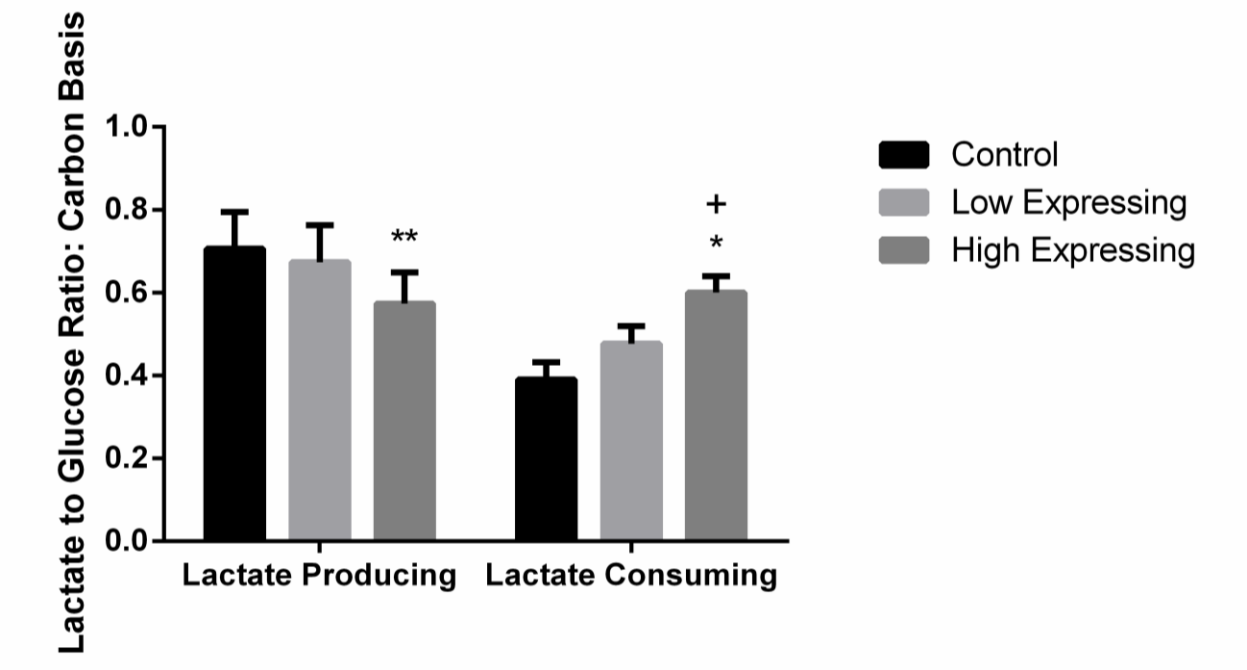

Figure 4-A-5. Comparison of lactate to glucose flux, on a carbon basis, which is a proxy of net cytosolic NADH balance. In the lactate-producing phase, a higher percentage indicates greater reliance upon lactate production for maintaining cytosolic redox. During this stage, glycolysis reduces NAD^+ to NADH and lactate dehydrogenase (LDH) re-oxidizes NADH to NAD^+. In the lactate-consuming phase, a higher percentage indicates greater mitochondrial capacity to transport and dispose of LDH-derived NADH. During this stage, both glycolysis and lactate consumption generate NADH. Standard deviation shown. * Indicates statistically significant difference compared to the control (p=0.05). + Indicates statistically significant difference between the Low Expressing and High Expressing clones (p=0.05). ** Indicates statistically significant difference compared to the control (p=0.1).

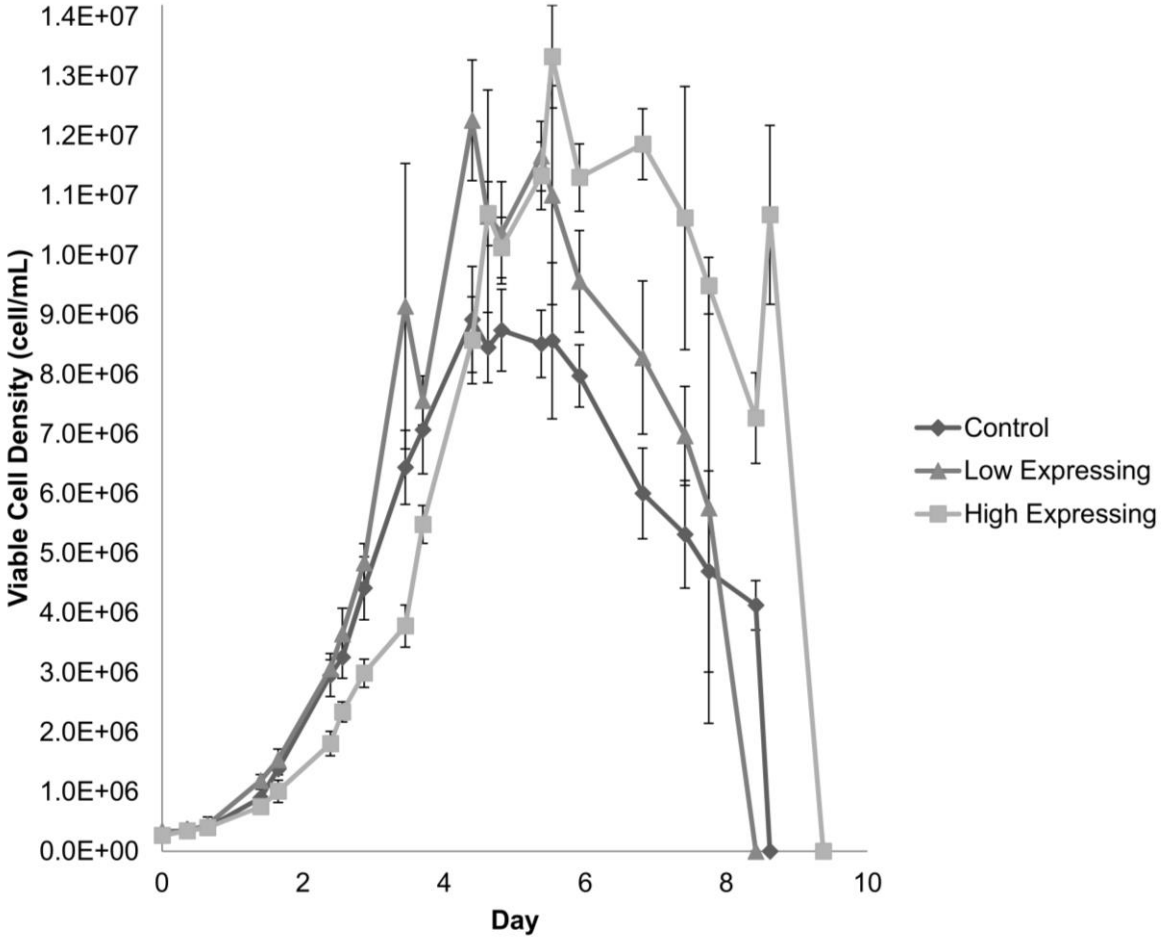

Figure 4-A-6. Viable cell density (VCD) over time. Standard deviation shown.

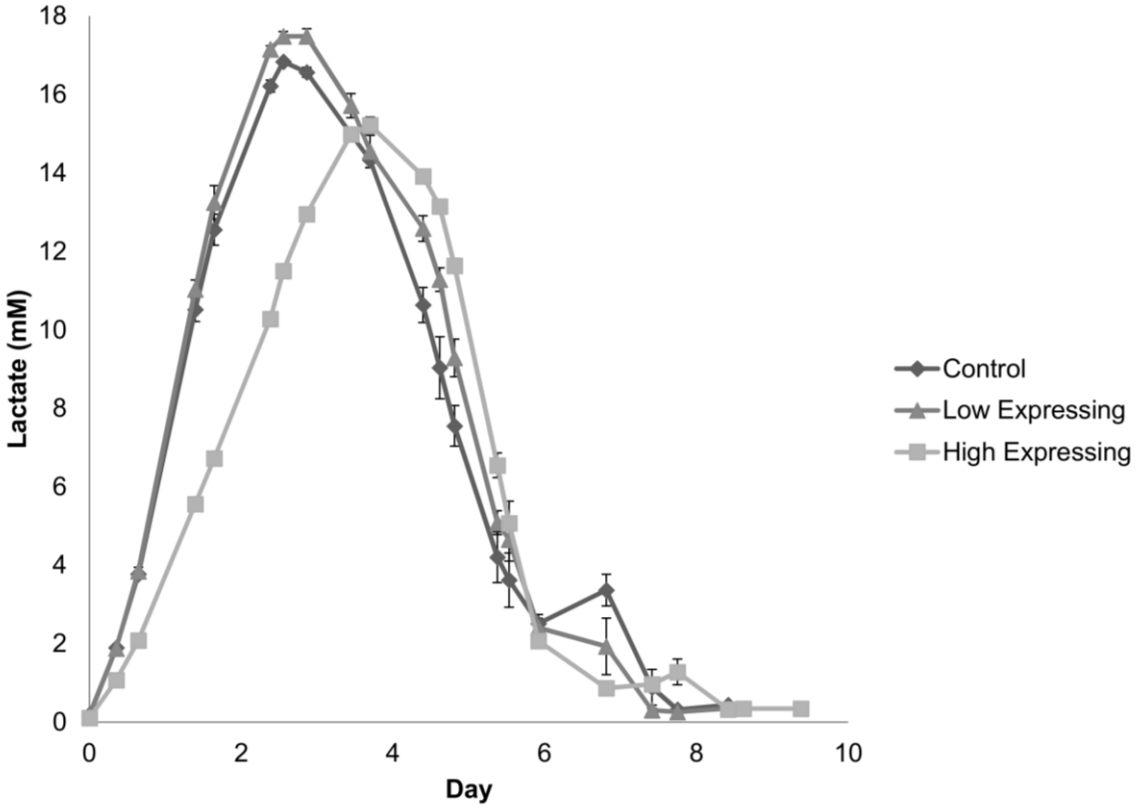

Figure 4-A-7. Lactate concentration over time. Standard deviation shown.

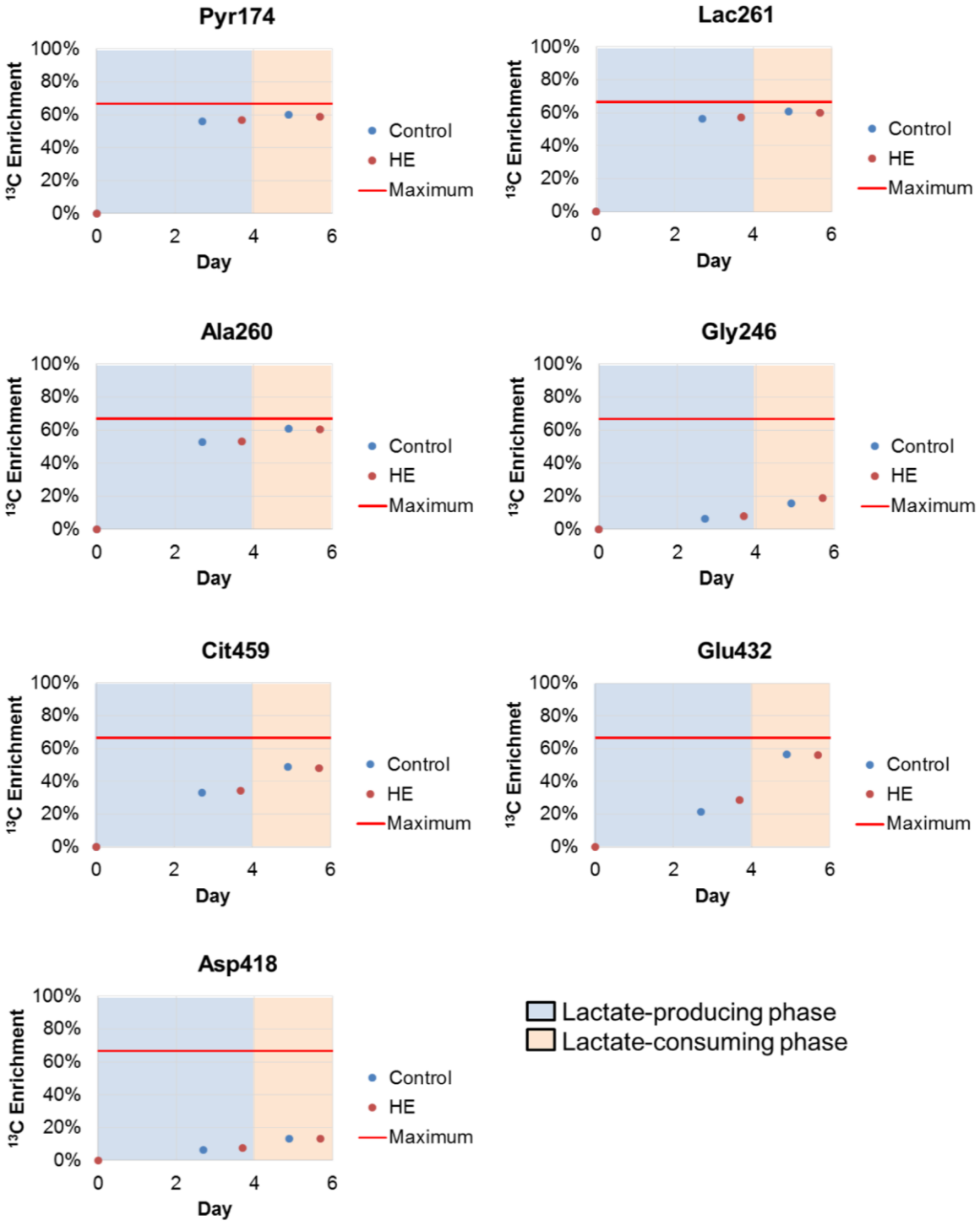

Figure 4-A-8. Average ^{13}C enrichments of intracellular metabolites at time points analyzed by ^{13}C MFA. The HE culture was sampled at later times due to delayed onset of lactate consumption. The red line shows the maximum enrichment achievable from the administered tracers (i.e., a 50:50 mixture of [U-$^{13}C_6$] and [1,2-$^{13}C_2$] glucose tracers).

Intracellular metabolites examined for labeling

Table 4-A-1. Ion fragments quantified via GCMS for the purpose of MFA. The number listed in the ion fragment column corresponds to the mass of fragment.

Ion Fragment	Node ID	Labeled Atom	Unlabeled Atom
Pyr 174	Pyr	1 2 3	C3 H12 O3 N Si
Lac 233	Lac	2 3	C8 H25 O2 Si2
Lac 261	Lac	1 2 3	C8 H25 O2 Si2
Ala 232	Ala	2 3	C8 H26 O N Si2
Ala 260	Ala	1 2 3	C8 H26 O2 N Si2
Gly 218	Gly	2	C8 H24 N O2 Si2
Gly 246	Gly	1 2	C8 H24 N O2 Si2
Suc 289	Suc	1 2 3 4	C8 H25 O4 Si2
Ser 288	Ser	2 3	C12 H34 N O Si2
Ser 362	Ser	2 3	C14 H40 N O2 Si3
Ser 390	Ser	1 2 3	C14 H40 N O3 Si3
Mal 419	Mal	1 2 3 4	C14 H39 O5 Si3
Asp 302	Asp	1 2	C12 H32 N O2 Si2
Asp 376	Asp	1 2	C14 H38 N O3 Si3
Asp 390	Asp	2 3 4	C14 H40 N O3 Si3
Asp 418	Asp	1 2 3 4	C14 H40 O4 N Si3
Glu 330	Glu.ms	2 3 4 5	C14 H36 N O2 Si2
Glu 358	Glu.ms	1 2 3 4 5	C12 H36 N O3 Si2
Glu 432	Glu.ms	1 2 3 4 5	C14 H42 O4 N Si3
Asn 417	Asn	1 2 3 4	C14 H41 N2 O3 Si3
Gln 431	Gln	1 2 3 4 5	C14 H43 N2 O3 Si3
Cit 459	Cit	1 2 3 4 5 6	C14 H39 O6 Si3

Carbon atom mapping of reaction network

Table 4-A-2. Reaction network carbon transitions.

Glycolysis	
PGI	G6P (abcdef) <-> F6P (abcdef)
PFK	F6P (abcdef) -> DHAP (cba) + GAP (def)
TPI	DHAP (abc) <-> GAP (abc)
GADPH	GAP (abc) <-> 3PG (abc)
Eno	3PG (abc) <-> PEP (abc)
PK	PEP (abc) -> Pyr (abc)
HK	Glc (abcdef) -> G6P (abcdef)
LDH	Lac (abc) <-> Pyr (abc)
Pentose Phosphate Pathway	
6PGDH	G6P (abcdef) -> Ru5P (bcdef) + CO2 (a)
R5PE	Ru5P (abcde) <-> X5P (abcde)
R5PI	Ru5P (abcde) <-> R5P (abcde)
TK1	X5P (abcde) + R5P (fghij) <-> GAP (hij) + S7P (fgabcde)
TK2	S7P (abcdefg) + GAP (hij) <-> E4P (defg) + F6P (abchij)
TK3	X5P (abcde) + E4P (fghi) <-> GAP (cde) + F6P (abfghi)
TCA Cycle	
PDH	Pyr (abc) -> AcCoA (bc) + CO2 (a)
SDH	Suc (abcd) <-> Fum (abcd)
Fum	Fum (abcd) <-> Mal (abcd)
MDH	Mal (abcd) <-> OAA (abcd)
CS	OAA (abcd) + AcCoA (ef) -> Cit (dcbfea)
ADH	aKG.m (abcde) -> Suc (bcde) + CO2 (a)
IDH	Cit (abcdef) <-> aKG.m (abcde) + CO2 (f)
Transport	
Glc IN	Glc.e (abcdef) -> Glc (abcdef)
Glc Labeled	Glc.l (abcdef) -> Glc.e (abcdef)
Lys IN	Lys.e (abcdef) -> Lys (abcdef)
Thr IN	Thr.e (abcd) -> Thr (abcd)
Phe IN	Phe.e (abcdefghi) -> Phe (abcdefghi)
Tyr IN	Tyr.e (abcdefghi) -> Tyr (abcdefghi)
Val IN	Val.e (abcde) -> Val (abcde)
Leu IN	Leu.e (abcdef) -> Leu (abcdef)
Ile IN	Ile.e (abcdef) -> Ile (abcdef)
Trp IN	Trp.e (abcdefghijk) -> Trp (abcdefghijk)
His IN	His.e (abcdef) -> His (abcdef)
Met IN	Met.e (abcde) -> Met (abcde)

R *aKG Produced	DummyaKG <-> aKGSink
Glu/Asp Antiporter	Glu.c (abcde) -> Glu.m (abcde)
Mal/aKG Antiporter	aKG.m (abcde) -> aKG.c (abcde)
Glu.c Contribution	0*Glu.c (abcde) -> Glu.ms (abcde)
Glu.m Contribution	0*Glu.m (abcde) -> Glu.ms (abcde)
Glu Sink	Glu.ms (abcde) -> PhoneyBaloneyGluSink (abcde)
Anaplerotic reactions	
ME	Mal (abcd) -> Pyr (abc) + CO2 (d)
PC	Pyr (abc) + CO2 (d) -> OAA (abcd)
ACL	Cit (abcdef) -> AcCoA.c (ed) + Mal (fcba)
Amino Acid Metabolism	
GLS	Gln (abcde) <-> Glu.m (abcde)
ASNS	Asp (abcd) <-> Asn (abcd)
SHT	Ser (abc) <-> Gly (ab) + MEETHF (c)
CYST	Ser (abc) <-> Cys (abc)
GS + SHT	CO2 (a) + MEETHF (b) -> Gly (ab)
Met Mtbl	Met (abcde) + Ser (fgh) -> Methyl (e) + Cys (fgh) + Suc (abcd)
PheTyr Mtbl	Phe (abcdefghi) -> Tyr (abcdefghi)
Thr Mtbl	Thr (abcd) -> Pyr (abc) + CO2 (d)
Histidase	His (abcdef) -> FormTHF (f) + Glu.c (abcde)
CBXase + Mutase	ProCoA (abc) + CO2 (d) -> Suc (abcd)
Trp Mtbl	Trp (abcdefghijk) -> CO2 (d) + CO2 (e) + Ala (abc) + aKetoadi (fghijk)
Trp2 Mtbl	aKetoadi (abcdef) -> CO2 (a) + CO2 (f) + AcCoA (bc) + AcCoA (de)
*GDH	aKG.m (abcde) + DummyaKG <-> Glu.m (abcde)
*ALT	Ala (abc) + aKG.c (defgh) + DummyaKG <-> Pyr (abc) + Glu.c (defgh)
*Ile Mtbl	Ile (abcdef) + aKG.c (ghijk) + DummyaKG -> AcCoA (de) + CO2 (a) + ProCoA (bcf) + Glu.c (ghijk)
*Leu Mtbl	Leu (abcdef) + aKG.c (ghijk) + CO2 (l) + DummyaKG -> CO2 (a) + AcCoA (bc) + AcCoA (ld) + AcCoA (ef) + Glu.c (ghijk)
*Tyr Mtbl	Tyr (abcdefghi) + aKG.c (jklmn) + DummyaKG -> CO2 (a) + Mal (defg) + AcCoA (bc) + AcCoA (hi) + Glu.c (jklmn)
*Val Mtbl	Val (abcde) + aKG.c (fghij) + DummyaKG -> Glu.c (fghij) + CO2 (a) + CO2 (e) + ProCoA (bcd)
*Lys Mtbl	Lys (abcdef) + aKG.c (ghijk) + aKG.c (lmnop) + DummyaKG + DummyaKG -> Glu.c (ghijk) + Glu.c (lmnop) + aKetoadi (abcdef)
*AST	OAA (abcd) + Glu.c (efghi) <-> Asp (abcd) + aKG.c (efghi) + DummyaKG
*Arg Mtbl	Arg (abcdef) + aKG.c (ghijk) + DummyaKG -> Glu.c (abcde) + Urea (f) + Glu.c (ghijk)
*PST	3PG (abc) + Glu.c (defgh) -> Ser (abc) + aKG.c (defgh) + DummyaKG
*Cys Mtbl	Cys (abc) + aKG.c (defgh) + DummyaKG -> Pyr (abc) + Glu.c (defgh)
Lumped Biomass Equation	

New Biomass 363pg	0.2178*Ala + 0.1368*Arg + 0.1712*Asp + 0.1046*Asn + 0.0526*Cys + 0.1168*Gln + 0.1401*Glu.c + 0.2389*Gly + 0.0519*His + 0.1176*Ile + 0.2048*Leu + 0.2069*Lys + 0.0501*Met + 0.0796*Phe + 0.1136*Pro + 0.1601*Ser + 0.1401*Thr + 0.016*Trp + 0.0661*Tyr + 0.151*Val + 0.1047*G6P + 0.0845*R5P + 0.0926*MEETHF + 0.0441*DHAP + 0.8985*AcCoA.c -> Biomass
Transport Exchange	
Ser Flux	Ser.e (abc) <-> Ser (abc)
Ala Flux	Ala.e (abc) <-> Ala (abc)
Arg Flux	Arg.e (abcdef) <-> Arg (abcdef)
Asp Flux	Asp.e (abcd) <-> Asp (abcd)
Gln Flux	Gln.e (abcde) <-> Gln (abcde)
Pro Flux	Pro.e (abcde) <-> Pro (abcde)
Asn Flux	Asn.e (abcd) <-> Asn (abcd)
Lac Flux	Lac.e (abc) <-> Lac (abc)
Gly Flux	Gly.e (ab) <-> Gly (ab)
Cys Flux	Cys.e (abc) <-> Cys (abc)
Glu Flux	Glu.e (abcde) <-> Glu.c (abcde)

95% confidence intervals associated with individual fluxes

Table 4-A-3. Net fluxes of control during lactate producing phase. Associated with Figure 4-4.

Pathway	Enzyme	Rxn	LB 95% CI	UB 95% CI	Value
Glycolysis	PGI	G6P <-> F6P	3.604	4.377	3.991
	PFK	F6P -> DHAP + GAP	3.544	4.317	3.931
	TPI	DHAP <-> GAP	3.497	4.271	3.884
	GADPH	GAP <-> 3PG	7.011	8.559	7.785
	Eno	3PG <-> PEP	6.836	8.316	7.576
	PK	PEP -> Pyr	6.836	8.316	7.576
	HK	Glc -> G6P	3.716	4.488	4.102
	LDH	Lac <-> Pyr	-7.096	-4.498	-5.797
PPP	6PGDH	G6P -> Ru5P + CO2	0.000	0.295	0.147
	R5PE	Ru5P <-> X5P	-0.064	0.133	0.034
	R5PI	Ru5P <-> R5P	0.056	0.158	0.107
	TK1	X5P + R5P <-> GAP + S7P	-0.032	0.066	0.017
	TK2	S7P + GAP <-> E4P + F6P	-0.032	0.066	0.017
	TK3	X5P + E4P <-> GAP + F6P	-0.032	0.066	0.017
TCA	PDH	Pyr -> AcCoA + CO2	1.831	4.030	2.931
	SDH	Suc <-> Fum	2.080	4.459	3.269
	Fum	Fum <-> Mal	2.080	4.459	3.269
	MDH	Mal <-> OAA	1.642	4.012	2.827
	CS	OAA + AcCoA -> Cit	2.133	4.381	3.257
	ADH	aKG.m -> Suc + CO2	1.928	4.287	3.108
	IDH	Cit <-> aKG.m + CO2	1.180	3.430	2.305
Transport	Glc IN	Glc.e -> Glc	3.716	4.488	4.102
	Lys IN	Lys.e -> Lys	0.249	0.366	0.308
	Thr IN	Thr.e -> Thr	0.138	0.178	0.158
	Phe IN	Phe.e -> Phe	0.087	0.129	0.108
	Tyr IN	Tyr.e -> Tyr	0.025	0.067	0.046
	Val IN	Val.e -> Val	0.197	0.319	0.258
	Leu IN	Leu.e -> Leu	0.202	0.316	0.259
	Ile IN	Ile.e -> Ile	0.116	0.185	0.151
	Trp IN	Trp.e -> Trp	0.044	0.109	0.076
	His IN	His.e -> His	0.071	0.127	0.099
	Met IN	Met.e -> Met	0.086	0.167	0.126
	Ser Flux	Ser.e <-> Ser	0.696	0.952	0.824
	Ala Flux	Ala.e <-> Ala	-0.771	-0.537	-0.654
	Arg Flux	Arg.e <-> Arg	0.164	0.289	0.227
	Asp Flux	Asp.e <-> Asp	-0.078	0.005	-0.036

	Gln Flux	Gln.e <-> Gln	0.832	1.058	0.945
	Pro Flux	Pro.e <-> Pro	0.112	0.129	0.121
	Asn Flux	Asn.e <-> Asn	0.351	0.522	0.437
	Lac Flux	Lac.e <-> Lac	-7.096	-4.498	-5.797
	Gly Flux	Gly.e <-> Gly	-0.377	-0.262	-0.319
	Cys Flux	Cys.e <-> Cys	0.056	0.153	0.104
	Glu Flux	Glu.e <-> Glu.c	0.011	0.091	0.051
	Glu/Asp Antiporter	Glu.c -> Glu.m	0.000	0.148	0.074
	Mal/aKG Antiporter	aKG.m -> aKG.c	0.000	0.100	0.050
Anaplerosis	ME	Mal -> Pyr + CO2	1.173	1.703	1.438
	PC	Pyr + CO2 -> OAA	0.111	0.550	0.330
	ACL	Cit -> AcCoA.c + Mal	0.886	1.021	0.953
Amino	GLS	Gln <-> Glu.m	0.708	0.934	0.821
Acid	ASNS	Asp <-> Asn	-0.410	-0.241	-0.326
Metabolism	SHT	Ser <-> Gly + MEETHF	0.305	0.367	0.336
	CYST	Ser <-> Cys	0.269	0.662	0.465
	GS + SHT	CO2 + MEETHF -> Gly	0.208	0.267	0.237
	Met Mtbl	Met + Ser -> Methyl + Cys + Suc	0.033	0.114	0.073
	PheTyr Mtbl	Phe -> Tyr	0.004	0.045	0.024
	Thr Mtbl	Thr -> Pyr + CO2	0.000	0.029	0.014
	Histidase	His -> FormTHF + Glu.c	0.016	0.073	0.044
	CBXase + Mutase	ProCoA + CO2 -> Suc	0.037	0.174	0.105
	Trp Mtbl	Trp -> CO2 + CO2 + Ala + aKetoadi	0.027	0.092	0.059
	Trp2 Mtbl	aKetoadi -> CO2 + CO2 + AcCoA + AcCoA	0.083	0.209	0.146
	*GDH	aKG.m <-> Glu.m	-0.997	-0.713	-0.855
	*ALT	Ala + aKG.c <-> Pyr + Glu.c	-0.944	-0.708	-0.826
	*Ile Mtbl	Ile + aKG.c -> AcCoA + CO2 + ProCoA + Glu.c	0.000	0.060	0.030
	*Leu Mtbl	Leu + aKG.c + CO2 -> CO2 + AcCoA + AcCoA + AcCoA + Glu.c	0.000	0.096	0.048
	*Tyr Mtbl	Tyr + aKG.c -> CO2 + Mal.c + AcCoA + AcCoA + Glu.c	0.000	0.019	0.010
	*Val Mtbl	Val + aKG.c -> Glu.c + CO2 + CO2 + ProCoA	0.037	0.158	0.098
	*Lys Mtbl	Lys + aKG.c + aKG.c -> Glu.c + Glu.c + aKetoadi	0.031	0.145	0.088
	*AST	OAA + Glu.c <-> Asp + aKG.c	-0.200	-0.016	-0.108

	*Arg Mtbl	Arg + aKG.c -> Glu.c + Urea + Glu.c	0.020	0.144	0.082
	*PST	3PG + Glu.c -> Ser + aKG.c	0.105	0.389	0.247
	*Cys Mtbl	Cys + aKG.c -> Pyr + Glu.c	0.402	0.773	0.588
Biomass Production	Biomass 398 pg	0.2388*Ala + 0.15*Arg + 0.1877*Asp + 0.1147*Asn + 0.0577*Cys + 0.1281*Gln + 0.1536*Glu.c + 0.2619*Gly + 0.0569*His + 0.129*Ile + 0.2245*Leu + 0.2268*Lys + 0.0549*Met + 0.0872*Phe + 0.1246*Pro + 0.1755*Ser + 0.1536*Thr + 0.0175*Trp + 0.0725*Tyr + 0.1656*Val + 0.1148*G6P + 0.0927*R5P + 0.1015*MEETHF + 0.0484*DHAP + 0.9851*AcCoA.c -> Biomass	0.899	1.036	0.967

Table 4-A-4. Exchange fluxes of control during lactate producing phase. Associated with Figure 4-4.

Pathway	Enzyme	Rxn	LB 95% CI	UB 95% CI	Value
TCA	IDH	Cit <-> aKG.m + CO2	0.000	0.7155	0.358
Amino	GLS	Gln <-> Glu.m	0.000	1.485	0.743
Acid	ASNS	Asp <-> Asn	0.000	3.8813	1.941
Metabolism	SHT	Ser <-> Gly + MEETHF	0.372	1.6458	1.009
	ALT	Ala + aKG.c <-> Pyr + Glu.c	0.000	2.8246	1.412
	AST	OAA + Glu.c <-> Asp + aKG.c	0.087	1.5429	0.815
Transport	Ser Flux	Ser.e <-> Ser	0.000	1.8807	0.940
	Ala Flux	Ala.e <-> Ala	0.000	0.1416	0.071
	Asp Flux	Asp.e <-> Asp	0.000	3.9289	1.964
	Lac Flux	Lac.e <-> Lac	0.000	0.1355	0.068
	Gly Flux	Gly.e <-> Gly	0.077	0.6427	0.360

Table 4-A-5. Net fluxes of low expressing (LE) during lactate producing phase. Associated with Figure 4-4.

Pathway	Enzyme	Rxn	LB 95% CI	UB 95% CI	Value
Glycolysis	PGI	G6P <-> F6P	3.165	4.029	3.597
	PFK	F6P -> DHAP + GAP	3.113	3.973	3.543
	TPI	DHAP <-> GAP	3.069	3.929	3.499
	GADPH	GAP <-> 3PG	6.153	7.874	7.014
	Eno	3PG <-> PEP	5.977	7.630	6.803
	PK	PEP -> Pyr	5.977	7.630	6.803
	HK	Glc -> G6P	3.273	4.133	3.703
	LDH	Lac <-> Pyr	-6.151	-3.833	-4.992
PPP	6PGDH	G6P -> Ru5P + CO2	0.000	0.305	0.152
	R5PE	Ru5P <-> X5P	-0.060	0.147	0.043
	R5PI	Ru5P <-> R5P	0.052	0.158	0.105
	TK1	X5P + R5P <-> GAP + S7P	-0.030	0.073	0.022
	TK2	S7P + GAP <-> E4P + F6P	-0.030	0.073	0.022
	TK3	X5P + E4P <-> GAP + F6P	-0.030	0.073	0.022
TCA	PDH	Pyr -> AcCoA + CO2	1.758	3.654	2.706
	SDH	Suc <-> Fum	1.621	3.879	2.750
	Fum	Fum <-> Mal	1.621	3.879	2.750
	MDH	Mal <-> OAA	1.603	3.635	2.619
	CS	OAA + AcCoA -> Cit	1.977	4.125	3.051
	ADH	aKG.m -> Suc + CO2	1.539	3.722	2.631
	IDH	Cit <-> aKG.m + CO2	1.083	3.230	2.156
Transport	Glc IN	Glc.e -> Glc	3.273	4.133	3.703
	Lys IN	Lys.e -> Lys	0.218	0.374	0.296
	Thr IN	Thr.e -> Thr	0.131	0.222	0.177
	Phe IN	Phe.e -> Phe	0.087	0.142	0.114
	Tyr IN	Tyr.e -> Tyr	0.006	0.059	0.032
	Val IN	Val.e -> Val	0.163	0.340	0.251
	Leu IN	Leu.e -> Leu	0.191	0.326	0.258
	Ile IN	Ile.e -> Ile	0.110	0.235	0.173
	Trp IN	Trp.e -> Trp	0.015	0.071	0.043
	His IN	His.e -> His	0.064	0.135	0.100
	Met IN	Met.e -> Met	0.047	0.112	0.080
	Ser Flux	Ser.e <-> Ser	0.539	0.831	0.685
	Ala Flux	Ala.e <-> Ala	-0.608	-0.410	-0.509
	Arg Flux	Arg.e <-> Arg	0.131	0.267	0.199
	Asp Flux	Asp.e <-> Asp	-0.064	0.022	-0.021
	Gln Flux	Gln.e <-> Gln	0.619	0.814	0.716
	Pro Flux	Pro.e <-> Pro	0.106	0.121	0.113

	Asn Flux	Asn.e <-> Asn	0.320	0.555	0.437
	Lac Flux	Lac.e <-> Lac	-6.151	-3.833	-4.992
	Gly Flux	Gly.e <-> Gly	-0.280	-0.188	-0.234
	Cys Flux	Cys.e <-> Cys	0.055	0.127	0.091
	Glu Flux	Glu.e <-> Glu.c	-0.130	-0.008	-0.069
	Glu/Asp Antiporter	Glu.c -> Glu.m	0.000	0.164	0.082
	Mal/aKG Antiporter	aKG.m -> aKG.c	0.008	0.261	0.134
Anaplerosis	ME	Mal -> Pyr + CO2	0.811	1.297	1.054
	PC	Pyr + CO2 -> OAA	0.128	0.469	0.298
	ACL	Cit -> AcCoA.c + Mal	0.836	0.956	0.896
Amino	GLS	Gln <-> Glu.m	0.503	0.698	0.600
Acid	ASNS	Asp <-> Asn	-0.450	-0.217	-0.333
Metabolism	SHT	Ser <-> Gly + MEETHF	0.257	0.308	0.282
	CYST	Ser <-> Cys	0.260	0.664	0.462
	GS + SHT	CO2 + MEETHF -> Gly	0.167	0.213	0.190
	Met Mtbl	Met + Ser -> Methyl + Cys + Suc	0.000	0.062	0.031
	PheTyr Mtbl	Phe -> Tyr	0.008	0.062	0.035
	Thr Mtbl	Thr -> Pyr + CO2	0.000	0.083	0.042
	Histidase	His -> FormTHF + Glu.c	0.013	0.083	0.048
	CBXase + Mutase	ProCoA + CO2 -> Suc	0.020	0.250	0.135
	Trp Mtbl	Trp -> CO2 + CO2 + Ala + aKetoadi	0.000	0.055	0.028
	Trp2 Mtbl	aKetoadi -> CO2 + CO2 + AcCoA + AcCoA	0.021	0.188	0.104
	*GDH	aKG.m <-> Glu.m	-0.776	-0.503	-0.639
	*ALT	Ala + aKG.c <-> Pyr + Glu.c	-0.816	-0.604	-0.710
	*Ile Mtbl	Ile + aKG.c -> AcCoA + CO2 + ProCoA + Glu.c	0.000	0.118	0.059
	*Leu Mtbl	Leu + aKG.c + CO2 -> CO2 + AcCoA + AcCoA + AcCoA + Glu.c	0.000	0.120	0.060
	*Tyr Mtbl	Tyr + aKG.c -> CO2 + Mal + AcCoA + AcCoA + Glu.c	0.000	0.029	0.014
	*Val Mtbl	Val + aKG.c -> Glu.c + CO2 + CO2 + ProCoA	0.013	0.189	0.101
	*Lys Mtbl	Lys + aKG.c + aKG.c -> Glu.c + Glu.c + aKetoadi	0.013	0.167	0.090
	*AST	OAA + Glu.c <-> Asp + aKG.c	-0.263	-0.019	-0.141
	*Arg Mtbl	Arg + aKG.c -> Glu.c + Urea + Glu.c	0.000	0.130	0.065
	*PST	3PG + Glu.c -> Ser + aKG.c	0.091	0.414	0.252

	*Cys Mtbl	Cys + aKG.c -> Pyr + Glu.c	0.327	0.717	0.522
Biomass Production	Biomass 363 pg	0.2178*Ala + 0.1368*Arg + 0.1712*Asp + 0.1046*Asn + 0.0526*Cys + 0.1168*Gln + 0.1401*Glu.c + 0.2389*Gly + 0.0519*His + 0.1176*Ile + 0.2048*Leu + 0.2069*Lys + 0.0501*Met + 0.0796*Phe + 0.1136*Pro + 0.1601*Ser + 0.1401*Thr + 0.016*Trp + 0.0661*Tyr + 0.151*Val + 0.1047*G6P + 0.0845*R5P + 0.0926*MEETHF + 0.0441*DHAP + 0.8985*AcCoA.c -> Biomass	0.930	1.064	0.997

Table 4-A-6. Exchange fluxes of low expressing (LE) during lactate producing phase. Associated with Figure 4-4.

Pathway	Enzyme	Rxn	LB 95% CI	UB 95% CI	Value
TCA	IDH	Cit <-> aKG.m + CO2	0	1.1067	0.55335
Amino Acid Metabolism	GLS	Gln <-> Glu.m	0	1.089	0.5445
	ASNS	Asp <-> Asn	0	2.6921	1.34605
	ALT	Ala + aKG.c <-> Pyr + Glu.c	0	2.3776	1.1888
	AST	OAA + Glu.c <-> Asp + aKG.c	0.1499	1.092	0.62095
Transport	Ser Flux	Ser.e <-> Ser	0	2.4757	1.23785
	Ala Flux	Ala.e <-> Ala	0	0.2092	0.1046
	Asp Flux	Asp.e <-> Asp	0	3.4407	1.72035
	Lac Flux	Lac.e <-> Lac	0	0.1598	0.0799
	Gly Flux	Gly.e <-> Gly	0	0.4771	0.23855

Table 4-A-7. Net fluxes of high expressing (HE) during lactate producing phase. Associated with Figure 4-4.

Pathway	Enzyme	Rxn	LB 95% CI	UB 95% CI	Value
Glycolysis	PGI	G6P <-> F6P	2.434	3.003	2.719
	PFK	F6P -> DHAP + GAP	2.413	2.960	2.687
	TPI	DHAP <-> GAP	2.380	2.927	2.653
	GADPH	GAP <-> 3PG	4.772	5.867	5.319
	Eno	3PG <-> PEP	4.686	5.773	5.230
	PK	PEP -> Pyr	4.686	5.773	5.230
	HK	Glc -> G6P	2.534	3.081	2.807
	LDH	Lac <-> Pyr	-3.982	-2.464	-3.223
PPP	6PGDH	G6P -> Ru5P + CO2	0.000	0.237	0.119
	R5PE	Ru5P <-> X5P	-0.045	0.116	0.035
	R5PI	Ru5P <-> R5P	0.039	0.121	0.080
	TK1	X5P + R5P <-> GAP + S7P	-0.023	0.058	0.018
	TK2	S7P + GAP <-> E4P + F6P	-0.023	0.058	0.018
	TK3	X5P + E4P <-> GAP + F6P	-0.023	0.058	0.018
TCA	PDH	Pyr -> AcCoA + CO2	1.900	3.313	2.607
	SDH	Suc <-> Fum	1.927	3.470	2.699
	Fum	Fum <-> Mal	1.927	3.470	2.699
	MDH	Mal <-> OAA	1.686	3.103	2.395
	CS	OAA + AcCoA -> Cit	2.095	3.577	2.836
	ADH	aKG.m -> Suc + CO2	1.914	3.449	2.681
	IDH	Cit <-> aKG.m + CO2	1.423	2.903	2.163
Transport	Glc IN	Glc.e -> Glc	2.534	3.081	2.807
	Lys IN	Lys.e -> Lys	0.215	0.309	0.262
	Thr IN	Thr.e -> Thr	0.098	0.134	0.116
	Phe IN	Phe.e -> Phe	0.060	0.094	0.077
	Tyr IN	Tyr.e -> Tyr	0.015	0.049	0.032
	Val IN	Val.e -> Val	0.105	0.137	0.121
	Leu IN	Leu.e -> Leu	0.143	0.179	0.161
	Ile IN	Ile.e -> Ile	0.082	0.113	0.097
	Trp IN	Trp.e -> Trp	0.011	0.047	0.029
	His IN	His.e -> His	0.062	0.112	0.087
	Met IN	Met.e -> Met	0.036	0.081	0.058
	Ser Flux	Ser.e <-> Ser	0.330	0.499	0.414
	Ala Flux	Ala.e <-> Ala	-0.461	-0.355	-0.408
	Arg Flux	Arg.e <-> Arg	0.096	0.161	0.128
	Asp Flux	Asp.e <-> Asp	-0.113	-0.052	-0.082
	Gln Flux	Gln.e <-> Gln	0.579	0.746	0.663
	Pro Flux	Pro.e <-> Pro	0.079	0.091	0.085

	Asn Flux	Asn.e <-> Asn	0.337	0.455	0.396
	Lac Flux	Lac.e <-> Lac	-3.982	-2.464	-3.223
	Gly Flux	Gly.e <-> Gly	0.079	0.116	0.098
	Cys Flux	Cys.e <-> Cys	0.050	0.102	0.076
	Glu Flux	Glu.e <-> Glu.c	-0.025	0.054	0.014
	Glu/Asp Antiporter	Glu.c -> Glu.m	0.000	0.066	0.033
	Mal/aKG Antiporter	aKG.m -> aKG.c	0.000	0.101	0.051
Anaplerosis	ME	Mal -> Pyr + CO2	0.820	1.175	0.998
	PC	Pyr + CO2 -> OAA	0.189	0.487	0.338
	ACL	Cit -> AcCoA.c + Mal	0.626	0.719	0.672
Amino	GLS	Gln <-> Glu.m	0.490	0.659	0.575
Acid	ASNS	Asp <-> Asn	-0.376	-0.259	-0.317
Metabolism	SHT	Ser <-> Gly + MEETHF	0.065	0.087	0.076
	CYST	Ser <-> Cys	0.191	0.410	0.300
	GS + SHT	CO2 + MEETHF -> Gly	0.000	0.016	0.008
	Met Mtbl	Met + Ser -> Methyl + Cys + Suc	0.000	0.043	0.022
	PheTyr Mtbl	Phe -> Tyr	0.000	0.035	0.017
	Thr Mtbl	Thr -> Pyr + CO2	0.000	0.029	0.015
	Histidase	His -> FormTHF + Glu.c	0.023	0.073	0.048
	CBXase + Mutase	ProCoA + CO2 -> Suc	0.000	0.026	0.013
	Trp Mtbl	Trp -> CO2 + CO2 + Ala + aKetoadi	0.000	0.035	0.017
	Trp2 Mtbl	aKetoadi -> CO2 + CO2 + AcCoA + AcCoA	0.071	0.166	0.118
	*GDH	aKG.m <-> Glu.m	-0.666	-0.491	-0.579
	*ALT	Ala + aKG.c <-> Pyr + Glu.c	-0.619	-0.502	-0.561
	*Ile Mtbl	Ile + aKG.c -> AcCoA + CO2 + ProCoA + Glu.c	0.000	0.025	0.012
	*Leu Mtbl	Leu + aKG.c + CO2 -> CO2 + AcCoA + AcCoA + AcCoA + Glu.c	0.000	0.025	0.012
	*Tyr Mtbl	Tyr + aKG.c -> CO2 + Mal + AcCoA + AcCoA + Glu.c	0.000	0.016	0.008
	*Val Mtbl	Val + aKG.c -> Glu.c + CO2 + CO2 + ProCoA	0.000	0.024	0.012
	*Lys Mtbl	Lys + aKG.c + aKG.c -> Glu.c + Glu.c + aKetoadi	0.062	0.152	0.107
	*AST	OAA + Glu.c <-> Asp + aKG.c	-0.172	-0.042	-0.107
	*Arg Mtbl	Arg + aKG.c -> Glu.c + Urea + Glu.c	0.000	0.057	0.029
	*PST	3PG + Glu.c -> Ser + aKG.c	0.071	0.176	0.123

	*Cys Mtbl	Cys + aKG.c -> Pyr + Glu.c	0.252	0.461	0.357
Biomass Production	Biomass 341 pg	0.2046*Ala + 0.1285*Arg + 0.1609*Asp + 0.0983*Asn + 0.0494*Cys + 0.1098*Gln + 0.1316*Glu.c + 0.2244*Gly + 0.0487*His + 0.1105*Ile + 0.1924*Leu + 0.1943*Lys + 0.0471*Met + 0.0747*Phe + 0.1068*Pro + 0.1504*Ser + 0.1316*Thr + 0.015*Trp + 0.0621*Tyr + 0.1419*Val + 0.0984*G6P + 0.0794*R5P + 0.087*MEETHF + 0.0415*DHAP + 0.844*AcCoA.c -> Biomass	0.7414	0.8518	0.7966

Table 4-A-8. Exchange fluxes of high expressing (HE) during lactate producing phase. Associated with Figure 4-4.

Pathway	Enzyme	Rxn	LB 95% CI	UB 95% CI	Value
TCA	IDH	Cit <-> aKG.m + CO2	0.0411	1.5426	0.79185
Amino Acid Metabolism	GLS	Gln <-> Glu.m	0	0.445	0.2225
	ASNS	Asp <-> Asn	0	1.8344	0.9172
	SHT	Ser <-> Gly + MEETHF	0.2508	0.673	0.4619
	ALT	Ala + aKG.c <-> Pyr + Glu.c	0	1.7645	0.88225
	AST	OAA + Glu.c <-> Asp + aKG.c	0.4405	1.2755	0.858
Transport	Lac Flux	Lac.e <-> Lac	0	0.1112	0.0556
	Ser Flux	Ser.e <-> Ser	0	0.4395	0.21975
	Ala Flux	Ala.e <-> Ala	0	0.1405	0.07025
	Asp Flux	Asp.e <-> Asp	0	2.8274	1.4137
	Gly Flux	Gly.e <-> Gly	0	0.0915	0.04575

Table 4-A-9. Net fluxes of control during lactate consuming phase. Associated with Figure 4-7.

Pathway	Enzyme	Rxn	LB 95% CI	UB 95% CI	Value
Glycolysis	PGI	G6P <-> F6P	-1.099	0.941	-0.079
	PFK	F6P -> DHAP + GAP	0.124	0.938	0.531
	TPI	DHAP <-> GAP	0.159	0.936	0.547
	GADPH	GAP <-> 3PG	0.864	1.872	1.368
	Eno	3PG <-> PEP	0.678	1.564	1.121
	PK	PEP -> Pyr	0.678	1.564	1.121
	HK	Glc -> G6P	0.680	0.960	0.820
	LDH	Lac <-> Pyr	0.563	0.716	0.640
PPP	6PGDH	G6P -> Ru5P + CO2	0.000	2.091	1.045
	R5PE	Ru5P <-> X5P	-0.005	1.307	0.651
	R5PI	Ru5P <-> R5P	0.002	0.643	0.322
	TK1	X5P + R5P <-> GAP + S7P	-0.002	0.653	0.325
	TK2	S7P + GAP <-> E4P + F6P	-0.002	0.653	0.325
	TK3	X5P + E4P <-> GAP + F6P	-0.002	0.653	0.325
TCA	PDH	Pyr -> AcCoA + CO2	1.452	2.497	1.974
	SDH	Suc <-> Fum	1.449	2.595	2.022
	Fum	Fum <-> Mal.m	1.449	2.595	2.022
	MDH	Mal.m <-> OAA	1.449	2.595	2.022
	CS	OAA + AcCoA -> Cit	1.550	2.674	2.112
	ADH	aKG.m -> Suc + CO2	1.431	2.571	2.001
	IDH	Cit <-> aKG.m + CO2	1.537	2.630	2.083
Transport	Glc IN	Glc.e -> Glc	0.680	0.960	0.820
	Lys IN	Lys.e -> Lys	0.005	0.020	0.013
	Thr IN	Thr.e -> Thr	0.006	0.033	0.020
	Phe IN	Phe.e -> Phe	0.002	0.014	0.008
	Tyr IN	Tyr.e -> Tyr	0.001	0.013	0.007
	Val IN	Val.e -> Val	0.004	0.024	0.014
	Leu IN	Leu.e -> Leu	0.032	0.069	0.050
	Ile IN	Ile.e -> Ile	0.007	0.032	0.020
	Trp IN	Trp.e -> Trp	0.001	0.017	0.009
	His IN	His.e -> His	0.002	0.016	0.009
	Met IN	Met.e -> Met	0.002	0.016	0.009
	Ser Flux	Ser.e <-> Ser	0.027	0.051	0.039
	Ala Flux	Ala.e <-> Ala	0.032	0.122	0.077
	Arg Flux	Arg.e <-> Arg	0.004	0.017	0.010
	Asp Flux	Asp.e <-> Asp	-0.005	0.015	0.005
	Gln Flux	Gln.e <-> Gln	-0.070	0.014	-0.028
	Pro Flux	Pro.e <-> Pro	0.003	0.010	0.006

	Asn Flux	Asn.e <-> Asn	-0.104	0.003	-0.051
	Lac Flux	Lac.e <-> Lac	0.563	0.716	0.640
	Gly Flux	Gly.e <-> Gly	-0.108	-0.052	-0.080
	Cys Flux	Cys.e <-> Cys	0.000	0.014	0.007
	Glu Flux	Glu.e <-> Glu.c	-0.060	-0.011	-0.035
	Glu/Asp Antiporter	Glu.c -> Glu.m	0.000	0.102	0.051
	Mal/aKG Antiporter	aKG.m -> aKG.c	0.009	0.135	0.072
Anaplerosis	ME	Mal.c -> Pyr + CO2	0.026	0.084	0.055
	PC	Pyr + CO2 -> OAA	0.086	0.238	0.162
	ACL	Cit -> AcCoA.c + Mal.c	0.023	0.077	0.050
Amino	GLS	Gln <-> Glu.m	-0.076	0.007	-0.035
Acid	ASNS	Asp <-> Asn	0.004	0.109	0.056
Metabolism	SHT	Ser <-> Gly + MEETHF	0.036	0.064	0.050
	CYST	Ser <-> Cys	0.080	0.429	0.254
	GS + SHT	CO2 + MEETHF -> Gly	0.030	0.058	0.044
	Met Mtbl	Met + Ser -> Methyl + Cys + Suc	0.000	0.013	0.007
	PheTyr Mtbl	Phe -> Tyr	0.000	0.007	0.004
	Thr Mtbl	Thr -> Pyr + CO2	0.000	0.026	0.013
	Histidase	His -> FormTHF + Glu.c	0.000	0.013	0.006
	CBXase + Mutase	ProCoA + CO2 -> Suc	0.000	0.034	0.017
	Trp Mtbl	Trp -> CO2 + CO2 + Ala + aKetoadi	0.000	0.016	0.008
	Trp2 Mtbl	aKetoadi -> CO2 + CO2 + AcCoA + AcCoA	0.000	0.019	0.009
	*GDH	aKG.m <-> Glu.m	-0.075	0.077	0.001
	*ALT	Ala + aKG.c <-> Pyr + Glu.c	0.028	0.120	0.074
	*Ile Mtbl	Ile + aKG.c -> AcCoA + CO2 + ProCoA + Glu.c	0.000	0.026	0.013
	*Leu Mtbl	Leu + aKG.c + CO2 -> CO2 + AcCoA + AcCoA + AcCoA + Glu.c	0.020	0.058	0.039
	*Tyr Mtbl	Tyr + aKG.c -> CO2 + Mal.c + AcCoA + AcCoA + Glu.c	0.002	0.010	0.006
	*Val Mtbl	Val + aKG.c -> Glu.c + CO2 + CO2 + ProCoA	0.000	0.016	0.008
	*Lys Mtbl	Lys + aKG.c + aKG.c -> Glu.c + Glu.c + aKetoadi	0.000	0.008	0.004
	*AST	OAA + Glu.c <-> Asp + aKG.c	0.008	0.112	0.060
	*Arg Mtbl	Arg + aKG.c -> Glu.c + Urea + Glu.c	0.000	0.010	0.005
	*PST	3PG + Glu.c -> Ser + aKG.c	0.107	0.469	0.288

	*Cys Mtbl	Cys + aKG.c -> Pyr + Glu.c	0.089	0.453	0.271
Biomass Production	Biomass 398 pg	0.2388*Ala + 0.15*Arg + 0.1877*Asp + 0.1147*Asn + 0.0577*Cys + 0.1281*Gln + 0.1536*Glu.c + 0.2619*Gly + 0.0569*His + 0.129*Ile + 0.2245*Leu + 0.2268*Lys + 0.0549*Met + 0.0872*Phe + 0.1246*Pro + 0.1755*Ser + 0.1536*Thr + 0.0175*Trp + 0.0725*Tyr + 0.1656*Val + 0.1148*G6P + 0.0927*R5P + 0.1015*MEETHF + 0.0484*DHAP + 0.9851*AcCoA.c -> Biomass	0.024	0.078	0.051

Table 4-A-10. Exchange fluxes of control during lactate consuming phase. Associated with Figure 4-7.

Pathway	Enzyme	Rxn	LB 95% CI	UB 95% CI	Value
TCA	IDH	Cit <-> aKG.m + CO2	0	0.156	0.078
Amino Acid Metabolism	ASNS	Asp <-> Asn	0	1.0698	0.5349
	SHT	Ser <-> Gly + MEETHF	0.601	3.6638	2.1324
	AST	OAA + Glu.c <-> Asp + aKG.c	0.0122	0.3127	0.16245
Transport	Ser Flux	Ser.e <-> Ser	0	0.5414	0.2707
	Ala Flux	Ala.e <-> Ala	0	0.1874	0.0937
	Asp Flux	Asp.e <-> Asp	0	0.8411	0.42055
	Lac Flux	Lac.e <-> Lac	4.9912	26.9638	15.9775
	Gly Flux	Gly.e <-> Gly	0.0818	0.5432	0.3125
	Cys Flux	Cys.e <-> Cys	0	3.795	1.8975

Table 4-A-11. Net fluxes of low expressing (LE) during lactate consuming phase.
Associated with Figure 4-7.

Pathway	Enzyme	Rxn	LB 95% CI	UB 95% CI	Value
Glycolysis	PGI	G6P <-> F6P	-0.963	0.683	-0.140
	PFK	F6P -> DHAP + GAP	0.101	0.680	0.390
	TPI	DHAP <-> GAP	0.098	0.681	0.389
	GADPH	GAP <-> 3PG	0.696	1.355	1.025
	Eno	3PG <-> PEP	0.431	1.081	0.756
	PK	PEP -> Pyr	0.431	1.081	0.756
	HK	Glc -> G6P	0.564	0.708	0.636
	LDH	Lac <-> Pyr	0.526	0.687	0.606
PPP	6PGDH	G6P -> Ru5P + CO2	0.000	1.621	0.811
	R5PE	Ru5P <-> X5P	-0.004	1.077	0.536
	R5PI	Ru5P <-> R5P	0.003	0.544	0.273
	TK1	X5P + R5P <-> GAP + S7P	-0.002	0.539	0.268
	TK2	S7P + GAP <-> E4P + F6P	-0.002	0.539	0.268
	TK3	X5P + E4P <-> GAP + F6P	-0.002	0.539	0.268
TCA	PDH	Pyr -> AcCoA + CO2	1.252	1.992	1.622
	SDH	Suc <-> Fum	1.245	2.042	1.643
	Fum	Fum <-> Mal.m	1.245	2.042	1.643
	MDH	Mal.m <-> OAA	1.245	2.042	1.643
	CS	OAA + AcCoA -> Cit	1.343	2.112	1.727
	ADH	aKG.m -> Suc + CO2	1.236	2.026	1.631
	IDH	Cit <-> aKG.m + CO2	1.280	2.063	1.671
Transport	Glc IN	Glc.e -> Glc	0.564	0.708	0.636
	Lys IN	Lys.e -> Lys	0.009	0.018	0.013
	Thr IN	Thr.e -> Thr	0.006	0.016	0.011
	Phe IN	Phe.e -> Phe	0.003	0.009	0.006
	Tyr IN	Tyr.e -> Tyr	0.001	0.008	0.004
	Val IN	Val.e -> Val	0.007	0.014	0.010
	Leu IN	Leu.e -> Leu	0.027	0.054	0.040
	Ile IN	Ile.e -> Ile	0.007	0.025	0.016
	Trp IN	Trp.e -> Trp	0.002	0.014	0.008
	His IN	His.e -> His	0.002	0.010	0.006
	Met IN	Met.e -> Met	0.003	0.014	0.008
	Ser Flux	Ser.e <-> Ser	0.019	0.038	0.028
	Ala Flux	Ala.e <-> Ala	0.008	0.053	0.030
	Arg Flux	Arg.e <-> Arg	0.006	0.014	0.010
	Asp Flux	Asp.e <-> Asp	0.001	0.017	0.009
	Gln Flux	Gln.e <-> Gln	-0.004	0.007	0.001
	Pro Flux	Pro.e <-> Pro	0.005	0.010	0.007

	Asn Flux	Asn.e <-> Asn	0.025	0.037	0.031
	Lac Flux	Lac.e <-> Lac	0.526	0.687	0.606
	Gly Flux	Gly.e <-> Gly	-0.089	-0.061	-0.075
	Cys Flux	Cys.e <-> Cys	0.000	0.011	0.006
	Glu Flux	Glu.e <-> Glu.c	-0.040	-0.016	-0.028
	Glu/Asp Antiporter	Glu.c -> Glu.m	0.000	0.063	0.032
	Mal/aKG Antiporter	aKG.m -> aKG.c	0.027	0.093	0.060
Anaplerosis	ME	Mal.c -> Pyr + CO2	0.039	0.075	0.057
	PC	Pyr + CO2 -> OAA	0.024	0.099	0.062
	ACL	Cit -> AcCoA.c + Mal.c	0.039	0.075	0.057
Amino	GLS	Gln <-> Glu.m	-0.012	-0.001	-0.006
Acid	ASNS	Asp <-> Asn	-0.031	-0.018	-0.024
Metabolism	SHT	Ser <-> Gly + MEETHF	0.040	0.056	0.048
	CYST	Ser <-> Cys	0.085	0.437	0.261
	GS + SHT	CO2 + MEETHF -> Gly	0.035	0.049	0.042
	Met Mtbl	Met + Ser -> Methyl + Cys + Suc	0.000	0.011	0.005
	PheTyr Mtbl	Phe -> Tyr	0.000	0.003	0.002
	Thr Mtbl	Thr -> Pyr + CO2	0.000	0.007	0.004
	Histidase	His -> FormTHF + Glu.c	0.000	0.007	0.003
	CBXase + Mutase	ProCoA + CO2 -> Suc	0.000	0.017	0.009
	Trp Mtbl	Trp -> CO2 + CO2 + Ala + aKetoadi	0.001	0.013	0.007
	Trp2 Mtbl	aKetoadi -> CO2 + CO2 + AcCoA + AcCoA	0.001	0.013	0.007
	*GDH	aKG.m <-> Glu.m	-0.059	0.012	-0.024
	*ALT	Ala + aKG.c <-> Pyr + Glu.c	0.001	0.047	0.024
	*Ile Mtbl	Ile + aKG.c -> AcCoA + CO2 + ProCoA + Glu.c	0.000	0.017	0.009
	*Leu Mtbl	Leu + aKG.c + CO2 -> CO2 + AcCoA + AcCoA + AcCoA + Glu.c	0.014	0.040	0.027
	*Tyr Mtbl	Tyr + aKG.c -> CO2 + Mal.c + AcCoA + AcCoA + Glu.c	0.000	0.004	0.002
	*Val Mtbl	Val + aKG.c -> Glu.c + CO2 + CO2 + ProCoA	0.000	0.004	0.002
	*Lys Mtbl	Lys + aKG.c + aKG.c -> Glu.c + Glu.c + aKetoadi	0.000	0.003	0.002
	*AST	OAA + Glu.c <-> Asp + aKG.c	-0.033	-0.012	-0.022
	*Arg Mtbl	Arg + aKG.c -> Glu.c + Urea + Glu.c	0.000	0.006	0.003
	*PST	3PG + Glu.c -> Ser + aKG.c	0.120	0.470	0.295

	*Cys Mtbl	Cys + aKG.c -> Pyr + Glu.c	0.092	0.444	0.268
Biomass Production	Biomass 363 pg	0.2178*Ala + 0.1368*Arg + 0.1712*Asp + 0.1046*Asn + 0.0526*Cys + 0.1168*Gln + 0.1401*Glu.c + 0.2389*Gly + 0.0519*His + 0.1176*Ile + 0.2048*Leu + 0.2069*Lys + 0.0501*Met + 0.0796*Phe + 0.1136*Pro + 0.1601*Ser + 0.1401*Thr + 0.016*Trp + 0.0661*Tyr + 0.151*Val + 0.1047*G6P + 0.0845*R5P + 0.0926*MEETHF + 0.0441*DHAP + 0.8985*AcCoA.c -> Biomass	0.043	0.084	0.063

Table 4-A-12. Exchange fluxes of low expressing (LE) during lactate consuming phase. Associated with Figure 4-7.

Pathway	Enzyme	Rxn	LB 95% CI	UB 95% CI	Value
Amino	ASNS	Asp <-> Asn	0.0258	0.6596	0.3427
Acid	SHT	Ser <-> Gly + MEETHF	0.5905	3.2054	1.89795
Metabolism	AST	OAA + Glu.c <-> Asp + aKG.c	0.1124	0.4211	0.26675
Transport	Ala Flux	Ala.e <-> Ala	0	0.2283	0.11415
	Asp Flux	Asp.e <-> Asp	0	0.6642	0.3321
	Asn Flux	Asn.e <-> Asn	0	26.6412	13.3206
	Gly Flux	Gly.e <-> Gly	0.0806	0.529	0.3048
	Cys Flux	Cys.e <-> Cys	0	5.4663	2.73315
	Lac Flux	Lac.e <-> Lac	6.0184	251.1219	128.57
	Ser Flux	Ser.e <-> Ser	0	0.5697	0.28485

Table 4-A-13. Net fluxes of high expressing (HE) during lactate consuming phase.
Associated with Figure 4-7.

Pathway	Enzyme	Rxn	LB 95% CI	UB 95% CI	Value
Glycolysis	PGI	G6P <-> F6P	-0.679	0.685	0.003
	PFK	F6P -> DHAP + GAP	0.196	0.683	0.439
	TPI	DHAP <-> GAP	0.174	0.681	0.428
	GADPH	GAP <-> 3PG	0.811	1.363	1.087
	Eno	3PG <-> PEP	0.391	0.985	0.688
	PK	PEP -> Pyr	0.391	0.985	0.688
	HK	Glc -> G6P	0.573	0.696	0.634
	LDH	Lac <-> Pyr	0.697	0.826	0.761
PPP	6PGDH	G6P -> Ru5P + CO2	0.000	1.384	0.692
	R5PE	Ru5P <-> X5P	-0.003	0.881	0.439
	R5PI	Ru5P <-> R5P	0.001	0.443	0.222
	TK1	X5P + R5P <-> GAP + S7P	-0.001	0.441	0.220
	TK2	S7P + GAP <-> E4P + F6P	-0.001	0.441	0.220
	TK3	X5P + E4P <-> GAP + F6P	-0.001	0.441	0.220
TCA	PDH	Pyr -> AcCoA + CO2	1.471	2.087	1.779
	SDH	Suc <-> Fum	1.570	2.202	1.886
	Fum	Fum <-> Mal.m	1.570	2.202	1.886
	MDH	Mal.m <-> OAA	1.570	2.202	1.886
	CS	OAA + AcCoA -> Cit	1.630	2.233	1.931
	ADH	aKG.m -> Suc + CO2	1.552	2.184	1.868
	IDH	Cit <-> aKG.m + CO2	1.577	2.206	1.891
Transport	Glc IN	Glc.e -> Glc	0.573	0.696	0.634
	Lys IN	Lys.e -> Lys	0.003	0.011	0.007
	Thr IN	Thr.e -> Thr	0.002	0.009	0.006
	Phe IN	Phe.e -> Phe	0.001	0.007	0.004
	Tyr IN	Tyr.e -> Tyr	0.000	0.007	0.004
	Val IN	Val.e -> Val	0.002	0.011	0.006
	Leu IN	Leu.e -> Leu	0.033	0.055	0.044
	Ile IN	Ile.e -> Ile	0.011	0.025	0.018
	Trp IN	Trp.e -> Trp	0.003	0.012	0.007
	His IN	His.e -> His	0.001	0.009	0.005
	Met IN	Met.e -> Met	0.002	0.012	0.007
	Ser Flux	Ser.e <-> Ser	0.034	0.049	0.042
	Ala Flux	Ala.e <-> Ala	0.038	0.066	0.052
	Arg Flux	Arg.e <-> Arg	0.003	0.011	0.007
	Asp Flux	Asp.e <-> Asp	0.004	0.016	0.010
	Gln Flux	Gln.e <-> Gln	-0.062	0.014	-0.024
	Pro Flux	Pro.e <-> Pro	0.002	0.006	0.004

	Asn Flux	Asn.e <-> Asn	-0.129	-0.034	-0.081
	Lac Flux	Lac.e <-> Lac	0.697	0.826	0.761
	Gly Flux	Gly.e <-> Gly	-0.094	-0.068	-0.081
	Cys Flux	Cys.e <-> Cys	-0.001	0.009	0.004
	Glu Flux	Glu.e <-> Glu.c	-0.016	-0.001	-0.008
	Glu/Asp Antiporter	Glu.c -> Glu.m	0.000	0.055	0.028
	Mal/aKG Antiporter	aKG.m -> aKG.c	0.000	0.063	0.032
Anaplerosis	ME	Mal.c -> Pyr + CO2	0.014	0.047	0.030
	PC	Pyr + CO2 -> OAA	0.075	0.180	0.128
	ACL	Cit -> AcCoA.c + Mal.c	0.013	0.045	0.029
Amino	GLS	Gln <-> Glu.m	-0.066	0.010	-0.028
Acid	ASNS	Asp <-> Asn	0.038	0.131	0.084
Metabolism	SHT	Ser <-> Gly + MEETHF	0.039	0.053	0.046
	CYST	Ser <-> Cys	0.212	0.564	0.388
	GS + SHT	CO2 + MEETHF -> Gly	0.036	0.049	0.043
	Met Mtbl	Met + Ser -> Methyl + Cys + Suc	0.000	0.010	0.005
	PheTyr Mtbl	Phe -> Tyr	0.000	0.004	0.002
	Thr Mtbl	Thr -> Pyr + CO2	0.000	0.005	0.003
	Histidase	His -> FormTHF + Glu.c	0.000	0.007	0.004
	CBXase + Mutase	ProCoA + CO2 -> Suc	0.007	0.023	0.015
	Trp Mtbl	Trp -> CO2 + CO2 + Ala + aKetoadi	0.002	0.012	0.007
	Trp2 Mtbl	aKetoadi -> CO2 + CO2 + AcCoA + AcCoA	0.002	0.012	0.007
	*GDH	aKG.m <-> Glu.m	-0.033	0.066	0.016
	*ALT	Ala + aKG.c <-> Pyr + Glu.c	0.037	0.067	0.052
	*Ile Mtbl	Ile + aKG.c -> AcCoA + CO2 + ProCoA + Glu.c	0.007	0.021	0.014
	*Leu Mtbl	Leu + aKG.c + CO2 -> CO2 + AcCoA + AcCoA + AcCoA + Glu.c	0.026	0.048	0.037
	*Tyr Mtbl	Tyr + aKG.c -> CO2 + Mal.c + AcCoA + AcCoA + Glu.c	0.000	0.006	0.003
	*Val Mtbl	Val + aKG.c -> Glu.c + CO2 + CO2 + ProCoA	0.000	0.006	0.003
	*Lys Mtbl	Lys + aKG.c + aKG.c -> Glu.c + Glu.c + aKetoadi	0.000	0.003	0.002
	*AST	OAA + Glu.c <-> Asp + aKG.c	0.034	0.124	0.079
	*Arg Mtbl	Arg + aKG.c -> Glu.c + Urea + Glu.c	0.000	0.007	0.004
	*PST	3PG + Glu.c -> Ser + aKG.c	0.226	0.578	0.402

	*Cys Mtbl	Cys + aKG.c -> Pyr + Glu.c	0.227	0.571	0.399
Biomass Production	Biomass 341 pg	0.2046*Ala + 0.1285*Arg + 0.1609*Asp + 0.0983*Asn + 0.0494*Cys + 0.1098*Gln + 0.1316*Glu.c + 0.2244*Gly + 0.0487*His + 0.1105*Ile + 0.1924*Leu + 0.1943*Lys + 0.0471*Met + 0.0747*Phe + 0.1068*Pro + 0.1504*Ser + 0.1316*Thr + 0.015*Trp + 0.0621*Tyr + 0.1419*Val + 0.0984*G6P + 0.0794*R5P + 0.087*MEETHF + 0.0415*DHAP + 0.844*AcCoA.c -> Biomass	0.016	0.053	0.034

Table 4-A-14. Exchange fluxes of high expressing (HE) during lactate consuming phase. Associated with Figure 4-7.

Pathway	Enzyme	Rxn	LB 95% CI	UB 95% CI	Value
TCA	SDH	Suc <-> Fum	0	1.2803	0.64015
	IDH	Cit <-> aKG.m + CO2	0	0.2198	0.1099
Amino Acid Metabolism	GLS	Gln <-> Glu.m	0.2211	0.5161	0.3686
	ASNS	Asp <-> Asn	0	1.0827	0.54135
	SHT	Ser <-> Gly + MEETHF	0.9106	2.6605	1.78555
	AST	OAA + Glu.c <-> Asp + aKG.c	0	0.2804	0.1402
Transport	Ser Flux	Ser.e <-> Ser	0	0.6406	0.3203
	Ala Flux	Ala.e <-> Ala	0	0.2297	0.11485
	Asp Flux	Asp.e <-> Asp	0	0.8068	0.4034
	Gly Flux	Gly.e <-> Gly	0.1709	0.6083	0.3896
	Cys Flux	Cys.e <-> Cys	0	0.6056	0.3028

References

[1] W. S. Ahn and M. R. Antoniewicz, “Towards dynamic metabolic flux analysis in CHO cell cultures.,” *Biotechnol. J.*, vol. 7, no. 1, pp. 61–74, Jan. 2012.

[2] S. R. Aggarwal, “What’s fueling the biotech engine-2011 to 2012.,” *Nat. Biotechnol.*, vol. 30, no. 12, pp. 1191–7, Dec. 2012.

[3] X. Xu, H. Nagarajan, N. E. Lewis, S. Pan, Z. Cai, X. Liu, W. Chen, M. Xie, W. Wang, S. Hammond, M. R. Andersen, N. Neff, B. Passarelli, W. Koh, H. C. Fan, J. Wang, Y. Gui, K. H. Lee, M. J. Betenbaugh, S. R. Quake, I. Famili, B. O. Palsson, and J. Wang, “The genomic sequence of the Chinese hamster ovary (CHO)-K1 cell line,” *Nat. Biotechnol.*, vol. 29, no. 8, pp. 1–8, Jul. 2011.

[4] J. Zhang, “Mammalian Cell Culture for Biopharmaceutical Production,” in *Manual of Industrial Microbiology and Biotechnology*, 3rd ed., no. 104, R. H. Baltz, A. L. Demain, and J. E. Davies, Eds. Washington, DC: ASM Press, 2010, pp. 157–178.

[5] S. S. Farid, “Process economics of industrial monoclonal antibody manufacture.,” *J. Chromatogr. B. Analyt. Technol. Biomed. Life Sci.*, vol. 848, no. 1, pp. 8–18, Mar. 2007.

[6] C. Altamirano, C. Paredes, a Illanes, J. J. Cairó, and F. Gòdia, “Strategies for fed-batch cultivation of t-PA producing CHO cells: substitution of glucose and glutamine and rational design of culture medium.,” *J. Biotechnol.*, vol. 110, no. 2, pp. 171–9, May 2004.

[7] J. Goswami, a J. Sinskey, H. Steller, G. N. Stephanopoulos, and D. I. C. Wang, “Apoptosis in batch cultures of Chinese hamster ovary cells.,” *Biotechnol. Bioeng.*, vol. 62, no. 6, pp. 632–40, Mar. 1999.

[8] a J. Mastrangelo, S. Zou, J. M. Hardwick, and M. J. Betenbaugh, “Antiapoptosis chemicals prolong productive lifetimes of mammalian cells upon Sindbis virus vector infection.,” *Biotechnol. Bioeng.*, vol. 65, no. 3, pp. 298–305, Nov. 1999.

[9] A. J. Mastrangelo, J. M. Hardwick, S. Zou, and M. J. Betenbaugh, “Part II. Overexpression of bcl-2 family members enhances survival of mammalian cells in response to various culture insults.,” *Biotechnol. Bioeng.*, vol. 67, no. 5, pp. 555–64, Mar. 2000.

[10] G. G. Chiang and W. P. Sisk, “Bcl-x(L) mediates increased production of humanized monoclonal antibodies in Chinese hamster ovary cells.,” *Biotechnol. Bioeng.*, vol. 91, no. 7, pp. 779–92, Sep. 2005.

[11] N. H. Simpson, R. P. Singh, a Perani, C. Goldenzon, and M. Al-Rubeai, “In hybridoma cultures, deprivation of any single amino acid leads to apoptotic death, which is

suppressed by the expression of the bcl-2 gene.," *Biotechnol. Bioeng.*, vol. 59, no. 1, pp. 90–8, Jul. 1998.

[12] M. Fussenegger, D. Fassnacht, R. Schwartz, J. a Zanghi, M. Graf, J. E. Bailey, and R. Pörtner, "Regulated overexpression of the survival factor bcl-2 in CHO cells increases viable cell density in batch culture and decreases DNA release in extended fixed-bed cultivation.," *Cytotechnology*, vol. 32, no. 1, pp. 45–61, Jan. 2000.

[13] H. Dorai, Y. S. Kyung, D. Ellis, C. Kinney, C. Lin, D. Jan, G. Moore, and M. J. Betenbaugh, "Expression of anti-apoptosis genes alters lactate metabolism of Chinese Hamster Ovary cells in culture.," *Biotechnol. Bioeng.*, vol. 103, no. 3, pp. 592–608, Jun. 2009.

[14] H. Le, S. Kabbur, L. Pollastrini, Z. Sun, K. Mills, K. Johnson, G. Karypis, and W.-S. Hu, "Multivariate analysis of cell culture bioprocess data--lactate consumption as process indicator.," *J. Biotechnol.*, vol. 162, no. 2–3, pp. 210–23, Dec. 2012.

[15] B. S. Majors, M. J. Betenbaugh, and G. G. Chiang, "Links between metabolism and apoptosis in mammalian cells: applications for anti-apoptosis engineering.," *Metab. Eng.*, vol. 9, no. 4, pp. 317–26, Jul. 2007.

[16] J. D. Young, "Metabolic flux rewiring in mammalian cell cultures," *Curr. Opin. Biotechnol.*, pp. 1–8, May 2013.

[17] L. Xie and D. I. Wang, "Material balance studies on animal cell metabolism using a stoichiometrically based reaction network.," *Biotechnol. Bioeng.*, vol. 52, no. 5, pp. 579–90, Dec. 1996.

[18] W. S. Ahn and M. R. Antoniewicz, "Parallel labeling experiments with [1,2-(13)C]glucose and [U-(13)C]glutamine provide new insights into CHO cell metabolism.," *Metab. Eng.*, vol. 15, pp. 34–47, Jan. 2013.

[19] N. Templeton, J. Dean, P. Reddy, and J. D. Young, "Peak antibody production is associated with increased oxidative metabolism in an industrially relevant fed-batch CHO cell culture.," *Biotechnol. Bioeng.*, vol. 110, no. 7, pp. 2013–2024, Feb. 2013.

[20] N. Sengupta, S. T. Rose, and J. a Morgan, "Metabolic flux analysis of CHO cell metabolism in the late non-growth phase.," *Biotechnol. Bioeng.*, vol. 108, no. 1, pp. 82–92, Jan. 2011.

[21] H. Dorai, D. Ellis, Y. S. Keung, M. Campbell, M. Zhuang, C. Lin, and M. J. Betenbaugh, "Combining high-throughput screening of caspase activity with anti-apoptosis genes for development of robust CHO production cell lines.," *Biotechnol. Prog.*, vol. 26, no. 5, pp. 1367–81, 2010.

[22] J. Greene, J. W. H. Jr, and J. P. Wikswo, “Rapid and Precise Determination of Cellular Amino Acid Flux Rates Using HPLC with Automated Derivatization with Absorbance,” *Agil. Appl. Note*, pp. 1–8, 2009.

[23] T. A. Murphy and J. D. Young, “ETA: robust software for determination of cell specific rates from extracellular time courses.,” *Biotechnol. Bioeng.*, vol. 110, no. 6, pp. 1748–1758, Jun. 2013.

[24] C. a Sellick, R. Hansen, A. R. Maqsood, W. B. Dunn, G. M. Stephens, R. Goodacre, and A. J. Dickson, “Effective quenching processes for physiologically valid metabolite profiling of suspension cultured Mammalian cells.,” *Anal. Chem.*, vol. 81, no. 1, pp. 174–83, Jan. 2009.

[25] J. Folch, M. Lees, and G. H. S. Stanley, “A simple method for the isolation and purification of total lipides from animal tissues,” *J. Biol. Chem.*, vol. 226, no. 1, pp. 497–509, Aug. 1957.

[26] M. R. Antoniewicz, J. K. Kelleher, and G. Stephanopoulos, “Elementary metabolite units (EMU): a novel framework for modeling isotopic distributions.,” *Metab. Eng.*, vol. 9, no. 1, pp. 68–86, Jan. 2007.

[27] K. Sheikh, J. Fo, and L. K. Nielsen, “Modeling Hybridoma Cell Metabolism Using a Generic Genome-Scale Metabolic Model of Mus musculus,” *Biotechnol. Prog.*, vol. 21, no. 1, pp. 112–121, 2005.

[28] H. Bonarius, G. Schmid, and J. Tramper, “Flux analysis of underdetermined metabolic networks: the quest for the missing constraints,” *Trends Biotechnol.*, vol. 15, no. 8, pp. 308–314, Aug. 1997.

[29] J. D. Young, “INCA: a computational platform for isotopically non-stationary metabolic flux analysis.,” *Bioinformatics*, vol. 30, no. 9, pp. 1333–5, May 2014.

[30] J. D. Young, J. L. Walther, M. R. Antoniewicz, and H. Yoo, “An Elementary Metabolite Unit (EMU) Based Method of Isotopically Nonstationary Flux Analysis,” *Biotechnology*, vol. 99, no. 3, pp. 686–699, 2008.

[31] M. R. Antoniewicz, J. K. Kelleher, and G. Stephanopoulos, “Determination of confidence intervals of metabolic fluxes estimated from stable isotope measurements.,” *Metab. Eng.*, vol. 8, no. 4, pp. 324–37, Jul. 2006.

[32] M. E. Smoot, K. Ono, J. Ruscheinski, P.-L. Wang, and T. Ideker, “Cytoscape 2.8: new features for data integration and network visualization.,” *Bioinformatics*, vol. 27, no. 3, pp. 431–2, Feb. 2011.

[33] C. a Schneider, W. S. Rasband, and K. W. Eliceiri, “NIH Image to ImageJ: 25 years of image analysis,” *Nat. Methods*, vol. 9, no. 7, pp. 671–675, Jun. 2012.

[34] J. Vance, “Phospholipid synthesis in a membrane fraction associated with mitochondria.,” *J. Biol. Chem.*, vol. 265, pp. 7248–7256, 1990.

[35] J. Meunier and T. Hayashi, “Sigma-1 Receptors Regulate Bcl-2 Expression by Reactive Oxygen Species-Dependent Transcriptional Regulation of Nuclear Factor B,” vol. 332, no. 2, pp. 388–397, 2010.

[36] F. Zagari, M. Jordan, M. Stettler, H. Broly, and F. M. Wurm, “Lactate metabolism shift in CHO cell culture: the role of mitochondrial oxidative activity.,” *N. Biotechnol.*, vol. 30, no. 2, pp. 238–245, Jun. 2013.

[37] W. S. Ahn and M. R. Antoniewicz, “Metabolic flux analysis of CHO cells at growth and non-growth phases using isotopic tracers and mass spectrometry.,” *Metab. Eng.*, vol. 13, no. 5, pp. 598–609, Sep. 2011.

[38] N. H. Simpson, R. P. Singh, a N. Emery, and M. Al-Rubeai, “Bcl-2 over-expression reduces growth rate and prolongs G1 phase in continuous chemostat cultures of hybridoma cells.,” *Biotechnol. Bioeng.*, vol. 64, no. 2, pp. 174–86, Jul. 1999.

[39] J. Li, C. L. Wong, N. Vijayasankaran, T. Hudson, and A. Amanullah, “Feeding lactate for CHO cell culture processes: Impact on culture metabolism and performance.,” *Biotechnol. Bioeng.*, vol. 109, no. 5, pp. 1173–86, May 2012.

[40] W. J. Placzek, J. Wei, S. Kitada, D. Zhai, J. C. Reed, and M. Pellecchia, “A survey of the anti-apoptotic Bcl-2 subfamily expression in cancer types provides a platform to predict the efficacy of Bcl-2 antagonists in cancer therapy.,” *Cell Death Dis.*, vol. 1, no. 5, p. e40, Jan. 2010.

[41] B. Figueroa, T. M. Sauerwald, a J. Mastrangelo, J. M. Hardwick, and M. J. Betenbaugh, “Comparison of Bcl-2 to a Bcl-2 deletion mutant for mammalian cells exposed to culture insults.,” *Biotechnol. Bioeng.*, vol. 73, no. 3, pp. 211–22, May 2001.

[42] H. Meents, B. Enenkel, H. M. Eppenberger, R. G. Werner, and M. Fussenegger, “Impact of coexpression and coamplification of sICAM and antiapoptosis determinants bcl-2/bcl-x(L) on productivity, cell survival, and mitochondria number in CHO-DG44 grown in suspension and serum-free media.,” *Biotechnol. Bioeng.*, vol. 80, no. 6, pp. 706–16, Dec. 2002.

[43] B. T. Tey, R. P. Singh, L. Piredda, M. Piacentini, and M. Al-Rubeai, “Influence of bcl-2 on cell death during the cultivation of a Chinese hamster ovary cell line expressing a chimeric antibody.,” *Biotechnol. Bioeng.*, vol. 68, no. 1, pp. 31–43, Apr. 2000.

[44] S. W. G. Tait and D. R. Green, “Mitochondria and cell death: outer membrane permeabilization and beyond.,” *Nat. Rev. Mol. Cell Biol.*, vol. 11, no. 9, pp. 621–32, Sep. 2010.

[45] Y. Wei, S. Pattingre, S. Sinha, M. Bassik, and B. Levine, “JNK1-mediated phosphorylation of Bcl-2 regulates starvation-induced autophagy.,” *Mol. Cell*, vol. 30, no. 6, pp. 678–88, Jul. 2008.

[46] A. Lewis, T. Hayashi, T. Su, and M. J. Betenbaugh, “Bcl-2 family in inter-organelle modulation of calcium signaling; roles in bioenergetics and cell survival.,” *J. Bioenerg. Biomembr.*, Sep. 2013.

[47] R. C. Murphy, E. Schneider, and K. W. Kinnally, “Overexpression of Bcl-2 suppresses the calcium activation of a mitochondrial megachannel.,” *FEBS Lett.*, vol. 497, no. 2–3, pp. 73–6, May 2001.

[48] S. Gupta, L. Cuffe, E. Szegezdi, S. E. Logue, C. Neary, S. Healy, and A. Samali, “Mechanisms of ER Stress-Mediated Mitochondrial Membrane Permeabilization.,” *Int. J. Cell Biol.*, vol. 2010, p. 170215, Jan. 2010.

[49] S. Orrenius, B. Zhivotovsky, and P. Nicotera, “Regulation of cell death: the calcium-apoptosis link.,” *Nat. Rev. Mol. Cell Biol.*, vol. 4, no. 7, pp. 552–65, Jul. 2003.

[50] A. Belzacq, H. L. A. Vieira, F. Verrier, I. Cohen, E. Larquet, F. Pariselli, P. X. Petit, A. Kahn, R. Rizzuto, C. Brenner, and G. Kroemer, “Bcl-2 and Bax Modulate Adenine Nucleotide Translocase Activity Bcl-2 and Bax Modulate Adenine Nucleotide Translocase Activity 1,” *Cancer Res.*, vol. 63, pp. 541–546, 2003.

[51] F. Zagari, M. Stettler, H. Broly, M. Wurm, and M. Jordan, “High expression of the aspartate–glutamate carrier Aralar1 favors lactate consumption in CHO cell culture,” *Pharm. Bioprocess.*, vol. 1, no. 1, pp. 19–27, 2013.

[52] F. M. Lasorsa, P. Pinton, L. Palmieri, G. Fiermonte, R. Rizzuto, and F. Palmieri, “Recombinant expression of the Ca(2+)-sensitive aspartate/glutamate carrier increases mitochondrial ATP production in agonist-stimulated Chinese hamster ovary cells.,” *J. Biol. Chem.*, vol. 278, no. 40, pp. 38686–92, Oct. 2003.

[53] D. Vaux, S. Cory, and J. Adams, “Bcl-2 gene promotes haemopoietic cell survival and cooperates with c-myc to immortalize pre-B cells.,” *Nature*, vol. 335, no. 29, pp. 440–442, 1988.

[54] R. J. Youle and A. Strasser, “The BCL-2 protein family: opposing activities that mediate cell death.,” *Nat. Rev. Mol. Cell Biol.*, vol. 9, no. 1, pp. 47–59, Jan. 2008.

[55] M. S. Lao and D. Toth, “Effects of ammonium and lactate on growth and metabolism of a recombinant Chinese hamster ovary cell culture.,” *Biotechnol. Prog.*, vol. 13, no. 5, pp. 688–91, 1997.

[56] K. Chen, Q. Liu, L. Xie, P. a Sharp, and D. I. Wang, “Engineering of a mammalian cell line for reduction of lactate formation and high monoclonal antibody production.,” *Biotechnol. Bioeng.*, vol. 72, no. 1, pp. 55–61, Jan. 2001.

[57] M. R. Antoniewicz, “Dynamic metabolic flux analysis--tools for probing transient states of metabolic networks.,” *Curr. Opin. Biotechnol.*, vol. 24, no. 6, pp. 973–8, Dec. 2013.

[58] M. R. Antoniewicz, D. F. Kraynie, L. a Laffend, J. González-Lergier, J. K. Kelleher, and G. Stephanopoulos, “Metabolic flux analysis in a nonstationary system: fed-batch fermentation of a high yielding strain of E. coli producing 1,3-propanediol.,” *Metab. Eng.*, vol. 9, no. 3, pp. 277–92, May 2007.

V: GLUTAMINE EXHAUSTION INDUCES LACTATE CONSUMPTION

Abstract

The push toward higher cell densities and product titers in mammalian cell bioprocesses is often accompanied by accumulation of inhibitory metabolites such as lactate. Accumulation of these toxic by-products is a predominant cause of cell death. Additionally, lactate accumulation is an indication that carbon sources are being used inefficiently, thus reducing yields of antibody and biomass. Therefore, we are investigating the causes of lactate accumulation and how it can be reversed by genetic engineering and/or medium optimization strategies.

We and others have observed that CHO (Chinese Hamster Ovary) cells are capable of not only producing but also consuming lactate under certain conditions. The switch to lactate consumption often accompanies the depletion of a preferred carbon source (such as glucose or glutamine) from the growth medium. In shake flask experiments, we observed that the specific lactate production rate was halved when the medium glutamine concentration was reduced from 8 to 4 mM. This corresponded with more efficient growth (30% higher specific growth rate and 40% higher peak viable cell density) as well as a 70% decrease in specific glucose consumption rate. Therefore, by reducing glutamine availability we were able to shift cell culture to a more efficient metabolic state involving both increased growth rate and decreased nutrient uptake.

Introduction

The increasing demand for protein based drugs, specifically monoclonal antibodies, has neatly corresponded with their clinical value in treatment of an increasing variety of diseases [1]. In 1987, with the protein therapeutic production market still largely in its infancy, the industry standard was 100 mg/L final antibody concentration. In 2007, significant progress had been made as select antibodies were reaching a final concentration of 5 g/L [2]. However, demands for this class of drug are still rising. In 1995 antibodies were 1% of the biopharmaceutical market. They were 22% of the market in 2002. Currently biopharmaceuticals (antibodies included) represent 10-25% of all new drugs to hit the US market [3]. This type of growth will not remain sustainable, as costs to the consumer are already remarkably high, without continued process innovation [4].

Lactate production from animal cell cultures has inhibited product generation for the past 30 years. In spite of all the innovation, lactate inhibition continues to be a significant problem. It not only requires energy from the cell that could have been used to produce antibody (poor efficiency), but additionally can begin to limit culture viability if sufficient concentrations are reached [2]. Additionally, there is less biomass generation as much of the incoming flux is going to produce lactate Traditionally companies have combated lactate accumulation by controlling the glucose feed, as when glucose is limiting the culture produces less lactate [5]. However, even though the lactate problem might be solved, another is created. When glucose is limited, many other fluxes are limited as well, including antibody production.

To control lactate production, other techniques that impose less consequences upon antibody production, are being explored. One method is limiting a specific nutrient's availability to determine if lactate accumulation can be halted or even reversed. We will quantify the impact

of nutrient availability through metabolic flux analysis (MFA) [6], a technique that is surprisingly uncommon in the cell culture industry. This makes our work novel to the industry. This lab seeks to measure the changes brought about by environmental changes to the cell wide metabolism. Only when a metabolic network is developed, can the holistic impact be determined on the cell.

Chinese hamster ovary (CHO) cells are used in this study as they are widely used in the industry for monoclonal antibody production. Currently, this cell line produces over 25 protein therapeutics, many of them being monoclonal antibodies [2]. They remain a popular choice for monoclonal antibody production because of their relative ease to perform a stable genetic modification upon (many genetic modifications are transient).

Materials and Methods

Cell line and medium

CHO-S, obtained from Invitrogen, is exclusively used for this study. CHO-S was cultured in CD-CHO, a proprietary Invitrogen media. Its contents, though widely known through independent measurement and quantification by this lab, are not accessible to the general public.

Shake Flask operation

A batch shake flask setup was developed to separately culture CHO-S in different experimental conditions. To do this, 125mL glass Erlenmeyer flasks were used. The culture is buffered from a filtered 10% CO_2 (mixed with air) feed into the head space of the flask and gases

are released into environment. The temperature and agitation rate are controlled by a Thermo Scientific Max Q 4000. Samples are taken through a hypodermic needle at regular intervals.

Analytical Methods

To determine amino acid concentrations of the media as they were cultured over time, an Agilent 1200 Series HPLC was used with a C18 column and multiple wavelength UV detector. A precolumn derivitization took place using OPA (O-phthaldialdehyde), as described in published method [7]. Glucose and lactate concentrations were determined using an YSI 2300 STAT Plus. Viable cell density was determined using a hemocytometer using 0.1% (w/v) trypan blue to dilute and stain. To determine intracellular metabolite concentrations an Agilent 7890A gas chromatography was used in conjunction with an Agilent 5975C mass spec.

Extracellular Metabolite Flux

Determination of extracellular fluxes is critical to the constraint of your overall metabolic network. Intracellular fluxes are inherently constrained by the incoming and outgoing fluxes of the cell. This equation assumes that the culture is at steady state in growth rate as well as metabolic flux of interest. The equation is reported as found in the literature [8]. The *qs* term is the specific rate of production (or consumption), and the μ term specific growth rate. *S* is the substrate concentration, and S_0 the initial concentration. X_0 is the initial cell concentration.

$$[S] = [S]_0 + \frac{q_s X_0}{\mu}(e^{\mu t} - 1) \quad (5\text{-}1)$$

Glutamine degrades spontaneously in addition to the cellular uptake of it, so it has a different version of the above equation for determination of extracellular flux [9]. The decomposition was determined to be first order with respect to glutamine concentration, and was experimentally determined to be 0.081 $days^{-1}$. The equation used for glutamine flux is:

$$[GLN] = [GLN]_0 e^{-kt} + \frac{q_{GLN}\left(e^{-kt} - e^{\mu t}\right)}{k+\mu} X_0 \quad (5\text{-}2)$$

There is only one time in the cell growth cycle that steady state exists: the exponential phase. Subsequently, all the flux measurements are specific to the exponential phase of cell growth.

Intracellular Metabolite Determination

To determine intracellular metabolite concentration, the following process was used in the stated order. Quenching is first and required to cease all metabolic activity. To this end, ammonium bicarbonate (AMBIC) (0.85% w/v) is mixed in a 60/40 methanol/Water solution and cooled to -40°C [10] and the temperature maintained in a CaCl solution [11]. After drawing enough media to quench 10 million cells, the cell laden media is forcefully ejected into the quench solution to allow for rapid cooling.

Extraction is then required to remove all the metabolites from the cell [12]. Derivatization is necessary as without it the metabolites of interest are not volatile enough to be analyzed in GC/MS [13]. A MOX-TBDMS (tert-butyl-dimethy-silyl) derivatization is used.

Results and Discussion

In the cell culture world, there are several variants of CHO. Some exhibit the ability to readily consume lactate, many do not. The reason why some cells have this ability can be as simple as enzyme expression (notably lactate dehydrogenase) to convert lactate back into pyruvate. However, even when the cell does express the enzyme, lactate production still occurs, sometimes at a rate that becomes toxic to the cell. Increased lactate production is a common trait in nearly all immortalized cell lines, but for reasons that are not fully understood. One of the more common explanations has to do with managing the redox balance (in NADH/NAD+) associated with energy production of ATP, the central energy currency of biology.

Methods for limiting lactate accumulation in the industry are straightforward, limit glucose availability and lactate levels will remain low [14]. Inherently, this limits antibody production. This is the reason why the ability of a culture to consume the lactate that it produces is a huge advantage. CHO-S has this native ability, where other varieties such as CHO-K1, will largely accumulate lactate. We and others have observed this effect [15].

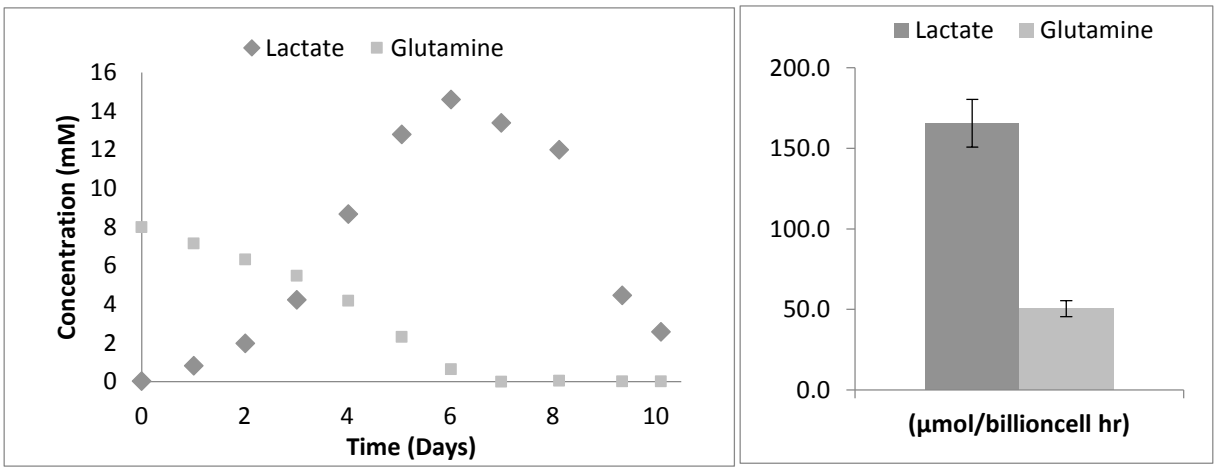

Figure 5-1. Lactate and glutamine profiles (8 mM [GLN]). Bar chart is representative of fluxes of lactate and glutamine.

Taking note of Figure 5-1, one can see when the glutamine is close to being exhausted from the culture, net lactate production switches to net consumption. It also represents a novel way to approach the lactate problem. If one could limit the amount of glutamine available, it might be possible to continually force the cell to consume the lactate that it had produced. This is a concept that to our knowledge has not been directly explored at this point based upon existing literature. As can be seen in Figure 5-2, glutamine is exhausted and lactate consumed while the culture is exiting exponential growth. This represents a significant shift in intracellular fluxes as the incoming nutrient source has changed. A glucose profile and flux is also determined to exhibit the most significant incoming flux in the cell. As mentioned prior, glucose availability is a significant factor in lactate production.

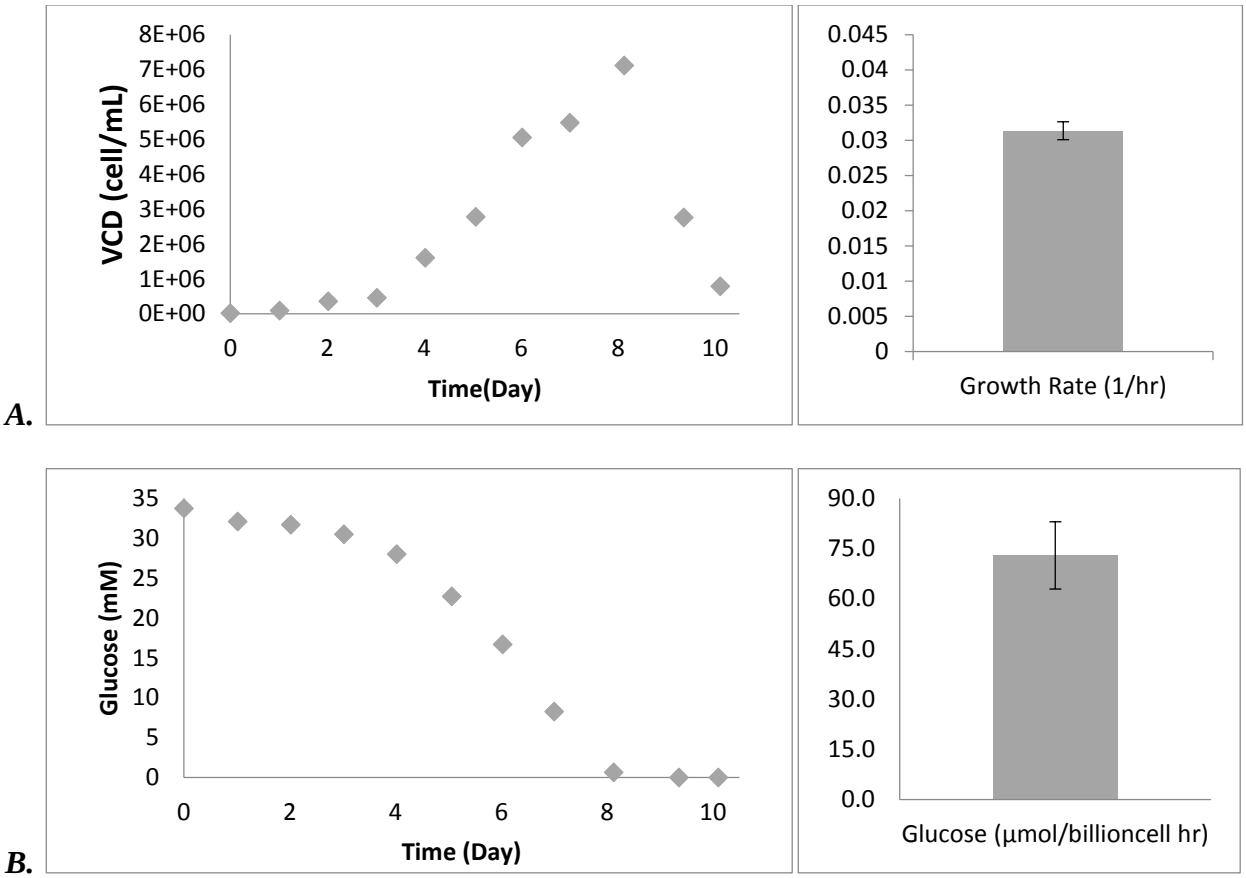

Figure 5-2. Growth and glucose profiles (8 mM [GLN]). A. Growth profile and growth rate of CHO-S. B. Glucose concentration profile and representative flux.

The potential of limiting glutamine to limit lactate was further explored. To do so, a similar experiment was designed where the initial glutamine concentration was halved to 4mM. Lactate was further reduced, and interestingly enough, again corresponded with the exhaustion of glutamine from the culture (Figure 5-3).

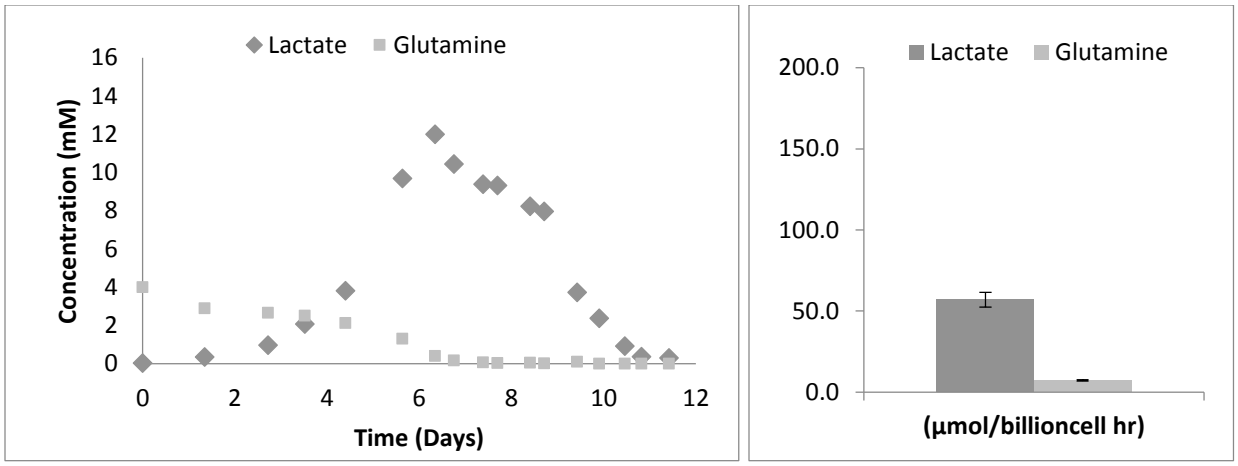

Figure 5-3. Lactate and glutamine profiles (4 mM [GLN]). Fluxes of lactate and glutamine plotted on same scale as 8mM [GLN].

These results indicate a lactate production rate that is less than half of the higher glutamine concentration. Upon observation of the growth profile (Figure 5-4), it can be seen that in spite of reduced nutrient availability, the culture was able to thrive, maintain, and even slightly increase growth rate. The fact that glucose consumption was reduced and growth rate was maintained in spite of limited glutamine suggests that the cell was forced into a more efficient state of metabolism. Less lactate was made and more biomass was generated.

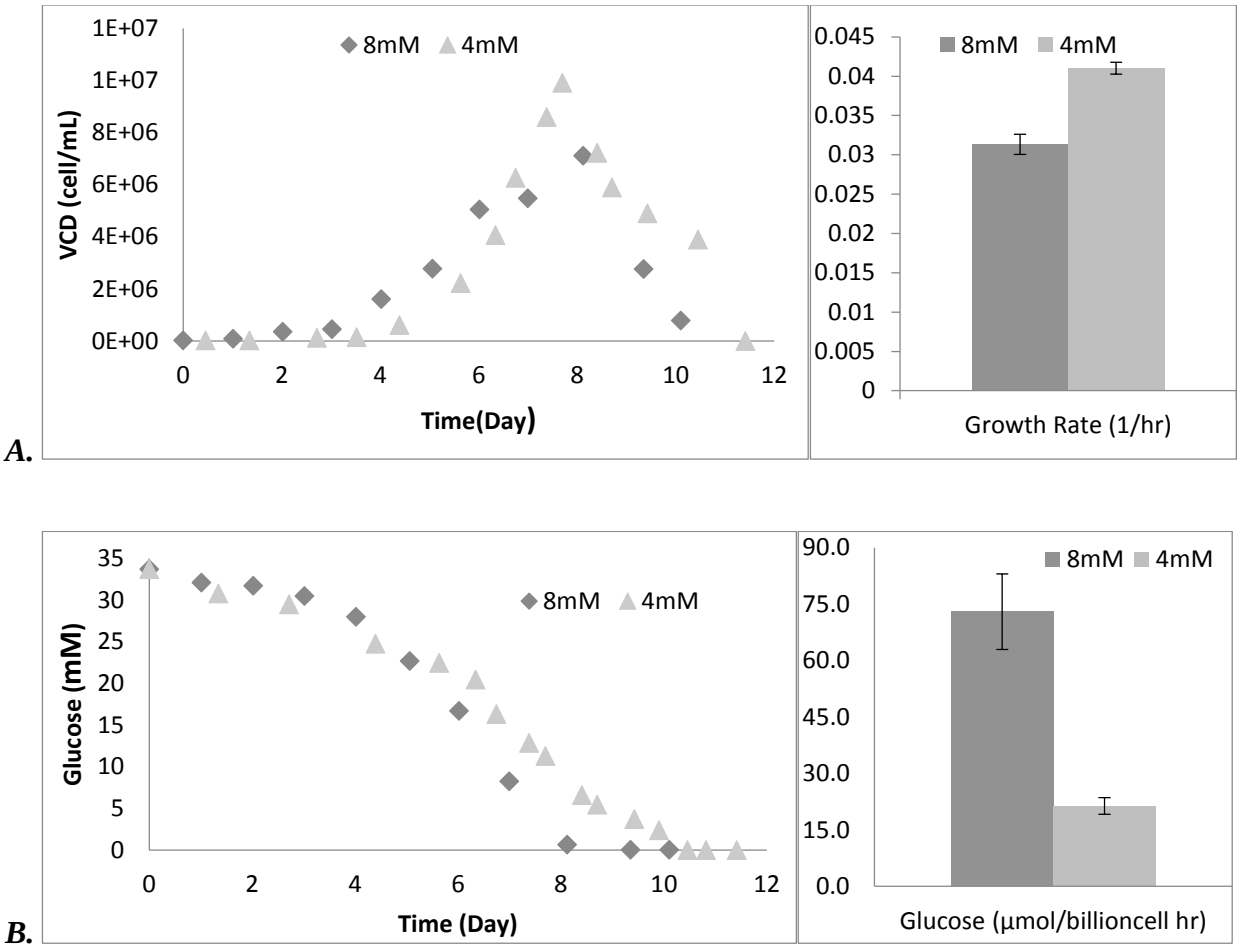

Figure 5-4. Growth and glucose characterization. A. Growth profile and growth rate of CHO-S with 4mM initial concentration of glutamine. B. Glucose concentration profile and representative flux.

The reprogramming of the metabolic network occurring during the lactate "switch" is of utmost interest. Metabolic flux analysis would provide a fundamental understanding of how a cell is performing in these specific conditions. To this end, an appropriate quenching method was explored. As mentioned in the methods, a NaCl quench [16] and AMBIC quench were each performed on the same culture at the same time to allow for quantitative comparison of intracellular metabolite concentrations.

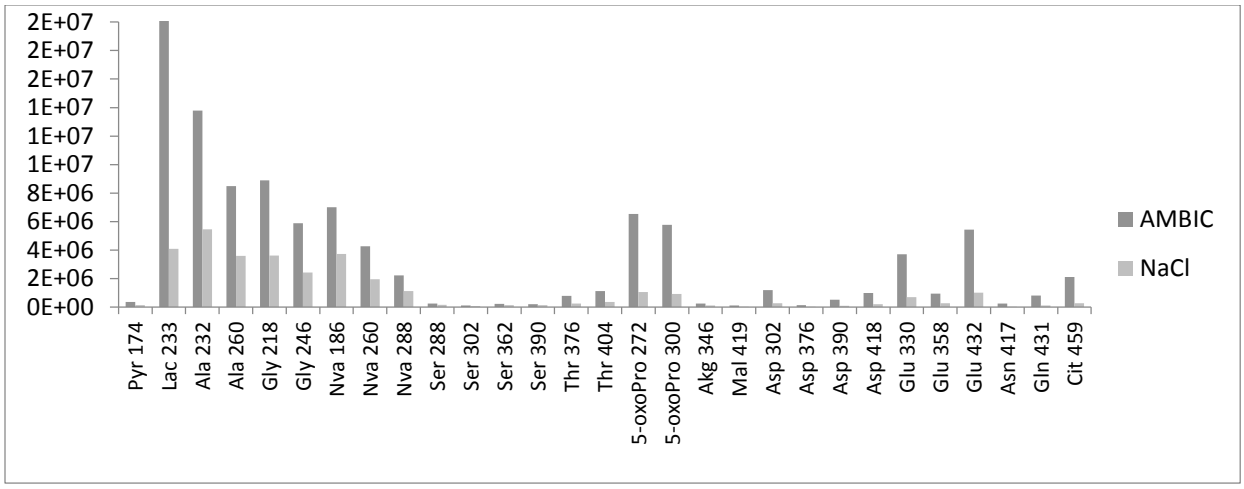

Figure 5-5. Total ion counts (y-axis) of various metabolites as determined with GC/MS. Direct comparison between quenching methods to determine which method provides greater recovery.

Each of the isotopic fragments (bound to TBDMS derivative) shown are what separated into the polar phase during extraction (both organic and polar phases are generated). These are the total ion counts that were measured for with within the range of 300,000-and 30,000,000. Other metabolites that did not fall inside this range are not shown, as the ion detector used is not accurate outside of this range. It should be noted that the total ion counts achieved for the NaCl quench were in general high enough to accurately measure for. However, it is more difficult to say whether or not the composition measured for in the GC/MS is comparable to the composition inside a cell due to the low recovery.

Conclusions

Metabolic flux analysis has already proven its resourcefulness in determining extracellular fluxes. A successful new feeding technique would be of great interest to the industry, but is only the fringe of the benefits provided by MFA. Providing a cell wide

metabolic network will provide new information regarding the causes of lactate accumulation, an issue that has troubled the protein therapeutic industry for 30 years. With a metabolic network, media compositions can be optimized or genetic modifications can appropriately be made. To this end, future work will involve quantifying the differences between the wild type CHO and CHO that has been engineered to over express proteins that provide death pathway resistance. Other research has already shown the advantages to doing this [15], especially when multiple genes are expressed. This is another research pursuit that will be attacked in parallel with media formulations. Having a reliable means to measure for metabolite concentrations, which has now been determined, will prove to be a critical marker in further applying MFA.

References

[1] G. Seth, P. Hossler, J. Chong, and Y. W. Hu, "Engineering Cells for Cell Culture Bioprocessing – Physiological Fundamentals," *Adv Biochem Engin/Biotechnol*, vol. 101, no. June, pp. 119–164, 2006.

[2] K. P. Jayapal, K. F. Wlaschin, M. G. S. Yap, and W.-S. Hu, "Recombinant Protein Therapeutics from CHO Cells — 20 Years and Counting," *SBE Spec. Sect. CHO Consort.*, pp. 40–47, 2006.

[3] J. R. Birch and Y. Onakunle, "Biopharmaceutical proteins: opportunities and challenges.," *Methods Mol. Biol.*, vol. 308, pp. 1–16, Jan. 2005.

[4] S. S. Farid, "Established Bioprocesses for Producing Antibodies as a Basis for Future Planning," *Adv. Biochem. Eng. Biotechnol.*, vol. 101, pp. 1–42, 2006.

[5] C. Altamirano, A. Illanes, S. Becerra, J. J. Cairó, and F. Gòdia, "Considerations on the lactate consumption by CHO cells in the presence of galactose.," *J. Biotechnol.*, vol. 125, no. 4, pp. 547–56, Oct. 2006.

[6] W. Wiechert, "13C Metabolic Flux Analysis," *Metab. Eng.*, vol. 3, pp. 195–206, Apr. 2001.

[7] J. Greene, J. W. H. Jr, and J. P. Wikswo, "Rapid and Precise Determination of Cellular Amino Acid Flux Rates Using HPLC with Automated Derivatization with Absorbance," *Agil. Appl. Note*, pp. 1–8, 2009.

[8] C. Zupke and G. Stephanopoulos, "Intracellular flux analysis in hybridomas using mass balances and in vitro (13)C nmr.," *Biotechnol. Bioeng.*, vol. 45, no. 4, pp. 292–303, Feb. 1995.

[9] S. S. Ozturk and B. O. Palsson, "Chemical decomposition of glutamine in cell culture media: effect of media type, pH, and serum concentration.," *Biotechnol. Prog.*, vol. 6, no. 2, pp. 121–8, 1990.

[10] C. a Sellick, R. Hansen, A. R. Maqsood, W. B. Dunn, G. M. Stephens, R. Goodacre, and A. J. Dickson, "Effective quenching processes for physiologically valid metabolite profiling of suspension cultured Mammalian cells.," *Anal. Chem.*, vol. 81, no. 1, pp. 174–83, Jan. 2009.

[11] W. P. Byrne and R. H. Bryan, "A calcium chloride solution, dry-ice, low temperature bath," *J. Chem. Educ.*, vol. 47, no. 5, p. 361, 1970.

[12] J. Folch, M. Lees, and G. H. S. Stanley, “A simple method for the isolation and purification of total lipides from animal tissues,” *J. Biol. Chem.*, vol. 226, no. 1, pp. 497–509, Aug. 1957.

[13] M. R. Antoniewicz, *Comprehensive Analysis of Metabolic Pathways Through the Combined Use of Multiple Isotopic Tracers by*. 2006, pp. 1–370.

[14] K. F. Wlaschin and W. Hu, “Fedbatch Culture and Dynamic Nutrient Feeding,” *Adv. Biochem. Eng.*, no. 101, pp. 43–74, 2006.

[15] H. Dorai, Y. S. Kyung, D. Ellis, C. Kinney, C. Lin, D. Jan, G. Moore, and M. J. Betenbaugh, “Expression of anti-apoptosis genes alters lactate metabolism of Chinese Hamster Ovary cells in culture.,” *Biotechnol. Bioeng.*, vol. 103, no. 3, pp. 592–608, Jun. 2009.

[16] S. Dietmair, N. E. Timmins, P. P. Gray, L. K. Nielsen, and J. O. Krömer, “Towards quantitative metabolomics of mammalian cells: development of a metabolite extraction protocol.,” *Anal. Biochem.*, vol. 404, no. 2, pp. 155–64, Sep. 2010.

VI: THE METABOLIC REPROGRAMMING OF INDUSTRIAL ANTIBODY EXPRESSING CHO

Abstract

Eleven CHOK1SV clones were cultured in three-liter fed-batch reactors, and ^{13}C MFA was applied to assess the early stationary phase of metabolism. Eight of the clones used the glutamine synthetase (GS) expression system to express IgG. Four of the clones were genetically manipulated to be apoptosis-resistant, expressing engineered Bcl-2Δ. Central metabolism was significantly altered in response to the added metabolic load of antibody production. As net NADH production by TCA cycle and glycolysis increased in CHOK1SV, specific antibody production likewise increased. The expression of Bcl-2Δ led to a further increase in NADH production that was accompanied by even greater specific mAb productivity. Increased TCA cycling, and decreased lactate production, were also independently associated with specific productivity. However, while lactate production was reduced in high-producing clones, total glycolytic flux increased in relation to specific productivity. Furthermore, high-producing clones generated recombinant protein at a rate roughly equivalent to that of biomass-associated protein (carbon molar basis). These findings underscore the connection between oxidative metabolic states and recombinant antibody generation, and define the unique metabolic alterations inherent in industrial cell culture.

Introduction

In previous work, metabolic flux analysis (MFA) has been successfully applied to individual IgG producing CHO clones cultured in fed-batch. GS-CHO lines were studied in five-liter bioreactors, where dissolved oxygen, partial CO_2 pressure, and temperature were optimized [1] for the stationary phase. It was later applied to a DHFR-CHO line grown in 24 deep-well plates, and assessed at four different stages of culture, including the stationary phase [2]. Since culture conditions change substantially over the time course of a fed-batch, multiple phases were considered to determine how central metabolism rewires itself over the course of a run. MFA has also been applied to better understand the relationship between metabolism and apoptosis [3], and anti-apoptosis engineering has been successfully applied to increase final product titer in fed-batch culture [4].

In this work, we sought to find common metabolic phenotypes associated with high specific productivity. We examined the early stationary phase, as specific productivity was previously determined to begin to peak during this phase. Since Bcl-2Δ expression has been previously shown to have increased mitochondrial enzymatic activity and reduced lactate production, traits associated with increased specifc productivity, we also assess the utility of expressing Bcl-2Δ expressing clones. A total of four unique IgGs were produced, both by CHOK1SV-GS and a Bcl-2Δ clone, making for a total of eight clones. Additionally, non-producing CHOK1SV and Bcl-2Δ clones are considered to better understand how central metabolism responds to forced IgG expression. While this study is by no means a large scale study for industrial cell culture work, it is to our knowledge the largest ^{13}C MFA study ever conducted upon IgG producing CHO cells. This large scale ^{13}C MFA was conducted to

differentiate between the metabolic phenotypes unique to individual clones, and the observable metabolic trends amongst multiple producing clones.

Materials and Methods

Cell Culture

Eleven different Lonza CHOK1-SV lines were cultured at Janssen. Three of the lines functionally served as non-producing controls: CHOK1SV, CHOK1SV-GS, and Bcl-2Δ. CHOK1SV served as the parent to the other ten lines, and in addition to not producing antibody, is the only heterogenous (non-clonal) line. The other ten lines are clonal. CHOK1SV-GS was transfected with a blank GS plasmid, and it contained neither light nor heavy chain. Bcl-2Δ was generated by transfecting CHOK1SV with the engineered anti-apoptotic protein of the same name, and following G418 selection, screening for minimal caspase 3/7 activity. Eight of the lines were antibody secreting, all transfected using Lonza's GS system. A total of four separate monoclonal antibodies were produced, denoted M1−M4. Two of these antibodies are IgG1, one IgG2, and one IgG4. The lineage of the eleven lines is described in Figure 6-1.

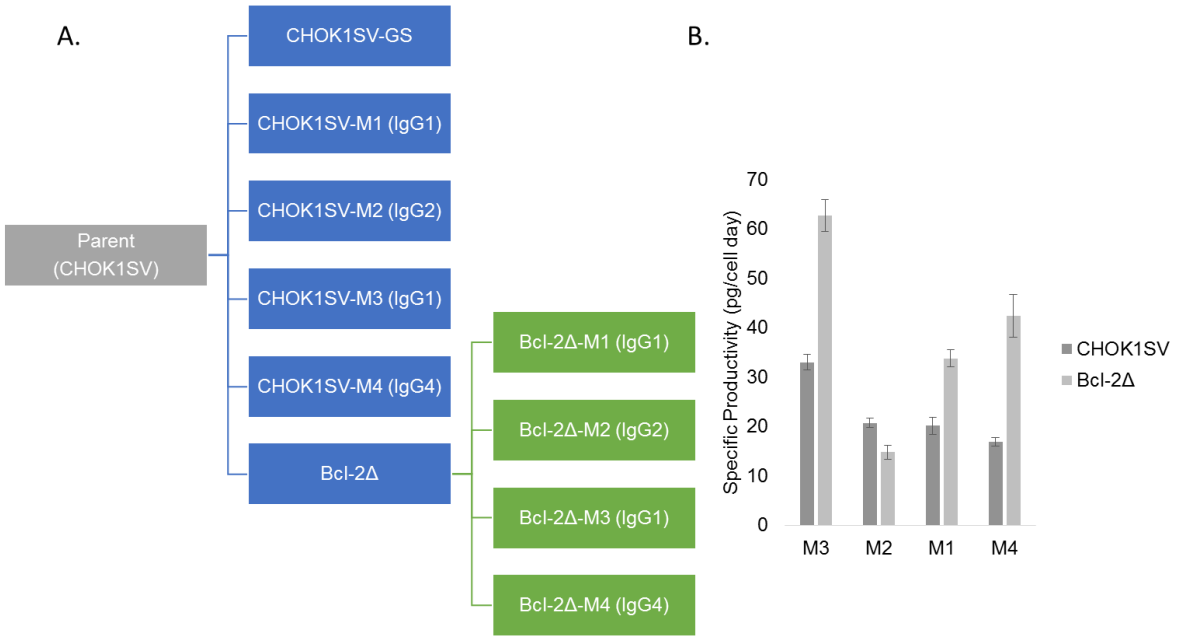

Figure 6-1. Cell lines. A. Genetic lineage of the 11 clones used in this study. **B.** Specific productivity of 8 IgG producing clones.

All antibody producing clones were screened for productivity, expression stability, and product quality. Between five to ten thousand clones were examined to obtain a high performance clone.

Fed-batch reactor conditions

Three -liter Millipore Mobius fed-batch reactors with pH, temperature, agitation, and dissolved oxygen (DO) controls were used for cell culture. pH was set to 7 and maintained between 6.9 and 7.1. Temperature was held at 36.5°C for the entire experiment. Agitation was set to 200 RPM. Oxygen was set to sparge at 40% DO, maintaining DO between 40-100%. Initially, cultures were inoculated into a 1-liter working volume. Culture volume rose to a final working volume of no higher than 1.2 L. Cultures were grown in batch mode for the first 3 days.

Reactors were fed on Day 3 and 4 with glucose, amino acids, vitamins, and minerals. At each daily feed addition, glucose was fed to reach 3 g/L concentration. The non-GS clones, namely the parental CHOK1SV and the Bcl-2Δ daughter, were fed glutamine to 6 mM concentration. The GS-clones were not supplemented with glutamine.

On Day 5 the feeding scheme changed, when glucose was fed to 6 g/L in all reactors and glutamine to 8 mM concentration in the non-GS clones. At day 5, the ^{13}C tracer was introduced, and 2 days passed without any additional feeds to the reactor. A summary of the experimental timeline is provided in Table 6-1.

Table 6-1. Experimental timeline. Days 5-7 are shaded to indicate the presence of ^{13}C glucose.

Day	0	1	2	3	4	5	6	7
Event	Inoculate at 4E5 cell/mL			Feed	Feed	Feed ^{13}C		Final Quench

Cultures were sampled throughout the 7 days, with an increased sampling frequency following exposure to ^{13}C glucose.

Determination of specific consumption/production rates

An Innovatis Cedex was used to determine the cell density. Amino acid concentration was determined using an Agilent 1200 series high performance liquid chromatograph (HPLC). Amino acid concentration was accurately quantified by UV absorbance detection, following pre-injection sample derivatization with orthophthaldildehyde (OPA), according to protocol [5].

Glucose, lactate, ammonia, glutamate, glutamine, and IgG concentration were determined using a Roche Cedex BioHT. Specific growth rate was determined by application of the following three equations:

$$\frac{dX}{dt} = \mu_{net} X \quad (6\text{-}1)$$

$$\frac{dX_d}{dt} = k_d X \quad (6\text{-}2)$$

$$\mu_{net} = \mu_g - k_d \quad (6\text{-}3)$$

Where net specific growth rate (μ_{net}), specific death rate (k_d), and gross growth rate (μ_g) were determined by regressing the viable cell density (X) and dead cell density (X_d). Specific production/consumption rates were determined using the following equation:

$$\frac{dC_i}{dt} = q_i X - k_i C_i \quad (6\text{-}4)$$

Where C_i represents the metabolite concentration at the *ith* measured time, q_i the specific production rate (negative if consumed), and k_i the first order degradation content. Glutamine was the only amino acid found to have a non-negligible degradation constant, with a half life of approximately 8 days. Regression to determine specific rates was performed using the ETA software package.

Isotope labeling experiments

On day 5 of culture, the glucose concentration was raised to 6 g/L. This glucose addition was a 50/50 (by molarity) mixture of [1,2-$^{13}C_2$]glucose and [U-$^{13}C_6$]glucose, beginning the ^{13}C labeled experiment (Figure 6-A-1). Since there was no media exchange, natural glucose made up between 30-50% of the final glucose concentration post ^{13}C glucose feed. Cultures were quenched several times over the next two days, in order to assess isotopic steady state. Sufficient volume was removed from the reactor to obtain approximately 10 million cells, which were immediately quenched in a 60% methanol, 40% ammonium bicarbonate aqueous solution pre-cooled to -40°C [6]. Once the quenching solution had been removed, polar metabolites were extracted using an 8:4:3 chloroform: methanol: water solution [7]. Chloroform and water/methanol form a biphasic solution, with the metabolites of interest partitioning to the less dense aqueous upper phase.

Gas chromatography mass spectroscopy (GCMS) analysis

After extraction, the samples were derivatized as described previously [2]. Derivatized polar metabolites were injected via split mode into an Agilent 7890B gas chromatograph employing an Agilent HP5-MS column (30m x 0.25mm i.d. x 0.25µm). The split ratio was varied from 1:2 to 1:10 in order to achieve accurately quantifiable signal (i.e., sufficient signal-to-noise ratio without oversaturating the detector). For the same reason, injection volume was varied from 0.5 to 2µL. The GC inlet was fixed at 270°C, and helium flow rate was 1 mL/min. The GC oven was initially set at 80°C and held for 5 minutes, ramped at 20°C/min to 140°C, ramped at 4°C/min to 280°C, and held for 5 minutes. To manage widely varying sample metabolite concentrations, the Agilent 5977A MS gain factor was adjusted in timed event mode.

Scan mode allowed all mass spectra between 100-500 m/z to be recorded, and raw ion chromatograms were integrated using a custom MATLAB program which applied consistent integration bounds and baseline corrections to each fragment ion [8].

To determine the relative ratio of [1,2-$^{13}C_2$]glucose, [U-$^{13}C_6$]glucose, and natural glucose, Di-O-isopropylidene propionate derivatization was performed. An Agilent 7890 gas chromatograph was used with an Agilent DB-5MS column (30m x 0.25mm i.d. x 0.25µm). 1 µL of sample was injected in splitless mode. Following injection, the GC oven was held at 80°C for 1 minute, ramped at 20°C/min to 280°C and held for 4 minutes, and again ramped by 40°C/min to 325°C and held for 0 minutes.

Reaction network

A reaction network was generated as described previously [3]. Individual cell dry mass was determined for each of the 13 clones used in this study. In total, there were 111 reactions, 22 extracellular metabolites, and two macromolecular products (biomass and antibody).

^{13}C metabolic flux analysis (MFA)

INCA was used to fit a metabolic model [9] to the experimental data, as described previously [3]. All models generated were overdetermined with approximately 100 degrees of freedom. Isotopic and metabolic steady-state were independently verified for all 13 cell lines. Model visualization was aided by Cytoscape [10].

Two-way hierarchical clustering

Ward's method was used to first cluster cell lines, based upon their respective flux map. Then, individual reactions were clustered together (making the analysis two-way). To generate the heat map, Z-scores were generated by using the following equation:

$$Z = \frac{V_{i,j} - \overline{V_i}}{s_{i,j}}$$

Where $V_{i,j}$ represents an individual carbon flux (e.g., $V_{HK,CHOK1SV}$), $\overline{V_i}$ the average carbon flux calculated over all cell lines, and $s_{i,j}$ the standard deviation associated with flux $V_{i,j}$.

Results

^{13}C metabolic flux analysis was performed upon a parental CHOK1SV line and ten daughter clones. Eight of the eleven lines were selected by Lonza's glutamine synthetase (GS) system, and then industrially screened for immunoglobulin (IgG) expression. All eight producing clones were generated independently, starting from the polyclonal CHOK1SV line. Amongst the eight clones, four model IgGs were produced. Two clones produced IgG1, one clone IgG2, and another clone IgG4. Past experiments concluded that specific productivity was at or near its peak during day 5-7 (data not shown). Therefore, this phase was intentionally examined to assess the unique demands posed to central metabolism by antibody production in a 3L fed-batch reactor. Fundamentally, the determination of a shared metabolic phenotype among high-producing clones is the central objective of this work.

Trends of productivity

To make for straightforward comparison, the clones have been ranked in order of specific productivity (Figure 6-1). Each IgG is produced by one CHOK1SV and one Bcl-2Δ clone. For this reason, the two clones producing the same IgG are often compared head-to-head. In ¾ of the cases explored in this study, the Bcl-2Δ clone significantly outperformed the CHOK1SV clone in specific productivity.

To provide insight about the increased metabolic demands required of the cell to produce an IgG for industrial purposes, a stoichiometric comparison was performed [11]. Here, the protein requirements for biomass production are compared to the antibody production requirements (Figure 6-2).

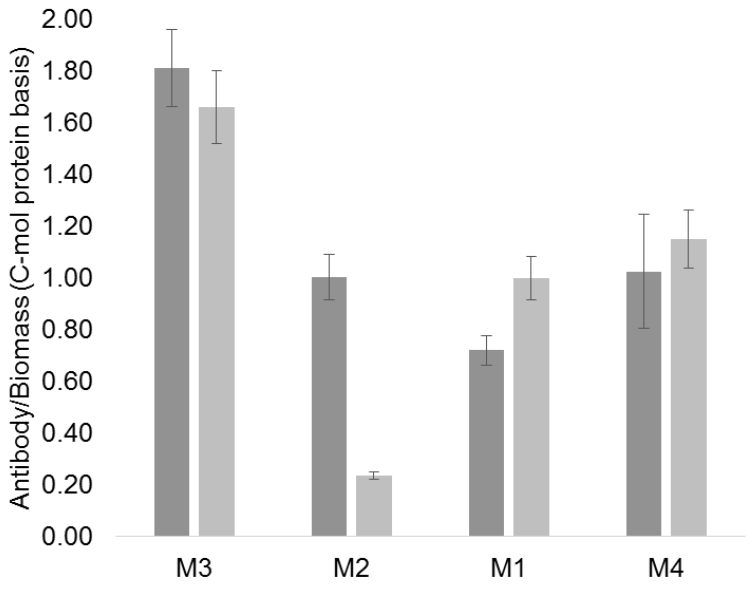

Figure 6-2. Protein demands. Relative comparison of protein production rates. Antibody production is compared relative to biomass (specifically, the protein content of cellular biomass). A ratio of 1 indicates equivalent rates of protein synthesis associated with either biomass or antibody production.

By utilizing a compositional analysis of biomass [12], and experimentally determining growth rate and dry cell mass, the rate of protein synthesis for biomass on a C-molar basis was quantified. Likewise, the measured specific rate of antibody production was converted to a C-molar basis by determination of the antibody's amino acid composition. In multiple instances, protein demand for antibody synthesis exceeded that of biomass. When the ratio of antibody/biomass synthesis is equal to 1, the total protein demand upon the cell doubles.

The GS system augments the endogenous capacity of the cell to produce glutamine, providing a selectable marker for isolation of stable clones [13]. However, GS was found to also lead to the secretion of glutamine into the extracellular media (Figure 6-3A), indicative of glutamine synthesis in excess of anabolic demand for protein synthesis.

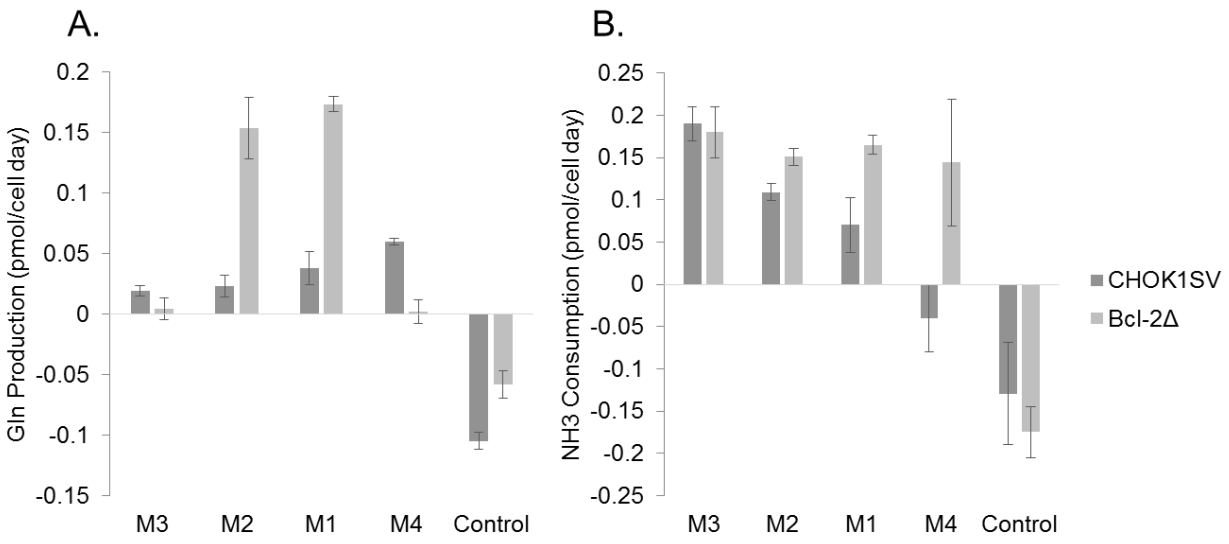

Figure 6-3. Metrics of Glutamine Synthetase (GS) overexpression. A. Glutamine production. Negative values indicate consumption. **B.** Ammonia consumption. Negative values indicate production.

Interestingly, the rate of extracellular glutamine flux was found to correspond negatively with specific productivity. In contrast to the GS-clones, the parental CHOK1SV and Bcl-2Δ lines were found to consume glutamine, with Bcl-2Δ consuming glutamine at roughly half the rate of the control CHOK1SV. This was in agreement with previous work using CHO-S [3].

Corresponding with glutamine synthesis, the majority of the producing clones consumed ammonia. To produce glutamine, GS adds an amine group to glutamate, which can be provided by ammonia. Ammonia consumption positively correlated with specific productivity, especially in the CHOK1SV background (Figure 6-3-B). The two lines considered without the GS system were both found to produce ammonia at rates similar to the ammonia consumption rate of the GS clone.

Metabolic flux analysis (MFA)

Figure 6-4 represents the flux map from 3 separate CHOK1SV lines. When GS was overexpressed, the relative amount of carbon directed to the mitochondria increased.

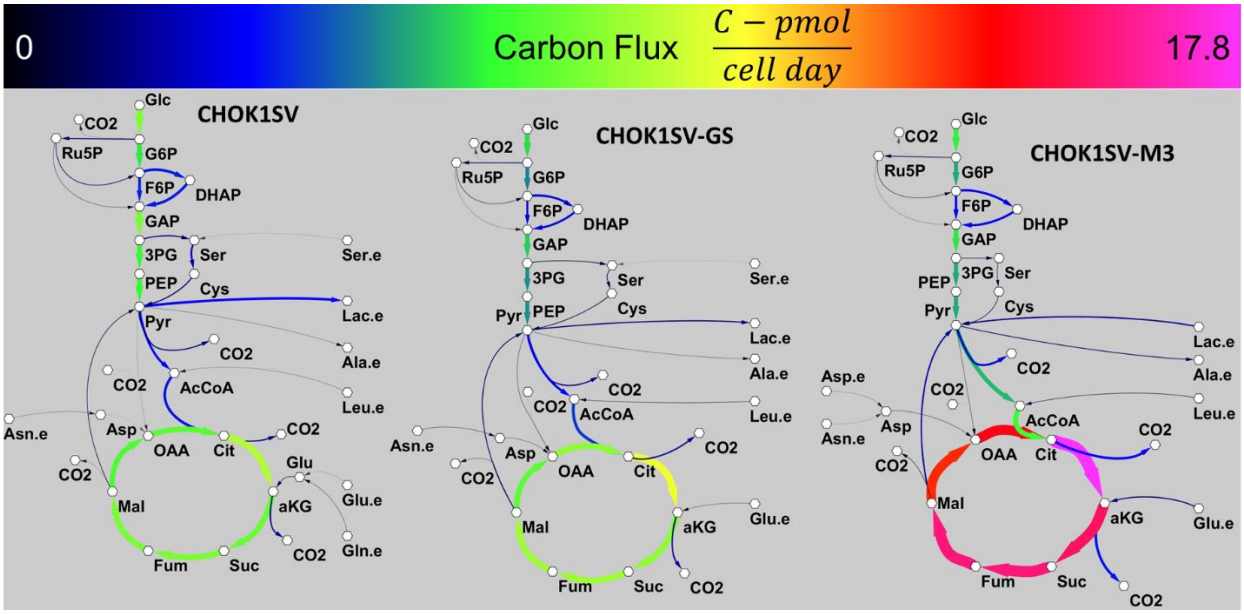

Figure 6-4. Metabolic flux analysis. Major carbon fluxes are shown. Both width and color of directional arrows are proportional to the magnitude of carbon flux.

This can largely be attributed to a reduction in lactate production, which was reduced by over 50% in CHOK1SV-GS when compared to CHOK1SV. All the more impressive is the impact upon central metabolism when a GS-CHO cell is forced to produce antibody. While total carbon consumption decreased by 30% in CHOK1SV-M3 (Figure 6-A-2), increased flux to the TCA cycle exceeded 30%. If the CO_2 generating reactions of the TCA cycle were summed together, CO_2 generation nearly doubled (Figure 6-A-3). Much of this increase to the TCA cycle can be

attributed to a net lactate consumption flux. As Figure 6-4 demonstrates, an upregulated TCA cycle was a hallmark of high specific productivity.

Like CHOK1SV-M3, Bcl-2Δ clones demonstrated significantly increased TCA cycling. However, not only was the TCA cycle upregulated relative to the parental Bcl-2Δ clone, it was upregulated relative to the CHOK1SV producing the equivalent IgG. This is best represented in the heat map of Figure 6-5.

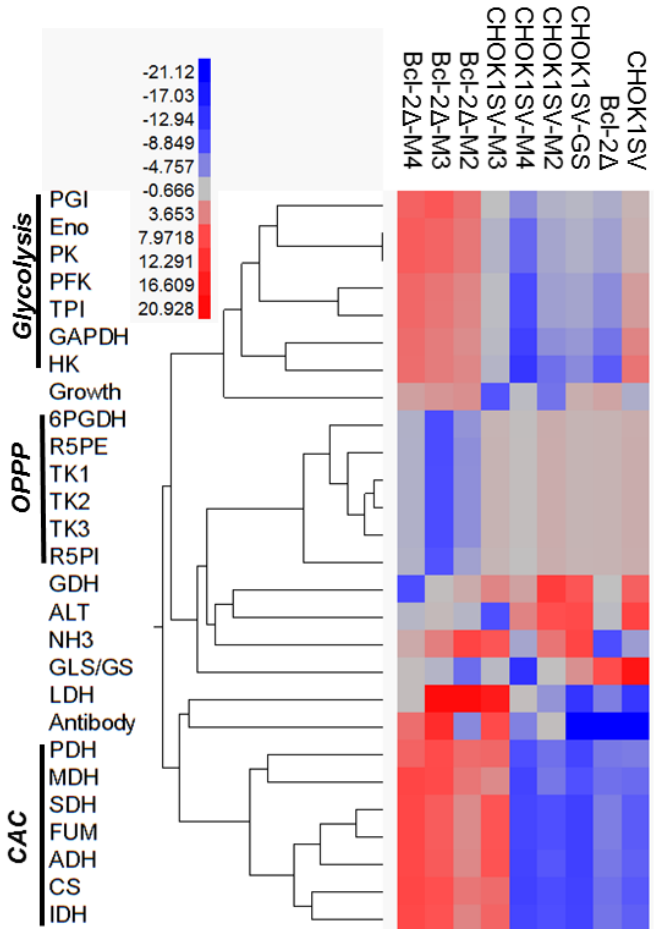

Figure 6-5. Central metabolism fluxes and specific antibody production. Maps generated by two-way hierarchical clustering using Ward's method.

Here, a two-way hierarchical clustering was performed upon the Z-scores of each individual metabolic reaction. Based upon hierarchical clustering, the most similarility was found between the control, Bcl-2Δ, and CHOK1SV groups. Notably, CHOK1SV-M3 was placed into the Bcl-2Δ group. Clustering was then applied to the individual fluxes. While the pathways were grouped together, the individual reactions were all free to be sorted. Considerable separation amongst the clones was observed in glycolysis and the TCA cycle.

Two rate limiting reactions [14] of the TCA cycle are considered further in Figure 6-6.

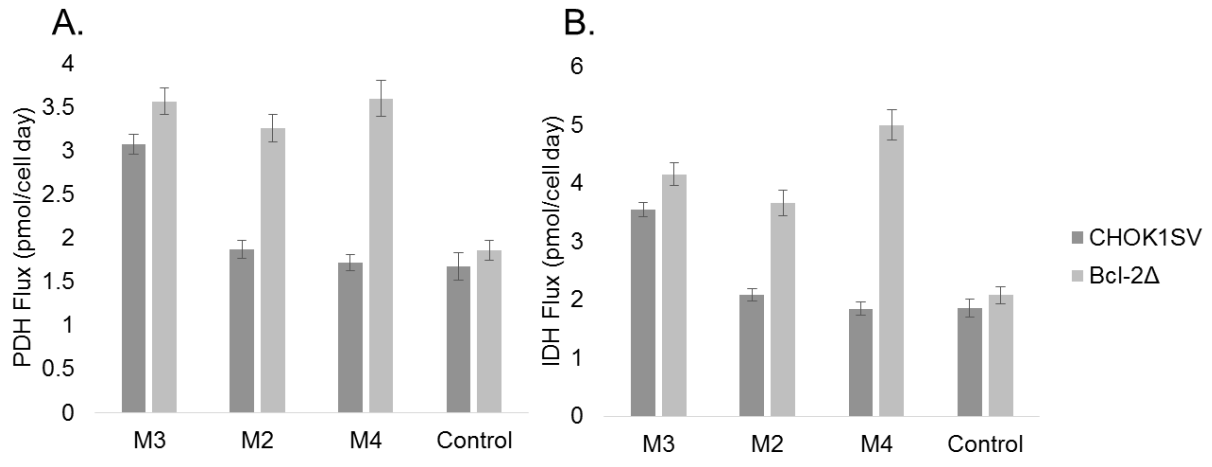

Figure 6-6. TCA Cycle fluxes. A. Pyruvate dehydrogenase (PDH) flux. **B.** Isocitrate dehydrogenase (IDH) flux.

Both in the case of pyruvate dehydrogenase (PDH) and isocitrate dehydrogenase (IDH), overall flux increased as specific productivity increased. Among the top three producing clones, PDH and IDH flux increased significantly relative to their respective parental control. In CHOK1SV-M3, PDH and IDH flux increased by 80% and 90% respectively. Additionally, glycolysis was also found to be upregulated in high producing clones, especially in Bcl-2Δ clones. Two rate

limiting glycolytic reactions, hexokinase (HK) and phosphofructokinase (PFK), both significantly increased in all Bcl-2Δ producers when compared to their control (Figure 6-7) [14].

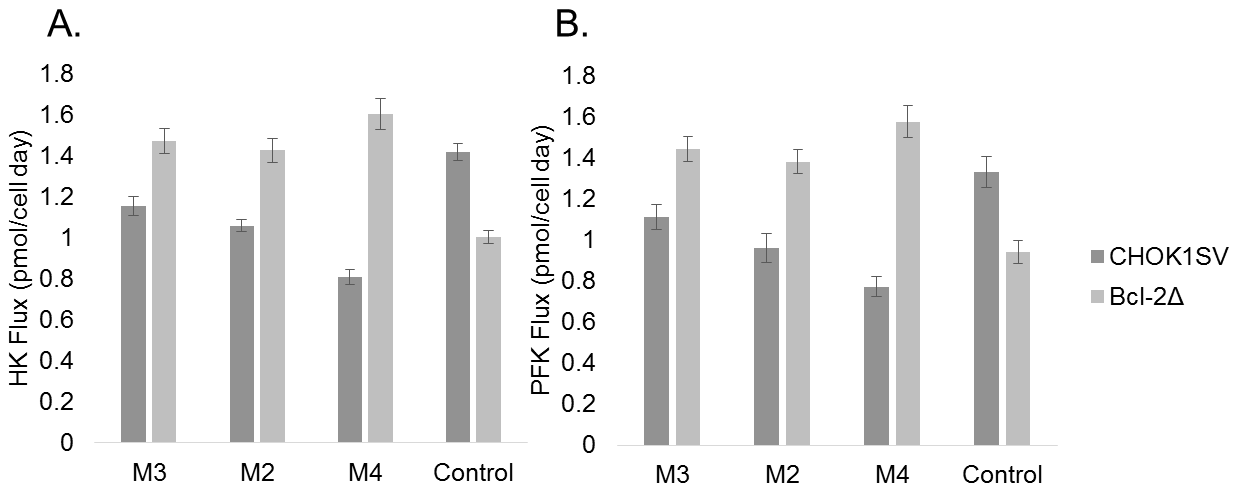

Figure 6-7. **Glycolytic fluxes**. **A.** Hexokinase (HK) flux. **B.** Phosphofructokinase (PFK) flux.

As reported by Figure 6-5, specific productivity corresponded with lactate dehydrogenase (LDH) more strongly than any other flux. When glycolytic flux is increased and carbon allocation to the mitochondria was increased, however, it often corresponded with higher specific productivity (Figure 6-8A).

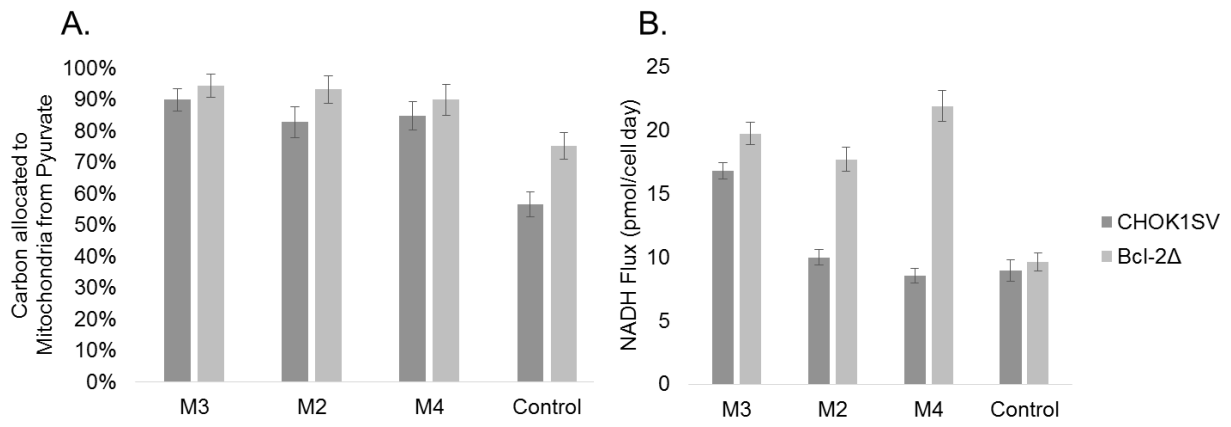

Figure 6-8. The mitochondria and NADH production. A. Carbon directed from pyruvate to mitochondria. Percentage determined based upon mass balance of the pyruvate node. **B.** Net NADH production. Net production was determined by summing together: glyceraldehyde-6-phosphate dehydrogenase (GAPDH), lactate dehydrogenase (LDH), pyruvate dehydrogenase (PDH), isocitrate dehydrogenase (IDH), alpha-ketoglutarate dehydrogenase (ADH), and malate dehydrogenase (MDH). Redox reactions outside of the TCA cycle and glycolysis were not included in the NADH flux reported.

Relative to CHOK1SV, Bcl-2 clones consistently had higher carbon allocation to the mitochondria. When the carbon of pyruvate is directed to the mitochondria, it can lead to the reduction of NAD^+ in the TCA cycle. When pyruvate is directed to lactate, however, it is associated with the oxidation of NADH. For this reason, it is often meaningful to consider the impact of glycolysis and the TCA cycle upon redox (Figure 6-8B). Here, net NADH production was determined, an indicator for oxidative phosphorylation (OXPHOS). Of all the reactions considered, only LDH was found to oxidize NADH in this study. When net NADH production was highest, it corresponded with the highest specific productivity in both CHOK1SV and Bcl-2Δ.

Discussion

Oxidative metabolism

A common theme of this work was the relationship between oxidative metabolism and specific productivity. All of the clones considered here employ the CHOK1SV-GS system. Previous work in DHFR based expression in CHO has found similar results [2]. While only a single clone was considered in that study, snapshots of the metabolic phenotype of the different stages of a fed-batch process were captured. During the stationary (peak productivity) phase, TCA cycle flux was found to peak (similar to the phase considered in this study). Additionally, the NADH/NAD^+ ratio was reported to fall. For this to happen, the rate of OXPHOS would likely be in excess of the TCA cycle (and other NAD^+ reducing reactions). TCA cycling simultaneously peaked with specific productivity both in GS and DHFR CHO clones.

In this work, peak NADH flux was observed in the highest producing clones from both CHOK1SV and Bcl-2Δ. As NADH flux was reduced in CHOK1SV, specific productivity consistently followed suit. If quasi-metabolic steady state is assumed, then the net production (reduction) of NADH must be met by equivalent consumption (oxidation). While oxidation can actually be in excess of reduction in CHO fed-batch culture [2], the positive correlation with enhanced specific productivity still holds.

Synthesis of protein is energetically expensive. 3 ATP equivalents are necessary to form one peptide bond [15]. This does not consider the energy necessary to package and secrete a protein. To generate this ATP, the cell has multiple pathways at its disposal. Independently engaging the glycolytic pathway, fermenting glucose to produce lactate, is a viable means for ATP generation. ATP is generated and while NAD^+ is reduced to NADH by glyceraldehyde-3-phosphate dehydrogenase, it is oxidized back to NAD^+ by LDH [16]. Thus glycolysis, in this

energetic sense, can operate independently of other pathways. However, this metabolic behavior is not typically associated with higher titers [17]. The presence of lactate as a byproduct in solution is not typically sufficient to harm growth or titers [18]. After all, lactate has successfully been fed to control pH in a CHO fed-batch reactor [19]. Instead, it is the metabolic phenotype associated with the production of lactate that correlates with poor productivity [20]. Alternatively, the cell can direct glycolytic flux to the mitochondria and engage the TCA cycle in conjunction with OXPHOS to generate ATP. Considering the respiratory quotients typically observed in CHO cells [21], a highly active TCA cycle generating CO_2 strongly corresponds with high oxygen uptake rates. Likewise, higher rates of oxygen uptake rate strongly correspond with high antibody production rates in CHO cells [22]. Considering the quantified increase in protein demand (Figure 6-2) and the associative required energy, it is rational that the cell would engage more efficient catabolic pathways for energy production. Efforts to increase the oxidative activity of the cell have clear potential to increase specific productivity.

Increased flux through the pentose phosphate pathway (PPP) often correlates with increased TCA cycling [1,2]. As much as 100% of glucose consumed can be directed through the PPP. In this study, as much as 30% of glucose consumed was directed to the PPP, but no more. This was actually in agreement with previous work examining CHO-K1 clones in the stationary phase of growth [23,24]. As to why more flux wasn't directed to the PPP in this GS-CHO study, it is possible that the experimental timing played a significant factor. This experiment ended at day seven while producing cultures ranged from 92-98% viability (Figure 6-A-4). The full production run time typically lasts eighteen days.

In relative terms, Bcl-2Δ clones directed more carbon flux to the mitochondria (Figure 6-8A), corroborating prior work [3]. This was true when carbon flux was expressed on either an

absolute or relative basis (Figure 6-6). This was not only true for the controls, but all IgG producing clones as well. Bcl-2Δ is known to modulate and maintain mitochondrial permeability by preventing the release of cytochrome-c into the intramembrane space [25]. Not only is the integrity of the mitochondrial membrane upheld, cytochrome-c is more readily available to participate in the electron transport chain of OXPHOS. While cytochrome c was not specifically measured in this work, there are molecular reasons for Bcl-2Δ to allow for enhanced oxidative metabolism.

With Bcl-2Δ clones directing greater flux (absolute basis) to the mitochondria, increased glycolytic flux coincided. The fact that Bcl-2Δ IgG producing clones consistently exhibited significantly increased glycolytic flux (Figure 6-7), yet directed more of it to the mitochondria (6-8A), clearly indicates that the additional glucose consumed was not directed to lactate. This finding, in conjunction with greater net NADH production (Figure 6-8B), may relate to the mitochondria of Bcl-2Δ clones having a greater capacity for redox exchange compared to their CHOK1SV pair. As discussed prior, lactate production oxidizes NADH making it possible for glycolysis to continue. However, so does OXPHOS. Yet NAD^+ cannot freely cross the mitochondrial membranes. The Aspartate/Glutamate shuttle provides this function allowing for NAD^+ equivalents to be transported back to the cytosol. Prior work has already shown lactate production to decrease in the presence of increased Asp/Glu expression [26,27].

Increased glycolytic flux alone doesn't necessarily lead to increased specific productivity. When comparing the CHOK1SV lines, the IgG producing clones all exhibited lesser glycolytic flux than their parental control. Yet in the case where increased glycolytic flux leads to an increased percentage of flux directed to the mitochondria, as was the case in Bcl-2Δ, this often corresponded with increased specific productivity (relative to CHOK1SV).

Practical applications

Genetic targets. Bcl-2Δ was consistently associated with enhanced oxidative metabolism, and has significant potential for industrial application. Of the four varieties of IgG being considered for this study, it increased specific productivity by an average of 70%. Considering the general lack of increase in cell specific productivity over the past twenty years, and the fact that this was accomplished in the widely used CHOK1SV-GS system, this finding was substantial [28,29]. While Bcl-2Δ is associated with reduced peak exponential growth, it overall leads to increased integral viable cell density (IVCD), by hindering the progression of apoptosis [3]. As has been reported previously, final titer often directly correlates to IVCD [30].

In addition to Bcl-2Δ, two TCA cycle enzymes have been identified for genetic modification. Both PDH and IDH have been identified as rate limiting steps of the TCA cycle [14]. Overexpression of PDH would increase the amount of carbon directed into the mitochondria. However, expression of PDH may be difficult, as PDH is an enzyme complex. For this reason, so far efforts have been made to inhibit PDH kinase (PDHK) through RNA interference. Encouragingly, they have been met with success increases to specific productivity [31]. Still, overexpression of PDH is not impossible, as similar efforts have been made to optimize the ratio of LC:HC [32]. Overexpression of IDH would also serve to bolster the TCA cycle, and it is not a complex. IDH which uses NAD^+ as a cofactor (IDH3) is of interest here, but the specific isoform still will need to be determined, as all three isoforms of IDH3 were previously identified in CHO transcriptomic work [33]. Since IDH3α was more highly expressed (than the other isozymes) in previous CHO transcriptomic work [34], overexpressingIDHβ or IDHγ may prove effective.

Increasing glycolytic flux at least has conditional industrial application. The fact that it corresponded with enhanced specific productivity is contrary to previous work that has attempted to limit glycolytic flux by controlled feeding of glucose to fed-batch CHO cultures. Increasing either HK or PFK, both rate limiting enzymes of glycolysis, will only be effective if the mitochondria has the increased capacity for redox exchange (involving the Asp/Glu transporter). This is why we state only conditional industrial application. After all, the control CHOK1SV line had increased glycolytic flux but also generated considerably more lactate (and produced no IgG). Figure 6-8B suggests increased mitochondrial redox capacity was the case for all Bcl-2Δ clones. Regardless, while limiting glucose availability in media in an effort to limit lactate production may be effective (to that end) [30,35], it may limit specific productivity (Figure 6-1 and 6-7).

Screening methods. Both ammonia production and glutamine production can serve as viable screening methods for clones capable of achieving higher titers (Figure 6-3). Assuming that the push for higher viable cell densities continues [36], ammonia will become more and more of an obstacle to higher titers. This is because ammonia negatively affects growth rate. The ammonia concentrations achieved even in this seven day study were high enough to potentially impact growth rate, as indicated by previous work [18,37] Here, we find a strong correlation among high ammonia consumption and high specific productivity in CHOK1SV clones. Therefore, selecting clones with high ammonia consumption will benefit IVCD in addition to specific productivity.

Production of glutamine corresponded negatively with specific productivity. When glutamine is produced from glutamate, it demands ATP. This is desirable for the purpose of cell growth and antibody production, but undesirable when the excess glutamine is directed to excretion. Additionally, the secretion of glutamine into the media poses risk for cell line stability. This is because it is the absence of glutamine from media that serves as the selective criteria for GS-transfected CHO cells. A loss of stability poses a substantial risk, as it can lead to inconsistent batch to batch performance. Excreted glutamine may not be a harmless byproduct of GS-CHO cells.

Appendix

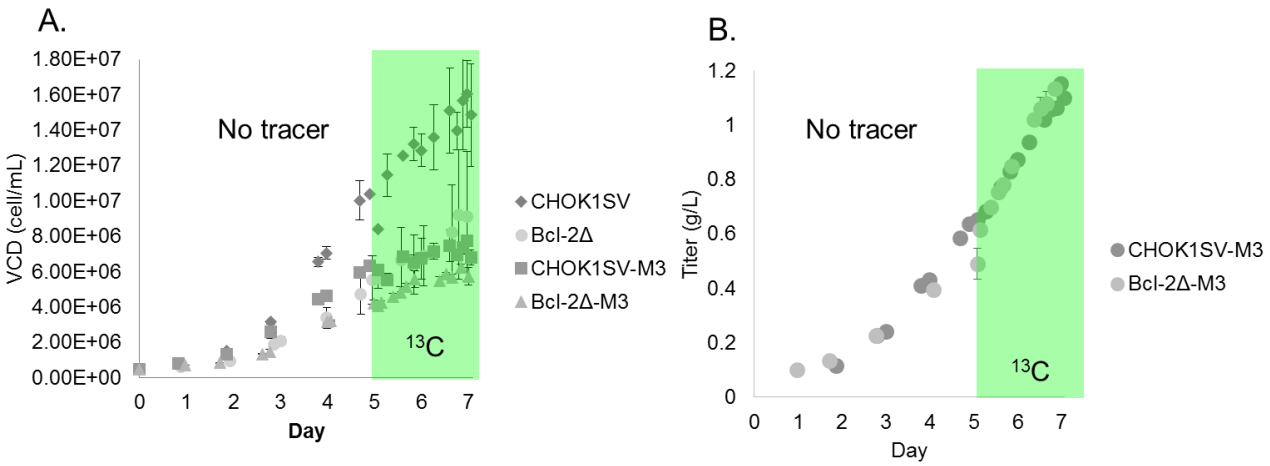

Figure 6-A-1. ^{13}C labeled culture profile. A. Viable cell density (VCD) over culture life. **B.** Antibody concentration (titer) over culture life.

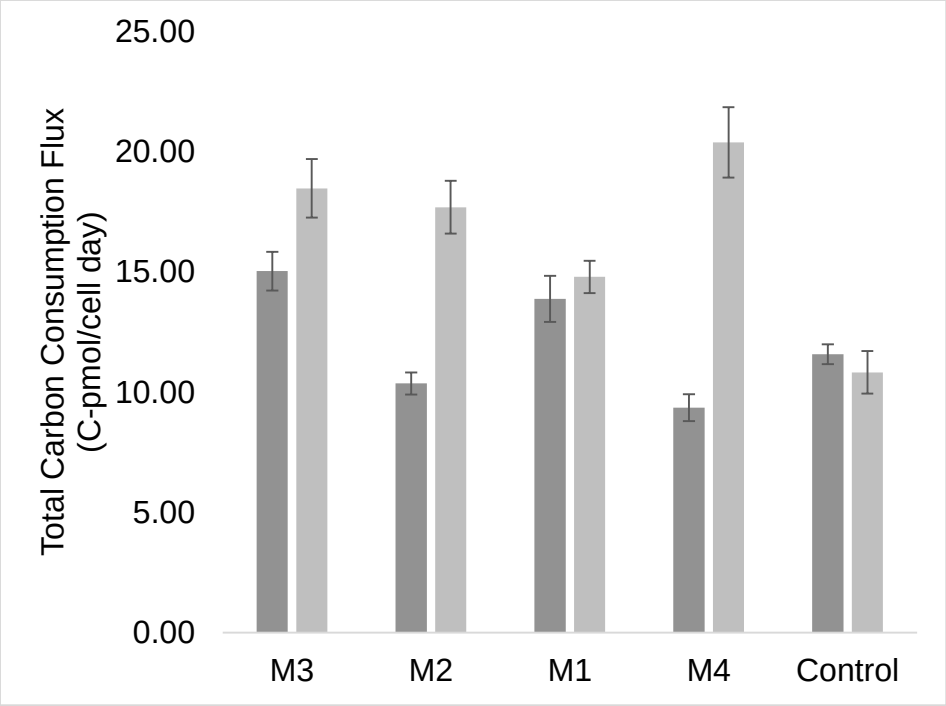

Figure 6-A-2. Total carbon consumption. All consumed metabolites included.

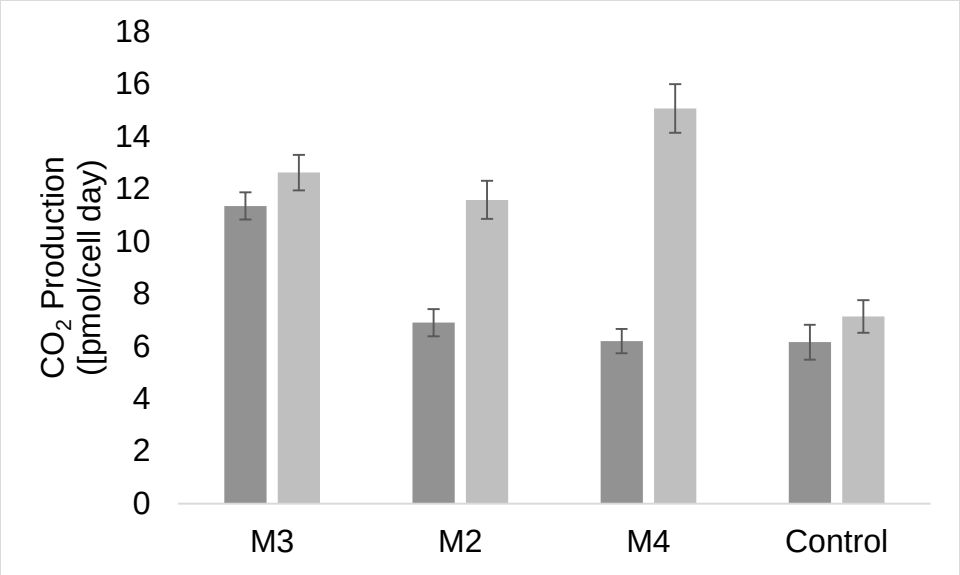

Figure 6-A-3. Total CO_2 production. All CO_2 producing and consuming reactions included.

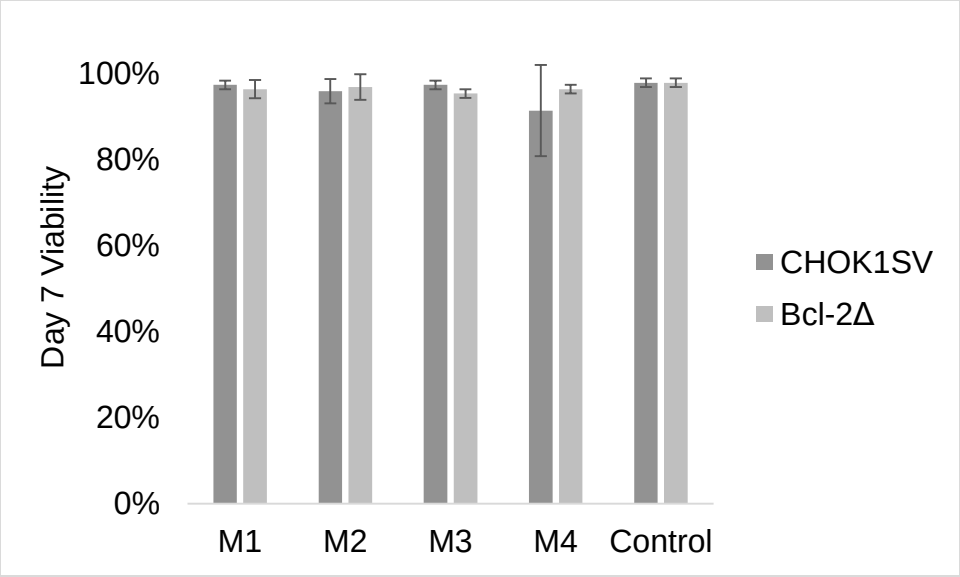

Figure 6-A-4. Viability at Day 7. End of experiment.

95% confidence intervals associated with individual fluxes

Table 6-A-1. Net fluxes of CHOK1SV. Associated with Figure 6-4 and 6-5.

Pathway	Enzyme	Rxn	LB	UB	Value
Glycolysis	PGI	G6P <-> F6P	0.784	1.488	1.136
	PFK	F6P -> DHAP + GAP	1.180	1.483	1.332
	TPI	DHAP <-> GAP	1.176	1.480	1.328
	GADPH	GAP <-> 3PG	2.553	2.960	2.757
	Eno	3PG <-> PEP	1.801	2.890	2.345
	PK	PEP -> Pyr	1.801	2.890	2.345
	HK	Glc -> G6P	1.334	1.497	1.415
	LDH	Lac <-> Pyr	-1.400	-1.037	-1.219
PPP	6PGDH	G6P -> Ru5P + CO2	0.000	0.623	0.311
	R5PE	Ru5P <-> X5P	-0.006	0.411	0.202
	R5PI	Ru5P <-> R5P	0.004	0.212	0.108
	TK1	X5P + R5P <-> GAP + S7P	-0.003	0.205	0.101
	TK2	S7P + GAP <-> E4P + F6P	-0.003	0.205	0.101
	TK3	X5P + E4P <-> GAP + F6P	-0.003	0.205	0.101
TCA	PDH	Pyr -> AcCoA + CO2	1.366	1.973	1.670
	SDH	Suc <-> Fum	1.743	2.375	2.059
	Fum	Fum <-> Mal	1.743	2.375	2.059
	MDH	Mal <-> OAA	1.553	2.190	1.872
	CS	OAA + AcCoA -> Cit	1.638	2.234	1.936
	ADH	aKG.m -> Suc + CO2	1.709	2.334	2.021
	IDH	Cit <-> aKG.m + CO2	1.557	2.165	1.861
Transport	Glc IN	Glc.e -> Glc	1.334	1.497	1.415
	Lys IN	Lys.e -> Lys	0.013	0.023	0.018
	Thr IN	Thr.e -> Thr	0.009	0.014	0.012
	Phe IN	Phe.e -> Phe	0.007	0.016	0.012
	Tyr IN	Tyr.e -> Tyr	0.008	0.019	0.013
	Val IN	Val.e -> Val	0.011	0.027	0.019
	Leu IN	Leu.e -> Leu	0.058	0.093	0.075
	Ile IN	Ile.e -> Ile	0.009	0.037	0.023
	Trp IN	Trp.e -> Trp	0.014	0.025	0.019
	His IN	His.e -> His	0.004	0.014	0.009
	Met IN	Met.e -> Met	0.017	0.027	0.022
	Ser Flux	Ser.e <-> Ser	0.073	0.087	0.080
	Ala Flux	Ala.e <-> Ala	-0.143	-0.108	-0.125

	Arg Flux	Arg.e <-> Arg	0.025	0.037	0.031
	Asp Flux	Asp.e <-> Asp	-0.049	-0.032	-0.040
	Gln Flux	Gln.e <-> Gln	0.091	0.118	0.105
	Pro Flux	Pro.e <-> Pro	0.007	0.012	0.010
	Asn Flux	Asn.e <-> Asn	0.087	0.102	0.094
	Lac Flux	Lac.e <-> Lac	-1.400	-1.037	-1.219
	Gly Flux	Gly.e <-> Gly	-0.058	-0.044	-0.051
	Cys Flux	Cys.e <-> Cys	-0.002	0.009	0.004
	Glu Flux	Glu.e <-> Glu.c	0.021	0.082	0.052
	Glu/Asp Antiporter	Glu.c -> Glu.m	0.042	0.170	0.106
	Mal/aKG Antiporter	aKG.m -> aKG.c	0.000	0.092	0.046
Anaplerosis	ME	Mal -> Pyr + CO2	0.194	0.409	0.302
	PC	Pyr + CO2 -> OAA	0.000	0.159	0.079
	ACL	Cit -> AcCoA.c + Mal	0.056	0.095	0.075
Amino	GLS	Gln <-> Glu.m	0.081	0.109	0.095
Acid	ASNS	Asp <-> Asn	-0.093	-0.078	-0.086
Metabolism	SHT	Ser <-> Gly + MEETHF	0.034	0.044	0.039
	CYST	Ser <-> Cys	0.022	1.141	0.581
	GS + SHT	CO2 + MEETHF -> Gly	0.028	0.035	0.032
	Met Mtbl	Met + Ser -> Methyl + Cys + Suc	0.013	0.023	0.018
	PheTyr Mtbl	Phe -> Tyr	0.000	0.010	0.005
	Thr Mtbl	Thr -> Pyr + CO2	0.000	0.003	0.001
	Histidase	His -> FormTHF + Glu.c	0.000	0.010	0.005
	CBXase + Mutase	ProCoA + CO2 -> Suc	0.002	0.036	0.019
	Trp Mtbl	Trp -> CO2 + CO2 + Ala + aKetoadi	0.013	0.023	0.018
	Trp2 Mtbl	aKetoadi -> CO2 + CO2 + AcCoA + AcCoA	0.013	0.025	0.019
	*GDH	aKG.m <-> Glu.m	-0.268	-0.134	-0.201
	*ALT	Ala + aKG.c <-> Pyr + Glu.c	-0.145	-0.107	-0.126
	*Ile Mtbl	Ile + aKG.c + -> AcCoA + CO2 + ProCoA + Glu.c	0.000	0.027	0.013
	*Leu Mtbl	Leu + aKG.c + CO2 -> CO2 + AcCoA + AcCoA + AcCoA + Glu.c	0.040	0.076	0.058
	*Tyr Mtbl	Tyr + aKG.c -> CO2 + Mal + AcCoA + AcCoA + Glu.c	0.005	0.021	0.013

	*Val Mtbl	Val + aKG.c -> Glu.c + CO2 + CO2 + ProCoA	0.000	0.015	0.007
	*Lys Mtbl	Lys + aKG.c + aKG.c + -> Glu.c + Glu.c + aKetoadi	0.000	0.006	0.003
	*AST	OAA + Glu.c <-> Asp + aKG.c	-0.043	-0.018	-0.031
	*Arg Mtbl	Arg + aKG.c -> Glu.c + Urea + Glu.c	0.013	0.027	0.020
	*PST	3PG + Glu.c -> Ser + aKG.c	0.014	1.132	0.573
	*Cys Mtbl	Cys + aKG.c -> Pyr + Glu.c	0.039	1.158	0.599
Biomass Production	Biomass 233pg	0.1099*Asp + 0.0899*Glu.c + 0.0671*Asn + 0.1028*Ser + 0.0333*His + 0.1533*Gly + 0.0878*Arg + 0.1398*Ala + 0.0424*Tyr + 0.0338*Cys + 0.0969*Val + 0.0322*Met + 0.051*Phe + 0.0755*Ile + 0.1314*Leu + 0.1328*Lys + 0.075*Gln + 0.0103*Trp + 0.0729*Pro + 0.0899*Thr + 0.0594*MEETHF + 0.0543*CO2 + 0.5767*AcCoA.c + 0.0284*DHAP + 0.0543*R5P + 0.0672*G6P -> Biomass	0.097	0.164	0.130

Table 6-A-2. Exchange fluxes of CHOK1SV. Associated with Figure 6-4 and 6-5.

Pathway	Enzyme	Rxn	LB	UB	Value
PPP	TK3	X5P + E4P <-> GAP + F6P	0.000	1.517	0.758
Amino	GLS	Gln <-> Glu.m	0.623	2.746	1.684
Acid	ASNS	Asp <-> Asn	0.000	1.060	0.530
Metabolism	SHT	Ser <-> Gly + MEETHF	0.189	25.122	12.656
Transport	Ser Flux	Ser.e <-> Ser	0.000	7.468	3.734
	Ala Flux	Ala.e <-> Ala	0.000	2.005	1.002
	Asp Flux	Asp.e <-> Asp	0.000	1.009	0.505
	Gln Flux	Gln.e <-> Gln	5.923	92.461	49.192
	Lac Flux	Lac.e <-> Lac	0.000	1.774	0.887
	Gly Flux	Gly.e <-> Gly	0.051	5.291	2.671
	*ALT	Ala + aKG.c <-> Pyr + Glu.c	0.000	12.931	6.466
	*AST	OAA + Glu.c <-> Asp + aKG.c	0.286	20.811	10.548

Table 6-A-3. Net fluxes of CHOK1SV-GS. Associated with Figure 6-4 and 6-5.

Pathway	Enzyme	Rxn	LB	UB	Average
Glycolysis	PGI	G6P <-> F6P	0.679	1.146	0.912
	PFK	F6P -> DHAP + GAP	0.937	1.138	1.038
	TPI	DHAP <-> GAP	0.931	1.132	1.032
	GADPH	GAP <-> 3PG	1.981	2.267	2.124
	Eno	3PG <-> PEP	1.447	2.190	1.818
	PK	PEP -> Pyr	1.447	2.190	1.818
	HK	Glc -> G6P	1.049	1.160	1.105
	LDH	Lac <-> Pyr	-0.634	-0.497	-0.565
PPP	6PGDH	G6P -> Ru5P + CO2	0.000	0.411	0.205
	R5PE	Ru5P <-> X5P	-0.009	0.266	0.129
	R5PI	Ru5P <-> R5P	0.007	0.145	0.076
	TK1	X5P + R5P <-> GAP + S7P	-0.004	0.133	0.064
	TK2	S7P + GAP <-> E4P + F6P	-0.004	0.133	0.064
	TK3	X5P + E4P <-> GAP + F6P	-0.004	0.133	0.064
TCA	PDH	Pyr -> AcCoA + CO2	1.470	1.814	1.642
	SDH	Suc <-> Fum	1.795	2.236	2.016
	Fum	Fum <-> Mal	1.795	2.236	2.016
	MDH	Mal <-> OAA	1.552	2.098	1.825
	CS	OAA + AcCoA -> Cit	1.820	2.213	2.017
	ADH	aKG.m -> Suc + CO2	1.754	2.180	1.967
	IDH	Cit <-> aKG.m + CO2	1.695	2.099	1.897
Transport	Glc IN	Glc.e -> Glc	1.049	1.160	1.105
	Lys IN	Lys.e -> Lys	0.024	0.036	0.030
	Thr IN	Thr.e -> Thr	0.016	0.021	0.019
	Phe IN	Phe.e -> Phe	0.010	0.021	0.015
	Tyr IN	Tyr.e -> Tyr	0.016	0.031	0.023
	Val IN	Val.e -> Val	0.018	0.038	0.028
	Leu IN	Leu.e -> Leu	0.097	0.144	0.120
	Ile IN	Ile.e -> Ile	0.021	0.059	0.040
	Trp IN	Trp.e -> Trp	0.012	0.025	0.019
	His IN	His.e -> His	0.006	0.018	0.012
	Met IN	Met.e -> Met	0.020	0.032	0.026
	Ser Flux	Ser.e <-> Ser	0.043	0.061	0.052
	Ala Flux	Ala.e <-> Ala	-0.152	-0.124	-0.138
	Arg Flux	Arg.e <-> Arg	0.036	0.052	0.044

	Asp Flux	Asp.e <-> Asp	-0.017	0.003	-0.007
	Gln Flux	Gln.e <-> Gln	-0.018	-0.006	-0.012
	Pro Flux	Pro.e <-> Pro	0.013	0.017	0.015
	Asn Flux	Asn.e <-> Asn	0.123	0.147	0.135
	Lac Flux	Lac.e <-> Lac	-0.634	-0.497	-0.565
	Gly Flux	Gly.e <-> Gly	-0.020	-0.005	-0.013
	Cys Flux	Cys.e <-> Cys	-0.001	0.017	0.008
	Glu Flux	Glu.e <-> Glu.c	0.055	0.116	0.085
	Glu/Asp Antiporter	Glu.c -> Glu.m	0.138	0.271	0.205
	Mal/aKG Antiporter	aKG.m -> aKG.c	0.056	0.162	0.109
Anaplerosis	ME	Mal -> Pyr + CO2	0.183	0.542	0.363
	PC	Pyr + CO2 -> OAA	0.000	0.309	0.155
	ACL	Cit -> AcCoA.c + Mal	0.104	0.138	0.121
Amino	GLS	Gln <-> Glu.m	-0.034	-0.021	-0.027
Acid	ASNS	Asp <-> Asn	-0.133	-0.109	-0.121
Metabolism	SHT	Ser <-> Gly + MEETHF	0.024	0.034	0.029
	CYST	Ser <-> Cys	0.006	0.686	0.346
	GS + SHT	CO2 + MEETHF -> Gly	0.012	0.020	0.016
	Met Mtbl	Met + Ser -> Methyl + Cys + Suc	0.013	0.025	0.019
	PheTyr Mtbl	Phe -> Tyr	0.000	0.010	0.005
	Thr Mtbl	Thr -> Pyr + CO2	0.000	0.002	0.001
	Histidase	His -> FormTHF + Glu.c	0.000	0.011	0.005
	CBXase + Mutase	ProCoA + CO2 -> Suc	0.006	0.052	0.029
	Trp Mtbl	Trp -> CO2 + CO2 + Ala + aKetoadi	0.010	0.023	0.016
	Trp2 Mtbl	aKetoadi -> CO2 + CO2 + AcCoA + AcCoA	0.010	0.027	0.018
	*GDH	aKG.m <-> Glu.m	-0.245	-0.109	-0.177
	*ALT	Ala + aKG.c <-> Pyr + Glu.c	-0.167	-0.135	-0.151
	*Ile Mtbl	Ile + aKG.c -> AcCoA + CO2 + ProCoA + Glu.c	0.005	0.043	0.024
	*Leu Mtbl	Leu + aKG.c + CO2 -> CO2 + AcCoA + AcCoA + AcCoA + Glu.c	0.069	0.116	0.093
	*Tyr Mtbl	Tyr + aKG.c -> CO2 + Mal + AcCoA + AcCoA + Glu.c	0.009	0.028	0.019

	*Val Mtbl	Val + aKG.c -> Glu.c + CO2 + CO2 + ProCoA	0.000	0.018	0.009
	*Lys Mtbl	Lys + aKG.c + aKG.c -> Glu.c + Glu.c + aKetoadi	0.000	0.009	0.004
	*AST	OAA + Glu.c <-> Asp + aKG.c	-0.108	-0.075	-0.091
	*Arg Mtbl	Arg + aKG.c -> Glu.c + Urea + Glu.c	0.017	0.034	0.025
	*PST	3PG + Glu.c -> Ser + aKG.c	0.024	0.703	0.364
	*Cys Mtbl	Cys + aKG.c -> Pyr + Glu.c	0.026	0.706	0.366
Biomass Production	Biomass 281pg	0.1326*Asp + 0.1085*Glu.c + 0.0809*Asn + 0.1239*Ser + 0.0402*His + 0.1849*Gly + 0.1059*Arg + 0.1686*Ala + 0.0511*Tyr + 0.0407*Cys + 0.1169*Val + 0.0388*Met + 0.0615*Phe + 0.091*Ile + 0.1585*Leu + 0.1602*Lys + 0.0905*Gln + 0.0124*Trp + 0.088*Pro + 0.1085*Thr + 0.0717*MEETHF + 0.0654*CO2 + 0.6955*AcCoA.c + 0.0342*DHAP + 0.0654*R5P + 0.0811*G6P -> Biomass	0.150	0.198	0.174

Table 6-A-4. Exchange fluxes of CHOK1SV-GS. Associated with Figure 6-4 and 6-5.

Pathway	Enzyme	Rxn	LB	UB	Value
PPP	TK3	X5P + E4P <-> GAP + F6P	0.000	0.884	0.442
TCA	IDH	Cit <-> aKG.m + CO2	1.809	102.196	52.003
Amino Acid Metabolism	ASNS	Asp <-> Asn	0.000	5.926	2.963
	SHT	Ser <-> Gly + MEETHF	0.065	2.204	1.134
	*ALT	Ala + aKG.c <-> Pyr + Glu.c	0.000	6.586	3.293
	*AST	OAA + Glu.c <-> Asp + aKG.c	1.886	6.246	4.066
Transport	Ser Flux	Ser.e <-> Ser	0.000	1.923	0.961
	Ala Flux	Ala.e <-> Ala	0.000	1.013	0.507
	Asp Flux	Asp.e <-> Asp	0.000	2.619	1.309
	Gln Flux	Gln.e <-> Gln	0.308	1.054	0.681
	Lac Flux	Lac.e <-> Lac	0.000	0.879	0.439
	Gly Flux	Gly.e <-> Gly	0.083	1.733	0.908

Table 6-A-5. Net fluxes of CHOK1SV-M2. Associated with Figure 6-5.

Pathway	Enzyme	Rxn	LB	UB	Average
Glycolysis	PGI	G6P <-> F6P	0.401	1.103	0.752
	PFK	F6P -> DHAP + GAP	0.822	1.099	0.960
	TPI	DHAP <-> GAP	0.818	1.095	0.957
	GADPH	GAP <-> 3PG	1.835	2.191	2.013
	Eno	3PG <-> PEP	1.378	2.055	1.716
	PK	PEP -> Pyr	1.378	2.055	1.716
	HK	Glc -> G6P	1.002	1.115	1.058
	LDH	Lac <-> Pyr	-0.352	-0.202	-0.277
PPP	6PGDH	G6P -> Ru5P + CO2	0.000	0.650	0.325
	R5PE	Ru5P <-> X5P	-0.006	0.428	0.211
	R5PI	Ru5P <-> R5P	0.004	0.221	0.113
	TK1	X5P + R5P <-> GAP + S7P	-0.003	0.214	0.106
	TK2	S7P + GAP <-> E4P + F6P	-0.003	0.214	0.106
	TK3	X5P + E4P <-> GAP + F6P	-0.003	0.214	0.106
TCA	PDH	Pyr -> AcCoA + CO2	1.668	2.073	1.870
	SDH	Suc <-> Fum	2.113	2.546	2.330
	Fum	Fum <-> Mal	2.113	2.546	2.330
	MDH	Mal <-> OAA	1.685	2.313	1.999
	CS	OAA + AcCoA -> Cit	1.950	2.358	2.154
	ADH	aKG.m -> Suc + CO2	2.076	2.508	2.292
	IDH	Cit <-> aKG.m + CO2	1.874	2.285	2.079
Transport	Glc IN	Glc.e -> Glc	1.002	1.115	1.058
	Lys IN	Lys.e -> Lys	0.027	0.047	0.037
	Thr IN	Thr.e -> Thr	0.026	0.054	0.040
	Phe IN	Phe.e -> Phe	0.013	0.024	0.019
	Tyr IN	Tyr.e -> Tyr	0.011	0.023	0.017
	Val IN	Val.e -> Val	0.028	0.036	0.032
	Leu IN	Leu.e -> Leu	0.080	0.114	0.097
	Ile IN	Ile.e -> Ile	0.025	0.060	0.042
	Trp IN	Trp.e -> Trp	0.010	0.022	0.016
	His IN	His.e -> His	0.030	0.057	0.043
	Met IN	Met.e -> Met	0.009	0.023	0.016
	Ser Flux	Ser.e <-> Ser	0.065	0.077	0.071
	Ala Flux	Ala.e <-> Ala	-0.152	-0.121	-0.136
	Arg Flux	Arg.e <-> Arg	0.032	0.046	0.039
	Asp Flux	Asp.e <-> Asp	0.032	0.045	0.038
	Gln Flux	Gln.e <-> Gln	-0.041	-0.006	-0.023
	Pro Flux	Pro.e <-> Pro	0.020	0.024	0.022

	Asn Flux	Asn.e <-> Asn	-0.007	0.014	0.003
	Lac Flux	Lac.e <-> Lac	-0.352	-0.202	-0.277
	Gly Flux	Gly.e <-> Gly	-0.014	0.000	-0.007
	Cys Flux	Cys.e <-> Cys	0.001	0.012	0.006
	Glu Flux	Glu.e <-> Glu.c	0.189	0.241	0.215
	Glu/Asp Antiporter	Glu.c -> Glu.m	0.222	0.285	0.253
	Mal/aKG Antiporter	aKG.m -> aKG.c	0.000	0.019	0.009
Anaplerosis	ME	Mal -> Pyr + CO2	0.235	0.642	0.438
	PC	Pyr + CO2 -> OAA	0.000	0.377	0.189
	ACL	Cit -> AcCoA.c + Mal	0.060	0.090	0.075
Amino	GLS	Gln <-> Glu.m	-0.059	-0.024	-0.042
Acid	ASNS	Asp <-> Asn	0.001	0.022	0.012
Metabolism	SHT	Ser <-> Gly + MEETHF	0.020	0.028	0.024
	CYST	Ser <-> Cys	0.060	0.678	0.369
	GS + SHT	CO2 + MEETHF -> Gly	0.013	0.020	0.016
	Met Mtbl	Met + Ser -> Methyl + Cys + Suc	0.003	0.017	0.010
	PheTyr Mtbl	Phe -> Tyr	0.000	0.010	0.005
	Thr Mtbl	Thr -> Pyr + CO2	0.000	0.029	0.014
	Histidase	His -> FormTHF + Glu.c	0.022	0.049	0.036
	CBXase + Mutase	ProCoA + CO2 -> Suc	0.011	0.045	0.028
	Trp Mtbl	Trp -> CO2 + CO2 + Ala + aKetoadi	0.006	0.017	0.012
	Trp2 Mtbl	aKetoadi -> CO2 + CO2 + AcCoA + AcCoA	0.010	0.030	0.020
	*GDH	aKG.m <-> Glu.m	-0.247	-0.175	-0.211
	*ALT	Ala + aKG.c <-> Pyr + Glu.c	-0.168	-0.134	-0.151
	*Ile Mtbl	Ile + aKG.c -> AcCoA + CO2 + ProCoA + Glu.c	0.011	0.045	0.028
	*Leu Mtbl	Leu + aKG.c + CO2 -> CO2 + AcCoA + AcCoA + AcCoA + Glu.c	0.050	0.083	0.066
	*Tyr Mtbl	Tyr + aKG.c -> CO2 + Mal + AcCoA + AcCoA + Glu.c	0.000	0.017	0.008
	*Val Mtbl	Val + aKG.c -> Glu.c + CO2 + CO2 + ProCoA	0.000	0.007	0.004
	*Lys Mtbl	Lys + aKG.c + aKG.c + -> Glu.c + Glu.c + aKetoadi	0.000	0.017	0.009
	*AST	OAA + Glu.c <-> Asp + aKG.c	-0.017	0.008	-0.005
	*Arg Mtbl	Arg + aKG.c -> Glu.c + Urea + Glu.c	0.015	0.030	0.022
	*PST	3PG + Glu.c -> Ser + aKG.c	0.062	0.686	0.374
	*Cys Mtbl	Cys + aKG.c -> Pyr + Glu.c	0.067	0.685	0.376

Antibody Production	Antibody Flux M2	503.5*Ala + 290.3*Arg + 386.2*Asp + 325.7*Asn + 250.2*Cys + 418.4*Gln + 444.9*Glu.c + 653.1*Gly + 160.6*His + 205.8*Ile + 658.5*Leu + 539.8*Lys + 94.27*Met + 345.3*Phe + 617.5*Pro + 1285*Ser + 683.1*Thr + 143*Trp + 367.8*Tyr + 853.6*Val -> Antibody	1.87E-05	2.27E-05	2.07E-05
Biomass Production	Biomass 292pg	0.1378*Asp + 0.1127*Glu.c + 0.0841*Asn + 0.1288*Ser + 0.0418*His + 0.1922*Gly + 0.1101*Arg + 0.1752*Ala + 0.0531*Tyr + 0.0423*Cys + 0.1215*Val + 0.0403*Met + 0.0639*Phe + 0.0946*Ile + 0.1647*Leu + 0.1664*Lys + 0.094*Gln + 0.0128*Trp + 0.0914*Pro + 0.1127*Thr + 0.0745*MEETHF + 0.068*CO2 + 0.7227*AcCoA.c + 0.0355*DHAP + 0.068*R5P + 0.0842*G6P -> Biomass	0.082	0.125	0.104

Table 6-A-6. Exchange fluxes of CHOK1SV-M2. Associated with Figure 6-5.

Pathway	Enzyme	Rxn	LB	UB	Average
PPP	TK2	S7P + GAP <-> E4P + F6P	0.000	4.965	2.482
	TK3	X5P + E4P <-> GAP + F6P	0.000	0.845	0.423
Amino	SHT	Ser <-> Gly + MEETHF	0.298	3.516	1.907
Acid	*ALT	Ala + aKG.c <-> Pyr + Glu.c	0.000	6.711	3.355
Metabolism	*AST	OAA + Glu.c <-> Asp + aKG.c	4.328	30.615	17.471
Transport	Ser Flux	Ser.e <-> Ser	0.000	1.532	0.766
	Ala Flux	Ala.e <-> Ala	0.026	0.910	0.468
	Asp Flux	Asp.e <-> Asp	0.000	2.307	1.153
	Gln Flux	Gln.e <-> Gln	0.296	0.738	0.517
	Asn Flux	Asn.e <-> Asn	0.000	18.636	9.318
	Lac Flux	Lac.e <-> Lac	0.000	0.784	0.392
	Gly Flux	Gly.e <-> Gly	0.090	1.052	0.571

Table 6-A-7. Net fluxes of CHOK1SV-M3. Associated with Figure 6-4 and 6-5.

Pathway	Enzyme	Rxn	LB	UB	Average
Glycolysis	PGI	G6P <-> F6P	0.736	1.237	0.986
	PFK	F6P -> DHAP + GAP	0.991	1.233	1.112
	TPI	DHAP <-> GAP	0.988	1.230	1.109
	GADPH	GAP <-> 3PG	2.072	2.461	2.266
	Eno	3PG <-> PEP	1.747	2.216	1.982
	PK	PEP -> Pyr	1.747	2.216	1.982
	HK	Glc -> G6P	1.066	1.244	1.155
	LDH	Lac <-> Pyr	0.565	0.746	0.656
PPP	6PGDH	G6P -> Ru5P + CO2	0.000	0.416	0.208
	R5PE	Ru5P <-> X5P	-0.005	0.274	0.134
	R5PI	Ru5P <-> R5P	0.003	0.143	0.073
	TK1	X5P + R5P <-> GAP + S7P	-0.002	0.137	0.067
	TK2	S7P + GAP <-> E4P + F6P	-0.002	0.137	0.067
	TK3	X5P + E4P <-> GAP + F6P	-0.002	0.137	0.067
TCA	PDH	Pyr -> AcCoA + CO2	2.846	3.293	3.069
	SDH	Suc <-> Fum	3.714	4.200	3.957
	Fum	Fum <-> Mal	3.714	4.200	3.957
	MDH	Mal <-> OAA	3.072	3.707	3.390
	CS	OAA + AcCoA -> Cit	3.377	3.837	3.607
	ADH	aKG.m -> Suc + CO2	3.626	4.106	3.866
	IDH	Cit <-> aKG.m + CO2	3.315	3.776	3.545
Transport	Glc IN	Glc.e -> Glc	1.066	1.244	1.155
	Lys IN	Lys.e -> Lys	0.038	0.070	0.054
	Thr IN	Thr.e -> Thr	0.030	0.035	0.033
	Phe IN	Phe.e -> Phe	0.014	0.033	0.023
	Tyr IN	Tyr.e -> Tyr	0.014	0.033	0.023
	Val IN	Val.e -> Val	0.037	0.064	0.050
	Leu IN	Leu.e -> Leu	0.131	0.186	0.159
	Ile IN	Ile.e -> Ile	0.051	0.100	0.075
	Trp IN	Trp.e -> Trp	0.020	0.039	0.030
	His IN	His.e -> His	0.009	0.030	0.020
	Met IN	Met.e -> Met	0.015	0.035	0.025
	Ser Flux	Ser.e <-> Ser	0.037	0.059	0.048
	Ala Flux	Ala.e <-> Ala	-0.391	-0.322	-0.356
	Arg Flux	Arg.e <-> Arg	0.038	0.062	0.050
	Asp Flux	Asp.e <-> Asp	0.073	0.094	0.083
	Gln Flux	Gln.e <-> Gln	-0.028	-0.010	-0.019
	Pro Flux	Pro.e <-> Pro	0.027	0.032	0.030

	Asn Flux	Asn.e <-> Asn	0.063	0.103	0.083
	Lac Flux	Lac.e <-> Lac	0.565	0.746	0.656
	Gly Flux	Gly.e <-> Gly	-0.059	-0.033	-0.046
	Cys Flux	Cys.e <-> Cys	0.007	0.028	0.018
	Glu/Asp Antiporter	Glu.c -> Glu.m	0.327	0.403	0.365
	Mal/aKG Antiporter	aKG.m -> aKG.c	0.000	0.025	0.013
	Glu Flux	Glu.e <-> Glu.c	0.309	0.374	0.341
Anaplerosis	ME	Mal -> Pyr + CO2	0.501	0.880	0.690
	PC	Pyr + CO2 -> OAA	0.000	0.326	0.163
	ACL	Cit -> AcCoA.c + Mal	0.048	0.077	0.062
Amino	GLS	Gln <-> Glu.m	-0.051	-0.033	-0.042
Acid	ASNS	Asp <-> Asn	-0.087	-0.046	-0.066
Metabolism	SHT	Ser <-> Gly + MEETHF	0.040	0.052	0.046
	CYST	Ser <-> Cys	0.066	0.453	0.260
	GS + SHT	CO2 + MEETHF -> Gly	0.034	0.045	0.039
	Met Mtbl	Met + Ser -> Methyl + Cys + Suc	0.009	0.029	0.019
	PheTyr Mtbl	Phe -> Tyr	0.000	0.018	0.009
	Thr Mtbl	Thr -> Pyr + CO2	0.000	0.003	0.002
	Histidase	His -> FormTHF + Glu.c	0.000	0.022	0.011
	CBXase + Mutase	ProCoA + CO2 -> Suc	0.043	0.098	0.071
	Trp Mtbl	Trp -> CO2 + CO2 + Ala + aKetoadi	0.014	0.033	0.023
	Trp2 Mtbl	aKetoadi -> CO2 + CO2 + AcCoA + AcCoA	0.024	0.060	0.042
	*GDH	aKG.m <-> Glu.m	-0.362	-0.283	-0.323
	*ALT	Ala + aKG.c <-> Pyr + Glu.c	-0.398	-0.324	-0.361
	*Ile Mtbl	Ile + aKG.c -> AcCoA + CO2 + ProCoA + Glu.c	0.034	0.083	0.059
	*Leu Mtbl	Leu + aKG.c + CO2 -> CO2 + AcCoA + AcCoA + AcCoA + Glu.c	0.096	0.150	0.123
	*Tyr Mtbl	Tyr + aKG.c -> CO2 + Mal + AcCoA + AcCoA + Glu.c	0.001	0.027	0.014
	*Val Mtbl	Val + aKG.c -> Glu.c + CO2 + CO2 + ProCoA	0.000	0.027	0.014
	*Lys Mtbl	Lys + aKG.c + aKG.c -> Glu.c + Glu.c + aKetoadi	0.003	0.034	0.018
	*AST	OAA + Glu.c <-> Asp + aKG.c	-0.148	-0.103	-0.126
	*Arg Mtbl	Arg + aKG.c -> Glu.c + Urea + Glu.c	0.022	0.047	0.035
	*PST	3PG + Glu.c -> Ser + aKG.c	0.136	0.523	0.329
	*Cys Mtbl	Cys + aKG.c -> Pyr + Glu.c	0.092	0.479	0.286

Biomass Production	Biomass 288pg	0.1728*Ala + 0.1086*Arg + 0.1359*Asp + 0.08294*Asn + 0.04176*Cys + 0.09274*Gln + 0.1112*Glu.c + 0.1895*Gly + 0.04118*His + 0.09331*Ile + 0.1624*Leu + 0.1642*Lys + 0.03974*Met + 0.06307*Phe + 0.09014*Pro + 0.127*Ser + 0.1112*Thr + 0.01267*Trp + 0.05242*Tyr + 0.1198*Val + 0.08309*G6P + 0.06708*R5P + 0.07344*MEETHF + 0.03505*DHAP + 0.7128*AcCoA.c + 0.06708*CO2 -> Biomass	0.067	0.108	0.087
Antibody Production	Antibody M3	484.6*Ala + 196*Arg + 368.9*Asp + 309.1*Asn + 220.2*Cys + 441*Gln + 427.2*Glu.c + 647.7*Gly + 145.8*His + 258.1*Ile + 666.1*Leu + 641.8*Lys + 79.98*Met + 276.1*Phe + 667*Pro + 1300*Ser + 689.9*Thr + 154.4*Trp + 403.3*Tyr + 844.5*Val -> Antibody	2.99E-05	3.60E-05	3.29E-05

Table 6-A-8. Exchange fluxes of CHOK1SV-M3. Associated with Figure 6-4 and 6-5.

Pathway	Enzyme	Rxn	LB	UB	Average
Glycolysis	LDH	Lac <-> Pyr	6.459	4236.200	2121.329
PPP	TK3	X5P + E4P <-> GAP + F6P	0.000	0.535	0.268
Amino	ASNS	Asp <-> Asn	0.857	4.224	2.541
Acid	SHT	Ser <-> Gly + MEETHF	0.326	1.349	0.838
Metabolism	CYST	Ser <-> Cys	0.000	0.224	0.112
	*ALT	Ala + aKG.c <-> Pyr + Glu.c	0.000	4.031	2.015
Transport	Ser Flux	Ser.e <-> Ser	0.000	0.802	0.401
	Ala Flux	Ala.e <-> Ala	0.015	0.636	0.326
	Asp Flux	Asp.e <-> Asp	0.000	1.432	0.716
	Gln Flux	Gln.e <-> Gln	0.000	0.271	0.135
	Asn Flux	Asn.e <-> Asn	0.000	9.755	4.877
	Lac Flux	Lac.e <-> Lac	0.000	0.538	0.269
	Gly Flux	Gly.e <-> Gly	0.207	0.756	0.482

Table 6-A-9. Net fluxes of CHOK1SV-M4. Associated with Figure 6-5.

Pathway	Enzyme	Rxn	LB	UB	Average
Glycolysis	PGI	G6P <-> F6P	0.514	0.870	0.692
	PFK	F6P -> DHAP + GAP	0.682	0.866	0.774
	TPI	DHAP <-> GAP	0.678	0.862	0.770
	GADPH	GAP <-> 3PG	1.416	1.726	1.571
	Eno	3PG <-> PEP	1.109	1.610	1.360
	PK	PEP -> Pyr	1.109	1.610	1.360
	HK	Glc -> G6P	0.739	0.877	0.808
	LDH	Lac <-> Pyr	-0.208	-0.084	-0.146
PPP	6PGDH	G6P -> Ru5P + CO2	0.000	0.290	0.145
	R5PE	Ru5P <-> X5P	-0.006	0.189	0.092
	R5PI	Ru5P <-> R5P	0.003	0.101	0.052
	TK1	X5P + R5P <-> GAP + S7P	-0.003	0.094	0.046
	TK2	S7P + GAP <-> E4P + F6P	-0.003	0.094	0.046
	TK3	X5P + E4P <-> GAP + F6P	-0.003	0.094	0.046
TCA	PDH	Pyr -> AcCoA + CO2	1.528	1.902	1.715
	SDH	Suc <-> Fum	1.808	2.285	2.046
	Fum	Fum <-> Mal	1.808	2.285	2.046
	MDH	Mal <-> OAA	1.407	1.902	1.654
	CS	OAA + AcCoA -> Cit	1.693	2.123	1.908
	ADH	aKG.m -> Suc + CO2	1.699	2.163	1.931
	IDH	Cit <-> aKG.m + CO2	1.617	2.065	1.841
Transport	Glc IN	Glc.e -> Glc	0.739	0.877	0.808
	Lys IN	Lys.e -> Lys	0.034	0.069	0.052
	Thr IN	Thr.e -> Thr	0.035	0.051	0.043
	Phe IN	Phe.e -> Phe	0.016	0.030	0.023
	Tyr IN	Tyr.e -> Tyr	0.028	0.044	0.036
	Val IN	Val.e -> Val	0.056	0.088	0.072
	Leu IN	Leu.e -> Leu	0.022	0.050	0.036
	Ile IN	Ile.e -> Ile	0.044	0.097	0.071
	Trp IN	Trp.e -> Trp	0.003	0.011	0.007
	His IN	His.e -> His	0.021	0.036	0.028
	Met IN	Met.e -> Met	0.005	0.015	0.010
	Ser Flux	Ser.e <-> Ser	0.050	0.076	0.063
	Ala Flux	Ala.e <-> Ala	-0.173	-0.141	-0.157
	Arg Flux	Arg.e <-> Arg	0.011	0.022	0.016
	Asp Flux	Asp.e <-> Asp	0.037	0.059	0.048
	Gln Flux	Gln.e <-> Gln	-0.066	-0.055	-0.060
	Pro Flux	Pro.e <-> Pro	0.016	0.022	0.019

	Asn Flux	Asn.e <-> Asn	0.167	0.216	0.192
	Lac Flux	Lac.e <-> Lac	-0.208	-0.084	-0.146
	Gly Flux	Gly.e <-> Gly	-0.038	-0.023	-0.030
	Cys Flux	Cys.e <-> Cys	0.015	0.029	0.022
	Glu Flux	Glu.e <-> Glu.c	0.138	0.186	0.162
	Glu/Asp Antiporter	Glu.c -> Glu.m	0.319	0.483	0.401
	Mal/aKG Antiporter	aKG.m -> aKG.c	0.159	0.310	0.234
Anaplerosis	ME	Mal -> Pyr + CO2	0.388	0.670	0.529
	PC	Pyr + CO2 -> OAA	0.000	0.218	0.109
	ACL	Cit -> AcCoA.c + Mal	0.046	0.088	0.067
Amino	GLS	Gln <-> Glu.m	-0.083	-0.071	-0.077
Acid	ASNS	Asp <-> Asn	-0.203	-0.154	-0.179
Metabolism	SHT	Ser <-> Gly + MEETHF	0.028	0.039	0.033
	CYST	Ser <-> Cys	0.043	0.442	0.242
	GS + SHT	CO2 + MEETHF -> Gly	0.022	0.031	0.026
	Met Mtbl	Met + Ser -> Methyl + Cys + Suc	0.000	0.010	0.005
	PheTyr Mtbl	Phe -> Tyr	0.005	0.020	0.012
	Thr Mtbl	Thr -> Pyr + CO2	0.012	0.029	0.021
	Histidase	His -> FormTHF + Glu.c	0.015	0.030	0.022
	CBXase + Mutase	ProCoA + CO2 -> Suc	0.074	0.138	0.106
	Trp Mtbl	Trp -> CO2 + CO2 + Ala + aKetoadi	0.000	0.008	0.004
	Trp2 Mtbl	aKetoadi -> CO2 + CO2 + AcCoA + AcCoA	0.008	0.046	0.027
	*GDH	aKG.m <-> Glu.m	-0.407	-0.240	-0.324
	*ALT	Ala + aKG.c <-> Pyr + Glu.c	-0.198	-0.163	-0.181
	*Ile Mtbl	Ile + aKG.c -> AcCoA + CO2 + ProCoA + Glu.c	0.032	0.085	0.059
	*Leu Mtbl	Leu + aKG.c + CO2 -> CO2 + AcCoA + AcCoA + AcCoA + Glu.c	0.000	0.024	0.012
	*Tyr Mtbl	Tyr + aKG.c -> CO2 + Mal + AcCoA + AcCoA + Glu.c	0.025	0.047	0.036
	*Val Mtbl	Val + aKG.c -> Glu.c + CO2 + CO2 + ProCoA	0.031	0.064	0.047
	*Lys Mtbl	Lys + aKG.c + aKG.c -> Glu.c + Glu.c + aKetoadi	0.008	0.044	0.026
	*AST	OAA + Glu.c <-> Asp + aKG.c	-0.236	-0.180	-0.208
	*Arg Mtbl	Arg + aKG.c -> Glu.c + Urea + Glu.c	0.000	0.008	0.004
	*PST	3PG + Glu.c -> Ser + aKG.c	0.051	0.449	0.250
	*Cys Mtbl	Cys + aKG.c -> Pyr + Glu.c	0.060	0.458	0.259

Biomass Production	Biomass 191pg	0.0901*Asp + 0.0737*Glu.c + 0.055*Asn + 0.0842*Ser + 0.0273*His + 0.1257*Gly + 0.072*Arg + 0.1146*Ala + 0.0348*Tyr + 0.0277*Cys + 0.0795*Val + 0.0264*Met + 0.0418*Phe + 0.0619*Ile + 0.1077*Leu + 0.1089*Lys + 0.0615*Gln + 0.0084*Trp + 0.0598*Pro + 0.0737*Thr + 0.0487*MEETHF + 0.0445*CO2 + 0.4727*AcCoA.c + 0.0232*DHAP + 0.0445*R5P + 0.0551*G6P -> Biomass	0.098	0.186	0.142
Antibody Production	Antibody Flux M4	504*Ala + 210.9*Arg + 372.5*Asp + 298.8*Asn + 222.4*Cys + 485.7*Gln + 458.1*Glu.c + 684.9*Gly + 120.4*His + 206*Ile + 658.4*Leu + 593.8*Lys + 107.8*Met + 305.2*Phe + 617.7*Pro + 1299*Ser + 710.6*Thr + 155.9*Trp + 406.9*Tyr + 797*Val -> Antibody	1.50E-05	1.85E-05	1.68E-05

Table 6-A-10. Exchange fluxes of CHOK1SV-M4. Associated with Figure 6-5.

Pathway	Enzyme	Rxn	LB	UB	Average
PPP	TK3	X5P + E4P <-> GAP + F6P	0.000	0.525	0.263
Amino Acid Metabolism	ASNS	Asp <-> Asn	0.000	2.403	1.202
	SHT	Ser <-> Gly + MEETHF	0.189	1.967	1.078
	*ALT	Ala + aKG.c <-> Pyr + Glu.c	0.000	2.961	1.480
	*AST	OAA + Glu.c <-> Asp + aKG.c	1.570	14.170	7.870
Transport	Ser Flux	Ser.e <-> Ser	0.000	1.398	0.699
	Ala Flux	Ala.e <-> Ala	0.130	0.735	0.432
	Asp Flux	Asp.e <-> Asp	0.000	2.403	1.202
	Gln Flux	Gln.e <-> Gln	0.388	1.256	0.822
	Lac Flux	Lac.e <-> Lac	0.000	0.566	0.283
	Gly Flux	Gly.e <-> Gly	0.109	0.938	0.524

Table 6-A-11. Net fluxes of Bcl-2Δ. Associated with Figure 6-4 and 6-5.

Pathway	Enzyme	Rxn	LB	UB	Average
Glycolysis	PGI	G6P <-> F6P	0.557	1.056	0.807
	PFK	F6P -> DHAP + GAP	0.834	1.050	0.942
	TPI	DHAP <-> GAP	0.829	1.045	0.937
	GADPH	GAP <-> 3PG	1.776	2.093	1.934
	Eno	3PG <-> PEP	1.437	2.023	1.730
	PK	PEP -> Pyr	1.437	2.023	1.730
	HK	Glc -> G6P	0.942	1.068	1.005
	LDH	Lac <-> Pyr	-0.528	-0.306	-0.417
PPP	6PGDH	G6P -> Ru5P + CO2	0.000	0.440	0.220
	R5PE	Ru5P <-> X5P	-0.007	0.287	0.140
	R5PI	Ru5P <-> R5P	0.005	0.153	0.079
	TK1	X5P + R5P <-> GAP + S7P	-0.004	0.144	0.070
	TK2	S7P + GAP <-> E4P + F6P	-0.004	0.144	0.070
	TK3	X5P + E4P <-> GAP + F6P	-0.004	0.144	0.070
TCA	PDH	Pyr -> AcCoA + CO2	1.618	2.068	1.843
	SDH	Suc <-> Fum	1.996	2.645	2.321
	Fum	Fum <-> Mal	1.996	2.645	2.321
	MDH	Mal <-> OAA	1.626	2.244	1.935
	CS	OAA + AcCoA -> Cit	1.870	2.445	2.157
	ADH	aKG.m -> Suc + CO2	1.908	2.530	2.219

	IDH	Cit <-> aKG.m + CO2	1.770	2.351	2.060
Transport	Glc IN	Glc.e -> Glc	0.942	1.068	1.005
	Lys IN	Lys.e -> Lys	0.058	0.103	0.081
	Thr IN	Thr.e -> Thr	0.037	0.058	0.047
	Phe IN	Phe.e -> Phe	0.012	0.032	0.022
	Tyr IN	Tyr.e -> Tyr	0.029	0.051	0.040
	Val IN	Val.e -> Val	0.043	0.088	0.066
	Leu IN	Leu.e -> Leu	0.019	0.083	0.051
	Ile IN	Ile.e -> Ile	0.031	0.093	0.062
	Trp IN	Trp.e -> Trp	0.002	0.028	0.015
	His IN	His.e -> His	0.031	0.052	0.041
	Met IN	Met.e -> Met	0.005	0.020	0.012
	Ser Flux	Ser.e <-> Ser	0.045	0.090	0.067
	Ala Flux	Ala.e <-> Ala	-0.240	-0.191	-0.215
	Arg Flux	Arg.e <-> Arg	0.013	0.026	0.020
	Asp Flux	Asp.e <-> Asp	0.026	0.061	0.044
	Gln Flux	Gln.e <-> Gln	0.036	0.080	0.058
	Pro Flux	Pro.e <-> Pro	0.011	0.014	0.012
	Asn Flux	Asn.e <-> Asn	0.164	0.194	0.179
	Lac Flux	Lac.e <-> Lac	-0.528	-0.306	-0.417
	Gly Flux	Gly.e <-> Gly	-0.062	-0.041	-0.052
	Cys Flux	Cys.e <-> Cys	0.013	0.033	0.023
	Glu Flux	Glu.e <-> Glu.c	0.044	0.146	0.095
	Glu/Asp Antiporter	Glu.c -> Glu.m	0.267	0.481	0.374

	Mal/aKG Antiporter	aKG.m -> aKG.c	0.168	0.352	0.260
Anaplerosis	ME	Mal -> Pyr + CO2	0.428	0.722	0.575
	PC	Pyr + CO2 -> OAA	0.000	0.207	0.103
	ACL	Cit -> AcCoA.c + Mal	0.083	0.111	0.097
Amino	GLS	Gln <-> Glu.m	0.023	0.068	0.045
Acid	ASNS	Asp <-> Asn	-0.183	-0.153	-0.168
Metabolism	SHT	Ser <-> Gly + MEETHF	0.038	0.049	0.044
	CYST	Ser <-> Cys	0.012	0.496	0.254
	GS + SHT	CO2 + MEETHF -> Gly	0.028	0.039	0.034
	Met Mtbl	Met + Ser -> Methyl + Cys + Suc	0.000	0.014	0.007
	PheTyr Mtbl	Phe -> Tyr	0.003	0.023	0.013
	Thr Mtbl	Thr -> Pyr + CO2	0.022	0.043	0.032
	Histidase	His -> FormTHF + Glu.c	0.025	0.046	0.036
	CBXase + Mutase	ProCoA + CO2 -> Suc	0.060	0.137	0.098
	Trp Mtbl	Trp -> CO2 + CO2 + Ala + aKetoadi	0.000	0.026	0.013
	Trp2 Mtbl	aKetoadi -> CO2 + CO2 + AcCoA + AcCoA	0.038	0.095	0.067
	*GDH	aKG.m <-> Glu.m	-0.529	-0.310	-0.419
	*ALT	Ala + aKG.c <-> Pyr + Glu.c	-0.261	-0.200	-0.230
	*Ile Mtbl	Ile + aKG.c -> AcCoA + CO2 + ProCoA + Glu.c	0.018	0.080	0.049
	*Leu Mtbl	Leu + aKG.c + CO2 -> CO2 + AcCoA + AcCoA + AcCoA + Glu.c	0.000	0.061	0.031
	*Tyr Mtbl	Tyr + aKG.c -> CO2 + Mal + AcCoA + AcCoA + Glu.c	0.031	0.061	0.046
	*Val Mtbl	Val + aKG.c -> Glu.c + CO2 + CO2 + ProCoA	0.027	0.072	0.049

	*Lys Mtbl	Lys + aKG.c + aKG.c -> Glu.c + Glu.c + aKetoadi	0.036	0.081	0.058
	*AST	OAA + Glu.c <-> Asp + aKG.c	-0.217	-0.170	-0.193
	*Arg Mtbl	Arg + aKG.c -> Glu.c + Urea + Glu.c	0.000	0.012	0.006
	*PST	3PG + Glu.c -> Ser + aKG.c	0.016	0.494	0.255
	*Cys Mtbl	Cys + aKG.c -> Pyr + Glu.c	0.033	0.516	0.275
Biomass Production	Biomass 206pg	0.0972*Asp + 0.0795*Glu.c + 0.0593*Asn + 0.0908*Ser + 0.0295*His + 0.1356*Gly + 0.0777*Arg + 0.1236*Ala + 0.0375*Tyr + 0.0299*Cys + 0.0857*Val + 0.0284*Met + 0.0451*Phe + 0.0667*Ile + 0.1162*Leu + 0.1174*Lys + 0.0663*Gln + 0.0091*Trp + 0.0645*Pro + 0.0795*Thr + 0.0525*MEETHF + 0.048*CO2 + 0.5098*AcCoA.c + 0.0251*DHAP + 0.048*R5P + 0.0594*G6P -> Biomass	0.163	0.217	0.190

Table 6-A-12. Exchange fluxes of Bcl-2Δ. Associated with Figure 6-4 and 6-5.

Pathway	Enzyme	Rxn	LB	UB	Average
Glycolysis	LDH	Lac <-> Pyr	0.000	4.304	2.152
PPP	TK3	X5P + E4P <-> GAP + F6P	0.026	1.051	0.538
Amino Acid Metabolism	GLS	Gln <-> Glu.m	0.450	3.249	1.850
	ASNS	Asp <-> Asn	0.000	2.083	1.042
	SHT	Ser <-> Gly + MEETHF	0.091	4.692	2.391
	*ALT	Ala + aKG.c <-> Pyr + Glu.c	0.000	1.689	0.844
	*AST	OAA + Glu.c <-> Asp + aKG.c	0.215	5.116	2.666
Transport	Ser Flux	Ser.e <-> Ser	0.000	6.095	3.048
	Ala Flux	Ala.e <-> Ala	0.126	1.212	0.669
	Asp Flux	Asp.e <-> Asp	0.000	1.986	0.993
	Lac Flux	Lac.e <-> Lac	0.069	0.858	0.464
	Gly Flux	Gly.e <-> Gly	0.000	1.712	0.856

Table 6-A-13. Net fluxes of Bcl-2Δ–M2. Associated with Figure 6-5.

Pathway	Enzyme	Rxn	LB	UB	Average
Glycolysis	PGI	G6P <-> F6P	1.259	1.513	1.386
	PFK	F6P -> DHAP + GAP	1.267	1.499	1.383
	TPI	DHAP <-> GAP	1.256	1.488	1.372
	GADPH	GAP <-> 3PG	2.516	2.981	2.748
	Eno	3PG <-> PEP	2.460	2.925	2.693
	PK	PEP -> Pyr	2.460	2.925	2.693
	HK	Glc -> G6P	1.311	1.539	1.425
	LDH	Lac <-> Pyr	0.343	0.441	0.392
PPP	6PGDH	G6P -> Ru5P + CO2	0.000	0.121	0.060
	R5PE	Ru5P <-> X5P	-0.018	0.066	0.024
	R5PI	Ru5P <-> R5P	0.011	0.055	0.033
	TK1	X5P + R5P <-> GAP + S7P	-0.009	0.033	0.012
	TK2	S7P + GAP <-> E4P + F6P	-0.009	0.033	0.012
	TK3	X5P + E4P <-> GAP + F6P	-0.009	0.033	0.012
TCA	PDH	Pyr -> AcCoA + CO2	2.947	3.558	3.252
	SDH	Suc <-> Fum	3.450	4.375	3.912
	Fum	Fum <-> Mal	3.450	4.375	3.912
	MDH	Mal <-> OAA	3.387	4.207	3.797
	CS	OAA + AcCoA -> Cit	3.504	4.281	3.892
	ADH	aKG.m -> Suc + CO2	3.403	4.301	3.852
	IDH	Cit <-> aKG.m + CO2	3.244	4.079	3.662
Transport	Glc IN	Glc.e -> Glc	1.311	1.539	1.425
	Lys IN	Lys.e -> Lys	0.098	0.144	0.121
	Thr IN	Thr.e -> Thr	0.060	0.092	0.076
	Phe IN	Phe.e -> Phe	0.026	0.054	0.040
	Tyr IN	Tyr.e -> Tyr	0.022	0.050	0.036
	Val IN	Val.e -> Val	0.043	0.070	0.056
	Leu IN	Leu.e -> Leu	0.109	0.200	0.155
	Ile IN	Ile.e -> Ile	0.036	0.112	0.074
	Trp IN	Trp.e -> Trp	0.064	0.093	0.079
	His IN	His.e -> His	0.020	0.048	0.034
	Met IN	Met.e -> Met	0.014	0.053	0.033
	Ser Flux	Ser.e <-> Ser	0.112	0.143	0.127
	Ala Flux	Ala.e <-> Ala	-0.300	-0.214	-0.257
	Arg Flux	Arg.e <-> Arg	0.052	0.089	0.070
	Asp Flux	Asp.e <-> Asp	0.089	0.120	0.105
	Gln Flux	Gln.e <-> Gln	-0.204	-0.104	-0.154
	Pro Flux	Pro.e <-> Pro	0.032	0.045	0.038

	Asn Flux	Asn.e <-> Asn	-0.017	0.034	0.009
	Lac Flux	Lac.e <-> Lac	0.343	0.441	0.392
	Gly Flux	Gly.e <-> Gly	-0.011	0.030	0.010
	Cys Flux	Cys.e <-> Cys	-0.002	0.029	0.013
	Glu Flux	Glu.e <-> Glu.c	0.331	0.416	0.373
	Glu/Asp Antiporter	Glu.c -> Glu.m	0.344	0.658	0.501
	Mal/aKG Antiporter	aKG.m -> aKG.c	0.000	0.257	0.128
Anaplerosis	ME	Mal -> Pyr + CO2	0.222	0.597	0.409
	PC	Pyr + CO2 -> OAA	0.000	0.264	0.132
	ACL	Cit -> AcCoA.c + Mal	0.180	0.281	0.230
Amino	GLS	Gln <-> Glu.m	-0.240	-0.140	-0.190
Acid	ASNS	Asp <-> Asn	-0.003	0.049	0.023
Metabolism	SHT	Ser <-> Gly + MEETHF	0.029	0.056	0.043
	CYST	Ser <-> Cys	0.022	0.163	0.092
	GS + SHT	CO2 + MEETHF -> Gly	0.008	0.030	0.019
	Met Mtbl	Met + Ser -> Methyl + Cys + Suc	0.000	0.039	0.019
	PheTyr Mtbl	Phe -> Tyr	0.000	0.029	0.015
	Thr Mtbl	Thr -> Pyr + CO2	0.013	0.048	0.030
	Histidase	His -> FormTHF + Glu.c	0.004	0.033	0.018
	CBXase + Mutase	ProCoA + CO2 -> Suc	0.003	0.082	0.042
	Trp Mtbl	Trp -> CO2 + CO2 + Ala + aKetoadi	0.058	0.087	0.072
	Trp2 Mtbl	aKetoadi -> CO2 + CO2 + AcCoA + AcCoA	0.103	0.162	0.133
	*GDH	aKG.m <-> Glu.m	-0.477	-0.142	-0.309
	*ALT	Ala + aKG.c <-> Pyr + Glu.c	-0.295	-0.201	-0.248
	*Ile Mtbl	Ile + aKG.c -> AcCoA + CO2 + ProCoA + Glu.c	0.003	0.079	0.041
	*Leu Mtbl	Leu + aKG.c + CO2 -> CO2 + AcCoA + AcCoA + AcCoA + Glu.c	0.047	0.138	0.092
	*Tyr Mtbl	Tyr + aKG.c -> CO2 + Mal + AcCoA + AcCoA + Glu.c	0.007	0.049	0.028
	*Val Mtbl	Val + aKG.c -> Glu.c + CO2 + CO2 + ProCoA	0.000	0.019	0.010
	*Lys Mtbl	Lys + aKG.c + aKG.c -> Glu.c + Glu.c + aKetoadi	0.035	0.086	0.060
	*AST	OAA + Glu.c <-> Asp + aKG.c	-0.066	0.001	-0.032
	*Arg Mtbl	Arg + aKG.c -> Glu.c + Urea + Glu.c	0.011	0.051	0.031
	*PST	3PG + Glu.c -> Ser + aKG.c	0.041	0.157	0.099
	*Cys Mtbl	Cys + aKG.c -> Pyr + Glu.c	0.036	0.177	0.107

Antibody Production	Antibody Flux M2	503.5*Ala + 290.3*Arg + 386.2*Asp + 325.7*Asn + 250.2*Cys + 418.4*Gln + 444.9*Glu.c + 653.1*Gly + 160.6*His + 205.8*Ile + 658.5*Leu + 539.8*Lys + 94.27*Met + 345.3*Phe + 617.5*Pro + 1285*Ser + 683.1*Thr + 143*Trp + 367.8*Tyr + 853.6*Val -> Antibody	1.19E-05	1.76E-05	1.47E-05
Biomass Production	Biomass 382pg	0.1802*Asp + 0.1475*Glu.c + 0.11*Asn + 0.1685*Ser + 0.0546*His + 0.2514*Gly + 0.144*Arg + 0.2292*Ala + 0.0695*Tyr + 0.0554*Cys + 0.1589*Val + 0.0527*Met + 0.0837*Phe + 0.1238*Ile + 0.2154*Leu + 0.2177*Lys + 0.123*Gln + 0.0168*Trp + 0.1196*Pro + 0.1475*Thr + 0.0974*MEETHF + 0.089*CO2 + 0.9454*AcCoA.c + 0.0465*DHAP + 0.089*R5P + 0.1102*G6P -> Biomass	0.190	0.297	0.244

Table 6-A-14. Exchange fluxes of Bcl-2Δ–M2. Associated with Figure 6-5.

Pathway	Enzyme	Rxn	LB	UB	Average
Glycolysis	LDH	Lac <-> Pyr	2.994	12.470	7.732
PPP	TK3	X5P + E4P <-> GAP + F6P	0.000	0.202	0.101
Amino Acid Metabolism	GLS	Gln <-> Glu.m	0.593	1.205	0.899
	ASNS	Asp <-> Asn	0.000	0.587	0.294
	SHT	Ser <-> Gly + MEETHF	0.267	1.250	0.758
	*ALT	Ala + aKG.c <-> Pyr + Glu.c	0.000	0.298	0.149
Transport	Ser Flux	Ser.e <-> Ser	0.000	0.264	0.132
	Ala Flux	Ala.e <-> Ala	0.000	0.131	0.066
	Asp Flux	Asp.e <-> Asp	0.000	0.284	0.142
	Asn Flux	Asn.e <-> Asn	0.000	0.793	0.397
	Lac Flux	Lac.e <-> Lac	0.000	0.084	0.042
	Gly Flux	Gly.e <-> Gly	0.014	0.241	0.127

Table 6-A-15. Net fluxes of Bcl-2Δ–M3. Associated with Figure 6-4 and 6-5.

Pathway	Enzyme	Rxn	LB	UB	Average
Glycolysis	PGI	G6P <-> F6P	1.335	1.571	1.453
	PFK	F6P -> DHAP + GAP	1.326	1.562	1.444
	TPI	DHAP <-> GAP	1.318	1.555	1.436
	GADPH	GAP <-> 3PG	2.639	3.112	2.875
	Eno	3PG <-> PEP	2.596	3.068	2.832
	PK	PEP -> Pyr	2.596	3.068	2.832
	HK	Glc -> G6P	1.352	1.588	1.470
	LDH	Lac <-> Pyr	0.468	0.592	0.530
PPP	6PGDH	G6P -> Ru5P + CO2	0.000	0.067	0.034
	R5PE	Ru5P <-> X5P	-0.011	0.036	0.012
	R5PI	Ru5P <-> R5P	0.008	0.032	0.020
	TK1	X5P + R5P <-> GAP + S7P	-0.006	0.018	0.006
	TK2	S7P + GAP <-> E4P + F6P	-0.006	0.018	0.006
	TK3	X5P + E4P <-> GAP + F6P	-0.006	0.018	0.006
TCA	PDH	Pyr -> AcCoA + CO2	3.272	3.853	3.562
	SDH	Suc <-> Fum	4.013	4.849	4.431
	Fum	Fum <-> Mal	4.013	4.849	4.431
	MDH	Mal <-> OAA	3.930	4.661	4.296
	CS	OAA + AcCoA -> Cit	3.926	4.668	4.297
	ADH	aKG.m -> Suc + CO2	3.913	4.719	4.316
	IDH	Cit <-> aKG.m + CO2	3.768	4.530	4.149
Transport	Glc IN	Glc.e -> Glc	1.352	1.588	1.470
	Lys IN	Lys.e -> Lys	0.114	0.172	0.143
	Thr IN	Thr.e -> Thr	0.072	0.106	0.089
	Phe IN	Phe.e -> Phe	0.032	0.059	0.046
	Tyr IN	Tyr.e -> Tyr	0.037	0.067	0.052
	Val IN	Val.e -> Val	0.071	0.091	0.081
	Leu IN	Leu.e -> Leu	0.156	0.266	0.211
	Ile IN	Ile.e -> Ile	0.092	0.174	0.133
	Trp IN	Trp.e -> Trp	0.012	0.047	0.029
	His IN	His.e -> His	0.030	0.060	0.045
	Met IN	Met.e -> Met	0.013	0.050	0.031
	Ser Flux	Ser.e <-> Ser	0.145	0.183	0.164
	Ala Flux	Ala.e <-> Ala	-0.208	-0.123	-0.165
	Arg Flux	Arg.e <-> Arg	0.052	0.091	0.071
	Asp Flux	Asp.e <-> Asp	0.066	0.103	0.085
	Gln Flux	Gln.e <-> Gln	-0.023	0.014	-0.004
	Pro Flux	Pro.e <-> Pro	0.055	0.066	0.061

	Asn Flux	Asn.e <-> Asn	-0.020	0.029	0.005
	Lac Flux	Lac.e <-> Lac	0.468	0.592	0.530
	Gly Flux	Gly.e <-> Gly	0.052	0.071	0.062
	Cys Flux	Cys.e <-> Cys	0.004	0.035	0.020
	Glu Flux	Glu.e <-> Glu.c	0.152	0.258	0.205
	Glu/Asp Antiporter	Glu.c -> Glu.m	0.332	0.627	0.479
	Mal/aKG Antiporter	aKG.m -> aKG.c	0.133	0.388	0.261
Anaplerosis	ME	Mal -> Pyr + CO2	0.224	0.409	0.316
	PC	Pyr + CO2 -> OAA	0.000	0.061	0.031
	ACL	Cit -> AcCoA.c + Mal	0.119	0.177	0.148
Amino	GLS	Gln <-> Glu.m	-0.070	-0.033	-0.051
Acid	ASNS	Asp <-> Asn	0.007	0.057	0.032
Metabolism	SHT	Ser <-> Gly + MEETHF	0.012	0.022	0.017
	CYST	Ser <-> Cys	0.034	0.119	0.076
	GS + SHT	CO2 + MEETHF -> Gly	0.000	0.006	0.003
	Met Mtbl	Met + Ser -> Methyl + Cys + Suc	0.000	0.037	0.019
	PheTyr Mtbl	Phe -> Tyr	0.001	0.029	0.015
	Thr Mtbl	Thr -> Pyr + CO2	0.005	0.041	0.023
	Histidase	His -> FormTHF + Glu.c	0.012	0.043	0.027
	CBXase + Mutase	ProCoA + CO2 -> Suc	0.057	0.138	0.097
	Trp Mtbl	Trp -> CO2 + CO2 + Ala + aKetoadi	0.000	0.034	0.017
	Trp2 Mtbl	aKetoadi -> CO2 + CO2 + AcCoA + AcCoA	0.050	0.120	0.085
	*GDH	aKG.m <-> Glu.m	-0.579	-0.277	-0.428
	*ALT	Ala + aKG.c <-> Pyr + Glu.c	-0.263	-0.169	-0.216
	*Ile Mtbl	Ile + aKG.c -> AcCoA + CO2 + ProCoA + Glu.c	0.057	0.138	0.097
	*Leu Mtbl	Leu + aKG.c + CO2 -> CO2 + AcCoA + AcCoA + AcCoA + Glu.c	0.080	0.191	0.136
	*Tyr Mtbl	Tyr + aKG.c -> CO2 + Mal + AcCoA + AcCoA + Glu.c	0.010	0.052	0.031
	*Val Mtbl	Val + aKG.c -> Glu.c + CO2 + CO2 + ProCoA	0.000	0.012	0.006
	*Lys Mtbl	Lys + aKG.c + aKG.c -> Glu.c + Glu.c + aKetoadi	0.039	0.098	0.069
	*AST	OAA + Glu.c <-> Asp + aKG.c	-0.033	0.031	-0.001
	*Arg Mtbl	Arg + aKG.c -> Glu.c + Urea + Glu.c	0.017	0.056	0.036
	*PST	3PG + Glu.c -> Ser + aKG.c	0.035	0.089	0.062
	*Cys Mtbl	Cys + aKG.c + -> Pyr + Glu.c	0.050	0.133	0.091

Antibody Production	Antibody M3	484.6*Ala + 196*Arg + 368.9*Asp + 309.1*Asn + 220.2*Cys + 441*Gln + 427.2*Glu.c + 647.7*Gly + 145.8*His + 258.1*Ile + 666.1*Leu + 641.8*Lys + 79.98*Met + 276.1*Phe + 667*Pro + 1300*Ser + 689.9*Thr + 154.4*Trp + 403.3*Tyr + 844.5*Val -> Antibody	5.64E-05	6.89E-05	6.27E-05
Biomass Production	Biomass 273pg	0.1288*Asp + 0.1054*Glu.c + 0.0786*Asn + 0.1204*Ser + 0.039*His + 0.1797*Gly + 0.1029*Arg + 0.1638*Ala + 0.0497*Tyr + 0.0396*Cys + 0.1136*Val + 0.0377*Met + 0.0598*Phe + 0.0885*Ile + 0.154*Leu + 0.1556*Lys + 0.0879*Gln + 0.012*Trp + 0.0854*Pro + 0.1054*Thr + 0.0696*MEETHF + 0.0636*CO2 + 0.6757*AcCoA.c + 0.0332*DHAP + 0.0636*R5P + 0.0788*G6P -> Biomass	0.177	0.262	0.219

Table 6-A-16. Exchange fluxes of Bcl-2Δ-M3. Associated with Figure 6-4 and 6-5.

Pathway	Enzyme	Rxn	LB	UB	Average
Glycolysis	LDH	Lac <-> Pyr	1.157	1.963	1.560
PPP	TK3	X5P + E4P <-> GAP + F6P	0.000	0.272	0.136
Amino	GLS	Gln <-> Glu.m	1.169	5.660	3.415
Acid	ASNS	Asp <-> Asn	0.000	8.379	4.190
Metabolism	SHT	Ser <-> Gly + MEETHF	0.081	0.290	0.185
	*ALT	Ala + aKG.c <-> Pyr + Glu.c	0.000	0.129	0.065
	*AST	OAA + Glu.c <-> Asp + aKG.c	0.118	18.178	9.148
Transport	Ser Flux	Ser.e <-> Ser	0.000	0.151	0.075
	Ala Flux	Ala.e <-> Ala	0.055	0.163	0.109
	Asp Flux	Asp.e <-> Asp	0.000	3.256	1.628
	Asn Flux	Asn.e <-> Asn	0.000	7.565	3.783
	Lac Flux	Lac.e <-> Lac	0.000	0.058	0.029
	Gly Flux	Gly.e <-> Gly	0.000	0.289	0.145

Table 6-A-17. Net fluxes of Bcl-2Δ-M4. Associated with Figure 6-5.

Pathway	Enzyme	Rxn	LB	UB	Average
Glycolysis	PGI	G6P <-> F6P	1.392	1.736	1.564
	PFK	F6P -> DHAP + GAP	1.429	1.728	1.578
	TPI	DHAP <-> GAP	1.422	1.721	1.572
	GADPH	GAP <-> 3PG	2.846	3.445	3.146
	Eno	3PG <-> PEP	2.780	3.382	3.081
	PK	PEP -> Pyr	2.780	3.382	3.081
	HK	Glc -> G6P	1.452	1.751	1.602
	LDH	Lac <-> Pyr	-0.321	0.000	-0.161
PPP	6PGDH	G6P -> Ru5P + CO2	0.000	0.183	0.091
	R5PE	Ru5P <-> X5P	-0.010	0.114	0.052
	R5PI	Ru5P <-> R5P	0.006	0.069	0.038
	TK1	X5P + R5P <-> GAP + S7P	-0.005	0.057	0.026
	TK2	S7P + GAP <-> E4P + F6P	-0.005	0.057	0.026
	TK3	X5P + E4P <-> GAP + F6P	-0.005	0.057	0.026
TCA	PDH	Pyr -> AcCoA + CO2	3.193	3.997	3.595
	SDH	Suc <-> Fum	4.906	6.017	5.461
	Fum	Fum <-> Mal	4.906	6.017	5.461
	MDH	Mal <-> OAA	4.558	5.554	5.056
	CS	OAA + AcCoA -> Cit	4.629	5.635	5.132
	ADH	aKG.m -> Suc + CO2	4.732	5.810	5.271
	IDH	Cit <-> aKG.m + CO2	4.490	5.512	5.001
Transport	Glc IN	Glc.e -> Glc	1.452	1.751	1.602
	Lys IN	Lys.e -> Lys	0.147	0.218	0.182
	Thr IN	Thr.e -> Thr	0.079	0.118	0.098
	Phe IN	Phe.e -> Phe	0.041	0.077	0.059
	Tyr IN	Tyr.e -> Tyr	0.030	0.067	0.049
	Val IN	Val.e -> Val	0.048	0.075	0.061
	Leu IN	Leu.e -> Leu	0.290	0.438	0.364
	Ile IN	Ile.e -> Ile	0.133	0.238	0.186
	Trp IN	Trp.e -> Trp	0.027	0.084	0.055
	His IN	His.e -> His	0.038	0.072	0.055
	Met IN	Met.e -> Met	0.020	0.066	0.043
	Ser Flux	Ser.e <-> Ser	0.263	0.313	0.288
	Ala Flux	Ala.e <-> Ala	-0.294	-0.199	-0.247
	Arg Flux	Arg.e <-> Arg	0.077	0.124	0.100
	Asp Flux	Asp.e <-> Asp	0.083	0.123	0.103
	Gln Flux	Gln.e <-> Gln	-0.021	0.018	-0.002
	Pro Flux	Pro.e <-> Pro	0.036	0.049	0.043

	Asn Flux	Asn.e <-> Asn	0.010	0.075	0.042
	Lac Flux	Lac.e <-> Lac	-0.321	0.000	-0.161
	Gly Flux	Gly.e <-> Gly	0.029	0.058	0.043
	Cys Flux	Cys.e <-> Cys	0.005	0.043	0.024
	Glu Flux	Glu.e <-> Glu.c	0.162	0.313	0.237
	Glu/Asp Antiporter	Glu.c -> Glu.m	1.006	1.360	1.183
	Mal/aKG Antiporter	aKG.m -> aKG.c	0.716	1.028	0.872
Anaplerosis	ME	Mal -> Pyr + CO2	0.486	0.741	0.614
	PC	Pyr + CO2 -> OAA	0.000	0.146	0.073
	ACL	Cit -> AcCoA.c + Mal	0.102	0.160	0.131
Amino	GLS	Gln <-> Glu.m	-0.061	-0.019	-0.040
Acid	ASNS	Asp <-> Asn	-0.047	0.019	-0.014
Metabolism	SHT	Ser <-> Gly + MEETHF	0.011	0.024	0.017
	CYST	Ser <-> Cys	0.186	0.350	0.268
	GS + SHT	CO2 + MEETHF -> Gly	0.000	0.011	0.005
	Met Mtbl	Met + Ser -> Methyl + Cys + Suc	0.007	0.054	0.030
	PheTyr Mtbl	Phe -> Tyr	0.016	0.053	0.034
	Thr Mtbl	Thr -> Pyr + CO2	0.026	0.069	0.047
	Histidase	His -> FormTHF + Glu.c	0.024	0.059	0.042
	CBXase + Mutase	ProCoA + CO2 -> Suc	0.107	0.213	0.160
	Trp Mtbl	Trp -> CO2 + CO2 + Ala + aKetoadi	0.018	0.075	0.046
	Trp2 Mtbl	aKetoadi -> CO2 + CO2 + AcCoA + AcCoA	0.127	0.220	0.173
	*GDH	aKG.m <-> Glu.m	-1.322	-0.963	-1.143
	*ALT	Ala + aKG.c <-> Pyr + Glu.c	-0.308	-0.198	-0.253
	*Ile Mtbl	Ile + aKG.c -> AcCoA + CO2 + ProCoA + Glu.c	0.107	0.213	0.160
	*Leu Mtbl	Leu + aKG.c + CO2 -> CO2 + AcCoA + AcCoA + AcCoA + Glu.c	0.232	0.380	0.306
	*Tyr Mtbl	Tyr + aKG.c -> CO2 + Mal + AcCoA + AcCoA + Glu.c	0.030	0.083	0.056
	*Val Mtbl	Val + aKG.c -> Glu.c + CO2 + CO2 + ProCoA	0.000	0.019	0.010
	*Lys Mtbl	Lys + aKG.c + aKG.c -> Glu.c + Glu.c + aKetoadi	0.091	0.164	0.127
	*AST	OAA + Glu.c <-> Asp + aKG.c	-0.116	-0.038	-0.077
	*Arg Mtbl	Arg + aKG.c -> Glu.c + Urea + Glu.c	0.046	0.095	0.071
	*PST	3PG + Glu.c -> Ser + aKG.c	0.051	0.182	0.117
	*Cys Mtbl	Cys + aKG.c -> Pyr + Glu.c	0.225	0.385	0.305

Antibody Production	Antibody Flux M4	504*Ala + 210.9*Arg + 372.5*Asp + 298.8*Asn + 222.4*Cys + 485.7*Gln + 458.1*Glu.c + 684.9*Gly + 120.4*His + 206*Ile + 658.4*Leu + 593.8*Lys + 107.8*Met + 305.2*Phe + 617.7*Pro + 1299*Ser + 710.6*Thr + 155.9*Trp + 406.9*Tyr + 797*Val -> Antibody	3.38E-05	5.08E-05	4.23E-05
Biomass Production	Biomass 257pg	0.1213*Asp + 0.0992*Glu.c + 0.074*Asn + 0.1133*Ser + 0.0368*His + 0.1691*Gly + 0.0969*Arg + 0.1542*Ala + 0.0468*Tyr + 0.0373*Cys + 0.1069*Val + 0.0355*Met + 0.0563*Phe + 0.0833*Ile + 0.1449*Leu + 0.1465*Lys + 0.0828*Gln + 0.0113*Trp + 0.0804*Pro + 0.0992*Thr + 0.0655*MEETHF + 0.0599*CO2 + 0.6361*AcCoA.c + 0.0313*DHAP + 0.0599*R5P + 0.0741*G6P -> Biomass	0.160	0.252	0.206

Table 6-A-18. Exchange fluxes of Bcl-2Δ-M4. Associated with Figure 6-5.

Pathway	Enzyme	Rxn	LB	UB	Average
Glycolysis	LDH	Lac <-> Pyr	0.000	0.302	0.151
PPP	TK3	X5P + E4P <-> GAP + F6P	0.000	0.881	0.440
Amino	GLS	Gln <-> Glu.m	3.400	17.810	10.605
Acid	SHT	Ser <-> Gly + MEETHF	0.039	0.346	0.192
Metabolism	*ALT	Ala + aKG.c <-> Pyr + Glu.c	0.000	0.200	0.100
Transport	Ser Flux	Ser.e <-> Ser	0.000	0.527	0.264
	Ala Flux	Ala.e <-> Ala	0.249	0.701	0.475
	Asp Flux	Asp.e <-> Asp	0.000	25.761	12.880
	Lac Flux	Lac.e <-> Lac	0.000	0.328	0.164
	Gly Flux	Gly.e <-> Gly	0.000	0.449	0.224

References

[1] N. Sengupta, S. T. Rose, and J. A. Morgan, "Metabolic flux analysis of CHO cell metabolism in the late non-growth phase.," *Biotechnol. Bioeng.*, vol. 108, no. 1, pp. 82–92, Jan. 2011.

[2] N. Templeton, J. Dean, P. Reddy, and J. D. Young, "Peak antibody production is associated with increased oxidative metabolism in an industrially relevant fed-batch CHO cell culture.," *Biotechnol. Bioeng.*, vol. 110, no. 7, pp. 2013–2024, Feb. 2013.

[3] N. Templeton, A. Lewis, H. Dorai, M. Campbell, K. D. Smith, S. E. Lang, M. J. Betenbaugh, and J. D. Young, "The impact of anti-apoptotic gene Bcl-2Δ expression on CHO central metabolism," *Metab. Eng.*, vol. 25, pp. 92–102, 2014.

[4] H. Dorai, Y. S. Kyung, D. Ellis, C. Kinney, C. Lin, D. Jan, G. Moore, and M. J. Betenbaugh, "Expression of anti-apoptosis genes alters lactate metabolism of Chinese Hamster Ovary cells in culture.," *Biotechnol. Bioeng.*, vol. 103, no. 3, pp. 592–608, Jun. 2009.

[5] J. Greene, J. W. H. Jr, and J. P. Wikswo, "Rapid and Precise Determination of Cellular Amino Acid Flux Rates Using HPLC with Automated Derivatization with Absorbance," *Agil. Appl. Note*, pp. 1–8, 2009.

[6] C. A. Sellick, R. Hansen, A. R. Maqsood, W. B. Dunn, G. M. Stephens, R. Goodacre, and A. J. Dickson, "Effective quenching processes for physiologically valid metabolite profiling of suspension cultured Mammalian cells.," *Anal. Chem.*, vol. 81, no. 1, pp. 174–83, Jan. 2009.

[7] J. Folch, M. Lees, and G. H. S. Stanley, "A simple method for the isolation and purification of total lipides from animal tissues," *J. Biol. Chem.*, vol. 226, no. 1, pp. 497–509, Aug. 1957.

[8] M. R. Antoniewicz, J. K. Kelleher, and G. Stephanopoulos, "Elementary metabolite units (EMU): a novel framework for modeling isotopic distributions.," *Metab. Eng.*, vol. 9, no. 1, pp. 68–86, Jan. 2007.

[9] J. D. Young, "INCA: a computational platform for isotopically non-stationary metabolic flux analysis.," *Bioinformatics*, vol. 30, no. 9, pp. 1333–5, May 2014.

[10] M. E. Smoot, K. Ono, J. Ruscheinski, P.-L. Wang, and T. Ideker, "Cytoscape 2.8: new features for data integration and network visualization.," *Bioinformatics*, vol. 27, no. 3, pp. 431–2, Feb. 2011.

[11] L. Xie and D. I. Wang, “Material balance studies on animal cell metabolism using a stoichiometrically based reaction network.,” *Biotechnol. Bioeng.*, vol. 52, no. 5, pp. 579–90, Dec. 1996.

[12] K. Sheikh, J. Fo, and L. K. Nielsen, “Modeling Hybridoma Cell Metabolism Using a Generic Genome-Scale Metabolic Model of Mus musculus,” *Biotechnol. Prog.*, vol. 21, no. 1, pp. 112–121, 2005.

[13] S. L. Bell, C. Bebbington, M. F. Scott, J. N. Wardell, R. E. Spier, M. E. Bushell, and P. G. Sanders, “Genetic engineering of hybridoma glutamine metabolism.,” *Enzyme Microb. Technol.*, vol. 17, no. 2, pp. 98–106, Feb. 1995.

[14] J. Wahrheit, J. Niklas, and E. Heinzle, “Metabolic control at the cytosol-mitochondria interface in different growth phases of CHO cells,” *Metab. Eng.*, pp. 1–13, Feb. 2014.

[15] G. Seth, P. Hossler, J. Chong, and Y. W. Hu, “Engineering Cells for Cell Culture Bioprocessing – Physiological Fundamentals,” *Adv Biochem Engin/Biotechnol*, vol. 101, no. June, pp. 119–164, 2006.

[16] J. G. Salway, *Medical Biochemistry at a Glance*, 3rd ed. West Sussex: John Wiley & Sons Inc., 2012, p. 169.

[17] J. Luo, N. Vijayasankaran, J. Autsen, R. Santuray, T. Hudson, A. Amanullah, and F. Li, “Comparative metabolite analysis to understand lactate metabolism shift in Chinese hamster ovary cell culture process.,” *Biotechnol. Bioeng.*, vol. 109, no. 1, pp. 146–156, Sep. 2011.

[18] S. S. Ozturk, M. R. Riley, and B. O. Palsson, “Effects of ammonia and lactate on hybridoma growth, metabolism, and antibody production.,” *Biotechnol. Bioeng.*, vol. 39, no. 4, pp. 418–31, Feb. 1992.

[19] J. Li, C. L. Wong, N. Vijayasankaran, T. Hudson, and A. Amanullah, “Feeding lactate for CHO cell culture processes: Impact on culture metabolism and performance.,” *Biotechnol. Bioeng.*, vol. 109, no. 5, pp. 1173–86, May 2012.

[20] H. Le, S. Kabbur, L. Pollastrini, Z. Sun, K. Mills, K. Johnson, G. Karypis, and W.-S. Hu, “Multivariate analysis of cell culture bioprocess data--lactate consumption as process indicator.,” *J. Biotechnol.*, vol. 162, no. 2–3, pp. 210–23, Dec. 2012.

[21] G. B. Nyberg, R. R. Balcarcel, B. D. Follstad, G. Stephanopoulos, and D. I. Wang, “Metabolism of peptide amino acids by Chinese hamster ovary cells grown in a complex medium.,” *Biotechnol. Bioeng.*, vol. 62, no. 3, pp. 324–35, Feb. 1999.

[22] Y.-M. Huang, W. Hu, E. Rustandi, K. Chang, H. Yusuf-makagiansar, and T. Ryll, “Maximizing productivity of CHO cell-based fed-batch culture using chemically defined

media conditions and typical manufacturing equipment.," *Biotechnol. Prog.*, vol. 26, no. 5, pp. 1400–10, 2010.

[23] W. S. Ahn and M. R. Antoniewicz, "Parallel labeling experiments with [1,2-(13)C]glucose and [U-(13)C]glutamine provide new insights into CHO cell metabolism.," *Metab. Eng.*, vol. 15, pp. 34–47, Jan. 2013.

[24] W. S. Ahn and M. R. Antoniewicz, "Metabolic flux analysis of CHO cells at growth and non-growth phases using isotopic tracers and mass spectrometry.," *Metab. Eng.*, vol. 13, no. 5, pp. 598–609, Sep. 2011.

[25] S. W. G. Tait and D. R. Green, "Mitochondria and cell death: outer membrane permeabilization and beyond.," *Nat. Rev. Mol. Cell Biol.*, vol. 11, no. 9, pp. 621–32, Sep. 2010.

[26] F. M. Lasorsa, P. Pinton, L. Palmieri, G. Fiermonte, R. Rizzuto, and F. Palmieri, "Recombinant expression of the Ca(2+)-sensitive aspartate/glutamate carrier increases mitochondrial ATP production in agonist-stimulated Chinese hamster ovary cells.," *J. Biol. Chem.*, vol. 278, no. 40, pp. 38686–92, Oct. 2003.

[27] F. Zagari, M. Stettler, H. Broly, M. Wurm, and M. Jordan, "High expression of the aspartate–glutamate carrier Aralar1 favors lactate consumption in CHO cell culture," *Pharm. Bioprocess.*, vol. 1, no. 1, pp. 19–27, 2013.

[28] F. M. Wurm, "Production of recombinant protein therapeutics in cultivated mammalian cells.," *Nat. Biotechnol.*, vol. 22, no. 11, pp. 1393–8, Nov. 2004.

[29] N. Carinhas, R. Oliveira, P. M. Alves, M. J. T. Carrondo, and A. P. Teixeira, "Systems biotechnology of animal cells: the road to prediction.," *Trends Biotechnol.*, vol. 30, no. 7, pp. 377–85, Jul. 2012.

[30] C. Altamirano, C. Paredes, a Illanes, J. J. Cairó, and F. Gòdia, "Strategies for fed-batch cultivation of t-PA producing CHO cells: substitution of glucose and glutamine and rational design of culture medium.," *J. Biotechnol.*, vol. 110, no. 2, pp. 171–9, May 2004.

[31] M. Zhou, Y. Crawford, D. Ng, J. Tung, A. F. J. Pynn, A. Meier, I. H. Yuk, N. Vijayasankaran, K. Leach, J. Joly, B. Snedecor, and A. Shen, "Decreasing lactate level and increasing antibody production in Chinese Hamster Ovary cells (CHO) by reducing the expression of lactate dehydrogenase and pyruvate dehydrogenase kinases.," *J. Biotechnol.*, vol. 153, no. 1–2, pp. 27–34, Apr. 2011.

[32] L. M. Barnes and A. J. Dickson, "Mammalian cell factories for efficient and stable protein expression.," *Curr. Opin. Biotechnol.*, vol. 17, no. 4, pp. 381–6, Aug. 2006.

[33] J. Becker, M. Hackl, O. Rupp, T. Jakobi, J. Schneider, R. Szczepanowski, T. Bekel, N. Borth, A. Goesmann, J. Grillari, C. Kaltschmidt, T. Noll, A. Pühler, A. Tauch, and K.

Brinkrolf, “Unraveling the Chinese hamster ovary cell line transcriptome by next-generation sequencing.,” *J. Biotechnol.*, vol. 156, no. 3, pp. 227–35, Dec. 2011.

[34] C. Clarke, P. Doolan, N. Barron, P. Meleady, S. F. Madden, D. DiNino, M. Leonard, and M. Clynes, “CGCDB: a web-based resource for the investigation of gene coexpression in CHO cell culture.,” *Biotechnol. Bioeng.*, vol. 109, no. 6, pp. 1368–70, Jun. 2012.

[35] C. Altamirano, A. Illanes, S. Becerra, J. J. Cairó, and F. Gòdia, “Considerations on the lactate consumption by CHO cells in the presence of galactose.,” *J. Biotechnol.*, vol. 125, no. 4, pp. 547–56, Oct. 2006.

[36] M. De Jesus and F. M. Wurm, “Manufacturing recombinant proteins in kg-ton quantities using animal cells in bioreactors.,” *Eur. J. Pharm. Biopharm.*, vol. 78, no. 2, pp. 184–8, Jun. 2011.

[37] T. Hassell, S. Gleave, and M. Butler, “Growth inhibition in animal cell culture,” *Appl. Biochem. Biotechnol.*, vol. 30, no. 1, pp. 29–41, 1991.

VII: CONCLUSIONS

Fundamentally, this dissertation accomplishes two goals:

First, the metabolic phenotypes associated with increasing antibody production in a fed-batch process were identified. Oxidative metabolism was consistently found to be correlated with increased antibody production, both in DHFR-CHO and GS-CHO lines. This was found to be true not only in terms of increased TCA cycling but also reduced lactate production. Increased net NADH and CO_2 production accompanied this finding. Similarly, as net NADPH production increased, specific antibody productivity followed suit.

The time dependency of fed-batch culture was elucidated, and the metabolism associated with peak exponential growth was markedly different from peak production phase. It is realistic that genetic manipulation to increase desirable metabolic traits of the production phase could be used to increase productivity, but this could have detrimental effects during the exponential growth phase. As a result, it may be important to implement metabolic engineering strategies using inducible genetic systems in order to regulate host cell metabolism in a time-dependent manner. Critically, all the aforementioned relationships were identified using industrially relevant CHO cell lines, all capable of achieving industrially relevant final antibody titers. This was possible due to the unique collaborative nature of this dissertation with multiple industry partners, including Amgen and Janssen.

Second, various approaches for enhancing the conditions associated with high product titers were implemented and evaluated. In one case, a genetic manipulation was employed to express Bcl-2Δ. Here, increased apoptotic resistance was incorporated into CHO cells with the

goal of augmenting IVCD. In addition to the expected increase in IVCD, we found that pyruvate metabolism was significantly rewired. Bcl-2Δ caused an increased percentage of pyruvate to enter the mitochondria to engage in oxidative metabolism while less was fermented to lactate. Furthermore, increased enzymatic activity was recorded in both TCA cycle and oxidative phosphorylation enzymes. In another case, a media optimization was implemented. When glutamine was limited in culture, specific growth rate was increased and lactate production reduced. If growth rate can be increased, higher IVCDs can be achieved in less time.

Practical applications to the biopharmaceutical industry

Efforts to increase flux to the mitochondria are expected to pay dividends in terms of antibody production. Nearly all the reactions of the TCA cycle were found to be upregulated in antibody-producing lines. Not only was this true when comparing the producer to the control, but as specific productivity increased, so did the given TCA cycle flux. Overexpressing pyruvate dehydrogenase (PDH) may be the most logical genetic manipulation to make, as it directly increases the total amount of carbon allocated to the mitochondria. Unfortunately, it is an enzyme complex, making expression difficult. However, overexpression of isocitrate dehydrogenase (IDH) also holds promise, as it too has been identified as a rate limiting enzyme [1]. IDH is not an enzyme complex, but three known NAD^+ isoforms exist [2]. To determine the correct IDH isoform to overexpress, RNA interference studies may assist in determining which isoform is most critical.

NADPH production likewise appears to be essential to high specific productivity. This relationship held true in both GS and DHFR CHO cell lines. However, while strong linear

relationships exist amongst individual TCA cycle reactions and productivity, the same cannot be said for individual reactions traditionally known for producing NADPH. Yet when NADPH producing fluxes malic enzyme (ME) and glucose-6-phosphate dehydrogenase (G6PDH) are summed together, a key correlation emerges. Thus, when both enzymes are overexpressed, further benefits can potentially be realized in terms of specific productivity.

Enhancing apoptotic resistance encourages increased mitochondrial activity, fostering conditions favorable for increased productivity. Perhaps not surprisingly, specific productivity in apoptotic resistant lines was generally higher than in control lines. While expressing Bcl-2Δ was associated with a decrease in specific growth rate, it led to a 40% gain in IVCD.

Future Work

As mentioned prior, time plays a major role in antibody production. Constitutive expression of a metabolic complex/enzyme to promote antibody production may be detrimental to the initial growth phase, which is frequently characterized by substantial lactate production. Therefore, it is imperative that an appropriate expression system is determined. Efforts to induce gene expression at reduced temperature [3] as well as tethering expression to a promoter naturally activated during peak productivity [4] both show promise.

Additionally, efforts to overexpress mitochondrial redox transporters, such as the Asp/ Glu transporter, may benefit the culture during both exponential growth and peak production (stationary-like) phase [5]. As described in the background, a lack of redox transport from the cytosol to the mitochondria may force the cell to generate lactate to maintain redox balance.

Expression of various isozymes of Asp/Glu transporters [6] gets at the root cause of lactate production, and deserves the special attention of MFA.

The relationship of NADPH production with antibody production merits further research. The relationship holds strongly in GS-CHO (CHOK1SV) clones, but not in the Bcl-2Δ variants. Oxidative metabolism is associated with the generation of reactive oxygen species (ROS), generated as byproduct of incomplete electron transfer. The fact that the correlation is weak in Bcl-2Δ clones compared to the sister GS-CHO clones may hypothetically be related to Bcl-2Δ's capacity to prevent mitochondrial permeabilization. An experiment measuring ROS production in all the GS-CHO lines, including the Bcl-2Δ clones, would be a first step to test this hypothesis. If there is a positive correlation between oxidative stress and NADPH production, genetic intervention would be warranted. Based primarily upon the DHFR-CHO findings, efforts to induce overexpression of G6PDH may have the greatest chance of improving titers. Be aware, however, that the pentose phosphate pathway fluxes have large confidence intervals, much larger than TCA cycle fluxes. This lessens the probability of the observed trend actually holding true.

Most of this work explored carbon metabolism. However, increased NH_3 consumption was associated with increased specific antibody production. After performing a mass balance on total nitrogen consumed or produced by the cell, a substantial portion of nitrogen (in one instance, more than half) was not accounted for by free amino acid production, antibody, or biomass (i.e. there are additional nitrogen sinks) (Figure 7-A-1). There is a realistic chance that a significant portion of this nitrogen may be demanded by other proteins (host cell protein) excreted extracellularly by the CHO cell. If host cell protein (HCP) were to account for all the unaccounted nitrogen, HCP would need to be 94% (± 45% s.d.) the summed rate of antibody and

biomass (based upon all GS-CHO lines tested). This corresponds with roughly 10%-30% of the total carbon consumed (Figure 7-A-2). This assumes that for each unaccounted nitrogen, stoichiometrically there are 4.1 carbons [7]. It is unlikely that HCP accounts for all the unaccounted nitrogen, but realistic that it accounts for a non-negligible portion. If there is any truth to this, a non-negligible amount of carbon would be demanded by HCP, carbon not currently accounted for. CO_2 production emanating from the TCA cycle may be overestimated in literature as well as our own metabolic models. A simple Bradford assay to determine the changing protein concentration extracellularly offers a reasonable starting point to test this hypothesis.

Contribution

The in-depth quantification of intracellular metabolism of both the GS and DHFR expression systems in multiple high-producing CHO cell lines during multiple phases of fed-batch culture is perhaps this work's most valuable contribution to the scientific community. All told, this body of work provides a step in the direction of using systems biology, not empirical analysis, to increase productivity in mammalian cell culture. This was primarily achieved by successful generation of ^{13}C-aided metabolic models and subsequent analysis to determine the biological significance of the results.

In an exercise of humility, the late mathematician/statistician George E.P. Box pragmatically stated:

Essentially, all models are wrong, but some are useful [8].

It is our hope and genuine belief that this body of work will prove to be useful.

Appendix

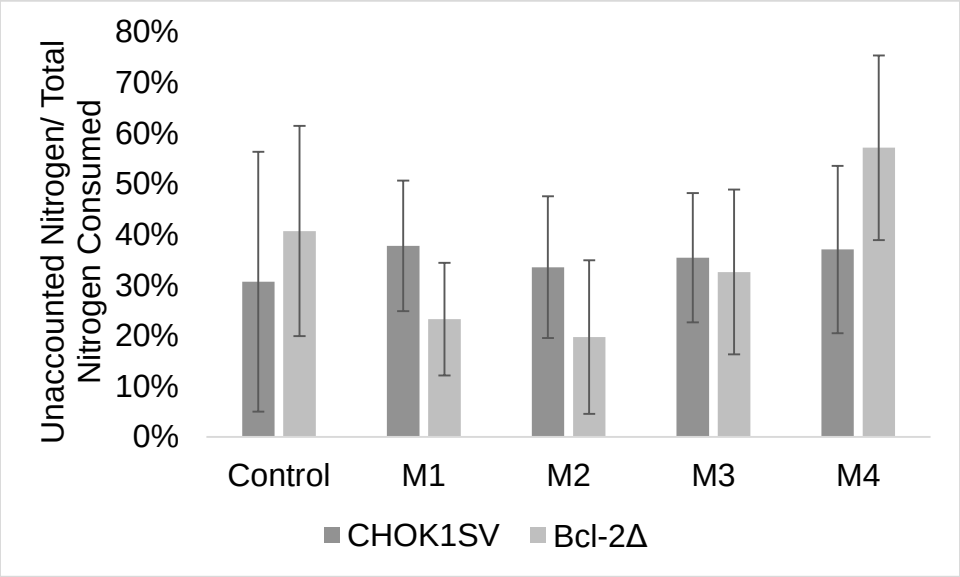

Figure 7-A-1. Unaccounted nitrogen associated with mass balance. Mass balance includes nitrogen associated with biomass and antibody generation, as well as amino acid production. Nitrogen balance does not account for host cell protein, or urea production.

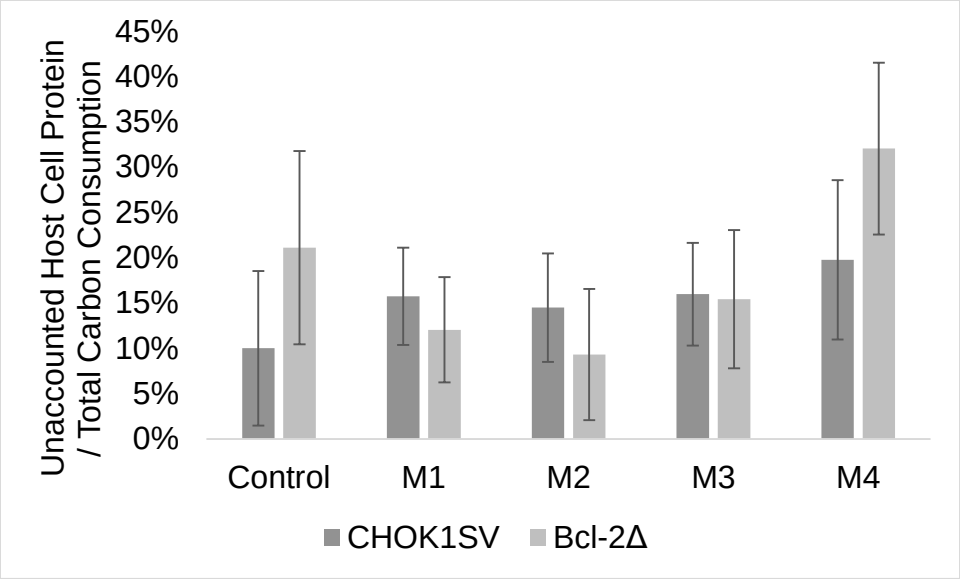

Figure 7-A-2. Unaccounted protein in the carbon mass balance. Calculation assumes 4.1 C/N and that all the unaccounted nitrogen is converted into protein.

References

[1] J. Wahrheit, J. Niklas, and E. Heinzle, “Metabolic control at the cytosol-mitochondria interface in different growth phases of CHO cells,” *Metab. Eng.*, pp. 1–13, Feb. 2014.

[2] S. Hammond, M. Kaplarevic, N. Borth, M. J. Betenbaugh, and K. H. Lee, “Chinese hamster genome database: An online resource for the CHO community at www.CHOgenome.org.,” *Biotechnol. Bioeng.*, vol. 109, no. 6, pp. 1353–1356, Nov. 2012.

[3] H. Thaisuchat, M. Baumann, J. Pontiller, F. Hesse, and W. Ernst, “Identification of a novel temperature sensitive promoter in CHO cells.,” *BMC Biotechnol.*, vol. 11, no. 1, p. 51, Jan. 2011.

[4] H. Le, N. Vishwanathan, A. Kantardjieff, I. Doo, M. Srienc, X. Zheng, N. Somia, and W.-S. Hu, “Dynamic gene expression for metabolic engineering of mammalian cells in culture.,” *Metab. Eng.*, vol. 20, pp. 212–20, Nov. 2013.

[5] F. Zagari, M. Stettler, H. Broly, M. Wurm, and M. Jordan, “High expression of the aspartate–glutamate carrier Aralar1 favors lactate consumption in CHO cell culture,” *Pharm. Bioprocess.*, vol. 1, no. 1, pp. 19–27, 2013.

[6] F. M. Lasorsa, P. Pinton, L. Palmieri, G. Fiermonte, R. Rizzuto, and F. Palmieri, “Recombinant expression of the Ca(2+)-sensitive aspartate/glutamate carrier increases mitochondrial ATP production in agonist-stimulated Chinese hamster ovary cells.,” *J. Biol. Chem.*, vol. 278, no. 40, pp. 38686–92, Oct. 2003.

[7] J. King, T. Jukes, and B. Clarke, *Non-darwinian evolution*, vol. 164, no. 3881. 1969, pp. 788–798.

[8] G. E. P. Box and N. R. Draper, *Empirical model-building and response surfaces. Wiley series in probability and mathematical statistics*. Oxford, England: John Wiley & Sons Inc., 1987, p. 669.